AGARD-AG-317

AGARD-AG-317

AGARD

ADVISORY GROUP FOR AEROSPACE RESEARCH & DEVELOPMENT
7 RUE ANCELLE 92200 NEUILLY SUR SEINE FRANCE

AGARDograph 317

Manual or the Flight of Flexible Aircraft in Turbulence

(Manuel sur le Vol des Avions Non-rigides en Milieu Turbulent)

NORTH ATLANTIC TREATY ORGANIZATION

AGARD

ADVISORY GROUP FOR AEROSPACE RESEARCH & DEVELOPMENT

7 RUE ANCELLE 92200 NEUILLY SUR SEINE FRANCE

AGARDograph 317

Manual on the Flight of Flexible Aircraft in Turbulence

(Manuel sur le Vol des Avions Non-rigides en Milieu Turbulent)

Edited by

John C. Houbolt

This AGARDograph was sponsored by the Structures and Materials Panel of AGARD.

North Atlantic Treaty Organization
Organisation du Traité de l'Atlantique Nord

The Mission of AGARD

According to its Charter, the mission of AGARD is to bring together the leading personalities of the NATO nations in the fields of science and technology relating to aerospace for the following purposes:

- Recommending effective ways for the member nations to use their research and development capabilities for the common benefit of the NATO community;
- Providing scientific and technical advice and assistance to the Military Committee in the field of aerospace research and development (with particular regard to its military application);
- Continuously stimulating advances in the aerospace sciences relevant to strengthening the common defence posture;
- Improving the co-operation among member nations in aerospace research and development,
- Exchange of scientific and technical information,
- Providing assistance to member nations for the purpose of increasing their scientific and technical potential;
- Rendering scientific and technical assistance, as requested, to other NATO bodies and to member nations in connection with research and development problems in the aerospace field.

The highest authority within AGARD is the National Delegates Board consisting of officially appointed senior representatives from each member nation. The mission of AGARD is carried out through the Panels which are composed of experts appointed by the National Delegates, the Consultant and Exchange Programme and the Aerospace Applications Studies Programme The results of AGARD work are reported to the member nations and the NATO Authorities through the AGARD series of publications of which this is one.

Participation in AGARD activities is by invitation only and is normally limited to citizens of the NATO nations

Published May 1991

ISBN 92-835-0617-0

Printed by Specialised Printing Services Limited
40 Chigwell Lane, Loughton, Essex IG10 3TZ

Dedication

The inspiration and motivation for the AGARD SMP activity which resulted in the publication of this ACARDograph was provided by Dr Gabriel (Daniel) Coupry. On 24 April 1985, Dr Coupry organized an informal group at the 60th SMP Meeting which recommended the publication of a manual containing updated gust statistics and new methods of computing loads and stresses induced by turbulence. The Panel accepted this recommendation and the Sub-Committee on "The Flight of Flexible Aircraft in Turbulence" was formed at the Fall, 1985 Meeting.

Dr Coupry retired from the Panel in June, 1987 and was retained as editor of the manual, at which time I was named as Chairman of the Sub-Committee. Work on the manual progressed in this manner until the untimely demise of Dr Coupry in June, 1988. The members of the Sub-Committee were unaminous in the desire to complete the manual and dedicate it to Dr Coupry. Dr John C.Houbolt agreed at that time to take over the duties of editor.

The manual is finished at last, and we can only hope that it would meet with Dr Coupry's approval We of the Sub-Committee, wholeheartedly dedicate it to Daniel — our colleague, our friend and our teacher.

Dédicace

Nous devons l'inspiration et la motivation du Panel AGARD SMP qui est à l'origine de cette AGARDographie au Docteur Gabriel (Daniel) Coupry Le 24 avril 1985, lors de la 60ème réunion du Panel SMP, le Docteur Coupry a réuni un groupe informel qui a proposé l'édition d'un manuel contenant des données statistiques mises à jour relatives aux rafales et aux nouvelles méthodes pour le calcul des charges et des sollicitations induites par la turbulence.

Cette proposition fut acceptée par le Panel et le sous-comité sur "le vol des avions non-rigides en milieu turbulent" qui a été crée lors de la réunion du Panel à l'automne 1985.

Le Docteur Coupry s'est retiré du Panel en juin 1987, mais il a été retenu comme maître d'oeuvre du manuel, à l'époque où je venais d'être nommé Président du sous-comité en question.

Les travaux de préparation de ce manuel se sont poursuivis ainsi jusqu'à son décès prématuré en juin 1988.

Les membres du sous-comité ont été unanimes pour mener à terme les travaux de ce document et pour le dédier au Docteur Coupry. Le Docteur John C.Houbolt a accepté alors de poursuivre et d'achever le manuel.

Le manuel est maintenant terminé et nous ne pouvons qu'espérer qu'il répond à ce qu'avait souhaité le Docteur Coupry Les membres du sous-comité, le dédient de tout coeur à Daniel — notre collègue, notre ami et notre maître.

Président du sous-comité sur le vol des avions non-rigides en milieu turbulent.

R.F.O'Connell
Chairman – Sub Committee on
The Flight of Flexible Aircraft in Turbulence

Structures and Materials Panel

Chairman: Mr Samuel L.Venneri
Director, Materials & Structures
Division (Code RM)
Office of Aeronautics & Space
Technology
NASA HQ
Washington DC 20546
United States

Deputy Chairman: Mr Roger Labourdette
Directeur Scientifique des
Structures
ONERA
29 ave de la Division Leclerc
92320 Chatillon
France

SUB-COMMITTEE ON
FLIGHT OF FLEXIBLE AIRCRAFT IN TURBULENCE

Chairman: Mr R F.O'Connell
Lockheed-California Co
P.O. Box 551
Burbank, CA 91520
United States

Members:		
	E.H Dowell	US
	H Forsching	GE
	R Freymann	LU
	J.J.Glaser	CA
	H.H.Ottens	NL
	J.Roustan	FR
	M.Rother	GE
	A.Salvetti	IT
	M Sancho	FR
	O Sensburg	GE
	C W Skingle	UK
	D.C.Thorby	UK
	A.F.Tovar de Lemos	PO
	A.P.Ward	UK
	R.J.Zwaan	NL

Technical Coordinator: J C Houbolt US

PANEL EXECUTIVE

Mr Murray C.McConnell (UK)

Mail from Europe:
AGARD—OTAN
Attn: SMP Executive
7, rue Ancelle
92200 Neuilly-sur-Seine
France

Mail from US and Canada:
AGARD—NATO
Attn: SMP Executive
APO New York 09777

Tel: 33 (1) 47 38 57 90 & 57 92
Telex: 610176F
Telefax: 33 (1) 47 38 57 99

Introduction

by

Dr John C.Houbolt
Chief Aeronautical Scientist (Retired)
NASA
Langley Research Center
Hampton, Va.
United States

Origin of the Manual. — The study of atmospheric turbulence and its influence on aircraft operation and design has been of concern to the Structures and Materials Panel almost continously since the inception of AGARD .Areas of interest have included the measurement and modeling of atmospheric turbulence, the response of airplanes, and the structural design as associated with turbulence encounter.

The past few years have seen a heightened interest in the turbulence or "gust" problem, particularly on analysis or reduction of turbulent encounter data, and on design procedures. In view of the varied and significant contributions that have been made, members of the SMP felt it would be appropriate to summarize the findings in the form of a manual. This compendium represents the manual that resulted. It is to be noted that the manual is divided into two parts; the first part deals with data collection and analysis, the second with certification procedures and analysis of airplane response. That the manual represents a collaborative effort can be noted from the Table of Contents, in general the various chapters come from authors representing the various countries involved.

Editorship. — It is to be noted that Gabriel Coupry was originally chosen too be Editor of this manual. With his passing, I was asked to take over and finish the work. Because of his contributions and continuous and longstanding keen interest in the atmospheric turbulence problem, and his beginning editorial efforts, this manual has been dedicated to him

Historical perspective. — To set the stage for the various chapters that ensue, it is felt appropriate to outline briefly the sequence of evolution of some of the earlier gust loads developments. The remainder of this introduction covers this perspective.

In the United States, gust studies started around 1915; the first published paper from NACA, in fact, dealt with the gust problem (Ref.1) It is to be noted that a basic gust loads equation was formulated almost at the beginning of gust loads studies, and that this general equation has prevailed to the present time as the basis for gust loads design. To outline briefly the nature of the derivation of this equation, consider that an airplane encounters a sharp edge or step function gust of intensity U, if we use quasi-steady aerodynamics and assume no vertical motion of the airplane, the lift due to the gust is given by

$$L = \frac{a}{2} \rho V^2 S \frac{U}{V} \tag{1}$$

The vertical acceleration increment, in g units, implied by a lift force of this magnitude follows as

$$\Delta n = \frac{L}{W} = \frac{a\rho SV}{2W} U \tag{2}$$

Equation (2) represents the root form of the gust loads equation for a discrete gust encounter This sharp edge gust concept was reported in 1931 in (Ref 2) and probably led to the first gust loads regulation in the United States in 1934 Prior to 1933, maneuver load factors for transports were reduced to 2 5 to 4.0 g. The cruising speed of the then newly-designed Boeing 247 airplane was about double that of the previous Ford Tri-motor, but the wing loading was about the same. Thus the possibility of gust loads becoming critical became significant

It was recognized that in reality, nonsteady aerodynamic effects due to gust penetration and due to airplane vertical response motion are present, and that the airplane would move vertically to alter the load Analysis indicated that these effects could be taken into account by introducing a factor K in the equation as follows

$$\Delta n = \frac{a\rho SV}{2W} KU \tag{3}$$

The factor K, reflecting the nonsteady effects, was designated the alleviation factor.

The first form of the alleviation factor K was based on wing loading W/S, a notion brought about mostly by empirical observation and gust tunnel results. A value of K=1 was set at W/S=16, increased to 1.22 at large wing loading and decreased

to zero for W/S=0 For design a value of U of around 30 fps was chosen. It should be noted that the density ρ, speed V, and gust intensity U, were given in terms of equivalent sea level values.

Around 1954 a more rational analysis indicated that the K values should be given in terms of the mass parameter

$$\mu = \frac{2W}{a\rho cgS}$$

This parameter was found in the derivation of the so-called revised gust loads formula (Ref.3) A 1-cos gust shape was used with a gradient distance of 12.5 chords. The assumptions in the analysis were: the airplane is a point mass, vertical motion only, and uniform spanwise gusts. Included were the Kussner unsteady lift function for gust penetration, and the Wagner function for airplane motion The equation for the alleviation function

$$K = \frac{.88\mu}{5.3 + \mu}$$

was derived by Haubolt. A gust design value of 50 fps was first used. Note, with this improved treatment, sea level values for density and speed are also used. (We may note that with U = 50 and a K of 7, the effective value for gust intensity is 35 fps, not far from the value of 30 used in the sharp edge gust treatment.)

In the early 1950s power spectral methods were introduced (Ref.4). It was found that an equation analogous to Equation (3) applied, namely

$$\sigma_{\Delta n} = \frac{a\rho SV}{2W} K_\phi \sigma_w \qquad (4)$$

We note that rms values replace intensity values, and that K_ϕ represents the alleviation factor found by the spectral approach.

In the application over the years, equations (3) and (4) have been used basically in two ways: 1, to deduce effective derived values of gust intensity, U, from flight measured values of Δn and 2, for stipulated or assigned values of U, to deduce airplane design load values for Δn. For equation (4), design values for load are arrived at by stipulating σ_w and a value for the number of standard deviations, for example: $U = 10\sigma_w$. The newer treatments also involve the use of true values for density, speed, and gust intensity, not the equivalent sea level values formerly used.

This brief insight sets the stage for the rest of the manual. A greatly expanded version of this perspective is to be found in (Ref 5)

REFERENCES

1 Wilson, E.B. Hunsacker, J C. "Theory of an Aeroplane Entering Gusts " NACA Report No. 1, Part 2, 1915

2 Rhode, R.V. Lundquist, E.E "Preliminary Study of Applied Load Factors in Bumpy Air." NACA Technical Note No 374, April 1931.

3. Pratt, K.G. Walker W.G. "A Revised Gust-Load Formula and A Reevaluation of V-G Data taken on Civil Transport Airplanes from 1933 to 1950." NACA Technical Report No. 1206, 1954.

4. Press, H Houbolt, J.C. "Some Applications of Generalized Harmonic Analysis to Gust Loads on Airplanes " IAS Jour. Aero. Sci., January 1955, pp. 17—26

5. Murrow, H.N. Pratt, K.G. Houbolt, J.C. "NACA/NASA Research Related to Evolution of U.S. Gust Design Criteria." AIAA Journal.

Contents

CHAPTER I
MEASUREMENT OF ATMOSPHERIC TURBULENCE

by

Harold N.Murrow
NASA Langley Research Center
United States
(retired)*

Introduction

The material contained herein is primarily a compilation of information that has already been published. The attached reference list should be adequate for clarifying points to any detail desired. The purpose of this chapter is to provide a description of the methodology required for measuring atmospheric turbulence in the form of true gust velocity. The content will include instrumentation requirements and selections used, flight assessments of the measurement system, some data reduction considerations, and finally some typical data obtained.

Atmospheric turbulence has always been of concern for aircraft. For example, the first NACA report written was on this subject (J. C. Hunsacker and E B. Wilson; "Report on Behavior of Aeroplanes in Gusts," NACA Rep. 1, 1915). Early aircraft designs were based on the concept of a rigid airplane and a single ramp-type gust with a gradient distance of ten wing chords and a specified maximum vertical velocity. An alleviation factor was applied for each airplane based on wing loading. Later, modifications were made to this procedure and a (1-cosine) shape was used with a gradient distance or time-to-peak of 12.5 chords and the alleviation was now based on the mass ratio. Assessments of turbulence encounters were made through measurements of vertical acceleration at or near the center of gravity of the airplane.

Subsequent aircraft developments led to many different configurations incorporating flexibility, wing sweep, etc.; operations covered wide ranges of speed and altitude, and new approaches to response analyses were pursued. In the early fifties, power spectral techniques of generalized harmonic analysis were introduced. Figure 1 (ref. 1) presents the input-output relation for this type of analysis. In this case, the atmospheric turbulence is desired in the form of a power spectrum, which takes into account the continuous nature and broad frequency content of the turbulence.
The two forms of turbulence measurement are depicted in figure 2. Individual gusts as sensed by a c.g. accelerometer on an aircraft are reduced to what is termed "derived gust velocity" which is normalized between different aircraft by the parameters of wing loading, lift curve slope, and the alleviation factor, K_g. Measurements of continuous turbulence where time histories of the actual air velocity fluctuations or "true gust velocity" is provided, are determined from in-situ sensors mounted on an aircraft. Additional instrumentation must be on-board to sense motions of the aircraft which are applied as corrections to measurements of the basic sensors. Figure 3 from reference 2 presents a comparison of results from the two methods of turbulence measurement as a function of time and distance. In this case, derived gust velocity values were determined at maximum acceleration points above selected threshold levels. It can be seen that the aircraft response effects present in the derived gust velocities result in significant differences between the two results.

*prepared while a NASA Distinguished Research Associate; now affiliated with Lockheed Engineering Sciences Co., Hampton, VA, USA

Methods for measuring time histories of air velocity fluctuations from onboard aircraft were being studied in the early 1950's. Parallel efforts in the U.S., at NACA (ref. 3) and Massachusetts Institute of Technology in that time period resulted in some early measurements which were limited by available instrumentation and computational capability. Advances in these two areas, specifically, inertial platform systems in the instrumentation area and fast Fourier transforms in the data processing area, have led to the practicality of obtaining accurate measurements of the three components of true gust velocity and the corresponding power spectra.

Mathematical Description of Atmospheric Turbulence

The equation for describing power spectra of turbulence that was proposed by von Karman is given in Figure 4. Note that two parameters are needed for a complete definition of a specific spectral curve, that is σ , the rms value, which defines the level or intensity and L, which is described as the "integral scale value." From the family of curves on the figure, it can be seen that L essentially defines the wavelength (or frequency) of the so-called "knee" of the curves. Examples of some early measurements are given in Figure 5 (from reference 2). These measurements did not extend far enough into the low frequency region to define the knee, however an indication of the relative intensity between three meteorological conditions is given. The importance of measurements at low frequencies or inverse wavelengths is shown in Figure 6. The frequency region for rigid body pitch and dutch roll modes for conventional transports is shown by the vertical band on the right of the figure. Note that for L values greater than 1000 feet response of these aircraft is relatively unaffected by L; however, for future supersonic transports which would cruise at M = 2.7 or greater, significant differences in response may result from different values of L. Figure 7 summarizes this result to indicate the importance of L values in response of a synthesized supersonic transport design. It is therefore important when measuring atmospheric turbulence, to include the long wavelength region (ref. 4).

Accurate power estimates in the higher frequency region of the measured spectra are also important. An example is studies related to the spanwise variation of turbulence. Several measurement programs have been conducted with this objective (ref. 5, for example), using ref. 6 for the theoretical basis, however, the maximum spanwise distance for the sampling aircraft that the author is aware of 60 ft. Other measurements of gust velocity at wing tips are refs. 7 and 8. Suffice it to say, however, that applications exist for accurate measurement data of atmospheric turbulence over the entire frequency range.

EQUATIONS FOR DETERMINING TRUE GUST VELOCITY

A discussion of instrumentation requirements will be presented later. At this point it should be stated that the basic sensors are used to make the primary measurements - air flow fluctuations - vertical, and horizontal (along and normal) to the aircraft flight direction. Aircraft motions - angles and angular rates - are measured for use in applying corrections to the basic flow measurements. Equations which are adequate to describe required measurements for deriving the three components of gust velocity are as follows (ref. 9):

$$\begin{array}{lcll} \text{GUST VELOCITY COMPONENT} & = & \left[\text{PRIMARY MEASUREMENT}\right] & + \left[\text{AIRCRAFT MOTION CORRECTIONS}\right] \\ & & & \underline{\text{LONGITUDINAL}} \\ u_g & = & [\Delta V] & + \left[v_{ax} \sin \bar{\psi} + v_{ay} \cos \bar{\psi}\right] \\ & & & \underline{\text{LATERAL}} \\ v_g & = & [V\beta] & + \left[-V\Delta\psi + v_{ax} \cos \bar{\psi} - v_{ay} \sin \bar{\psi} + l\dot{\psi} + V\alpha\Phi\right] \\ & & & \underline{\text{VERTICAL}} \\ w_g & = & [V\alpha] & + \left[-V\theta + v_{az} + l\dot{\theta} - V\beta\Phi\right] \end{array}$$

where vane angles and aircraft motions (velocities and rates) are increments from the mean value for the data run, and l is the distance from the flow sensors to the inertial platform.

If the sampling vehicle could be made to transverse the area of interest on a tight wire stretching across the region of interest so that it would not deviate from straight level flight in response to the turbulence, then highly responsive airflow sensors and a sensitive airspeed device would be adequate instrumentation. Since the airplane does respond to the rough air, a number of aircraft motion measurements are necessary to correct the basic measurements. All the terms to the right of the basic measurements in the equations are correction terms set up for use of an inertial platform (East-West and North-South components) due to aircraft response. ($\bar{\Psi}$ is the mean aircraft heading relative to true north). Equations for the determination of V and ΔV are:

$$V = \text{Mach No.} \times \text{Speed of Sound}$$

so that

$$\Delta V = V - \bar{V}$$

where

$$a = 65.77 \sqrt{T}$$

$$M = 5 \left\{ \left(\frac{q_c}{p} + 1 \right)^{2/7} - 1 \right\}^{1/2}$$

and q_c, p and $\bar{V}$ denote the impact pressure, the static pressure and the mean value of V for the run, respectively.

INSTRUMENTATION SYSTEM AND OPERATION

An instrumentation system that has been used successfully is described in reference 10. This system was installed on a B-57B airplane for the NASA program called MAT (Measurement of Atmospheric Turbulence). A list of measurement requirements is shown in Table I for all measurements except those from the inertial platform. As indicated earlier, these are required in the equations for determination of the three

components of gust velocity. As shown in the table, a NASA system has been developed that satisfied the requirements list. A discussion of these requirements is given in Reference 10. The basic (primary) measurements are α, β, ΔV, and V. Required ranges and allowable errors are shown. The angles, of course, depend on the speed of the sampling airplane in combination with the largest gusts expected and include aircraft motion. The sampling aircraft of ref. 10 operated at about M = 0.6; therefore, air fluctuations or turbulence velocities to around 80 fps could be measured assuming negligible aircraft motion. Phase matching is also important since terms are added together to obtain time histories of each component of gust velocity. Allowable phase errors requested for the present NASA program are given in Table II. The results for A_x, A_y, A_z, and $\dot{\theta}$, $\dot{\Phi}$, and $\dot{x}$ were less than was required. Aircraft motion measurement requirements are given in Table III. These are derived from inertial platform outputs.

Several types of flow angle sensors are shown in Figure 8. Reference 11 gives details on these and some other flight instrumentation components. The fixed vane type measures the aerodynamic lifting force on the vanes and relates this to angle-of-attack. The differential pressure probe measures the difference in pressure at two points on a spherical nose. The movable vane senses α or β directly. The relations used to determine α for the different sensors are:

Fixed Vane: Subsonic, $\alpha = \frac{F}{2\pi A_q}$

Supersonic, $\alpha = \frac{F\sqrt{M^2-1}}{4Aq}$

Differential Pressure Probe: $\alpha = \frac{\Delta P}{Kq}$

Free Movable Vane: $\alpha = \alpha$

Note that the accuracy of the first two depends on accurately measuring dynamic pressure, q. At NASA Langley, a movable vane assembly was engineered around 1950 and this design is still in use to date. The system is simple in that angles are measured directly. These vanes are shown on a nose boom attached to a sampling airplane in Figure 9. They are made of coated balsa and have low inertia and are mass balanced. Dry lubricant is used for the bearings to prevent "seizing" at very cold temperatures. The balsa is surprisingly rugged as evidenced by flights through storms where hail was prevalent and only slight damage was sustained. A cage that surrounds the vanes is attached to the boom to protect them from damage while the aircraft is on the ground. Note the nose boom in the photo. It is important that the natural frequency of the boom be above the frequency range of interest for the measurements. The boom shown here has a natural frequency of 26 Hz, whereas the data interest is only to 10 Hz or less. The length of the boom is also important. Since airflow is disturbed to pass around the airplane (upwash), a general rule is to place the vanes 1.5 body diameters ahead of the nose to minimize this effect. Characteristics of the vanes are shown in Figure 10. As long as the dynamic pressure is above approximately 16 psf, the vane natural frequency will be above the range of interest. The expected dynamic pressure at 70,000 ft. altitude will be slightly above this value. The damping will be about 1/4 critical, which is also considered acceptable. Other flow sensing methods have been or are being used. At the National Center for Atmospheric Research (NCAR) in the U.S., studies have been made with a system of five pressure measurements on the surface of a special nose section on an aircraft (ref. 12). In England, the RAE has used Conrad Yawmeters which consist of two hyperdermic tubes with angled ends. The pressure difference across each double tube is sensed and recorded. Details are given in refs. 13 and 14.

A sensitive airspeed system developed for use in the NASA MAT project to obtain the longitudinal turbulence component is illustrated by the schematic drawing in Figure 11, which is taken from reference 10. The principle of operation is first to obtain the steady-state true airspeed at the beginning of each data run by means of conventional measurements of impact and static pressure, and then to measure incremental pressures by means of separate auxiliary transducers during the remainder of the run. These auxiliary transducers are thus required to cover only the range of fluctuations caused by the turbulence and by the pilot in controlling the airplane, and the required pressure range is considerably reduced, with a resulting increase in accuracy and resolution. Valves A and B are ordinarily open during climb and speed changes so that pressures are equalized on both sides of the sensitive transducers (shown below valves A and B) and in the chambers shown. At the beginning of a data run, the pilot's data switch activates solenoids which close valves A and B to "lock" reference pressures which exist at that time in the volume chambers which are heavily insulated and thermostatically controlled so that thermal drifts do not cause detectable pressure changes on the sensitive transducers during the data-recording interval. Once valves A and B are closed, incremental total pressure and incremental static pressure are recorded for the remainder of the run in addition to coarse-resolution impact pressure and free-stream static pressure. Although the pilot can maintain a reasonably horizontal flight path during the run, small changes in altitude would contaminate the measurements of Δp_t (and thus the measurements of incremental true airspeed) at a low frequency if not removed in the data reduction by use of the incremental static pressure recording. To restate: what is needed for obtaining true airspeed fluctuations is Δq_c, or incremental impact pressure (equal to $\Delta p_t - \Delta p_s$), and this can be readily obtained in the postflight data reduction. The dynamic requirements of the static pressure measurements are not stringent since the airplane does not change altitude very rapidly. In order to improve the dynamics of the total pressure measurement, interchangeable restrictor orifices are installed in the pitot head at the front of the boom according to the anticipated altitude range for the particular mission. Their effect is to compensate for changes in damping (of the air column plumbing system) due to changes in density (temperature) with altitude.

Piezoelectric pressure sensors with capability of measuring a broad range of pressure with high sensitivity and accuracy have been used more recently (ref. 5). They are small and are not temperature sensitive and provide a digital output. These features provide more flexibility in location on the aircraft, particularly from the point of view of allowing reduction in length of tubing (and pneumatic volume) from orifices to the sensing element. It was found that these units were directionally sensitive to acceleration, but performance was satisfactory when they were selectively oriented.

Figure 12 shows the inertial platform setup. Accelerometers are mounted on the platform and integrated to give velocity. An on-board analog computer provides computations to obtain desired time histories for recording.

One measurement concern surrounding the derived velocities from the inertial platform centers on the so-called "Schuler" oscillation. The gyrostabilized element is responsive at a period of 84.4 minutes. (This is the natural period of a pendulum with arm length equal to the radius of the earth.) The amplitude of this oscillation is important as can be seen in Figure 13 since turbulence runs of about 10 minutes are desired. The maximum error on the horizontal velocities can be approximated by a linear trend (It is not possible to measure the Schuler oscillation at the end of the flight and trace back and correct velocities since the phase and amplitude may vary with time; however, it is believed that the oscillation amplitude at the end of the flight is the maximum since it always remains the same or increases.) As a matter of further interest some attempts have been made to determine Schuler oscillation while in-flight. Actual post-flight measurements from some NASA flights indicated that σ_{trend} is 1.6 fps or less for nearly all cases. The effect of this on resulting power spectra for the horizontal components is indicated in Figure 14. The computer-generated time

history of reference 15 was used for this study. In Figure 14(a), the ratio of trend to turbulence is 0.5, and in Figure 14(b) the ratio is 1.0. Since most turbulence data considered worthy of analysis has a σ greater than 4 fps, this trend effect is considered tolerable, but the Schuler oscillation should always be monitored to assure that it is within an acceptable level after a flight. It should also be considered that advanced inertial platforms may have smaller Schuler oscillation buildup.

The platform-mounted accelerometer for measuring vertical acceleration is not used for navigation. This accelerometer is susceptible to varying Coriolis forces during data runs due to changing ground tracks with respect to the earth's rotation. The change in the earth's gravity constant with altitude is another source of "zero" shift or error. Both of these sources lead to velocity trend errors for the integrated acceleration. One way of overcoming this difficulty is to integrate the accelerometer output in the postflight data reduction rather than to utilize onboard electronic integration. Points along the time history where the vertical airplane velocity is estimated to be zero are chosen to start and stop the integration. These start and stop times are chosen by inspection of the time history of the sensitive incremental static pressure, Δp ; that is, points are chosen where the slope of the time history is zero. A mean for the accelerometer output for this time range is then determined on the computer. When the mean (which is determined to a large number of digits and not limited to the resolution of the individual acceleration readings) is subtracted and the integration performed, the resulting velocity time history has thus been forced to start and stop at zero. This procedure has limitations, however, it is not easily automated into the data reduction process, and the location of exact points along the time history where zero vertical velocity occurs is difficult because of noise present in the time history of the sensitive static pressure. (This relatively high-frequency noise results from cross flow over the static port locations on the pitot-static head, particularly in severe turbulence.) Another disadvantage is that zero vertical velocity points may not occur at convenient locations near each end of the time history, and, in fact, for short pitch and yaw maneuvers, they may not occur at all. A more efficient procedure has been developed which accomplishes the same result but with greater accuracy and no limitation on the starting and stopping points. The basis for the procedure surrounds the fact that when an erroneous trend slope, k , is integrated over total time T, (with mean removed), a parabolic error with a maximum value at T/2 of $-kT^2/8$ results. The maximum error at T/2 is determined experimentally in the present case by double integration of the platform–mounted accelerometer output to obtain a time history of inertial displacement. This displacement is then compared with the time history of the pressure-derived altitude. An illustrative sketch of the procedure is given in Figure 15.

It should be noted that the end point of the time history of $\iint \Delta a_z(dt)^2$ has been forced to agree with the time history of Δh_p at the end of the run by an adjustment to the initial condition of the first integration; that is, the last integration is then $\int(Vaz-\overline{Vaz}+C)dt$, where $C=\Delta h_p(T)/T$ The procedure has been automated in the data reduction process. The displacement error at the midpoint of the run is obtained by averaging over $\pm 1/2$ second to minimize possible effects of the previously mentioned high-frequency noise on the time history of sensitive pressure altitude. The value of k obtained is applied as a detrend slope correction to the vertical airplane velocity obtained from the first integration. As a check on the overall procedure, in the example case the vertical airplane velocity V_{az} was again integrated after the detrending procedure and was compared with the pressure altitude. The resulting time histories for a twelve minute turbulence run at an altitude of 13,100 m (43,000 ft.) is shown in Figure 16. This particular turbulence run was of interest because of the unusually large altitude excursions. The amplitudes of the excursions obtained by the two methods agree quite well. Certainly all systematic parabolic errors between the two quantities has been eliminated. Thus, the airplane vertical velocity measurements must be essentially accurate to zero frequency.

Modern digital data recording methods are very precise. Pulse code modulation (PCM) on magnetic tape yields the capabilities shown in Figure 17.

Special pilot displays as shown in Figure 18 were used in the NASA flights primarily to prevent measurements from going off scale and to assess the turbulence intensity to determine if recording should begin. The intensity meter indicates the rms acceleration at the center of gravity of the aircraft. Selections are available for time averaging. It was found that about 5 sec. averaging was the most satisfactory. The outside temperature reading was of general interest relative to the nature of turbulence encounters.

Data Acquisition and Processing

Signals from all the sensors except the inertial platform (and the piezoelectric pressure sensors, when used) are analog signals. These are input to the digital data stream subject to being subjected to matched antialiasing filters.

A schematic of flight data recording and postflight data reduction is given in Figure 19. The flight tape is converted into two tapes, one for the high frequency channels at 200 samples per sec and the other for the inertial navigation system at 40 samples per sec. A procedure is applied for wildpoint removal, the digital channels are filtered, calibrations are applied, and then all data are merged into an engineering units tape (EU) at 40 samples per second. Gust velocity time histories are then derived according to the equations given earlier at 40 samples per second. The resulting data tape (shown as SPANMAT on the figure) is then used for the various analyses. Power spectra can be provided to 20 Hz, however most data are presented from 0-10 Hz.

Assessment of System Adequacy

Flight assessments of the instrumentation adequacy and accuracy are best made in smooth air. Results of such an assessment are given in reference 9. For the vertical component, oscillatory "roller-coaster" maneuvers are made at about the same frequency as the airplane would be expected to respond in rough air. Each term in the equation shown earlier is evaluated as shown in Figure 20, and the terms added. A summation of terms resulted in the time history of vertical gust velocity shown at the bottom of the figure. Since the run was in smooth air, the summation should have zero value; the residual is the error. The residual gust velocity shown in the figure is not considered excessive in view of the rather large amplitude of the induced pitching motions. It is seen that the lower frequency component of the maneuver (as evidenced by the downward trend of the $\hat{V\theta}$ oscillations) is completely counteracted by the downward trend of $\hat{V}_{az}$ as can be seen by the absence of any low-frequency trend in w_g. It is believed that at least one-half of the residual gust velocity oscillation can be accounted for by the upwash created at the flow-vane measuring station by the flow field of the airplane. Physically, the flow field around the oscillating wing extends upstream far enough to cause the vane measuring incremental angle-of-attack, $\hat{\alpha}$, to read high. Calculations for the NASA MAT airplane under average flight conditions give an induced upwash factor of about 10 percent of the angle of attack. Close inspection of figure 20 indicates that the residual gust velocity is nearly in phase with $\hat{V\alpha}$ (w_g appears to be lagging slightly), and that a 10 percent amplitude reduction in α would reduce the gust velocity oscillation considerably. However, this simple correction will not suffice for turbulence measurements, since it is based on quasi-static flow effects about the wing. Penetration of the turbulence flow field by the airplane, the dynamics of flow buildup about the wing due to turbulence, and propagation forward to the flow vane make such an upwash correction considerably more complicated. Some justification for not attempting such a correction here was the fact that a "noise hump" at 0.5 Hz was not discernible on the power spectra. The lack of such a power peak can probably be attributed to relatively low amplitude of the short-period motions of the MAT airplane. (Generally, the amplitude of pitching motions at 0.5 Hz is not greater than about one-third that shown in the figure.)

Results from a similar procedure to evaluate the accuracy of the lateral gust velocity component are shown in Figure 21. The results of the yawing oscillation are more important than the pitch results, since yawing motions of approximately this amplitude are constantly present for this airplane in turbulence of moderate intensity. In the figure, lateral gust velocity v_g is ±1 to ±2 ft./sec. This erroneous oscillation at a frequency of about 0.25 Hz (approximately the Dutch-roll frequency of the airplane) will probably be discernible in the time history of lateral gust velocity. The size of the resulting hump in the power spectrum at 0.25 Hz can be estimated by assuming that the noise is a sine wave with peak amplitude of ±2 ft./sec. The mean square, or power spectral area contribution, would thus be

$$\sigma^2_{\text{sine wave}} = \left[\frac{\text{Amplitude}}{\sqrt{2}}\right]^2$$

When the amplitude is ±2 ft./sec., the mean square would be 2 $(\text{ft./sec})^2$. If moderate intensity turbulence is assumed to have a standard deviation σ of 10 ft./sec., the total area under the power spectrum σ^2 would be 100 $\text{ft.}^2/\text{sec}^2$. The percentage area contribution of the noise arising from the yawing oscillation would thus be only 2 percent and would probably be obscured by normal fluctuations of the power estimates. The reason for the ±1 to ±2 ft./sec. residual gust velocity obtained in the yawing maneuver can probably be attributed to a small phase difference between the $\Delta\psi$ and $\hat{\beta}$ time histories which has not been taken into account. It is noted that the overall heading change (caused by the pilot's first rudder oscillation being slightly unsymmetrical) is compensated for quite adequately by the $\hat{V}_{ax} \cos(\bar{\Psi})$ term, so that zero gust velocity is effectively maintained at this lower frequency.

It is more difficult to assess the accuracy of the longitudinal component; however some speed-change maneuvers were performed. The results of one such maneuver are shown in Figure 22. These results primarily serve to show that the special measurements and data reduction procedures for obtaining incremental true airspeed are correct. Such a maneuver is not itself representative of motions encountered in turbulence. The steep inertial speed change ($\hat{V}_{ax} \sin \bar{\Psi}$) was caused by the pilot applying an abrupt power change. Changes of this steepness do not ordinarily occur during the turbulence runs since power settings are changed only slightly, if at all. Changes of this nature in true airspeed $\hat{V}$ might occur because of wind shear or mountain wave effects, however. Possible error in the longitudinal gust component which correlates with the maneuver is not apparent; however, very small errors could be masked by the low-intensity turbulence present. Observation of the motion records in turbulence indicates that the airplane itself does not respond appreciably to air motions in the longitudinal direction until somewhat longer wavelengths are reached.

STATISTICAL RELABILITY OF THE DATA

Since turbulence is a random process, all turbulence data must be treated in a statistical manner. Each individual power estimate that goes into describing the power spectral curve can be determined with certain confidence. The statistical reliability, as shown in Table IV, depends on the statistical degrees-of-freedom appropriate for that measurement. The degrees-of-freedom, in turn, depend on the resolution bandwidth for individual spectral estimates and the length of the individual turbulence sample. In order to have power estimates to define the spectra below the knee, a resolution bandwidth of 0.02 Hz has been selected. It is considered highly desirable that 24

degrees of freedom be realized, however, it is also recognized that this is very difficult to achieve. Individual turbulence sampling runs of at least 10 minutes are needed. In many cases, it is difficult to get stationary turbulence for 10-minute duration. Many researchers believe that nonstationary samples (or those with nonuniform intensity within a data run) will cause the resultant spectra to have a "weak" or rounded (not well defined) knee. This is clarified in reference 16, however, and a method is provided for determining the effects of nonhomogenity. If it is assumed that a turbulence sample can be described by the von Karman model with a certain integral scale value L, and the time history varies in the two ways shown in Figure 23 then the limits for the ratio of L_σ (the distance over which the change takes place) to L are shown on the right for "barely detectable" and "strongly rounding" of the knee of the resulting power spectrum.

Examples of Reduced Turbulence Data

Data will be presented and discussed for four example cases and will include time histories and power spectra for each case. These data were reported in refs. 17 and 18.

The first time histories presented are for convective turbulence encountered in clear air at an altitude of 0.3 km (1000 ft) above gently rolling terrain. Because of the length of this run (19.1 minutes), the first part of the time histories is shown in the upper part of figure 24 and the final portion in the lower part of the figure. The root-mean-square values were similar for all three turbulence components, i.e., about 1.2 m/s (4 fps).

Various methods have been proposed for determination of an appropriate value for the integral scale value, L, for a given data sample. Ref. 5 provides a method that appears worthy of consideration for estimating L. It involves fitting von Karman model type autocorrelation functions for various values of L to the experimentally derived autocorrelation functions. For the cases shown here, however, comparisons are made between measured and theoretical spectra according to the von Karman model to estimate L values.

The power spectra for these time histories are shown in Figure 25. The spectra are shown such that the area under the curves is equal to the variance or σ^2 . The abscissa values were obtained by converting frequency to inverse wavelength by use of the average true airspeed for each run. Symbols are shown for the five lowest frequency power estimates. Except for the first point, the estimates are at equal increments of approximately 0.01 Hz (10 Hz/1024). The points therefore appear closer together at higher values of $1/\lambda$ on the logarithmic scale. Superimposed upon the data are the theoretical von Karman-type curves with selected L values. Note that the slopes of the curves match at the higher frequencies. It is seen that an L value 300 m (1000 ft) is appropriate for the vertical component. The lateral component, however, has relatively higher power content at low frequencies and the L value is apparently in the range of 600 m (2000 ft). The longitudinal component fits well with an L value of 1200 m (4000 ft). This difference between components, of course, means that the turbulence is not isotropic in the long wavelength region. In the shorter wavelength region where previous measurements have been made, the turbulence appears to be isotropic.

The time histories for a high-altitude wind-shear case are presented in Figure 26. It should be noted that the vertical-scale sensitivities are decreased by a factor of two with respect to the preceding case and that the intensity is really much greater. The turbulence intensity for all three components is also increasing with time. As stated earlier, such nonhomogeneous (or nonstationary) behavior has generally been believed to be responsible for considerable rounding or smoothing of the "knee" on the power spectra. As was indicated in Figure 23, however, the change in intensity must be considerably more abrupt than shown here to provide a noticeable effect in

the resulting spectra. The significant low-frequency power present in the horizontal components is believed to be directly attributable to the changing horizontal wind field.

The low-frequency content can be thought of as a modulation of the mean value. Thus, the von Karman representation may not apply over the entire frequency region. A model of turbulence which includes mean modulation with a typical high-frequency amplitude-modulated random process superimposed has been suggested in Refs. 19 and 20. No pronounced low-frequency power is noted in the vertical component time history. These observations are substantiated in the corresponding power spectra shown in Figure 27. Note that while L = 300 m (1000 ft) is appropriate for the vertical component, L values of greater than 1800 m (6000 ft) would be necessary for the horizontal components in order to include the large power content at low frequencies.

The next case is a rotor-type turbulence encounter on the lee side of the Sierra Mountains in California at an altitude approximately level with the higher ridges. The onboard observer reported direct correlation of turbulence severity with the upwind terrain. Peak center-of-gravity acceleration increments of 1g were equaled or exceeded 80 times in this traverse of the rotor region, with maximum incremental accelerations of +2.2g and -1.8g. (The turbulence intensity approached that of a small thunderstorm.) Time histories of the three components of turbulence are given in Figure 28. The segments between 4-1/2 and 7-1/2 minutes of the longitudinal component where high-frequency oscillations are absent results from the sensitive airspeed measurement system being off-scale some of the time in the negative direction. The spectra for this case are given in Figure 29. All three spectra exhibit high low-frequency power; thus, if the von Karman expression is applicable in this region, L must be greater than 1800 m (6000 ft). It should be noted that the high-frequency part of the longitudinal spectrum, as well as σ_u, could be somewhat contaminated by the loss of the high-frequency fluctuations as a result of the partial off-scale condition previously mentioned. The flattening-out of the high-frequency end of the spectrum is not associated with this problem, but is a result of the use of the high-altitude restrictor provided for the pitot-static test head. The use of two different restrictors for flight operations above and below 9.1 km (30,000 ft) to provide the proper damping for the sensitive airspeed measurement was discussed earlier. In this particular case the high-altitude restrictor was installed, since the original mission for this flight was to seek high-altitude mountain-wave turbulence.

The fourth and final case considered herein is categorized as lee wave-generated turbulence which propogated upward and was encountered at an altitude of about 14.3 km (47,000 ft). The time histories are given in Figure 30. Notice that the vertical component contains at least three waves and possibly four. Patches of turbulence occur on the rising part of the last two waves; or at approximate 7-1/2 and 10 minutes from the start of the run. Apparently, the last two waves have not broken down into continuous turbulence as yet, or the displacement of the airplane has carried it out of the turbulent region of the wave. Inspection of the lateral and longitudinal components, where a very long wave can be seen, together with supplementary meteorological information, indicates that wind-shear effects were also present. Thus, this is not a classic case of pure mountain-wave turbulence. These time histories are of considerable interest, but whether power spectra description is appropriate is debatable since the turbulence is essentially noncontinuous. Power spectra were obtained, however, for the 12.6-minute run and are shown in Figure 31. A large amount of low-frequency power is present in all three components. This case is in contrast to that for wind-shear-alone where the vertical component contained relatively little low-frequency power.

Notation

A_i Area under input power spectrum.

A_o Area under output power spectrum.

a	Speed of sound, m/sec.(ft/sec)
a_n	Normal acceleration, g units or m/sec^2.(ft/sec^2)
$a_{n_{max}}$	Maximum value of normal acceleration, g units.
c/Cc	Damping divided by critical damping.
f_n	Natural frequency.
g	Acceleration due to gravity.
h_p	Pressure-derived altitude based on standard atmosphere table.
K_g	Gust factor.
k	Slope of erroneous linear trend in time history of airplane vertical velocity, also zero error in vertical accelerometer which when integrated produces this trend, m/sec^2 (ft/sec^2).
L	Scale of turbulence, m (ft.); also, wavelength (Figure 1 only).
l	Horizontal distance between inertial-platform (or body-mounted) accelerometers and flow-direction sensors, m (ft.).
m	Lift-curve slope, per radian.
p	Free-stream static pressure, Pa (psi).
p_t	Free-stream total pressure, pa (psi).
q	Dynamic pressure, $1/2\ \rho\ V^2$.
q_c	Impact pressure, $p_t - p$, Pa (psi).
S	Wing Area
T	Total duration of run, sec.; also, air temperature, degrees Kelvin, and also airplane transfer function (Figure 1 only).
t	Time, sec.
U_{de}	Derived gust velocity, defined as $\frac{2a_{n\,max}W}{m\rho_o SV_e K_g}$
u_g	Longitudinal component of gust velocity, positive in direction of flight path, m/sec. (ft./sec.).
V	True airspeed, m/sec (ft/sec).
v_{ax}	East-west component of incremental horizontal airplane velocity obtained from inertial platform, with arbitrary zero at instant that data switch is turned on, positive toward east, m/sec (ft/sec).
v_{ay}	North-south component of incremental horizontal airplane velocity obtained from inertial platform, with arbitrary zero at instant that data switch is turned on, positive toward north, m/sec (ft/sec).

v_{az} Incremental vertical airplane vehicle obtained from computer integration of output from vertically oriented accelerometer mounted on inertial-platform stabilized element, positive up, m/sec (ft/sec).

V_e Equivalent airspeed, $V\sqrt{\rho/\rho_o}$, m/sec (ft/sec)

V_x Horizontal airplane velocity along inertial platform east-west axis, positive toward east, m/sec (ft/sec).

V_y Horizontal airplane velocity along inertial-platform north-south axis, positive toward north, m/sec (ft/sec).

v_g Lateral component of gust velocity, positive toward right wind, m/sec (ft/sec).

W Airplane weight, lb.

w_a Airplane vertical velocity, m/sec (ft/sec); $= \int_0^t (a_n - \bar{a}_n)dt$ (comparable to v_{az} obtained from inertial platform except for probable presence of trend error).

w_g Vertical component of gust velocity, positive up, m/sec (ft/sec).

α Angle-of-attack, positive with flow-vane trailing edge up, rad.

α_v Vane-indicated angle-of-attack, radians (equivalent to α in MAT instrumentation).

β Angle of sideslip, positive with flow-vane trailing edge toward right wing, rad.

Δa_z Incremental vertical acceleration obtained from inertial platform with reference to 1g level flight, positive up, m/sec^2 (ft/sec^2).

Δh_p Incremental pressure-derived altitude with reference to value at beginning of run (see definition of h_p), positive when altitude increases, m (ft).

Δp Incremental free-stream static pressure with reference to value at beginning of run, Pa (psi).

Δp_t Incremental free-stream total pressure with reference to value at beginning of run, Pa (psi).

Δq_c Incremental impact pressure with reference to value at beginning of run, Pa (psi).

ΔV $V - \bar{V}$

θ Pitch attitude, measured in vertical plane, positive with nose up, rad.

$\dot{\theta}$ Pitch rate measured by body-mounted pitch rate transducer, positive with nose going up, rad/sec.

λ	Wavelength, or distance per cycle, m (ft).
ρ	Air density
ρ_o	Air density at sea level
Φ_i	Input power spectrum.
Φ_o	Output power spectrum of arbitrary airplane response.
ϕ	Roll attitude of airplane with reference to horizontal, positive with right wing down, rad.
ψ	Airplane heading, measured in a horizontal plane clockwise from north, always positive, deg or rad.
$\Delta\psi$	Incremental sensitive airplane heading with arbitrary zero at instant that data switch is turned on, measured in horizontal plane, positive with nose right, rad.
$\dot{\psi}$	Yaw rate measured by body-mounted yaw-rate transducer, positive with nose going right, rad/sec.
Ω	Reduced frequency, equal to ω/V, rad/m (rad/ft)
ω	Frequency, rad/sec

A bar over a symbol indicates average over the entire run.
A caret over a symbol indicates that the quantity is given with respect to the mean for the entire run; that is, the mean has been subtracted.

References

1. Houbolt, J. C.; Steiner, R.; and Pratt, K. G.: Dynamic Response of Airplanes to Atmospheric Turbulence Including Flight Data on Input and Response." NASA TR R-199, 1964.

2. Rhyne, R. H. and Steiner, Roy: Turbulence and Precipitation Problems Associated with Operation of Supersonic Transports. Presented at the American Meteorological Society Fourth Conference on Applied Meteorology, Hampton, Virginia, September 10-14, 1962.

3. Crane, H. L. and Chilton, R. G.: Measurement of Atmospheric Turbulence Over A Wide Range of Wavelength for One Meteorological Condition. NACA TN 3702, 1956.

4. Murrow, H. N. and Rhyne, R. H.: The MAT Project--Atmospheric Turbulence Measurements with Emphasis on Long Wavelengths. Proceedings of the Sixth Conference on Aerospace and Aeronautical Meteorology, (AIAA/AMS), pp. 313-316, November 1974.

5. Sleeper, Robert K: Spanwise Measurements of the Vertical Components of Atmospheric Turbulence. NASA TP 2963, 1990.

6. Houbolt, John C. and Sen, Assim: Cross-Spectral Functions Based on von Karman's Spectral Equations. NASA CR-2011, 1972.

7. Ganzer, Victor M.; Joppa, Robert G.; vander Wees, Gerrit: Analysis of Low Altitude Atmospheric Turbulence Data Measured in Flight. NASA CR-2886, 1977.

8. Foster, G. W.: Examples of Low Altitude Atmospheric Turbulence Measurements by Gnat XP505. Royal Aircraft Establishment TR 83026, 1983.

9. Rhyne, R. H.: Flight Assessment of an Atmospheric Turbulence Measurement System with Emphasis on Long Wavelengths. NASA TN D-8315, 1976.

10. Meissner, C. W, Jr.: A Flight Instrumentation System for Acquisition of Atmospheric Turbulence Data. NASA TN D-8314, 1976.

11. Rentz, E.: Evaluation and Utilization of Airplane Flight Loads Data. AFFDL-TR-68-52 (Part II), 1968.

12. Brown, E. N.; Friehe, C. A.; and Lenschow, D. H.: The Use of Pressure Fluctuations on the Nose of an Aircraft for Measuring Air Motion. AMS Journal of Climate and Applied Meteorology, Vol. 22, No. 1, January 1983, pp. 171-180.

13. Foster, G. W. and Poulter, R. L.: Gnat XP 505 Atmospheric Research Aircraft - Instrumentation and Data Processing. RAE TM FS(B)480, 1982.

14. Foster, G. W. and Jones, J. G.: Measurement and Analysis of Low Altitude Atmospheric Turbulence Obtained Using a Specially Instrumented Gnat Aircraft. AGARD SMP Workshop, Athens, Greece, September 1986.

15. Keisler, S. R. and Rhyne, R. H.: An Assessment of Prewhitening in Estimating Power Spectra of Atmospheric Turbulence at Long Wavelengths. NASA TN D-8288, 1976.

16. Mark, William D. and Fischer, Raymond W : Investigation of the Effects of Non-Homogeneous (or Nonstationary) Behavior on the Spectra of Atmospheric Turbulence. NASA CR-2745, 1976.

17. Rhyne, R. H.; Murrow, H. N.; and Sidwell, K. W.: Atmospheric Turbulence Power Spectral Measurements to Long Wavelengths for Several Meteorological Conditions. Proceedings of the NASA Safety and Operating Problems Conference, NASA Langley Research Center, Hampton, Virginia, October 18-20, 1976, pp. 271-287, NASA SP-416, 1976.

18. Murrow, Harold N.; McCain William E.; and Rhyne, Richard H.: Power Spectral Measurements of Clear-Air Turbulence to Long Wavelengths for Altitudes Up to 14000 meters. NASA TP-1979, 1982.

19. Reeves, Paul M.; Joppa, Robert G.; and Ganzer, Victor M.: A Non-Gaussian Model of Continuous Atmospheric Turbulence for Use in Aircraft Design. NASA CR-2639, January 1976.

20. Sidwell, Kenneth: A Mathematical Study of a Random Process Proposed as an Atmospheric Turbulence Model. NASA CR-145200, 1977.

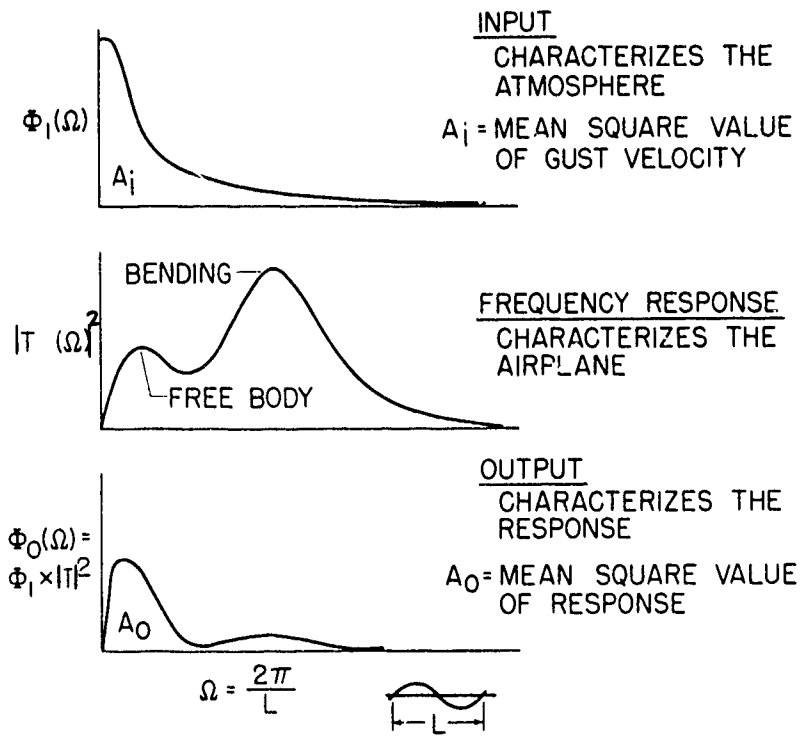

Figure 1 Input-Output Relation for Power Spectral Analysis

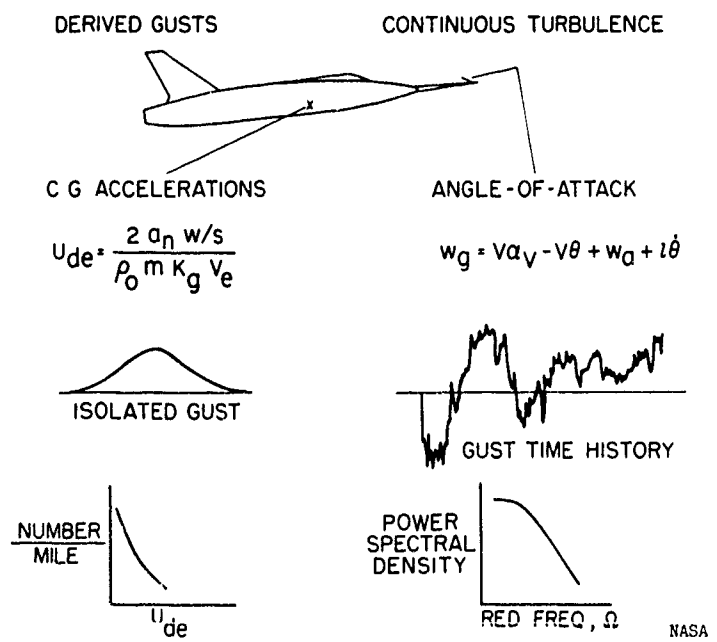

Figure 2. Methods of Measuring and Describing Atmospheric Turbulence

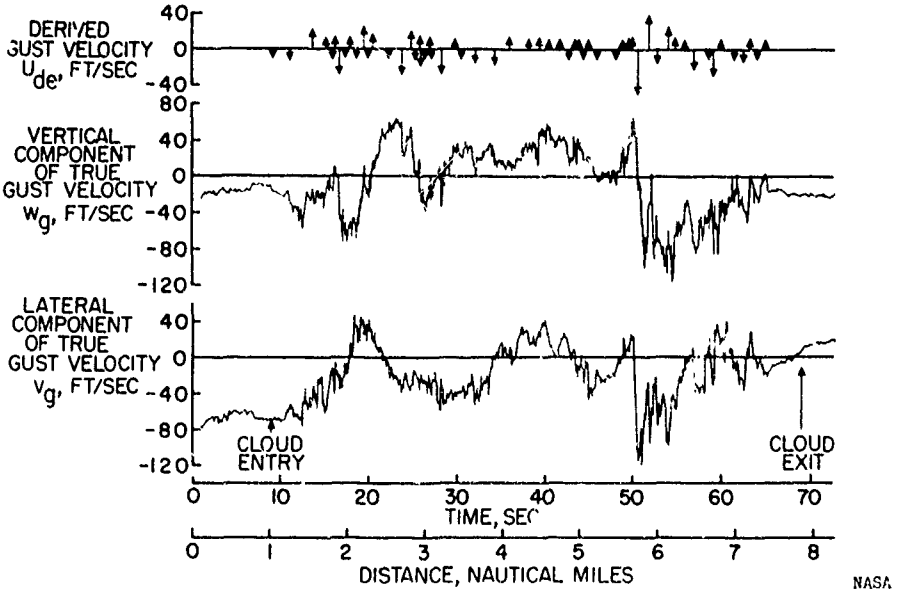

Figure 3 Comparison of Derived Gust Velocity Values with Vertical and Lateral Components of True Gust Velocity

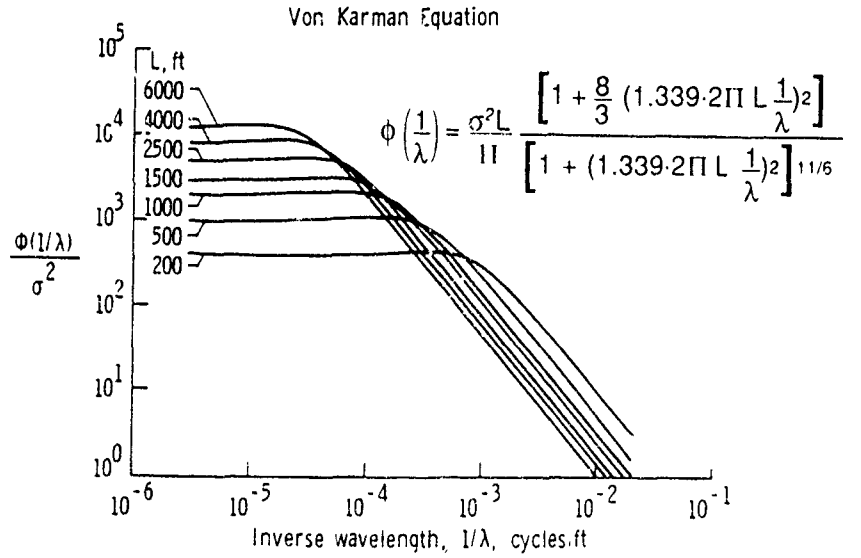

Figure 4. Theoretical Power Spectra for Various Values of L

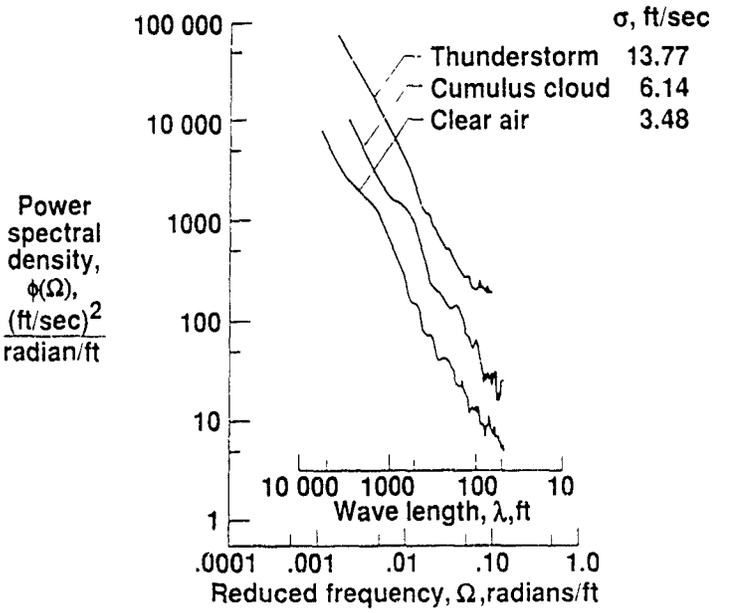

Figure 5 Measured Power Spectra for Three Weather Conditions

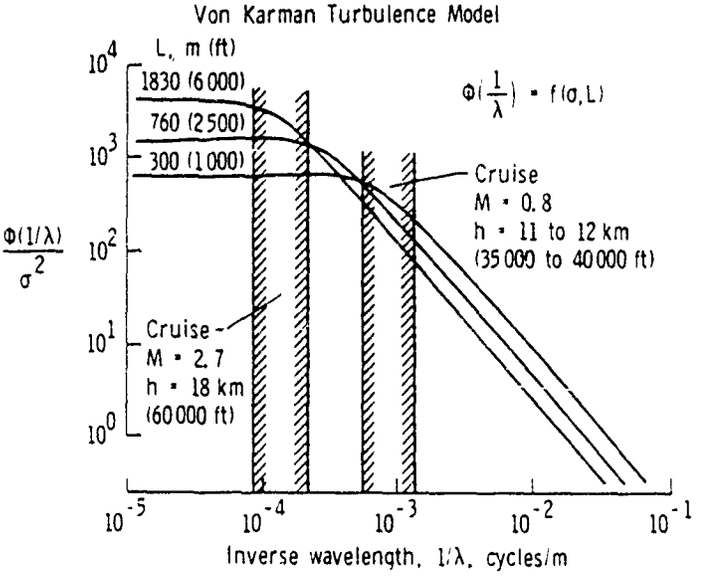

Figure 6 Regions of Primary Aircraft Response to Atmospheric Turbulence

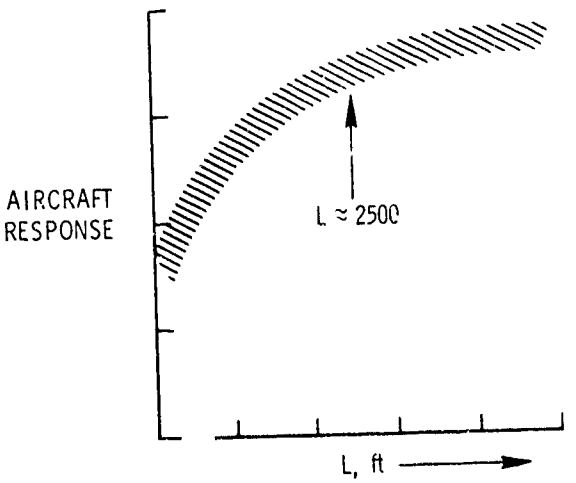

Figure 7 Significance of L for Supersonic Transport

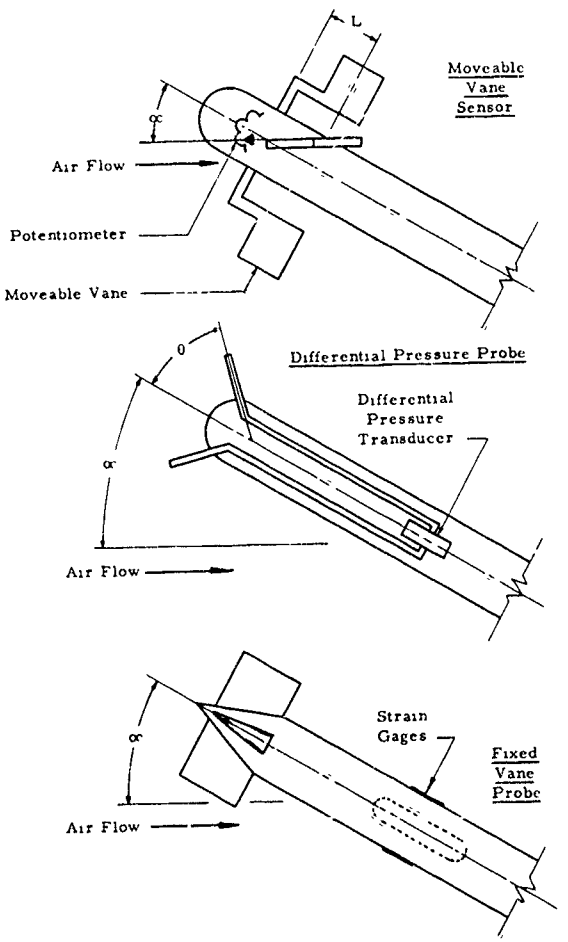

Figure 8 Three Sensors for Determining Angle-of-Attack

Figure 9 Nose Boom and Balsa Vanes Mounted on a Sampling Airplane

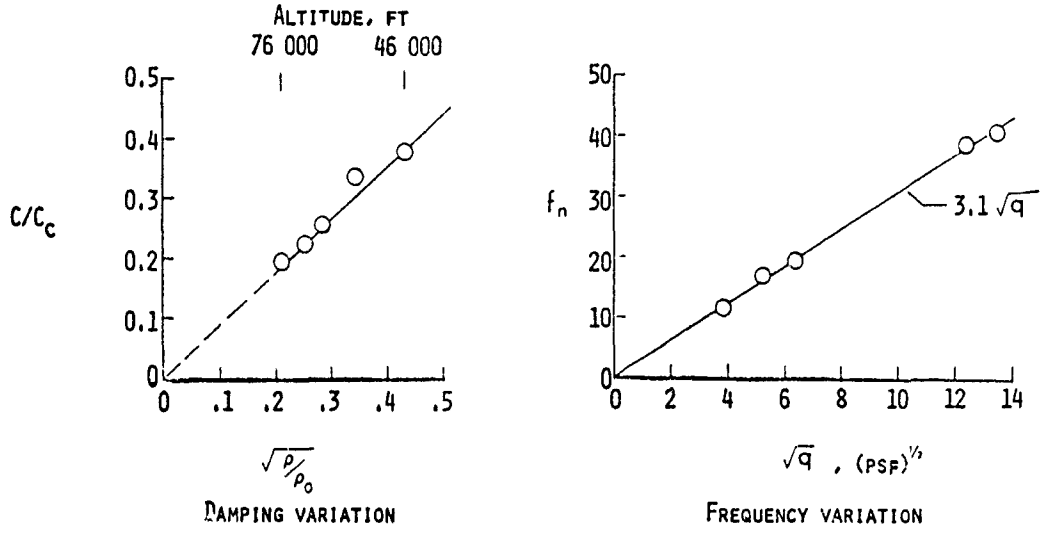

Figure 10. Frequency and Damping Characteristics of Balsa Vanes (From Wing Tunnel Tests)

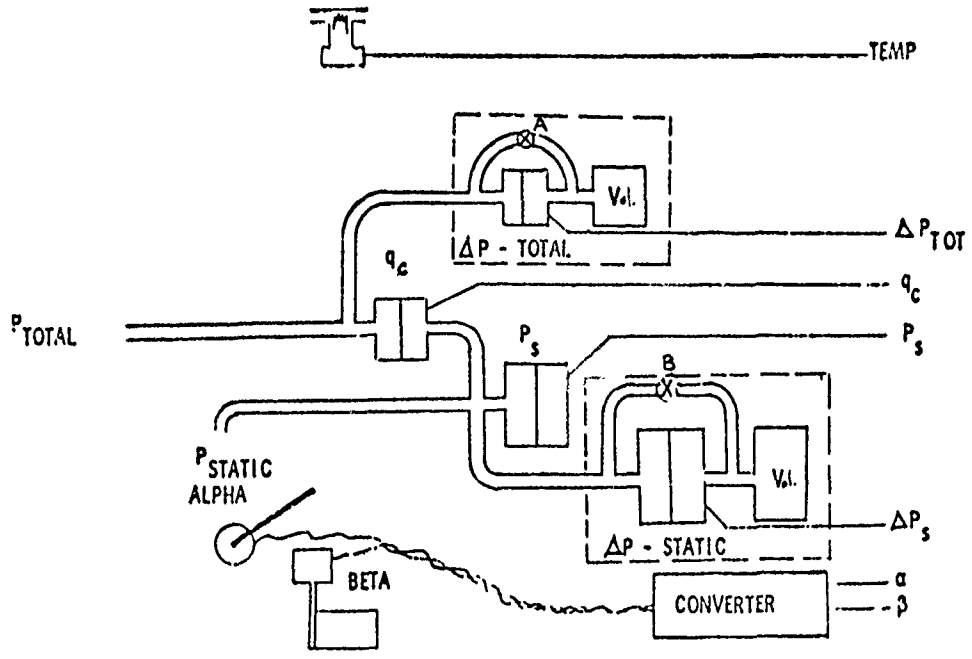

Figure 11. Airflow Measurements Including Diagram of Statoscope Device

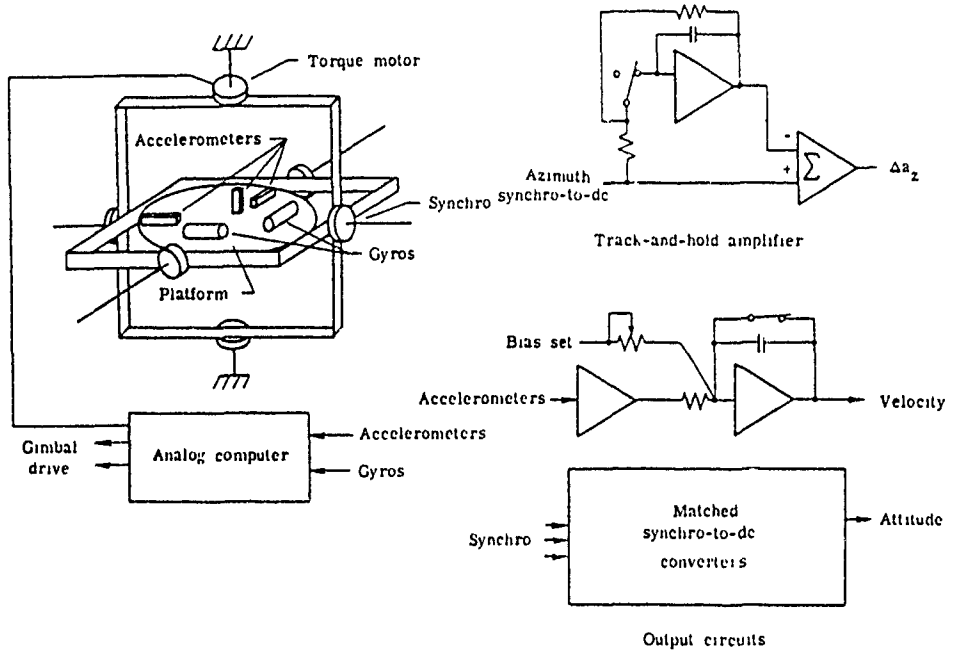

Figure 12. Setup for Inertial Platform Sensors

MAXIMUM EFFECT ON A 10 MINUTE TURBULENCE TIME HISTORY CAN BE APPROXIMATED BY A LINEAR TREND:

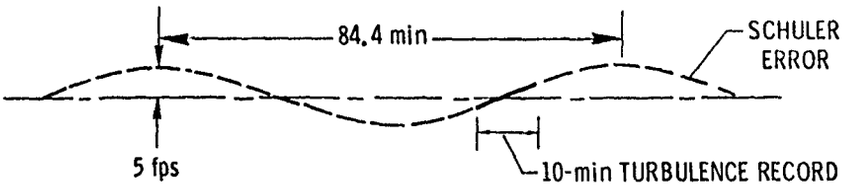

Figure 13 Typical Schuler Oscillation

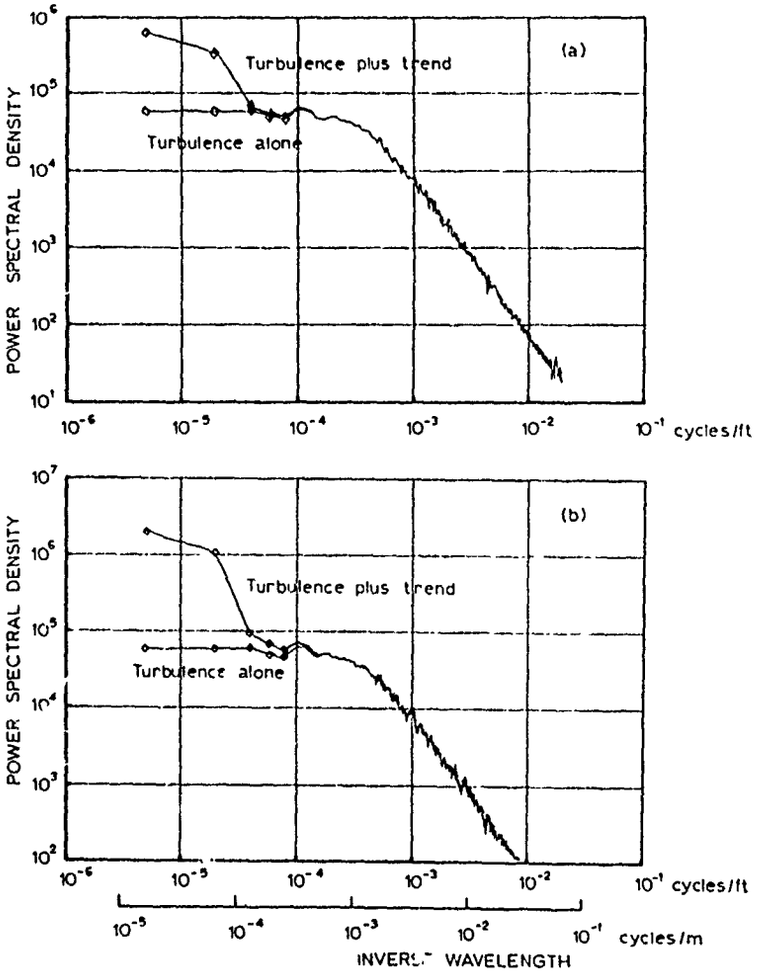

Figure 14. Effects of Linear Trend on Power Spectrum
(a) $\sigma_{trend}/\sigma_{turb} = 0.5$ and (b) $\sigma_{trend}/\sigma_{turb} = 1.0$

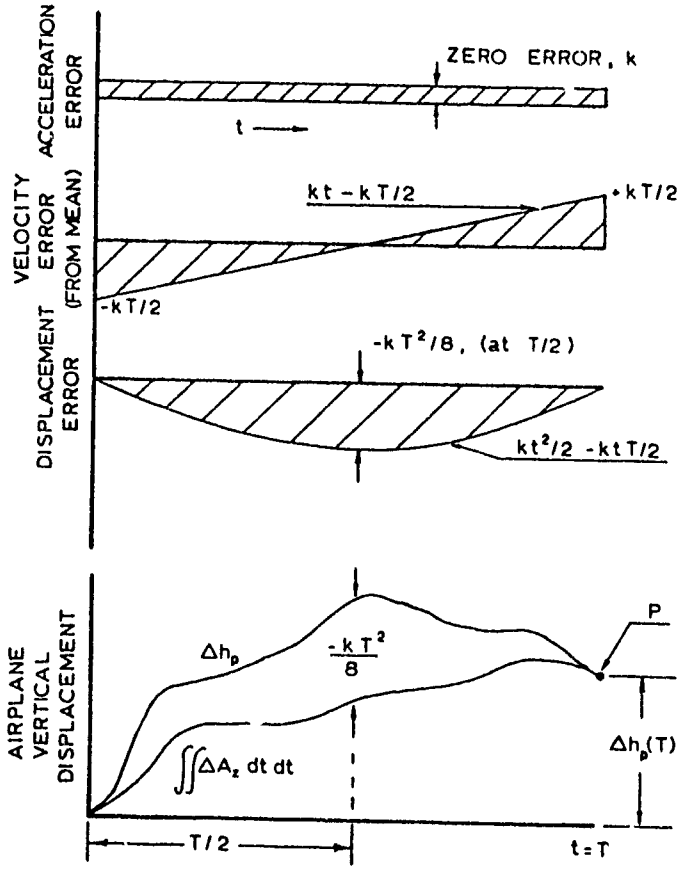

Figure 15. Description of Methods for Establishing Accelerometer Zero

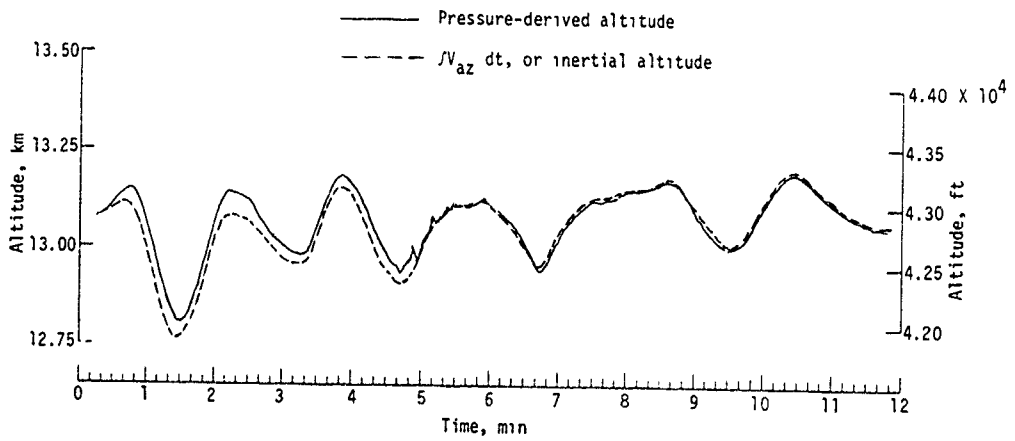

Figure 16. Comparison of Altitude Time Histories

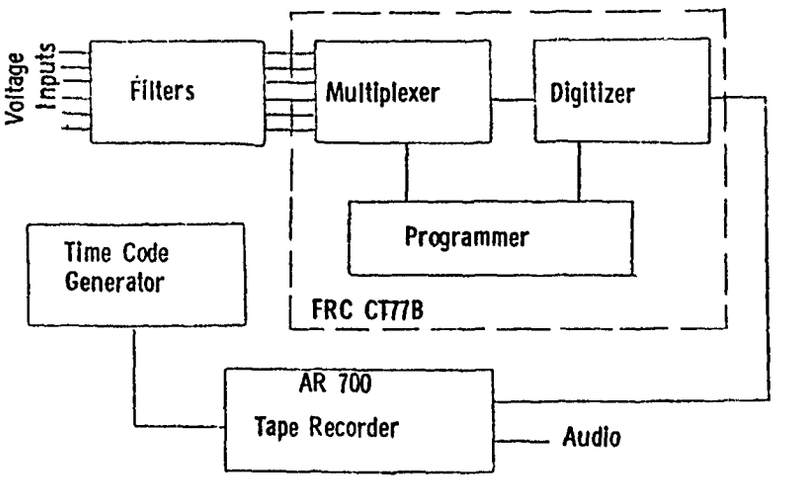

Figure 17 Data System Capability. (80 channels, 200 samples per sec , 10 bits per sample, 10-volt input range, 10 mv resolution, aliased voltages attenuated 60 db for 10-20 Hz, 1 5 hr. record time)

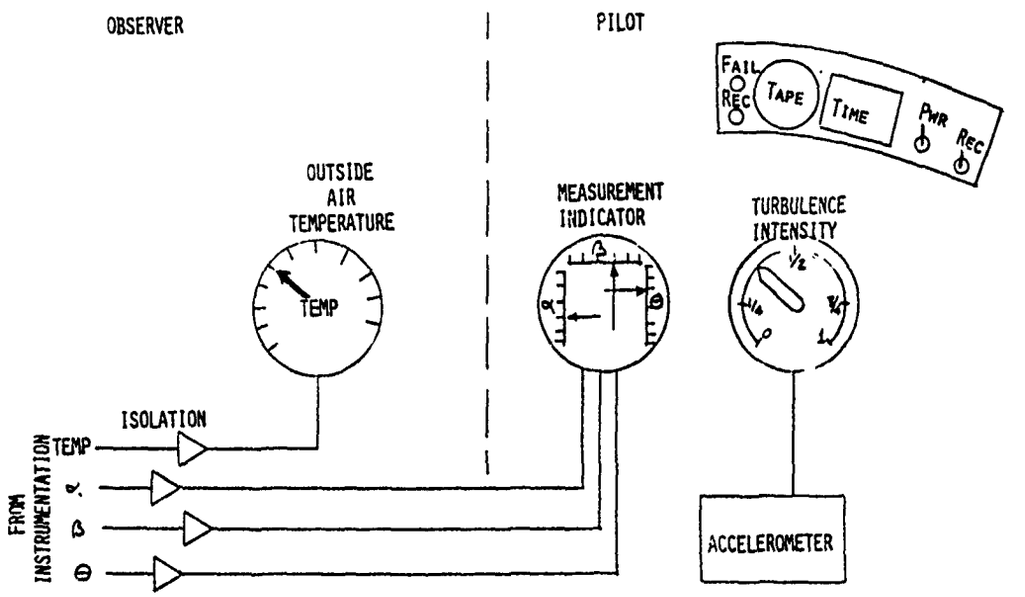

Figure 18 Cockpit Displays (Pilot Aids)

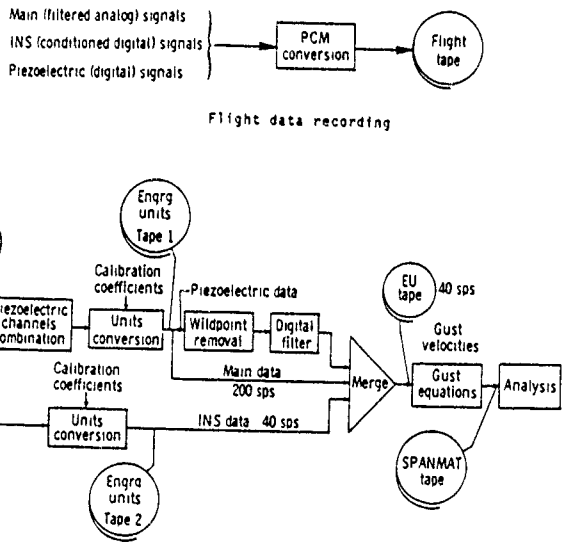

Figure 19 Flight Data Recording and Post-Flight Data Reduction Schematic

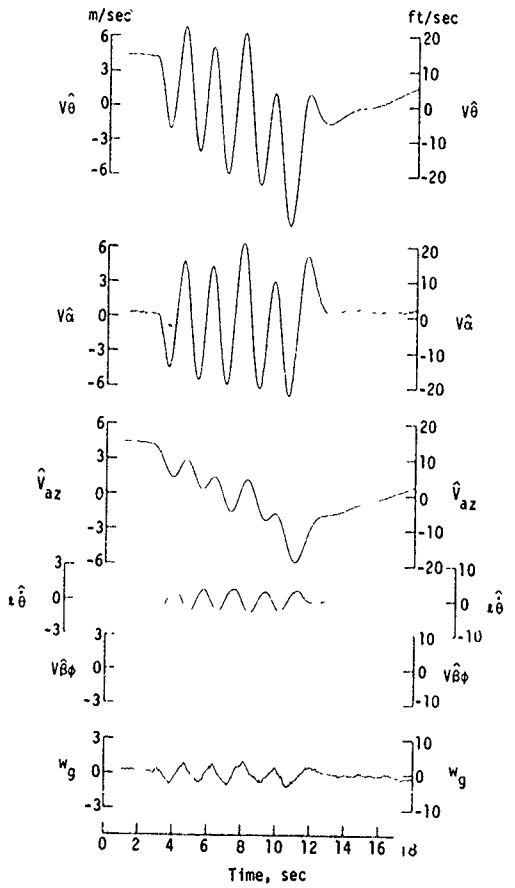

Figure 20. Results of Pitching Oscillation in Smooth Air

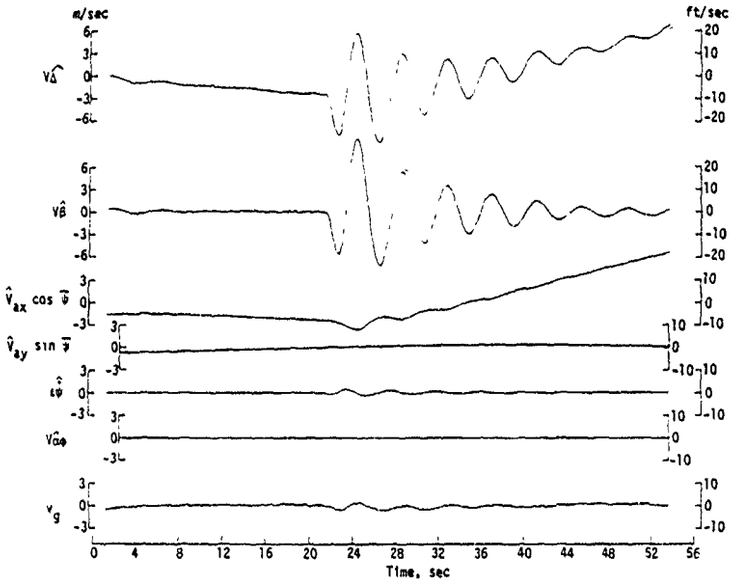

Figure 21. Results of Yawing Oscillation in Smooth Air

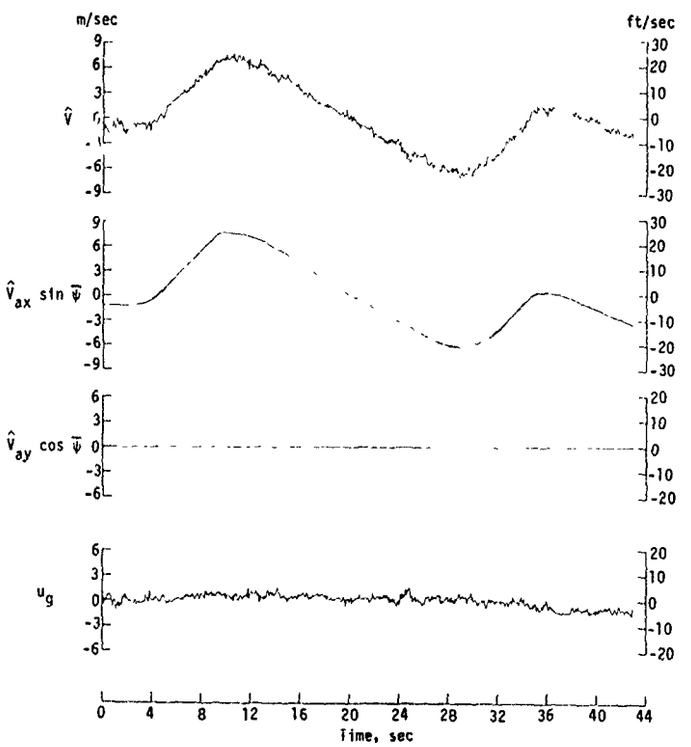

Figure 22. Results of Speed Change Maneuver in Slight Turbulence

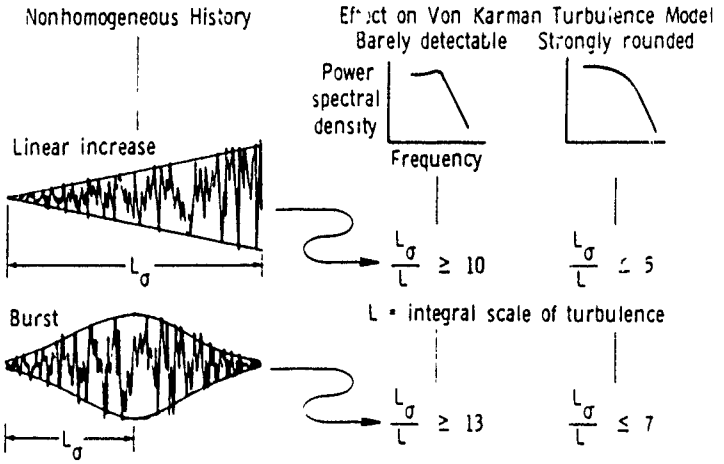

Figure 23. Significance of Nonhomogenuity on Measured Power Spectra

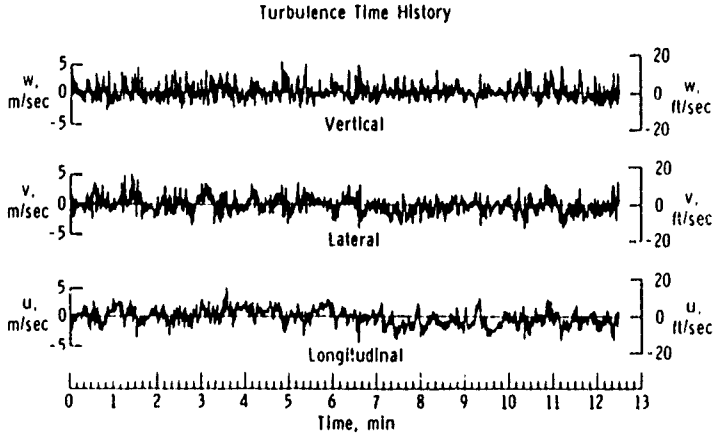

Figure 24 Turbulence Component Time Histories for Convective Case

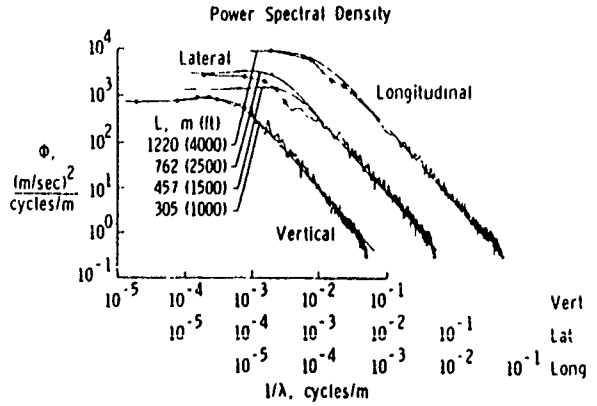

Figure 25 Power Spectra for Convective Case

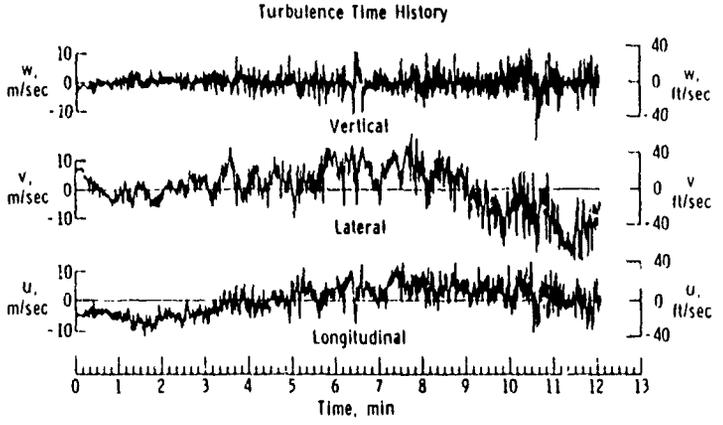

Figure 26 Turbulence Component Time Histories for A High-Altitude Wing-Shear Case

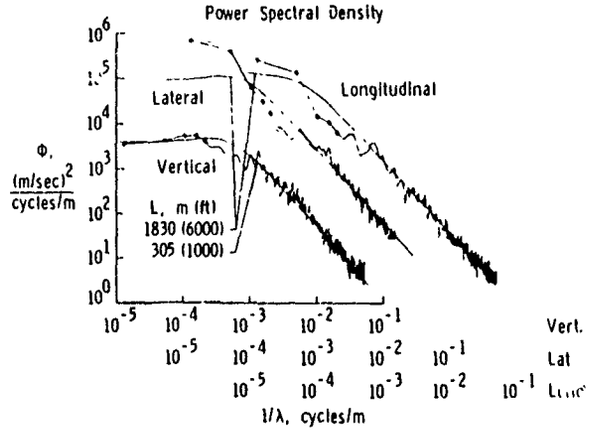

Figure 27. Power Spectra for the High-Altitude Wing-Shear Cas

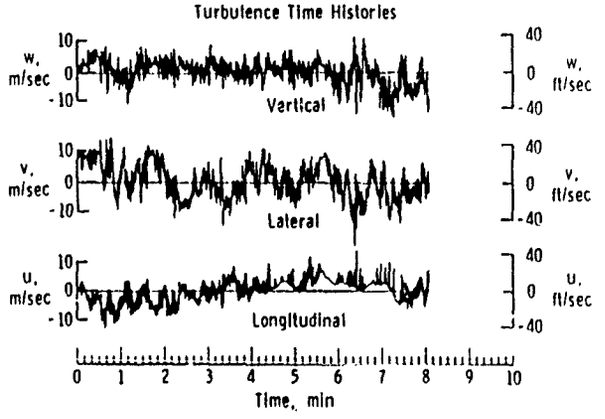

Figure 28. Turbulence Component Time Histones for the Rotor Case

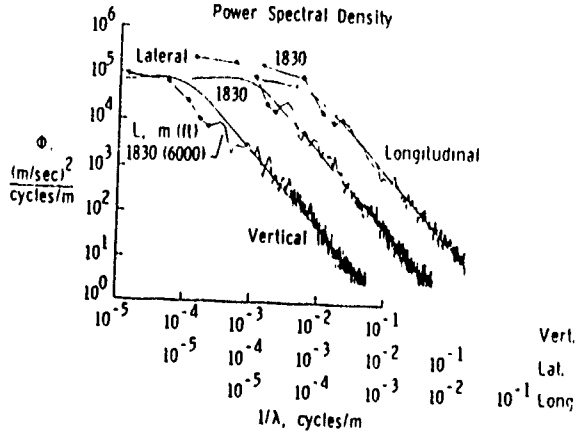

Figure 29 Power Spectra for the Rotor Case

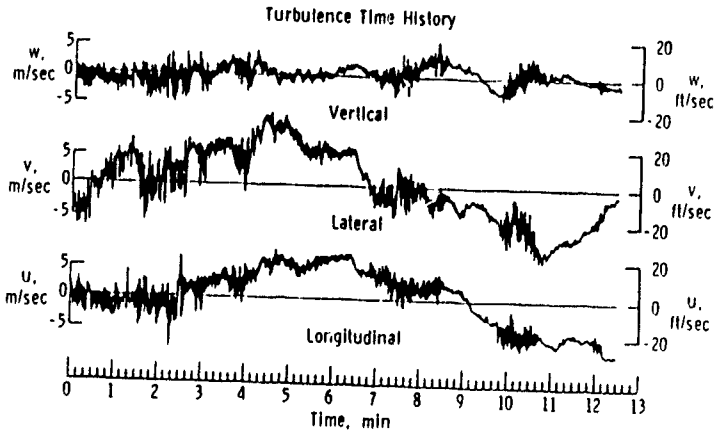

Figure 30. Turbulence Component Time Histones for the Mountain-Wave Case

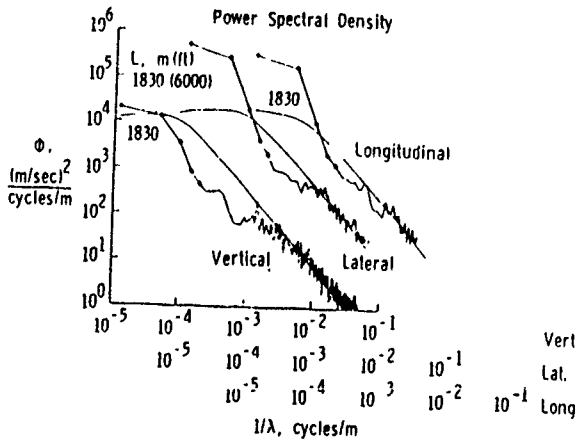

Figure 31. Power Spectra for the Mountain-Wave Case

Table I. Measurements List

Measurement	Range	Overall System Allowable Error (1σ)	Measured System Error at 25°C	±1 dB Upper Band Edge, Hz	Measured ±1 dB Upper Band Edge
α, Balsa Angle-of-Attack Flow Vane	±7.5°	0.09° Relative	0.03 (0.1)	10.0	6.00
β, Balsa Angle-of-Sideslip Flow Vane	±7.5°	0.09° Relative	0.03 (0.1)	10.0	6.00
$\dot{\phi}$, Pitch Rate	±1 r/sec	0.012 r/sec	0.01	5.0	> 10.00
$\dot{\psi}$, Yaw Rate	±1 r/sec	0.006 r/sec	0.005	5.0	> 10.00
$\dot{\phi}$, Roll Rate	±1 r/sec	0.012 r/sec	0.008	5.0	> 10.00
T, Free Air Temp. (Total Temp.)	±50°C	0.555°C	0.3°C	0.5	0.05
q_c, Impact Pressure	0-5 psid	0.03 psi	0.013	N/A	
p_s, Static Pressure	0-15 psia	0.1 psi	0.04	N/A	
Δp_s, Incremental Static Pressure	±0.25 psid ±0.1 psid	0.003 psi	0.0007 0.0003	N/A	
ΔP_T, Incremental Total Pressure	±0.25 psid ±0.1 psid	0.003 psi	0.0007 0.0003	10.0 10.0	5.00 3.00
A_n, C.G. Acceleration	±1 G	0.02 G	0.008	10.0	> 10.00
Time	0 - 365 days	0.001 sec		N/A	

Table II. Phase Matching Requirements

Measurement	Full-Scale Range	Allowable Phase Error, Degrees	Measured Relative Phase at 1 Hz, Degrees
θ	±7.5°	±1.50	- 0.75
$\Delta\psi$	±7.5°	±1.50	- 0.75
α and β	±7.5°	±1.70	< 0.25
ϕ	±20°	±0.92	- 0.75
$\dot{\theta}$, $\dot{\phi}$	±1 rad/sec	±1.40	- 1.50
$\dot{\psi}$	±0.5 rad/sec	±1.40	- 1.50
A_x, A_y	±1 G	±0.70	- 1.25
A_z	±3 G	±0.70	- 1.25
V_{ax}, V_{ay}, V_{az}	±50 ft/sec	±1.40	- 1.25
A_n	±1 G	±1.70	- 1.10
ψ	0 - 360°	±1.50	- 0.75
ΔP_{Total} HI	±0.25	±1.70	
ΔP_{Total} LO	±0.10	±1.70	

Table III. Measurements List-Airborne Inertial Data System (AIDS)

Measurement	Range	Overall System Allowable Error (1σ)	Measured System Error at 25°C	±1 dB Upper Band Edge, Hz	Measured ± dB Upper Band Edge, Hz
A_x, Accl Along x Axis	1 G to -1 G	.006 G	.005	5	>10
A_y, Accl. Along y Axis	1 G to -1 G	.006 G	.005	5	>10
A_z, Accl. Along z Axis	3 G to -3 G	.018 G	.013	5	>10
V_{ax}, Change in Vel. Along x Axis During Rec. Period	±100 fps	0.6 fps	0.4	5	>10
V_{ay}, Change in A/C Vel. Along y Axis During Rec. Period	±100 fps	0.6 fps	0.4	5	>10
V_{az}, Change in A/C Vel. Along z Axis During Rec. Period	±100 fps	0.6 fps	0.4	5	>10
ϕ, Roll Attitude of A/C	20 to 5° 5 to -5° -5 to -20°	0.16° 0.12° 0.16°	0.08 0.04 0.08	5	>10
θ, Pitch Attitude of A/C	7.5 to 4° 4 to -4° -4 to -7.5°	0.1° 0.08° 0.1°	0.03 0.03 0.03	5	>10
$\Delta\psi$, Relative Change in Azimuth Angle of A/C	±7.5°	0.08°	0.09°	5	>10
V_x, Total Vel. Along x Axis	2000 fps* 1000 fps	15 fps	6 fps	5 5	-- --
V_y, Total Vel. Along y Axis	2000 fps* 1000 fps	15 fps	6 fps	5 5	-- --
ψ, Azimuth	0 - 360°	0.5°	0.7°	5	>10

*Scale change.

Table IV. Statistical Reliability (Random Error of Individual Power Estimate)

Percent Confidence Band	Statistical Degrees of Freedom (2 B_e T)*	True spectral value lies between (a) and (b) of measured value.	
		(a)	(b)
95	24	0.61	1.94
	30	0.64	1.78
80	24	0.72	1.53
	30	0.74	1.45

* For B_e = 0.02 Hz; 24 degrees-of-freedom requires T = 600 sec.

CHAPTER II
ACQUISITION OF STATISTICAL GUST LOAD DATA BY COMMERCIAL AIRPLANES

by

J.B.de Jonge
National Aerospace Laboratory – NLR
P.O. Box 153
8300 AD Emmeloord
The Netherlands

CONTENTS

1. INTRODUCTION

As described in the previous chapter, knowledge about the nature and properties of atmospheric turbulence has been and is being obtained from measurements with specially instrumented "research"-aircraft.

On the other hand, our statistical information on the frequency of occurrance and intensity of gusts is largely based on relatively simple measurements, using simple recording devices, obtained over a period of more than half a century in commercial airplanes during normal operation.

These measurements are of an indirect nature, that means not the gust velocity itself but the aircraft response due to the gust is measured. Universally, the c.g vertical acceleration has been taken as response quantity to be measured.

This choice is quite understandable: in the first place the incremental vertical acceleration is (for a given aircraft weight) directly proportional to the incremental lift force due to the gust and thus an obvious measure of gust strength; in the second place the c.g acceleration is easy to measure with simple and reliable instrumentation.

In this chapter, a brief review will be presented of "historical" acceleration recording programmes carried out by NACA (and its successor NASA) and the RAE. Next, more recent recording programmes making use of acceleration data recorded with so-called ACMS (Aircraft Condition Monitoring Systems) will be discussed.

The methods used to reduce the acceleration data to "gust velocities" will be briefly described with specific reference to the differences in the various programmes.

In a summarizing discussion the possibility and desirability to extend the gust data base using "routine" ACMS recorded c.g acceleration data will come forward. To compare data from different sources it is essential that agreement on data reduction procedures be reached.

It will be argued that for this, a reduction method based on a continuous gust concept and an aircraft response including pitch appears the most appropriate.

2. VG RECORDS AND VGH RECORDS

For over 30 years, the NASA and its predecessor, the NACA, have collected data on the normal accelerations experienced by commercial transport airplanes. This research has been conducted with the cooperation of airplane manufacturers and airlines who have borne the cost of installing and transporting the instrumentation.

Starting in 1930, until 1950 measurements were made with the so-called VG recorder, (Ref. 1) a very simple device continuously recording the instantaneous acceleration vs indicated airspeed. An illustrative VG record is shown in figure 1. Essentially it provides an envelope of the maximum accelerations experienced over the airspeed range during the period (usually appr. 200 flight hours) covered by the record.

By its nature, the VG recorder is only suited to provide information about the maximum or extreme loads occurring; as illustrated in figure 2 the max. positive and negative acceleration recorded were usually the only recorded data evaluated. It should be borne in mind that in the thirties and early fourties, when fatigue was not a design consideration, statistical knowledge on extreme loads, as a basis for static design loads definition, was the prime information of interest. The VG recorder does not provide information on the flight altitude nor the time and hence the weight at which an acceleration peak occurred: these shortcomings were overcome in the so called VGH recorder. This device which was introduced in the early fifties is considerably more complicated than the VG recorder (Ref. 2).

It records simultaneously airspeed ("V"), c.g acceleration ("G") and altitude ("H") as a function of time.

Figure 3 shows a typical VGH record. Table 1 reviews the scope and size of the VGH and VG data samples obtained by NACA/NASA.

In the analysis of VGH data only gust-induced accelerations were considered, that means manoeuvre load occurrences (characterized by a longer duration) were eliminated.

Next, the acceleration peaks to be evaluated were selected using a criterion usually indicated as "Peak-between Means" criterion. The criterion is illustrated in figure 4. Between two successive crossings of the $n_z = 1$ level (or rather a narrow "threshold zone" around $n_z = 1$) only the acceleration peak value associated with the largest incremental acceleration is considered. This acceleration value is read off from the VGH-record together with the speed V and altitude H at the time of occurrance. Next, these

acceleration peak values Δn_z were reduced to "derived gust velocities" U_{de} using the well-known "Pratt formula".

$$U_{de} = \frac{\Delta n_z \; 2W/S}{\rho_o \; V_e \; C_{L_\alpha} \; . \; F(\mu g)} \qquad (1)$$

where: g = gravity constant
C_{L_α} = lift curve slope
ρ_o = air density at sea level
V_e = equivalent air speed
W = aircraft weight
S = wing area
ρ = true air density
$\bar{c}$ = wing mean chord
μg = "mass parameter" =

$$\frac{\rho g \bar{c} \; C_{L_\alpha}}{2W/S}.$$

The gust factor $F(\mu g)$ is given by the following expression:

$$F(\mu g) = \frac{.88 \; \mu g}{5.3 + \mu g}. \qquad (2)$$

The above expression is a close approximation of the result of a response calculation based on the following assumptions (see Ref. 4).

a With regard to the gust:
- The gust has a "1-cos" shape and a gust length equal to 25 chords.

b With regard to the aircraft response:
- The aircraft is infinitely stiff.
- The aircraft responds only in plunge but not in pitch.
- Aerodynamic inertia (both Küssner and Wagner effects) are includ

It may be noted that the instantaneous weight of the aircraft at the occurrance of the gust could only be estimated on the basis of average take-off weights and fuel consumption rates.

In principle the acceleration peaks obtained from VG records (see Fig. 2) were reduced in the same way, using estimated values of altitude and weight.

Results of analyses of VGH data and VG data have been presented in various reports (see e.g. Ref. 3). Figure 5, reproduced from reference 5, gives on overall summary result.

The following observations may be made:

- The gust intensity is strongly dependent on altitude and decreases with increasing altitude.
- The exceedance curve for each altitude is approximately the sum of two straight lines in a semi-logarithmic grid: these straight lines represent the exceedance curves for a "storm-turbulence"-component and a "non-storm" turbulence component respectively. The mathematical expression for the exceedance curve has the form

$$G(U_{de}) = G_1(0)e^{-U_{de}/a_1} + G_2(0)e^{-U_{de}/a_2}. \qquad (3)$$

The parameters $G_1(0)$, $G_2(0)$ and a_1 and a_2 are a function of altitude.

3. FATIGUE METER DATA

During more than twenty years, the Royal Aircraft Establishment RAE have collected c.g vertical acceleration data by means of so-called "fatigue-meters". The programme included 17 different types of aircraft and covered 30000 flight hours on 15000000 kms of flight (Ref. 7).

The fatigue meter, also indicated as "counting accelerometer", is a device which counts the number of exceedings of specific acceleration levels.

In order to avoid spurious countings due to small acceleration variations the counting of a level crossing is only completed after a second criterion has been met: exceeding of a specific level is counted after the signal has dropped below another "reset" level which is closer to the one-g level. This counting criterion which is usually indicated as "restricted level cross counting" is illustrated in figure 6. At intervals of a few minutes the counters were photographed together with an altimeter, airspeed indicator and clock.

It should be noted that no distinction between manoeuvre-induced accelerations and accelerations due to gust can be made. Hence, fatiguemeter data do include manoeuvre loads. The recorded acceleration data were reduced to "derived gust velocities" using equation (1), but two different expressions for the gust factor F were used based on a discrete gust approach and a continuous gust approach respectively.

i Discrete gust approach:
A gust factor $F(\mu_g, c)$ according to Zbozek (Ref. 6) is used, following from a response calculation based on the following assumptions:

a A "ramp type" gust with a fixed gradient distance of 100 ft. for a straight winged aircraft and (100 + ½b tan Λ) for an aircraft with span b and sweepback Λ.

b Like for the VGH-data reduction, the aircraft is assumed to be infinitely stiff and to respond in plunge only. Aerodynamic inertia is included.

ii Continuous gust approach:
Response calculations were made to continuous turbulence with a "von Karman" power spectral density. The scale of turbulence was taken equal to the altitude below 1000 ft and above that altitude increasing in proportion to the inverse density ratio (Ref. 7).

The aircraft was again assumed to be infinitely stiff and to respond in plunge only. Aerodynamic inertia and the effects of finite span and sweep back were included.

Results obtained for various aircraft types, in terms of "discrete gust velocity" occurrances, have been published in numerous RAE-reports (or ARC CP's). Reference 7 presents a summary of all results, including the presentation in terms of "PSD"-gust velocities.

Reference 8 presents a analysis of the obtained results in terms of "discrete" gusts.

Like for the VGH-data it has been found that the gust exceedance curve can be fitted with good accuracy by the sum of two straight lines in a semi logarithmic grid.

4. ACMS-RECORDED LOAD DATA

The gust load data described in the previous sub-chapter were obtained with simple recording devices during normal commercial flights of transport aircraft. Yet, the necessary equipment was specifically installed for these measurements and obviously the reading out of e.g the VGH traces or fatiguemeter-"pictures" and the processing of these data in a pre-computer age must have made these data acquisition programmes time consuming and costly.

Today much better opportunities for easy gust data acquisition exist.
Currently, all transport aircraft have recorders for the primary flight parameters.

Many, specifically the larger ones, are equipped with so-called Aircraft Condition Monitoring Systems (ACMS), formerly indicated as AIDS (Aircraft Integrated Data Systems).

These systems record a very large number of parameters (often several hundreds), including such quantities as e.g acceleration, speed, altitude, flap positions, instantaneous a.c weight etc. The ACMS-data are usually put on magnetic tape and these tapes are taken from the aircraft at regular intervals and transferred to the airline's computer facility. Here the data are scanned and processed using several application programs, usually as an aid for Aircraft Maintenance.

These ACMS recordings can easily be used to gather statistical gust load data in large quantities and at remarkably low cost!

For example, between 1974 and 1988 the National Aerospace Laboratory NLR has gathered ACMS-recorded service load data in 747 aircraft operated by KLM, SAS and Swissair (Ref. 9).

For each recorded flight, stored data include detailed mission profile information, thus values of successive peaks and troughs in the c.g acceleration trace. Time, flap position and bank angle at peak/trough occurrance are also noted.

These data were analyzed in the same way as the VGH recordings. (Peak selection according to "peak between means", reduction to U_{de} according to Pratt-formula).

In addition the acceleration peaks were reduced to U_{σ}-values using a PSD approach comparable to the one applied to the fatigue meter data, as described in reference 7.

The procedures applied and results obtained have been fully described and discussed in reference 10. Table 2 gives a summary of the U_{de}-distributions obtained.

It may be noted that the flight time covered in this programme, being about 100000 hours is more than two times the total time covered by VGH data, see table 1!

A Data Bank currently being set up by ONERA (Ref. 11) is even more impressive with respect to size.

Since 1980 data have been collected, in cooperation with CAA, about load factor occurrances with incremental values exceeding $|\Delta n_z| = 0.5$, as recorded with ACMS systems in aircraft of Britisch Airways. Since 1986, comparable data provided by Air France are also included.

This Data Base, including data obtained from 7 different aircraft types (ranging from BAC 1-11 to Concorde) covered already 370168 flight hours in May 1988 (Ref. 12)!

The ONERA Data Base contains information about the more "extreme" loading conditions and might be considered as a greatly improved version of the VG data: it may be noted that the current figure of 370000 hours approaches the figure of 500000 hours for the VG data (see Tab. 1) while the associated mileage is undoubtedly already larger.

5. DISCUSSION

In the previous subchapters "historical" gust data banks were reviewed and some examples recent gust data acquisition programmes using ACMS data were described.

It may be stated that, compared to the curren design lifetimes in the order of 90000 hours, the VGH-data bank and the fatigue meter data bank are actually pretty small. Even the VG data bank, main source of extreme value data is relatively small considering that limit load conditions are expected to occurr less than once in a lifetime.

At the same time comparison of the VGH program and fatigue meter data revealed another main problem: in all successive steps of the data acquisition such as elimation or inclusion of manoeuvre loads, peak/trough selection and reduction of accelerations to gust velocities the two programmes, showed small but essential differences, thus hampering a real "pooling" of the data sets.

On the other hand, thousands of aircraft are flying aroupd every day, permanently recording gust loads. These data are just eagerly waiting to be processed, so to speak!

Presently it has become possible to set up in international cooperation a vast gust data base from ACMS recordings in a short time and at relatively little cost.

It is essential then, however, that agreement be reached about the methods of data reduction. It should be stressed that processing all data in the same way is much more important than applying the "best" or most accurate reduction technique!

In the following, we will briefly discuss the elements on which agreement has to be reached.

a Inclusion or elimination of manoeuvre loads

It may be recalled that counting accelerometer data and also the 747 ACMS data processed by NLR included manoeuvre induced accelerations; these are reduced to "apparent gusts". As manoeuvres have predominantly a positive sign, these "apparent gusts" are largely upward, causing "asymmetry" in the derived gust spectra.
Probably, the observed larger number of "up-gusts" compared to "down gusts" (see e.g. Fig. 7) is largely due to this inclusion of manoeuvre induced accelerations.

In the processing of the VGH data, manoeuvre loads were visually distinguished from turbulence patches and eliminated. One may have doubts about the success of such a procedure in those cases were gust loads (having a short duration/high frequency character) are superimposed on "long duration" manoeuvre loads. This situation may occur e.g. when flying a low altitude "holding"-circuit.

Anyway, for processing ACMS-acceleration data other, fully "computerized", methods are required if one wishes to eliminate the manoeuvre load components.

For this, two methods can easily be defined:

- Filtering the acceleration signal using a "high pass" filter (e.g. with corner frequency 0.1 Hz) before application of the peak/trough selection criterion.
  This procedure was applied e.g. in the analysis of "routine" BAC 1-11 data, see reference 13.
  Unfortunately, "standard" ACMS systems only record unfiltered c.g. acceleration data. Recording of filtered data would imply addition of a filter, hence modification, of the ACMS system or a complex additional processing of the complete ACMS recorded acceleration trace in ground facilities. This may not always be feasible.
- If the bank angle ϕ at the time of the acceleration peak Δn_z is also recorded, a "correction" can be made by subtracting the load factor component due to the banking manoeuvre $\Delta n_{banking} = 1 - 1/\cos\phi$, hence Δn_z "corrected" = $\Delta n_z - (1-1/\cos\phi)$.
  This procedure has been applied to a batch of 3932 flights in the 747 ACMS Data Base of NLR (bank angle information was only available for the more recently recorded flights).
  Figure 8 gives the result obtained for load factor exceedings below 10000 ft altitude. Looking at the relative positions of the squares and triangles and the "positive" and "negative" curve respectively, on may note that the correction was very effective in obtaining symmetry.
  The above correction appears very attractive because of its simplicity but it must be admitted that the procedure has no effect on the load factors due to pitching manoeuvres.

b Peak/trough selection

Relevant peak/trough values in the acceleration history must be reduced to gust velocity-occurrances. Different criteria to select the relevant peak/trough values can be defined.

It may be recalled that for VGH data a "peak between means" criterion was used whereas the fatigue meter actually uses a so-called restricted level cross technique. In principle, both techniques will give different results unless the reset level for all fatigue meter counting levels is equal to 1.g.

In general, the "peak between means" criterion may imply a very drastic reduction in load peaks to be analysed, see figure 9a. However, the aircraft c.g. acceleration response shows a more or less pronounced "narrow band" character, centred around the short period response frequency. Figure 9b depicts a signal with a very pronounced "narrow band" character. In that case the "peak between means" criterion implies very little reduction; actually most peak selection criteria will yield about the same result.

In the authors opinion, the "peak between means" criterion is quite acceptable as "standard" peak recognition criterion.

c Reduction of accelerations to gust velocities

The reduction of recorded accelerations to "derived gust velocities" must be based on a response calculation, involving two aspects namely:

i the assumed nature of the "input" gust signal;
ii the assured response behaviour of the airplane.

With regard to the input signal, distinction can be made between "discrete" gust inputs and a continuous gust representation. The discrete gusts assumed in the past ("[1-cos]" bump of 25 chords or a ramp of 100 ft) lack physical realism and do not reflect in a satisfactory manner the nature of atmospheric turbulence.

Using the continuous gust approach a weighted average response is calculated, by integrating the product of aircraft transfer function squared times the power spectral density function of turbulence.

The relative sensitivity for gust frequencies (= wavelengths) is reflected by the transfer-function of the aircraft, while the relative importance of the various gust frequencies is defined by the Power Spectral Density function.

In the authors opinion there's no doubt that the continuous approach is physically much better founded and strongly to be preferred over any "discrete" approach.

With regard to the aircraft response behaviour it may be recalled that in all programmes reviewed in this chapter the "classical" assumption of response in plunge only was made. This assumption may have been of relatively little consequence when calculating the response to discrete gusts of specific length (although Ref. 14 indicates a considerable effect of pitch response for "old" aircraft types).

For PSD-approaches, on the other hand, it is believed that the inclusion of pitch response freedom is vitally important.

Figure 9 reproduced from reference 15 illustrates the distribution of response power for an aircraft response model with plunge only and pitch and plunge freedom respectively.

In case the airplane is free to respond in pitch, the "windcock"-effect will make the aircraft practically insentitive for low gust frequencies (= long gusts). If one assumes plunge response only one

greatly overestimates the response to long gusts, and the PSD function shows that there the main part of the atmospheric power is concentrated!

Hence, the calculated average response if one ignores pitch response is grossly erroneous. This might not be a big problem if the error made would be equally big for all aircraft. However, figure 10 already indicates that this is not the case: Two aircraft with the same μ but different cord length would have about the same response if pitch were included, but very different response if plunge only were considered!

[Note that the "discrete" Pratt-formula, giving a dependence on μ only, would give a better prediction than a PSD response calculation with plunge response only].

In conclusion, it is our belief that the reduction of acceleration data to "gustvelocities" should be based on a response calculation to continuous turbulence for an aircraft model which must include pitch response freedom.

In the next chapter a simple procedure which complies with the above criteria will be presented.

6. REFERENCES

1. Taback, I., The NACA Oil-Damped VG Recorder. NACA TN 2194, 1950.

2. Richardson, N.R., NACA VGH Recorder. NACA TN 2265, 1951.

3. Coleman, T.L., Trends in repeated Loads on Transport Airplanes. Paper presented at the 4th ICAF Symposium, Munich, June 1965 (ICAF Doc. Nr. 487).

4. Pratt, K.G., Walker, W.G., A Revised Gust-Load Formula and a re-evaluation on VG data taken on civil transport airplanes from 1933 to 1950. NASA Report 1206, 1964.

5. Press, H., Steiner, R., an approach to the problem of estimating severe and repeated gust loads for missile operations. NACS TN 4332, 1958.

6. Zbrozek, J.K., Gust Alleviation Factor (Parts I, II and III). ARC R &M 2970, 1953.

7. Kaynes, I.W., A summary of the Analysis of Gust Loads Recorded by Counting Accelerometers on Seventeen Types of Aircraft. AGARD Report No 605, 1972.

8. Bullen, N.I., A review of Counting Accelerometer Data on Aircraft Gust Loads. ARC CP 933, 1967.

9. de Jonge, J.B., Spiekhout, D.J., Use of AIDS Recorded Data for Asessing Service Load Experience. In ASTM SP 671, 1979.

10. de Jonge, J.B., v.d. Wekken, A.J.P., Noback, R., Acquisition of Gust Statistics from AIDS-Recorded Data.

11. Coupry, G., Progress in the analysis of atmospheric turbulence (in French). In AGARD Report No 738, June 1986.

12. Hutin, P.M., Coupry, G., Description of atmospheric turbulence (in French). ONERA Report Technique No 6/3567 RY 070 R, May 1988.

13. Payne, B.W., Dudman, A.E., Criffith, K.C., Re-assessment of Gust statitics using CAADRP Data. In AGARD Report No 734, 1987.

14. Card, V., A review of Measured Gust Responses in the Light of Modern Analysis Methods. In AGARD Report R-7341 ADDENDUM, June 1988.

15. Houbolt, J.C., Status Review of Atmospheric Turbulence and Aircraft Response.

TABLE 1
Scope and sizes of VGH and V-G data samples
(reproduced from Ref. 3)

Airline service	Airplane type	Propulsion	VGH data			V-G data		
			Number of:			Number of:		
			Airplanes	Airlines	Flight hours	Airplanes	Airlines	Flight hours
Feeder	A	2-engine piston	1	1	1278	27	7	91,089
	L	2-engine turboprop	2	1	2100	2	1	10,368
Short haul	B	2-engine piston	1	1	834	24	1	38,578
	C		1	1	676	7	3	11,215
	D		2	2	2418	3	1	13,327
	M	4-engine turboprop	3	3	7038	8	2	38,138
	N		1	1	1834	--	--	------
Long haul	E	4-engine piston	-	-	------	10	1	48,187
	F		1	1	1038	--	-	------
	G		1	1	673	24	5	69,757
	H		2	2	2555	6	2	23,148
	H-1		1	1	1062	5	1	14,953
	J		4	2	4666	--	-	------
	K		3	3	3908	4	1	15,387
	O-1	4-engine turbojet	2	2	2410	8	3	51,264
	O-2		2	2	2822	3	2	19,330
	O-3		2	1	1539	--	-	------
	P-1		-	-	-----	2	1	13,571
	P-2		2	1	2464	5	2	24,478
	P-3		1	1	1651	4	1	13,750
	Q		1	1	1222	4	1	10,103
Total					42,188			506,643

TABLE 2
Summary of U_{de}-data derived from 747 ACMS recordings
(reproduced from Ref. 10)

NUMBER OF FLIGHTS CONSIDERED 20205

ALTITUDE INTERVAL (FT)	TOTAL DISTANCE FLOWN (NM)	TOTAL TIME SPENT (HRS)	NUMBER OF GUST "OCCURRENCES" IN INDICATED VELOCITY INTERVALS ("M/SEC", EQUIV.) U P W A R D									
			2-3	3-4	4-5	5-7	7-9	9-11	11-13	13-16	16-20	> 20
< 1500	164144	1036.24	21251	20021	10406	5739	760	130	33	17	4	5
1500- 3000	217974	1161.64	20006 ε	12757 ε	4752 ε	2235	232	25	4		1	3
3000- 5000	299323	1332.37	14564 ε	8210 ε	2863	1153	115	19			1	1
5000-10000	731005	2618.93	13664 ε	6933	2369	978	81	20	3	1		2
10000-15000	799602	2269.57	4391 ε	1557	517	231	40	5	3			
15000-20000	787312	1973.36	1979 ε	557	195	86	19	5	2	1		
20000-25000	1058572	2417.90	1558	409	112	68	17	3	1			
25000-30000	3082351	6445.35	2946	783	199	84	14	4				
30000-35000	21421269	43841.93	13208	3077	746	285	43	8	2	2	1	2
35000-40000	18391713	37825.56	9001	1968	447	166	22	3				2
> 40000	113056	234.00	104	29	5	2						
ALL ALTITUDES	47066322	101156.85	102672 ε	56301 ε	22611 ε	11027	1343	222	48	21	7	15

ALTITUDE INTERVAL (FT)	TOTAL DISTANCE FLOWN (NM)	TOTAL TIME SPENT (HRS)	NUMBER OF GUST "OCCURRENCES" IN INDICATED VELOCITY INTERVALS ("M/SEC", EQUIV.) D O W N W A R D									
			2-3	3-4	4-5	5-7	7-9	9-11	11-13	13-16	16-20	> 20
< 1500	164144	1036.24	27251	12903	4092	1314	198	49	13	10	3	1
1500- 3000	217974	1161.64	18619 ε	8638 ε	2421 ε	772	58	20	24	11	8	
3000- 5000	299323	1332.37	11013 ε	4354 ε	1250	454	46	12	5	2	4	
5000-10000	731005	2618.93	10230 ε	4039	1228	485	57	14	8	1	2	
10000-15000	799602	2269.57	3524 ε	1017	303	154	22	8	1			
15000-20000	787312	1973.36	1780 ε	416	134	56	10	3	2	1		
20000-25000	1058572	2417.90	1363	318	78	22	10	1				
25000-30000	3082351	6445.35	2651	622	173	73	15	2				
30000-35000	21421269	43841.93	11890	2699	613	263	38	5				
35000-40000	18391713	37825.56	7859	1588	398	140	22	2	2			
> 40000	113056	234.00	92	24	5	2						
ALL ALTITUDES	47066322	101156.85	96272 ε	36618 ε	16506 ε	3735	476	116	55	25	17	1

ε STATISTICALLY UNRELIABLE DATA DUE TO RECORDING THRESHOLD OF 0.18 G

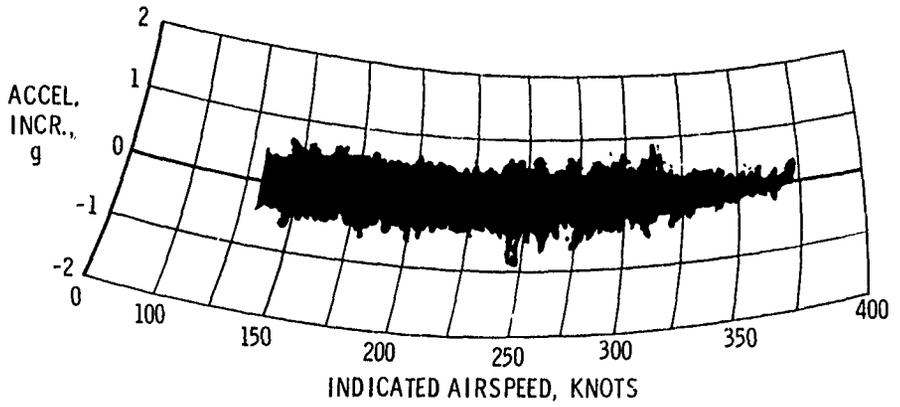

NASA

Fig. 1 Example of V-G record (200 flight hours). Reproduced from ref. 3

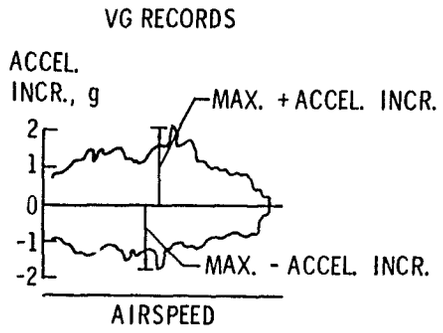

Fig. 2 Method of evaluating V-G records

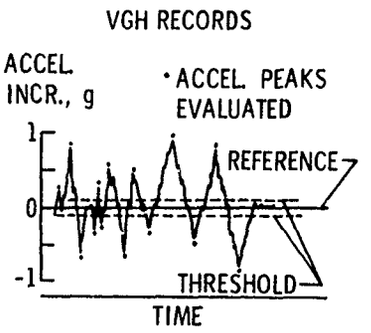

Fig. 4 Method of evaluating accelerations from VGH records, by the "Peak-between Means" criterion

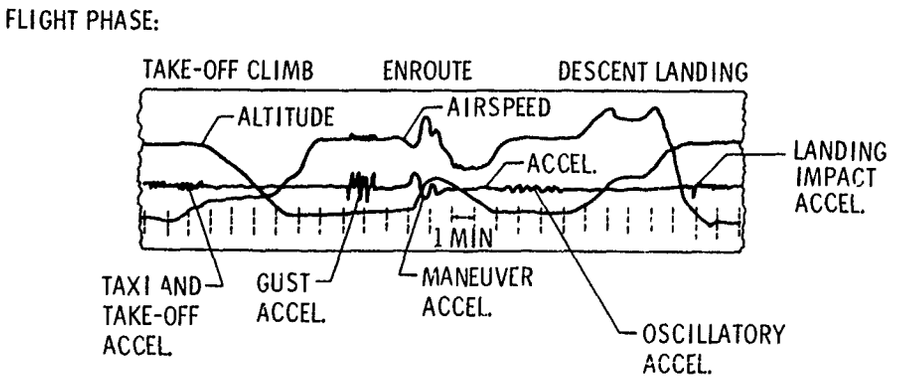

NASA

Fig. 3 Illustrative VGH record

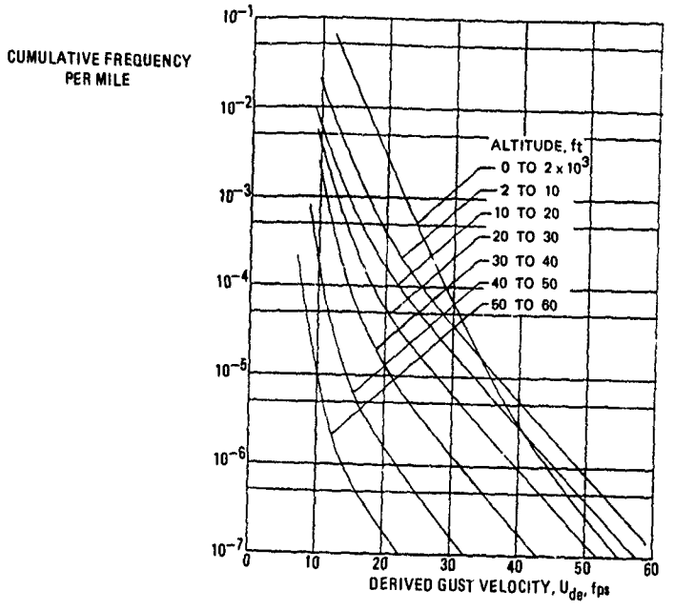

Fig. 5 Distribution of overall derived gust velocity $\bar{G}(U_{de})$ for airplanes at various altitudes, derived from VGH and VG data (from ref.

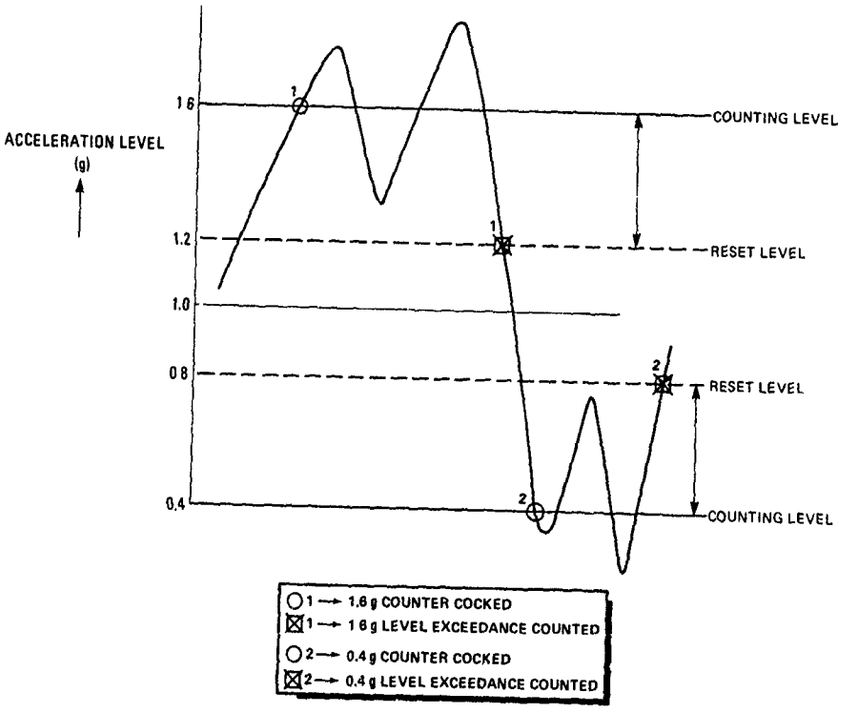

Fig. 6 Illustration of restricted level cross counting

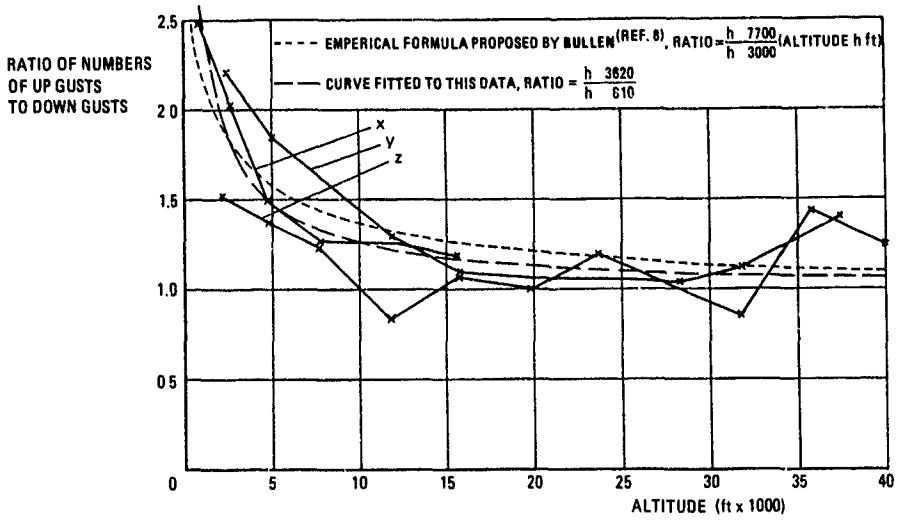

Fig. 7 Altitude variations of the ratio of up to down gusts of speeds greater than 6 m/s eas, by spectral gust response factors. Climb cruise and descent combined (reproduced from ref. 7)

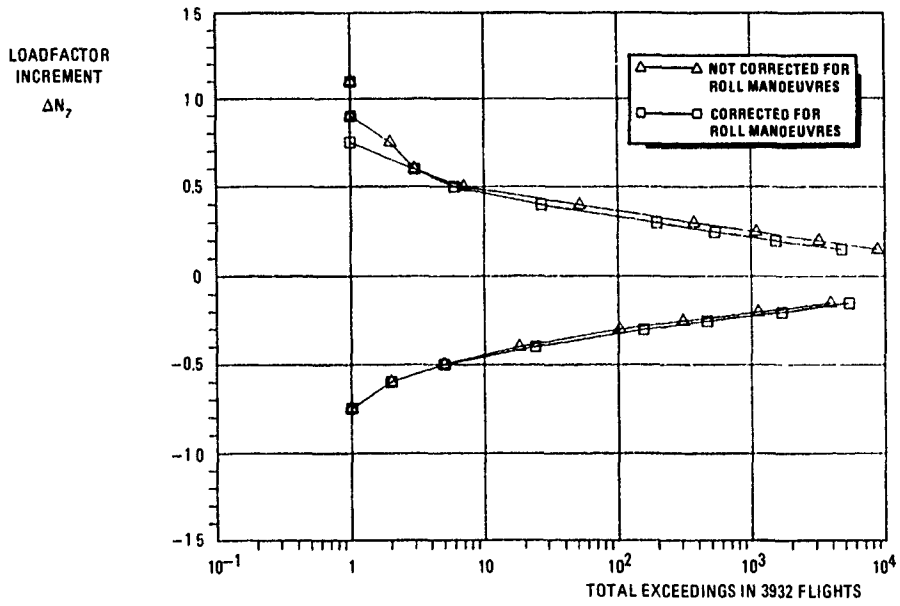

Fig. 8 Effect of bank angle correction on 747-ACMS recorded load factor spectra. (Altitude below 10000 ft)

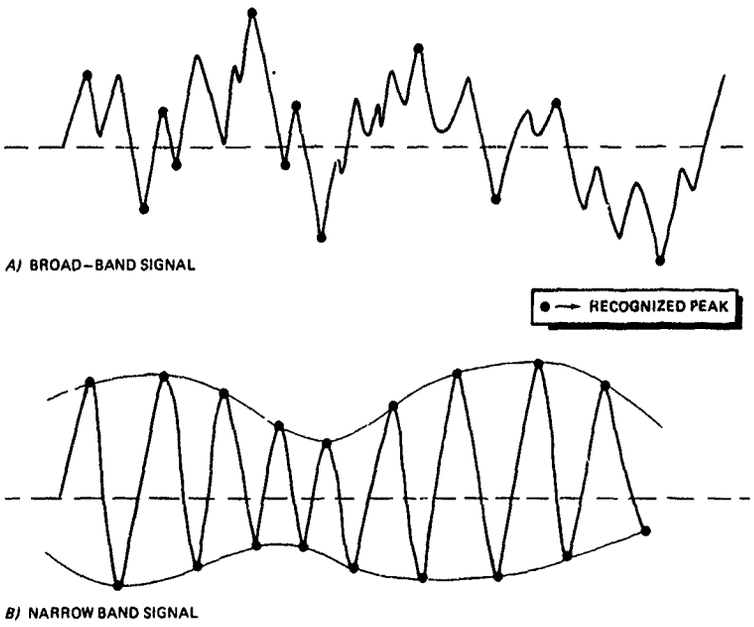

Fig. 9 Effect of signal-character on peak/trough reduction by peak-between means criterion

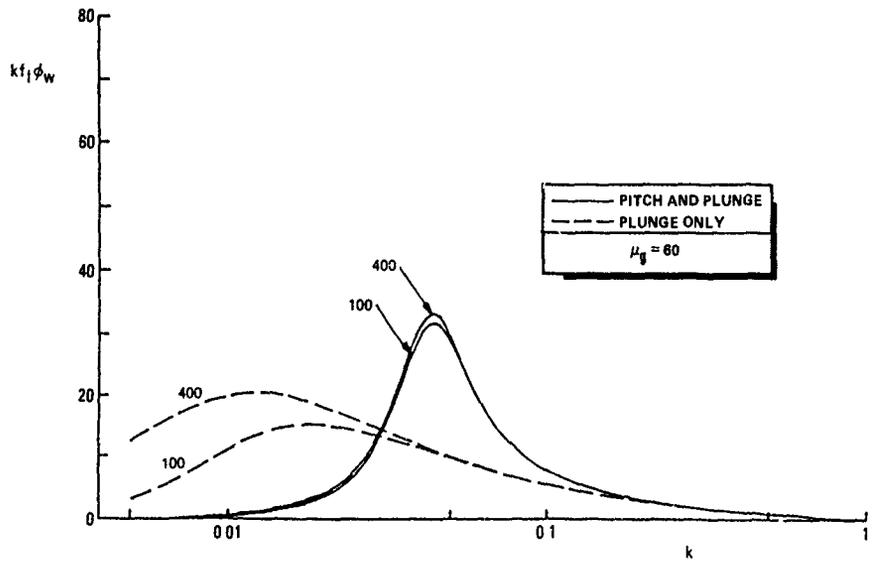

Fig 10 Distribution of response power for one and two degrees of freedom

CHAPTER III
IMPROVED REDUCTION OF GUST LOADS DATA FOR GUST INTENSITY

by

Gabriel (Daniel) Coupry* (Retired)
ONERA
29 av de la Division Leclerc
92320 Châtillon
France

CONTENTS

* This chapter was prepared with the technical support of M.Pierre-Marie Hutin, which the author wishes to acknowledge.

INTRODUCTION

This chapter deals with the reduction of load factor data to turbulence data, in view of proposing improved statistics of gusts. It will review the different methods available to achieve this process. A comprehensive analysis will be made to highlight the shortcomings and their consequences on the regulations.

The renewal of interest in turbulence comes from the new problems industry has to face:

- larger aspect ratio commercial airplanes,
- penetration of military aircraft at low altitude and high velocity,
- active control of flight and of loads,
- justification of increased fatigue life of existing commercial airplanes.

On one hand, one should keep in mind that exploration of turbulence by specially equipped aircraft (vanes, gyros, inertial platforms) has been, and is still, the only way to obtain time histories of turbulence from which are deduced the power spectral density and the integral scale; it provides a strong foundation for the methods based on the concept of continuous turbulence, but fails in providing statistics (e. g. exceedance curves) due to the small number of aircraft concerned. On the other hand, commercial airplanes fly millions of nautical miles per year, and encounter many patches of turbulence during their lives. They have been recently equipped with airborne recorders that collect information on accelerations at the center of gravity, indicated airspeed, altitude, weight and Mach number at the time of each event. During the same period, powerful computers became available which made it possible to record and analyze large data banks.

Thus the motivation and means appeared at nearly the same time, which lead research laboratories and industry to refine their analyses, taking into account the spanwise variations of gusts in isotropic turbulence and the balance of loads when continuous turbulence is the tool for certification. It also explains the new attempts described here to enlarge the data banks and consolidate the regulations.

The first attempt to reduce Δn data to turbulence data can be dated as early as the period 1931-1949, when Rhode and Donely assumed a one-degree-of-freedom response of the aircraft to a very simple isolated gust. Between 1950 and 1956, Pratt and Alii introduced the gust alleviation factor and the 1 - cosine gust, and worked on some 55,000 flight hours of data. Later (1956-1970), Press and Houbolt proposed the concept of continuous turbulence that lead to an amendment to FAR 25, prepared by Hoblit, which was widely accepted. This was followed by the works of Hall and Kaynes who, always with a one-degree-of-freedom system, introduced some spanwise distribution of the gusts. Very recently, Houbolt proposed a new method of reduction that takes into account the pitch degree of freedom of the airplane. In the meantime, collection of data was pursued, and Δn statistics are available for more than one million flight hours.

In its first part, this chapter will deal with the philosophy underlying the data reduction, and will raise the question of the meaning of a gust deduced from acceleration data; it will then describe some of the methods (Pratt, Hall, Houbolt). Finally, it will highlight the shortcomings (especially those due to the effect of pilot manoeuvres) and their impact on the regulations.

SYMBOLS

The notations used in this chapter are those used by J. C. Houbolt in his presentation to the AGARD Structures and Materials Panel in Athens in September, 1986:

a slope of the lift curve
A response transfer coefficient, as in $\sigma_{\Delta n} = A\sigma_w$
A_r aspect ratio
c wing chord
k reduced frequency, $k = \omega c/2V$
k_0 reduced frequency for zero crossings, $k_0 = \pi N_0 c/V$
k_s reduced short period frequency, $k_s = \omega_s c\backslash 2V$
L integral scale of turbulence
N_0 zero crossings per second, $N_0 = Vk_0/\pi c$
S wing area
U_d, U_e, U_t various gust intensity design values
V airplane speed
W airplane weight
α angle of attack of airplane in level flight referenced to the $C_L = 0$ crossing point
Δn incremental load factor due to gusts
μ mass parameter, $\mu = 2W/a\rho cgS$
ρ air density
σ_w rms value of gust intensity

$$\sigma_i = \frac{\sigma_w}{\sqrt{\pi}\left(\frac{2L}{c}\right)^{1/3}}$$

Φ_w power spectrum for gusts
ω angular frequency
Ω reduced frequency, $\Omega = \omega/V$
M Mach number

1. GENERAL CONSIDERATIONS

A description of atmospheric turbulence is essential in order to predict the loads an aircraft has to sustain during its normal life. As has been pointed out in the Introduction, statistics of gusts cannot be obtained by the very small number of aircraft specially equipped to measure time histories of turbulence. Consequently, one has to rely on Δn data collected on commercial flights and on some method to reduce these Δn data to gust data. Let us consider this last point: the prediction of the incremental load factor of an aircraft crossing a gust of a given slope is now easy through some sophisticated calculations. In contrast, it is impossible to derive a gust peak from a known Δn if one ignores the slope of the associated gust and all the details of the flight configuration (e. g., the static margin). In the past, various gust load formulas have been developed for the calculation of design gust loads on an aircraft, and used for the derivation of gust intensities from Δn data. Since it was first published in 1954, the alleviation factor approach of Pratt and Walker has gained almost universal acceptance and for many years has been a familiar part of the airworthiness requirements for both civil and military aircraft.

The original concept of the "Pratt formula" was to predict the peak accelerations due to discrete gusts on a given aircraft from the peak accelerations measured on another aircraft for flight through a discrete gust of the same shape and amplitude. Thus the derived gust velocity is not so much an absolute physical quantity, but is rather more a gust-load transfer factor

defined within the terms of the formula. As such, the method is most accurate when restricted to use on aircraft with very similar characteristics.

Use of very simple formulas to reduce Δn data was necessary at the time of Pratt, due to the poor computing facilities; it is still essential now, when one has to work on more than ten thousand events. All the methods described here will also be cheap tools for data reduction; they will all suffer the difficulties evoked for the Pratt formula. Consequently, one will have to keep in mind that description of gust statistics derived from Δn data is not a physical representation of turbulence, and should be applied with caution to airplanes that differ too much from those on which the primary information was collected.

At this point, it seems necessary to raise the question of the difficulties that come from the fact that generally (except for British Airways data), there is no means to separate accelerations due to pilot manoeuvres from those due to turbulence. This may not be important for large load factors, but surely contaminates the results for lower load factors.

Summarizing, the trend is now to use simple formulas for data reduction that could be used successfully for a large range of aircraft of very different weights, shapes and speeds, and that would take into account the two degrees of freedom of the rigid aircraft. This seems possible (work of J. C. Houbolt) because the flight mechanics of the different airplanes are to be kept in a narrow range for pilot acceptance.

In any event, whatever the efforts to refine the formulas, they will deliver a biased description of the turbulence that should be used very cautiously for certification purposes.

2. THE DIFFERENT METHODS

We will now describe some of the different methods that are now available to reduce Δn data to gust data; Pratt formula, Hall's method, and the new approach of J. C. Houbolt. All are based on an intensive use of the mass parameter

$$\mu = \frac{2\,W}{a\rho cgs}$$

that plays a fundamental role in airplane response to turbulence.

2.1 "Pratt Formula"

The most important feature of the Pratt formula is the introduction of the gust alleviation factor K in the formula that gives the load factor associated with a gust:

$$\Delta n = \frac{a\rho SV}{2\,W} K U_e \qquad (1)$$

Pratt and Walker (1954) made the following assumptions:

-The airplane is considered a point mass with vertical degree of freedom only.

-The number of zero crossings of the vertical acceleration is the same for all aircraft.

-The gust is a simple ramp of a given length until the maximum acceleration is reached.

-The gust is uniform in the spanwise direction.

With these assumptions one obtains the "Pratt formula":

$$K = \frac{.88\ \mu}{5.3 + \mu} \qquad (2)$$

The design gust velocities in current gust load requirements are based on the derivation, by the Pratt formula, of exceedance counts of center-of-gravity accelerations obtained, for the most part, from statistical data collected on U. S. transport aircraft prior to 1950 and supported by further data collected on European transport aircraft prior to 1960.

Later, the Pratt formula was improved by the introduction of the 1-cosine gust, 25 chords long, and still uniform in the spanwise direction.

2.2 The "Hall Method"

The Hall method is based on the assumption of continuous turbulence; that is, a stochastic process characterized by its power spectral density $\Phi_w(k)$ to which the power spectral density $\Phi_{\Delta n}(k)$ of the acceleration at the center-of-gravity is related by:

$$\Phi_{\Delta n}(k) = |T(k)|^2 \Phi_w(k) \qquad (3)$$

where T(k) is the transfer function of the aircraft.

J. Hall (1962) gives the following simple formula for T(k) for the case in which pitching and the effect of finite span on the lift due to atmospheric can be neglected:

$$|T(k)|^2 = (\rho S V a g/2W)^2 \frac{\beta^2}{p^2 + \beta^2} \times \left[\frac{B_1}{\alpha_1^2(1+B_1^2\beta^2)} + \frac{B_2}{\alpha_2^2(1+B_2^2\beta^2)} \right]$$

where:

$$\beta = 2\Omega L = \frac{4L\ k}{c}$$

$$p = \frac{L}{c\mu}$$

$$\alpha_1 = \frac{.26 + 2/\Lambda_T}{1 + .83M + .95M^2}$$

$$\alpha_2 = \frac{2 + 2/\Lambda_T}{1 + .83M + .95M^2}$$

$$B_1/\alpha_1^2 = \frac{\alpha_1 + 3\alpha_2}{4\ (\alpha_1 + \alpha_2)}$$

$$B_2/\alpha_2^2 = \frac{\alpha_2 + 3\alpha_1}{4\ (\alpha_1 + \alpha_2)}$$

$$B_1 = \frac{c}{L\alpha_1}$$

$$B_2 = \frac{c}{L\alpha_2}$$

The gust response factor K is then given by:

$$K^2 = \int_0^{+\infty} \frac{\beta^2}{p^2 + \beta^2} \times \left[\frac{B_1}{\alpha_1^2(1+B_1^2\beta^2)} + \frac{B_2}{\alpha_2^2(1+B_2^2\beta^2)} \right] \frac{\Phi_w(k)}{2\pi L\sigma_w^2} d\beta \qquad (4)$$

The first factor is associated with the acceleration that would occur if the gust produced lift instantaneously; the second factor is the coefficient for the unsteady lift function.

If the power spectral density of turbulence is represented by the Von Karman model, numerical integration must be carried out; on the contrary, if $\Phi_w(k)$ is represented by the Dryden model, integration can be achieved in closed form and gives the following result:

$$K^2 = \left(\frac{B_1}{2\alpha_1^2} \right) \frac{2 - 1/(1+p) + 1/(1+B_1)}{(1+p)(1+B_1)(1+pB_1)} + \left(\frac{B_2}{2\alpha_2^2} \right) \frac{2 - 1/(1+p) + 1/(1+B_2)}{(1+p)(1+B_2)(1+pB_2)} \qquad (5)$$

This formula is very easy to handle, but suffers the assumption of the Dryden model that does not seem realistic. In any event, it is progress in the sense that it takes into account the effect of unsteady aerodynamics and of the integral scale of turbulence.

Amazingly, as we will see later, whatever its shortcomings, it compares favorably with the "exact" values of K obtained by the J. C. Houbolt approach.

2.3 The Houbolt Method

The greatest part of this chapter will be devoted to the method proposed recently by J. C. Houbolt, which is very promising because it takes into account the two degrees of freedom of the rigid aircraft and the spanwise gust gradients.

The point spectrum chosen is the Von Karman spectrum, but written in the following form:

$$\Phi_w(k) = \sigma_1^2 \frac{\left(\frac{2L}{c} \right)^{5/3} \left[1 + \frac{8}{3} \left(1.339 \frac{2Lk}{c} \right)^2 \right]}{\left(1 + \left(1.339 \frac{2Lk}{c} \right)^2 \right)^{11/6}} \qquad (6)$$

where

$$\sigma_1^2 = \frac{\sigma_w^2}{\pi \left(\frac{2L}{c} \right)^{2/3}} \qquad (7)$$

This formulation makes all the spectra pass through the same points at high frequency, regardless of the scale of turbulence (figure 1).

The inclusion of the pitch degree of freedom has a pronounced influence on the output response. Figure 2 compares the distribution of response power for a single degree of freedom airplane with that of the two degree of freedom case. We note that there is a lot of response at low frequency for the single

degree of freedom case, and that the response depends on 2L/c. In contrast, the response power for the two degree of freedom airplane tends to concentrate around the short period frequency and the response is less sensitive to the value of 2L/c.

The response for incremental vertical acceleration is found to be:

$$\Delta n = \frac{V K_1}{c g \mu} U_e = \frac{V K_1}{c g \mu} R\sigma_1$$

$$= \frac{V K_1}{c g \mu} \frac{1}{\sqrt{\pi}} \left(\frac{c}{2 L} \right)^{1/3} R\sigma_w$$

where K_1 is the reduced gust alleviation factor associated with σ_1 and can be formulated as:

$$K_1^2 = \int_0^{+\infty} f_0(k) f_1(k) f_2(k) f_3(k) dk \qquad (8)$$

In the equation for K_1, $f_0(k)$ is the airplane transfer function, $f_1(k)$ is the unsteady lift function, $f_2(k)$ takes into account the spanwise gust variation, and

$$f_3(k) = \frac{\Phi_w(k)}{\sigma_1^2}$$

is the reduced gust power spectral density.

The specific equations used for $f_1(k)$ and $f_2(k)$, as proposed by J. C. Houbolt, are:

$$f_1(k) = \frac{1}{1 + 2.32 \nu k + \nu^2 k^2} \qquad (9)$$

$$f_2(k) \quad \frac{1 + .55 A_r k}{1 + .66 A_r k + .34 A_r^2 k^2} \qquad (10)$$

where

$$\nu = \frac{1.5}{\beta} \frac{A_r}{3 + A_r \beta}$$

with

$$\beta = \sqrt{1 - M^2}$$

Knowing the transfer function of the airplane makes it possible to compute "exactly" the value of K_1. Unfortunately, this is not practicable where more than ten thousand data points are to be reduced; consequently, Houbolt searched for a very simple formula that could give a very good approximation of the "exact" solution. The analysis was applied to a number of different airplanes and has shown that an acceptable approximation of the value of K_1 associated with equation (8) was given by:

$$K_1 = .95 \sqrt{\mu} \qquad (11)$$

Using equation (7) one can then derive the gust alleviation factor K as:

$$K = \frac{.95}{\sqrt{\pi}} \left(\frac{c}{2L} \right)^{1/3} \sqrt{\mu} \qquad (12)$$

Incidentally, we will note that, with the use of the $f_1(k)$ and $f_2(k)$ functions, there is no difficulty found in establishing realistic values of the zero crossing parameter N_0, without any arbitrary cut off of the integration. One finds:

$$N_0 = \frac{.475}{\pi\, c \sqrt{\mu}} \qquad (13)$$

Nevertheless, results of Houbolt's method reveal discrepancies up to 10% with the "exact" values of K derived from equation (8).

3. RESULTS AND DISCUSSION

3.1 Foreword

We have described in this chapter three of the methods commonly used to reduce load factors to gust data. These three methods are based essentially on the value of the mass parameter μ. The first (Pratt's formula) starts from a very simple description of the gust and derives the amplitude of the gust from the vertical acceleration of the aircraft; the second and third methods are based on the assumption of continuous turbulence, the Hall method with a one degree of freedom motion of the aircraft, the Houbolt method with a two degree of freedom description of the flight mechanics and the proposal of an approximate simple formula. Both Hall's and Houbolt's approach take into account the integral scale of turbulence. At this point, one could be puzzled by the fact that continuous turbulence and power spectral methods are used to reduce accelerations to isolated gust intensities through the K and N_0 values; this seems acceptable because, during its flight life, an airplane crosses gusts of various lengths, these lengths being distributed according to the power spectral density of turbulence.

Let us now compare, as functions of the mass parameter μ, the values of K associated with Pratt's and Houbolt's simple formulae. The results are given in figure (3) for different values of the integral scale of turbulence. They obviously show that both the absolute values and the shapes of the curves are extremely different, and, consequently, that one of the formulae is undoubtedly wrong.

Let us now compare the "exact" values of K, as given by the integral of equation (8), with the values given by the Houbolt formula (eqn. (12)). This has been achieved for 15 very different configurations of Boeing 747 airplanes, and the results are given in table (1) for an integral scale of 750 m.

MASS kg	TAS knots	ALTITUDE	MACH	μ	K EXACT	K HOUBOLT	% ERROR
222300	205	3843	.313	15.27	.413	.371	-10.2
213700	298	5512	.460	19.13	.454	.415	-8.6
315900	230	3283	.359	21.91	.486	.444	-8.6
275300	355	9931	.528	28.60	.540	.507	-6.1
230400	397	17464	.635	29.05	.538	.512	-5.0
207600	474	21036	.748	29.41	.529	.515	-2.6
317800	373	9902	.578	33.11	.574	.546	-4.9
202100	477	28970	.765	37.08	.584	.578	-1.0
236700	458	25722	.733	39.18	.603	.594	-1.5
312800	451	18110	.706	41.50	.621	.612	-1.4
233700	513	36074	.853	53.89	.666	.697	+4.7
244000	530	35133	.850	54.23	.665	.699	+4.5
255400	491	33028	.811	55.26	.684	.710	+3.2
287500	515	30954	.831	56.03	.689	.717	+4.1
269600	515	32906	.829	58.44	.696	.726	+4.3

Table 1

As can be seen from this table, errors up to 10% occur when comparing the two values of K, but they stay generally around 5%. As such, Houbolt's formula gives acceptable results, which clearly shows that Pratt's formula should no longer be considered valid.

Even so, errors of the order of 5% to 10% may result in greater errors in the exceedance curves, and improved simple methods should be sought.

3.2 Improved Houbolt Method

Table (1) exhibits negative errors for low values of μ and positive errors for large values of μ. This gives the idea of modifying equation (12) in the following way:

$$K = \frac{1}{\sqrt{\pi}} \left(\frac{c}{2L} \right)^{1/3} \frac{.95\sqrt{\mu}}{(b + h\mu)} \qquad (14)$$

where b and h should be determined by a root mean square fitting from the values given in table (1). The integral of equation (8) need be calculated only for these 15 configurations, and the thousands of events associated with the data recorded should then be reduced by equation (14) which is very easy to handle. In

equation (8), one should take the following as the value of $f_0(k)$ for the rigid body motion (two degrees of freedom):

$$f_0(k) = \frac{k^4 + \left(\frac{1}{\mu} - 2\,\alpha_g\, k_g^2 \right) k^2}{(k^2 - k_g^2)^2 + 4\alpha_g k_g^2 k^2}$$

where α_g is the non-dimensional damping of the aircraft.

The result of the mean square fitting is presented in figure (4) and gives the following values for b and h:

$$b = .846$$
$$h = .0035$$

The K values for the 15 configurations have been recalculated using equation (14) and the results are presented in table (2).

In table (2), K_{HC} stands for the K Houbolt modified according to equation (14).

One can see immediately from the table that the errors between K "exact" and K_{HC} are now limited to 2%, which is quite acceptable. The same process has been applied to the fleet of BAC 111 and Boeing 737 airplanes of British Airways with the same success.

MASS kg	TAS knots	ALTITUDE	MACH	μ	K EXACT	K_{HC}	% ERROR
222300	205	3843	.313	15.27	.413	.408	-1.2
213700	298	5512	.460	19.13	.454	.451	-0.7
315900	230	3283	.359	21.91	.486	.479	-1.4
275300	355	9931	.528	28.60	.540	.535	-1.0
230400	397	17464	.635	29.05	.538	.538	0.0
207600	474	21036	.748	29.41	.529	.541	+2.3
317800	373	9902	.578	33.11	.574	.567	-1.2
202100	477	28970	.765	37.08	.584	.592	+1.4
236700	458	25722	.733	39.18	.603	.604	+0.2
312800	451	18110	.706	41.50	.621	.617	-0.6
233700	513	36074	.853	53.89	.666	.673	+1.1
244000	530	35133	.850	54.23	.669	.674	+0.7
255400	491	33028	.811	55.26	.684	.678	-1.0
287500	515	30954	.831	56.03	.689	.685	-0.6
269600	515	32906	.829	58.44	.696	.689	-1.0

Table 2

(Editor's note: It is to be noted that the editor suggested equation (12), not only because it represented a fairly good approximation to K, but also because it led to a great simplification of some subsequent results. At the same time he derived another approximation that gave more accurate results, but Coupry did not have access to this second approximation. We present the report as Coupry wrote it, but include here the results that would have been obtained if he had access to the equation. The more accurate approximation for K that I found is

$$K = \frac{11.5}{\sqrt{\pi}} \left(\frac{c}{2L} \right)^{1/3} \sqrt{\frac{\mu}{110 + \mu}} \qquad (15)$$

which reflects the proper behavior at high values of μ. With this equation (and $2L/c = 180$) the results of table 2 would appear as (giving only the last three columns):

K EXACT	K_{HA}	% ERROR
.413	.412	-0.2
.454	.454	0.0
.486	.481	-1.0
.540	.536	-0.7
.538	.539	+0.3
.529	.542	+2.4
.574	.568	-1.1
.584	.542	-1.5
.603	.605	+0.3
.621	.618	-0.5
.666	.677	+1.6
669	.678	+1.4
.684	.682	-0.2
.689	.685	-0.5
.696	.695	-0.1

where K_{HA} refers to the use of equation (15). We see a rather remarkable agreement with the "exact" K values. We return now to a continuation of Coupry's writing.)

Summarizing, it seems that one of the best ways to reduce An data to turbulence data is to use the improved Houbolt method, that is, to "calibrate" equation (14) (Editor's change: use the better approximation of Houbolt, and "calibrate" equation (15))

by "exact" calculations on a small number of different flight conditions, and then to use this formula for the reduction of all the data.

3.3 Results

The core of the data that can be used with confidence is given by the British Airways records, where manoeuvre loads have been removed, for incremental Δn greater than 0.5. The best check of the methods is the comparison of the description of the atmosphere as deduced from different types of airplanes; if a method is acceptable, the descriptions should be very close to each other.

In six years of records on eight different types of aircraft, British Airways has analysed 1,209,462 hours of flight, in particular:

540,949 hours on Boeing 747
177,092 hours on Boeing 737
101,484 hours on BAC 111

For all these airplanes, the flight profile was known.

Three methods have been used to reduce the data; the Pratt formula, the Hall formula with a Dryden spectrum, and the Houbolt method. The Pratt formula failed completely to derive a consistent description of turbulence from the data recorded on the different types of airplanes.

Figures (5), (6), (7), and (8) show, for a given range of altitude, the number of exceedances of a given value of turbulence per 1000 nautical miles. The results have been derived from the use of Houbolt's formula, but the results using Hall's method are very close. Both the methods exhibit nearly the same description of the atmosphere, whatever the aircraft on which Δn has been recorded , which in some measure supports their validity. The greatest discrepancy occurs for the lowest altitude, presumably because the BAC 111 airplanes fly very often in the Berlin corridor at altitudes lower than 10,000 feet.

In conclusion, Houbolt's method derives, from Δn recorded on one type of aircraft, the probability of gust occurrence which, when applied to another (different) type of aircraft, makes it possible to predict its load factor exceedances with an acceptable accuracy. It is then obviously clear that Houbolt's reduction method provides a good tool for certification, at least for large gusts associated with Δn greater than 0.5.

3.4 Discussion

Another question is to decide whether or not Houbolt's technique provides a good description of the actual physical atmosphere. The feeling of the author is that this description is globally not too bad for the extreme gusts considered here, once a sufficient number of events exceed the reference level of turbulence. In such conditions, one could expect that the effect of the scatter of unknown parameters, as:

- actual transfer function
- exact value of $C_{L\alpha}$
- actual scale of turbulence
- actual detailed autopilot mode

should be averaged.

This conclusion is only valid for the British Airways flights, for which turbulence and manoeuvre loads have been clearly separated; consequently, the results exhibit symmetric exceedance curves for positive and negative gusts. Unfortunately, this separation has not been achieved for most of the records of

other fleets. In British Airways flights of the Boeing 747, for $\Delta n \leq 0.5$, 25% of the events are associated with pilot manoeuvres. As manoeuvres corresponding to large accelerations are rare, it is obvious that this percentage should increase for lower load factors, at least at low altitude, and that the exceedance curves for positive and negative gusts should not be symmetric, with a greater number of positive ones. This has been observed in NLR data, also recorded on Boeing 747 aircraft, but without turbulence-manoeuvre separation. In the range of altitude 0-5000 feet, the numbers of positive and negative accelerations greater than 0.3 g are 1452 and 449 respectively; they have a tendency to equality (.55 and .48) for $\Delta n \geq 0.5$.

4. CONCLUSIONS

The work presented here represents the analysis of more than a million hours of commercial flights by different countries (British Airways, Air France). The following points summarize the findings.

The formula of Pratt should be abandoned because it leads to atmospheric descriptions which are incoherent.

The formula of Hall, with an appropriate choice of scale, leads to a reasonably coherent description of the turbulence, relatively independent of the type of airplanes involved.

The formula of Houbolt supplies a good description of the atmosphere and leads to a coherent description of atmospheric turbulence, independent of the airplane. Means for analytically deriving the proper "K" for reduction purposes are given.

For strong turbulence, the number of exceedances per nautical mile of a given level of turbulence severity diminishes exponentially with the gust severity level.

For the slight levels of turbulence, the interpretation of measurements of turbulence is delicate because the accelerations due to manoeuvres represent a significant percentage of the overall acceleration records; it does not seem readily possible to separate gust and manoeuvre accelerations.

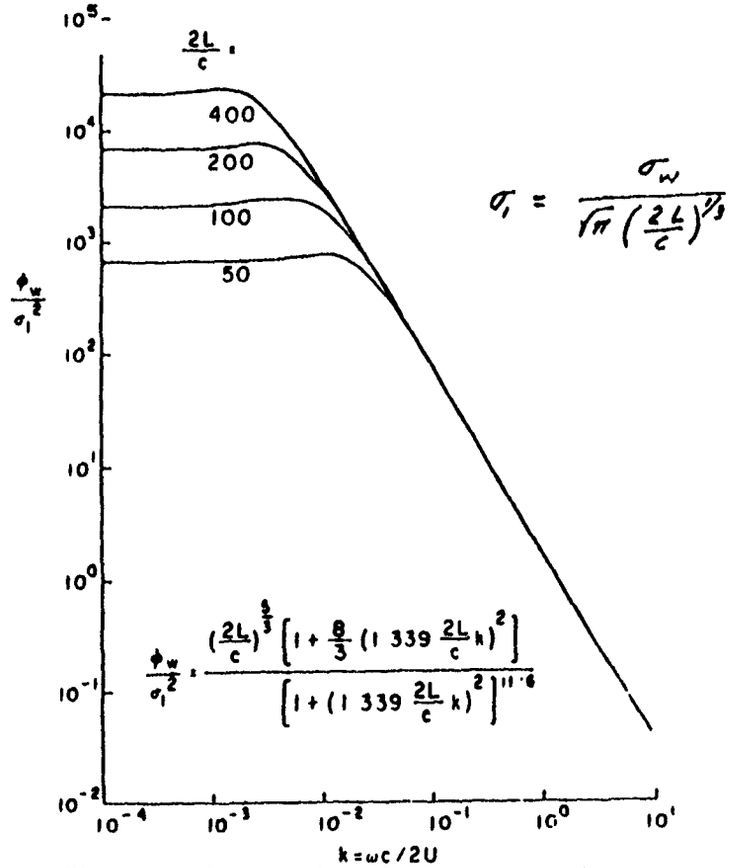

Figure 1.- Gust spectrum form used in analysis.

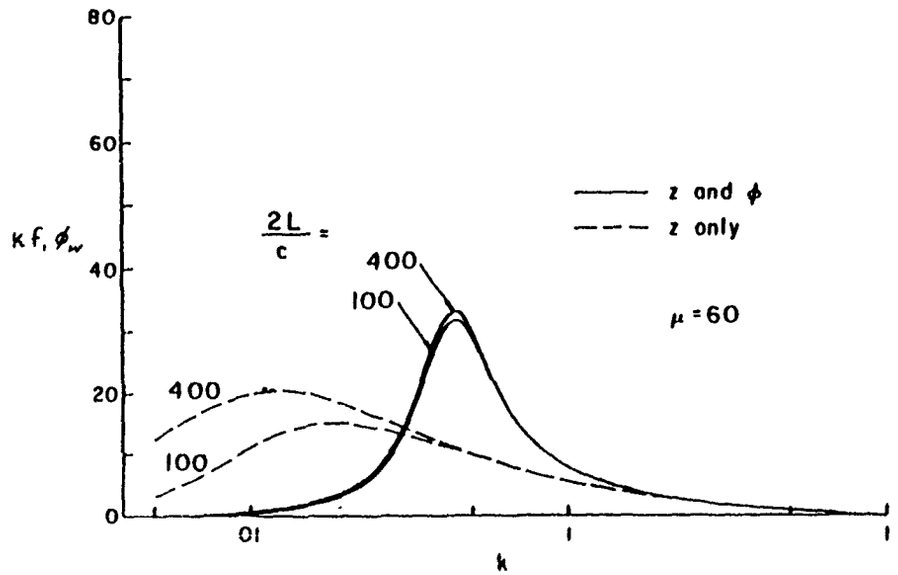

Figure 2.- Distribution of response power for one and two degrees of freedom.

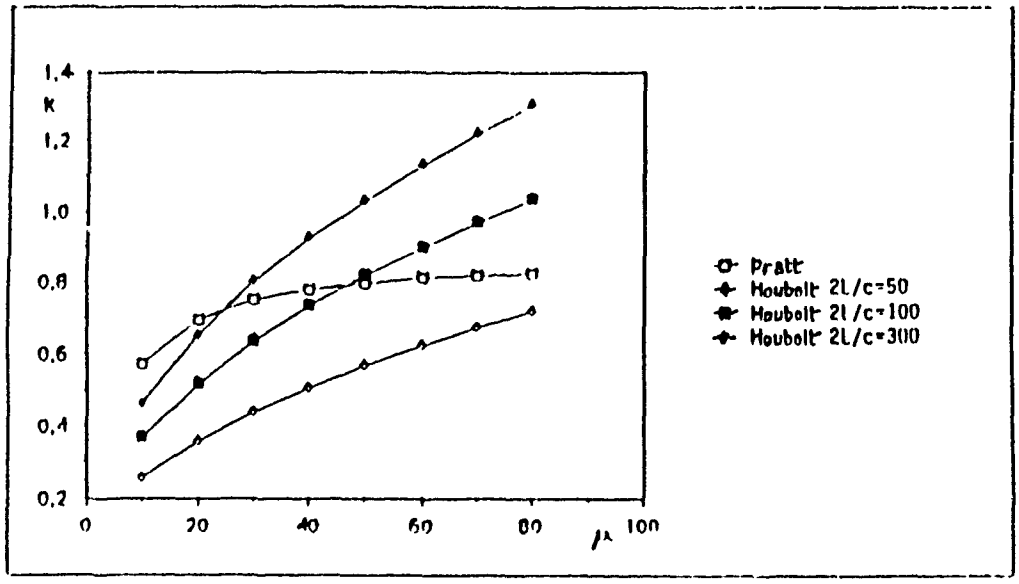

Figure 3.- Alleviation factors

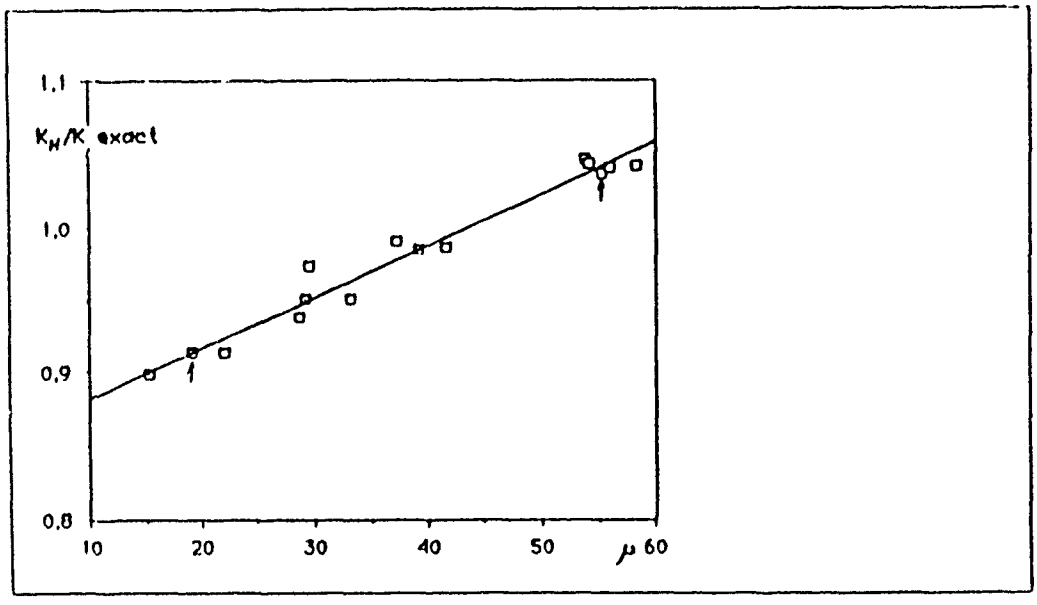

Figure 4.- Plot of K_H/K_{exact}

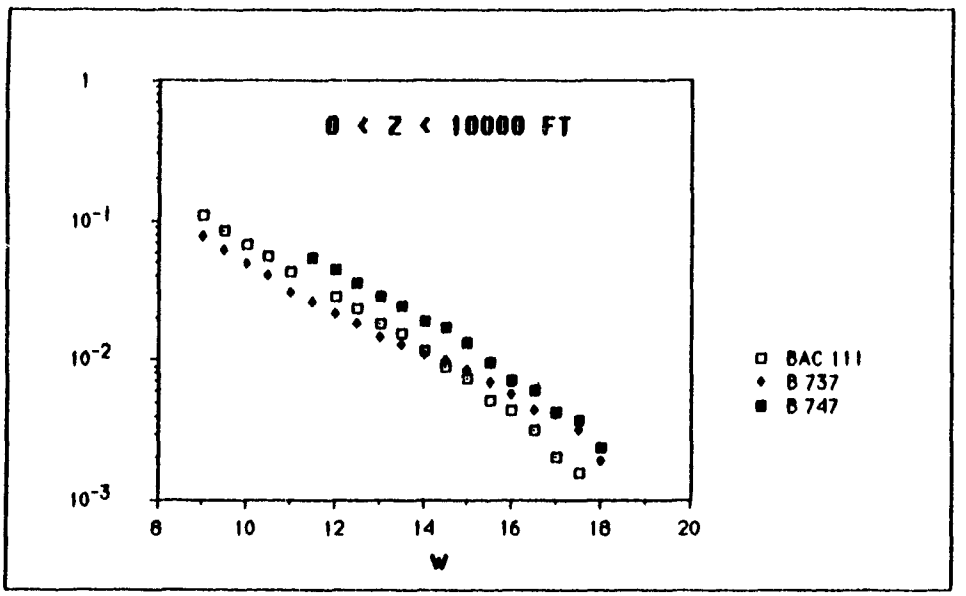

Figure 5.- Gust exceedances per 1000 nautical miles.

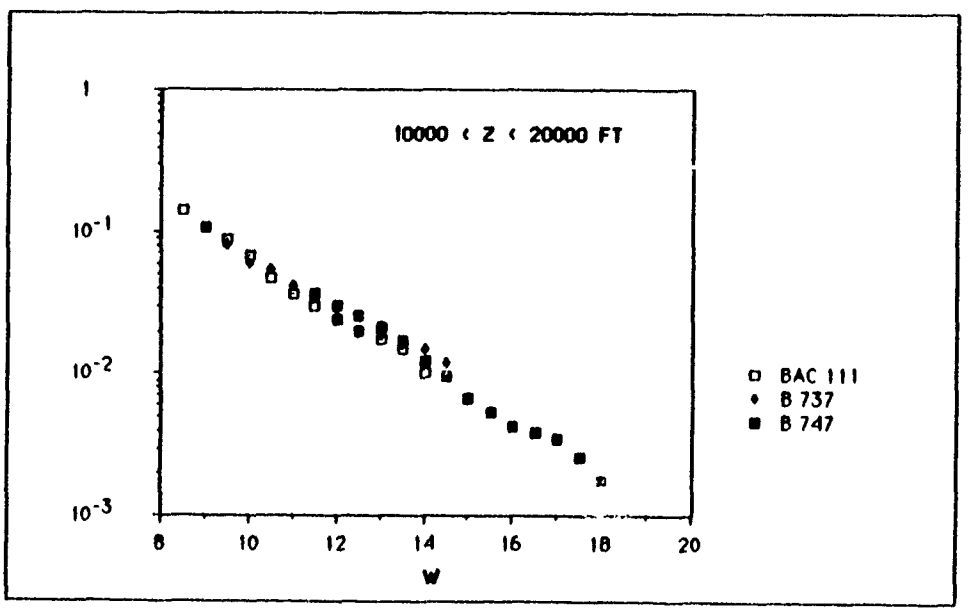

Figure 6.- Gust exceedances per 1000 nautical miles.

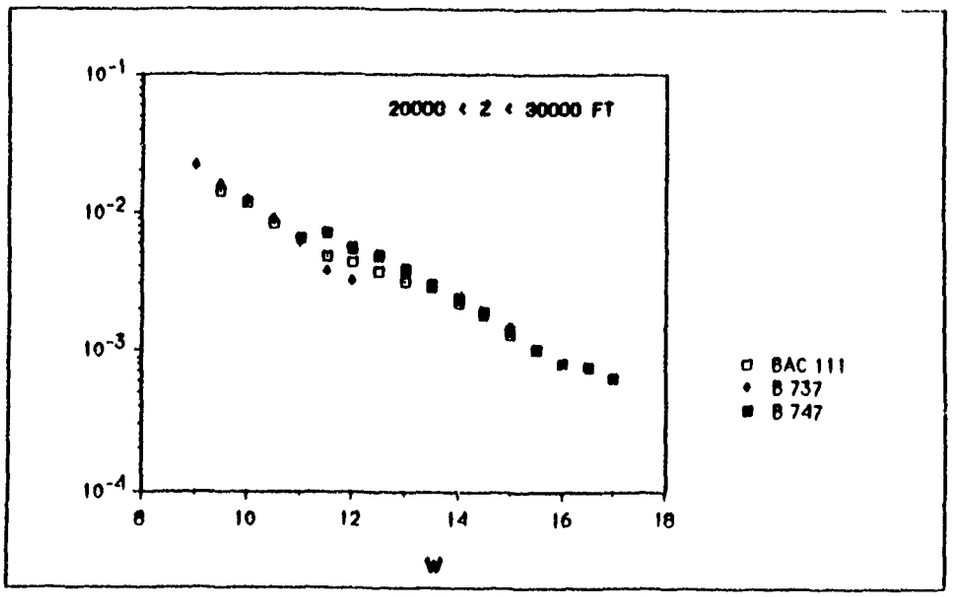

Figure 7.- Gust exceedances per 1000 nautical miles.

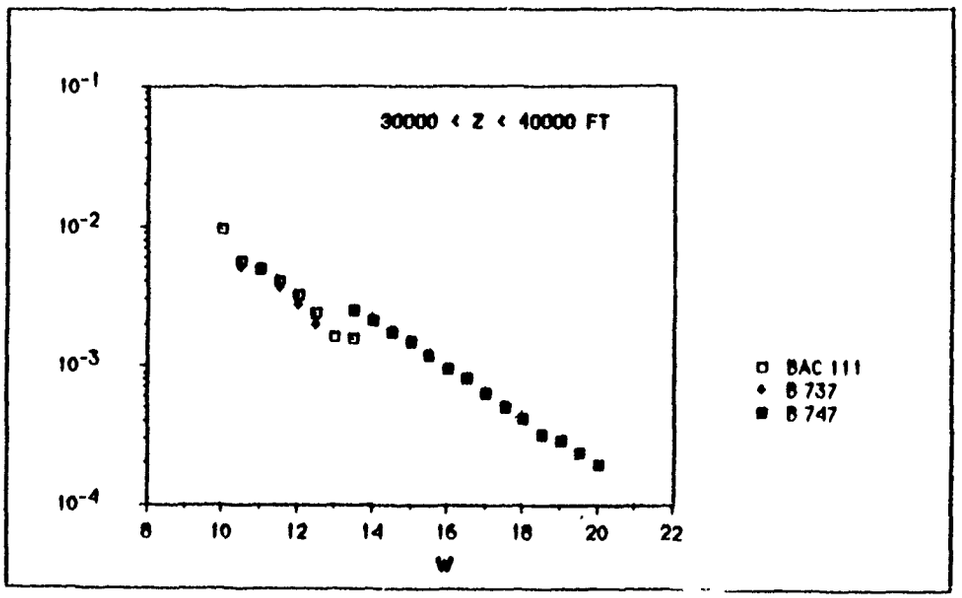

Figure 8.- Gust exceedances per 1000 nautical miles.

CHAPTER IV
CERTIFICATION PROCEDURES AND REQUIREMENTS

by

Terence J.Barnes
FAA
United States

and

Victor Card
CAA
Brabazon House
Redhill, Surrey RH1 1SQ
United Kingdom

CONTENTS

1. PHILOSOPHY AND EVOLUTION OF THE REGULATIONS (T. Barnes, FAA)

The underlying philosophy behind all structural loads criteria is that there should be an adequate margin between normal operating loads and design loads. Design load conditions are intended to produce load levels consistent with the load level which might be experienced once in the lifetime of an aircraft. In the early days of aircraft development, gust loads were assumed to be covered by conservative maneuver loads. As aircraft designs developed, however, the maneuver load criteria were reduced. Also it became apparent that parameters such as airspeed and wing loading were important in defining gust loads, and it was recognised that maneuver and gust loads should be treated separately.

A regulation must be sufficiently versatile to account for basic aircraft parameters, and operation. As aircraft became more flexible, it became necessary to account for dynamic response. While early criteria recognised only discrete gusts, more recent (current) criteria account for the continuous nature of atmospheric turbulence. Philosophically, however, as more detail and realism are added to the criteria it becomes increasingly difficult to define both realistic and design level criteria simultaneously.

To minimize analysis complication, some simplifying assumptions are made. For example, discrete gusts are assumed to have a one-minus-cosine shape, continuous turbulence and discrete gusts are separated, and each presumed to result in design level loads. Spanwise variation in gust velocity is ignored, and combinations of maneuvers, continuous turbulence and discrete gusts are not considered.

Since the recognition that turbulence produced significant structural loads (around 1915), there have been several significant steps in the development of gust criteria. The first gust criterion was the SHARP EDGED GUST formula. This was later modified to a formula specifying RAMP-PLATFORM GUSTS and later to ONE-MINUS-COSINE gusts. Finally, the criteria for CONTINUOUS TURBULENCE were developed. Figure 1 (taken from Reference 1) shows the chronology of Federal Regulatory gust loads criteria for transport aircraft design.

Reference 1, which was prepared by NASA with assistance from FAA, traces the evolution of gust design criteria in the U.S. particularly from the standpoint of the background research that was used to substantiate changes. Rather than reprint selected sections, this paper is considered to be an integral part of this manual. In the paper, the mathematical models of airplanes and atmospheric turbulence and their rationale are described. Emphasis is given to the revisions and refinements made starting in the 1920's up to the present time. The major steps, beginning with the sharp edged gust formula, are traced through the modified formula specifying ramp-platform gusts and later to one-minus-cosine gusts and finally to criteria for continuous gust analyses. The influence of aircraft design developments on design criteria development needs is also addressed. A brief summary of military criteria is included. Significant discussion is devoted to measurements that have been made, including onboard recordings, to provide an extensive data base of:

(1) atmospheric turbulence experienced in routine flight operations;

(2) specifically-instrumented research aircraft measurements to provide atmospheric characterisation for various flight and meteorological conditions; and

(3) comparisons of measured and calculated aircraft responses in turbulence.

2. DIGEST OF CERTIFICATION PROCEDURES (V.Card, CAA)

2.1 Discussion of Requirements

Loads due to gusts and turbulence have had a significant influence on aircraft design and the airworthiness criteria governing the strength of civil aircraft. Airworthiness Authorities have recognised from the early days of civil aviation that loads due to atmospheric disturbances may become design critical for certain parts of the structure. For modern civil aircraft the design of many of the primary structures (such as wings, empennages, fuselage and engine mounts) may be dictated by these load cases.

The two major airworthiness codes in use within the AGARD group of countries are the U.S. Federal Aviation Regulation (FAR) and the European Joint Airworthiness Requirements (JAR). The major gust requirements that these codes contain are summarised in Figure 2. As can be seen, both sets of requirements acknowledge two natural atmospheric phenomena which can lead to high external loads on aircraft structures - namely discrete gusts and continuous turbulence.

In the discrete gust description, gusts are assumed to be events which are sufficiently isolated for the motion of the aircraft to have subsided before the aircraft encounters the next. The gust is described as a specific time history of velocity fluctuation fixed in space. The gust loads are developed as a result of the deterministic response of the aircraft as it passes through the gust field.

In the continuous turbulence description, atmospheric fluctuations are assumed to occur in patches within which the gust velocity and the aircraft response varies continuously. It is not possible to relate any particular response load with any particular velocity fluctuation and, therefore, turbulence loads can only be described statistically.

2.2 Discrete Gust Requirements

In the basic discrete gust requirement of both FAR 25 and JAR 25 the disturbing gust takes the following form:-

$$U = \frac{U_{de}}{2} \left[1-\cos \left(\frac{2\pi s}{H} \right) \right] \qquad (1)$$

where:-

s = the distance penetrated into the gust (ft);

U_{de} = the derived gust velocity for design limit loads (ft/sec);

H = the gust gradient distance (ft);

U = the gust velocity at distance s (ft/sec).

Whilst the atmosphere is essentially random in nature and the pattern of air motion can take an almost infinite variety of forms this "1-cosine" description of discrete gusts is one which has found almost universal acceptance for aircraft design calculations. Although this gust model is arbitrary, it does closely represent the essential nature of many atmospheric disturbances. It is also advantageous because it provides an acceptable mathematical description of a discrete gust which facilitates the solution of the aircraft response equations. Historically this has enabled researchers to calculate reasonably accurate values of derived gust velocity from centre-of-gravity accelerations measured during routine operations. In this way design values of derived gust velocity have been set which have an acceptable probability of occurrence and which maintain the levels of strength of previously successful designs.

The gust velocities and associated design speeds which are to be assumed for the limit load calculations are as follows:-

(1) For flight at the design speed for maximum gust intensity (V_B), positive and negative rough air gusts of 66 fps EAS must be considered at altitudes between sea-level and 20,000 ft. The gust velocity may be reduced linearly from 66 fps EAS at 20,000 ft to 38 fps EAS at 50,000 ft.

(2) For flight at the design cruising speed (V_C), positive and negative gusts of 50 fps EAS must be considered at altitudes between sea-level and 20,000 ft. The gust velocity may be reduced linearly from 50 fps EAS at 20,000 ft to 25 fps EAS at 50,000 ft.

(3) For flight at the design diving speed (V_D), positive and negative gusts of 25 fps EAS must be considered at altitudes between sea-level and 20,000 ft. The gust velocity may be reduced linearly from 25 fps EAS at 20,000 ft to 12.5 fps EAS at 50,000 ft.

The scale of these design velocities is predicated upon certain assumptions concerning likely operational use. The main design condition is based upon flight at the design cruising speed (V_C). Normal operational practice implies that in areas of known severe turbulence flight at the rough air speed will be adopted. The rough air speed is a recommended operational speed which is often closely associated with the design speed for maximum gust intensity (V_B). In such a condition potentially more severe gusts must be expected. Therefore a higher design gust velocity is appropriate at the V_B speed. On the other hand, flight at speeds above the design cruising

speed is not a routine condition. Speed exceedances approaching the design diving speed have a very low probability of occurrence. Consequently, the probability of meeting an extreme gust whilst at the design diving speed is extremely remote. Therefore a lower design gust velocity is appropriate at the V_L speed.

Since gust loads are approximately proportional to the aircraft speed, the aeroplane structure is more gust tolerant at lower speeds and it is by no means certain that the V_B conditions, which are associated with the highest amplitude gusts, will provide the design cases. For modern designs, gust loads arising from the V_C and V_B cases tend to be of a similar magnitude, with the critical case sometimes depending upon the particular part of the structure under consideration. Therefore both conditions must be investigated in detail. Generally, the gust loads arising from the V_D cases tend to be lower than those from either the V_C cases or the V_B cases. Nevertheless they must still be investigated since they could prove critical for some components, for example the horizontal tailplane.

In normal useage the gust length is taken as fixed at a value equal to 25 times the mean geometric chord of the aircraft under consideration. For many aircraft a gust of such length tends to produce a maximum aircraft load factor and the highest values for some important loads such as bending moment and shear force near the root of the wing. For other parts of the aircraft, and particularly those structures for which the effects of flexibility are appreciable, a gust of a different gradient distance can often provide a more severe condition. For this reason the United Kingdom requires that the discrete gust investigation should take proper account of the dynamic amplification of stress that can occur due to flexibility and that the gradient distance of the gust should be varied to find the peak response for each part of the aircraft.

The formula given in 25.341(c) closely approximates the response of an aircraft to the discrete gust prescribed by 25.341(a). Its accuracy depends upon how closely the response of the aircraft agrees with the following assumptions :

(1) The aircraft can be treated as a rigid body.

(2) The aircraft forward speed is constant throughout the event.

(3) The aircraft can rise but cannot pitch.

(4) The unsteady aerodynamic effects can be approximated by the transient lift functions (Kussner and Wagner functions) for infinite aspect ratio.

In the original applications of this formula it was assumed that the lift increments of the fuselage and horizontal tail were negligible in comparison with the wing lift increment. Now it is common for the mass parameter to be based upon a whole aircraft lift curve slope. Loads on each lifting surface are subsequently calculated using the appropriate aerodynamic distributions, but with inertia relief effects based upon the aircraft load factor derived from the formula. Appropriate allowances would normally be made for pitching moment effects by adopting an overall aircraft load solution in which aerodynamic moments are balanced by the aircraft pitching inertia.

For an aircraft which is not conventional in relation to the layout of wing, fuselage and tailplane, or for an aircraft which is equipped with active controls, the simple formula may prove to be unconservative when compared to a more conventional aircraft. In such a case a more rational approach is allowed which solves the equations of motion for the rigid

aircraft to the prescribed gust. The normal approach is to use an aircraft model including just the rigid body degrees of freedom and any required control equations.

In the past, the gust analysis using the simple formula has assumed that the aircraft behaves as a collocation of rigid structures. No allowances were made for the effects of structural flexibility on :-

(1) The lift curve slope of the major aerodynamic surfaces.

(2) The distribution of lift across the span of the major lifting surfaces.

(3) The transient effects of the vibration modes of the structure (dynamic stress response).

For a wing with appreciable sweepback angle, the aero-elastic deformation of the wing under application of air load can result in :-

(1) A reduction in wing lift curve slope.

(2) A change in the span-wise wing lift distribution producing an appreciable inboard movement of the centre pressure on each wing.

(3) An increase in the stress over that resulting from a rigid wing concept due to dynamic stress response effects.

To cover such effects as (a) and (b) above, a quasi-static behaviour of the major aerodynamic surfaces can be assumed. Thus the elastic deformation of the surface is assumed to be in phase with the gust loading with no lift lag. The load distribution and corresponding deformation under load can then be treated in a similar manner to the steadily increasing application of load in the manouevring condition. The transient effects of flexibility are best covered by rational dynamic analysis of each design condition using a mathematical model of the flexible aircraft similar to that demanded for calculation of continuous turbulence loads.

2.3 Continuous Turbulence Requirements

2.3.1 Analytical Structural Modelling

Most forms of structural modelling can be classified into two main categories:

(i) beam modelling

(ii) finite element modelling

Regardless of the approach taken for structural modelling, a minimum acceptable level of sophistication, consistent with the complexity of the configuration under study, is necessary to satisfactorily represent the critical modes of deformation of the primary structure. It would not normally be necessary to include the control surface degrees of freedom unless it is desired to model the effects of an active control system. Wing-pylon mounted engines are often significant in the response to vertical turbulence and warrant particular attention in the modelling of the pylon, and pylon-engine and pylon-wing interfaces. Appropriate stiffness should be reflected in the modelling of aircraft structural components which would exhibit significant changes in stiffness under limit design flight conditions.

Where possible, the correctness of the structural representation should be demonstrated by comparison with the results of a ground vibration test. Appropriate stiffness adjustments can be made to ensure an adequate correlation.

2.3.2 Analytical Aerodynamic Modelling

Aerodynamic modelling for gust response requires the use of unsteady, two-dimensional strip theory or three-dimensional panel theory methods for compressible or incompressible flow. The choice of the appropriate technique depends upon the complexity of the dynamic structural motions and the flight speed envelope of the aircraft.

In order to represent accurately the important rigid body motions, surface aerodynamic data are commonly adjusted by weighting factors in such a way that ensures the aircraft overall stability derivatives are correct. Weighting factors for steady flow (k=0) are usually obtained by comparing aerodynamic wind tunnel test results with theoretical data.

3. REFERENCE

1) H. Murrow, K.G.Pratt and J. Houbolt

NACA/NASA Research Related to Evolution of U.S. Gust Criteria. Paper presented to AIAA 30th SDM.

Figure 1

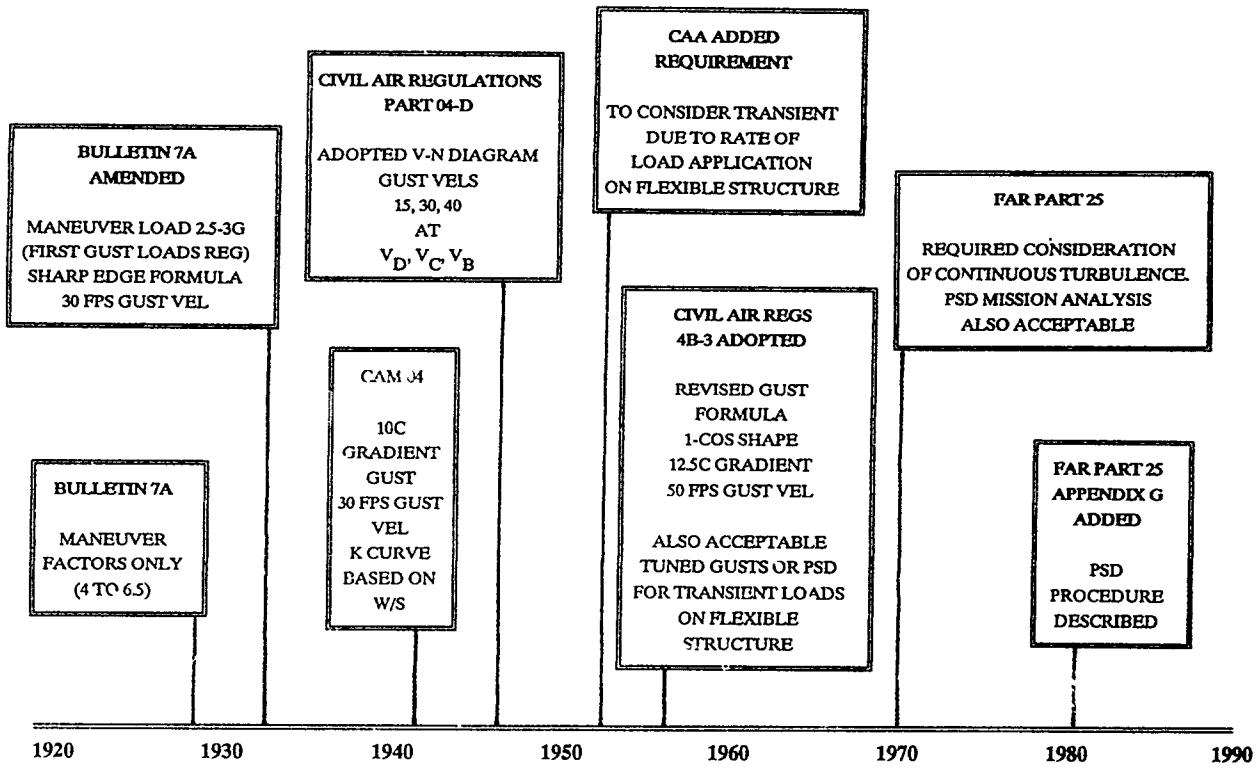

Chronology of federal regulatory gust loads transport design criteria

Figure 2

A SUMMARY OF THE MAIN GUST REQUIREMENTS IN USE IN THE AGARD COUNTRIES

JAR	U.K.National Variant to JAR	FAR	
Pratt Formula OR 12.5 c 1-cos rigid body solution 100% U_{de} AND 12.5 c 1-cos fully dynamic solution 90% U_{de}		Pratt Formula OR 12.5 c 1-cos rigid body solution 100% U_{de}	DISCRETE GUST
	1-cos with varying gradient distance 90% U_{de} fully dynamic solution H**1/3 reduction in gust velocity for gradients below 100 feet in length		TUNED DISCRETE GUST
Design Envelope Analysis with U_{sigma} = 85ft/sec at V_C A reduction in U_{sigma} to a value not below 75 ft/sec is allowed if justified on a rational basis OR Mission Analysis + supplementary Design Envelope Analysis with U_{sigma} = 60ft/sec at V_C All analyses to be fully dynamic solutions	Design Envelope Analysis with U_{sigma} = 85ft/sec at V_C A reduction in U_{sigma} to a value not below 75ft/sec is allowed if justified on a rational basis OR Mission Analysis + supplementary Design Envelope Analysis with U_{sigma} = 60ft/sec at V_C All analyses to be fully dynamic solutions	Design Envelope Analysis with U_{sigma} = 85ft/sec. at V_C A reduction in U_{sigma} to a value of 75ft/sec is allowed if justified by showing dynamic similarity with an aircraft with a satisfactory safety record OR Mission Analysis + supplementary Design Envelope Analysis with U_{sigma} = 60ft/sec at V_C All analyses to be fully dynamic solutions	CONTINUOUS TURBULENCE

U_{de} = 50 feet/sec EAS at V_C and at sea level; where V_C is the aircraft design cruising speed
U_{de} = 66 feet/sec EAS at V_B and at sea level; where V_B is the aircraft design speed for maximum gust intensity
U_{de} = 25 feet/sec EAS at V_D and at sea level; where V_D is the aircraft design diving speed

U_{sigma} = 85 feet/sec TAS (75 feet/sec TAS) at V_C and at sea level
U_{sigma} = 1.32 times the V_C value at V_B
U_{sigma} = 0.5 times the V_C value at V_D

CHAPTER V
GUST DESIGN PROCEDURES

by

H.Lusebrink and **R.Sonder**
Deutsche Airbus GmbH
Department EF3
Box 950109
2103 Hamburg 95
Germany

Table of Contents

List of Illustrations

1.0 Introduction

One of the most important structural design condition for civil and military transport aircraft are the vertical and lateral gust loads, which the A/C experiences, when flying in a turbulent atmosphere.
Complying with US and European Airworthiness Regulations, the A/C - manufacturer has to consider two basic gust concepts or models:

- The Discrete Gust Models
- The Continuous Turbulence PSD - Gust Models

The Discrete Gust Model is the older concept and was developed in the Thirties
During the years of application, the gust shape and intensities changed different times and have now been settled to the well-known truncated 1-cos shape with a constant Gust Gradient Distance (USA/Europe) or a variable one for UK.
The PSD-Methods were developed in the Sixties with the intention to supplement the Discrete Gust Analysis by methods, which take more account of modelling the dynamics of the flexible A/C structure and the real physical behaviour of the atmosphere as a random process.
After a transition phase with extensive international discussions an experience making with the new methods, the PSD-Models became part of the US - FAR 25 and European - JAR 25 Airworthines Requirements. Means-of-Compliances and Gust Intensity Parameters of both the Discrete and the PSD-Methods are provided in the Regulations completely independent of each other and no effort was made, to harmonize or to justify the different turbulence parameters.
However, the A/C-Manufacturer has to apply both the Discrete and one of the PSD-methods and to find out the most critical one for each A/C - component and then to design the structure for the envelope loads.
Application of the PSD-Methods implies, that the Dynamic Model of the A/C is linear and the linear relation between output and input power spectra of a linear system is applicable., In the requirement the turbulence intensity is described by its frequency dependent Power-Spectral-Density and the associated rms-values.
As a consequence or a matter of reason, the Dynamic Gust Load analysis should be performed in the frequency domain by means of Transfer- or Frequency-Response Functions.
The PSD - Methods cannot be directly applied to Non-Linear Dynamic Models, because the Superposition Principle does not hold in this case and Transfer-Functions are not defined
Therefore, approximative methods, based on a linearization of the non-linear system elements or Monte-Carlo-Methods with time-dependent sample signals, which should have the statistical characteristics given in the Requirements, have to be applied. Acceptance of the Airworthiness Authorities will be obtained, if the Linearization Methods provide conservative Design Loads.
If the dynamics of the A/C can be represented by a linear model, the Discrete Gust and PSD-analysis can be commonly treated in the Frequency Plane by determining Load - Transfer Functions in advance to the specific Gust Analysis.
Modern A/C have a variety of automatic control systems The influence of these systems on structural loads due to Discrete Gust and PSD-methods, including their failed and degraded states, has to be investigated
Before we start to describe recent and expected future Gust Load Analysis Methods, we will make the following assumptions:
The rigid body and flexible A/C dynamics can be represented by a *linear* Dynamic Model.
The Dynamic Equations of the Gust Problem and their solution with respect to loads will be presented in both Frequency and Time Plane notation.

Non-Linear dynamic analysis in the time plane will not be considered, because a compact formulation of the Equations of Motion is difficult and each type of Non-Linearity may need its own treatment. Particularly, structural non-linearities would exclude the application of modal methods from the dynamic analysis methods. Therefore, we will restrict the non-linear analysis to application of quasi-linearisation methods for sinosoidal or gaussian random signals in the frequency plane
From the variety of Unsteady Aerodynamic Theories we will select - or have in mind - the 3-dim - Doublet Lattice Method, when writing down the dynamic load equations and knowing furthermore that the Aerodynamic Influence Coefficient Matrix can easily be transformed from the panel-grid to structural nodal points by Matrix Methods. Kernal Function Methods or Modified Strip Theory results may be transformed to panel-force form, similiar to Doublet Lattice results.
Following this way we remain more flexible in structural modelling and are able to provide the Stress Office with Nodal Loads.
When desribing the Gust Analysis Procedures and their practical application, we will presume, that Load Transfer-Functions have already been previously calculated, in order to achieve a compact presentation of the essentials of the gust methods Determination of the Load Transfer Functions will be outlined in a separate chapter
Time Plane Analysis of the Dynamic Gust Problem has to be performed for modern A/C with digital flight control and alleviation systems containing a variety of non-linear elements.
For this purpose, the unsteady aerodynamic forces have to be transformed from the frequency plane to the time plane.
This will be achieved by approximating the elements of the modalised unsteady aerodynamic force matrix by PADE-type approximants, which allow to generate the Delta-pulse response matrix-kernals used in the Convolution Integral representation of the unsteady aerodynamic forces in the time plane.

2.0 Discrete Gust and Discrete Tuned Gust Analysis for Conventional Aircraft

2.1 Present Concepts of Gust Modelling

The Discrete Gust Methods, recently defined in the US and European Airworthiness Requirements, FAR 25 and JAR 25, consists of two variants.

- Discrete Gust - Constant Gust Gradient
- Discrete Tuned Gust - Variable Gust Gradient (UK)

2.2 Discrete Gust Shape

Both methods have in common the truncated 1-cos gust velocity distribution, which reads in space co-ordinates

$$U(x) = \begin{cases} \frac{1}{2} U_{mox} \left(1-\cos(\pi x/H) \right) & \text{for } 0 \le x \le 2H \\ 0 & \text{for } x < 0;\ x > 2H \end{cases}$$

$U(x)$ = Vertical or Lateral Gust Velocity Distribution in Space
x = Penetration Depth (ft)
U_{max} = Maximum Gust Velocity (ft/s)
$H = k \cdot \bar{C}$ = Gust Gradient Distance (ft)
k = factor on $\bar{C}$
$\bar{C}$ = Geometric Mean Chord of the Wing (ft)
$2H$ = Gust Length (ft)

When an A/C, flying with speed V penetrates the front of the space fixed gust field ($x = 0$) with its nose at time $t = 0$, the origin of the A/C Body-Axis geometric reference co-ordinate system at the nose, experiences a time-dependent gust velocity distribution, due to the Galilei-Transform

$$x = V \cdot t$$

yielding:

$$U(t) = \begin{cases} \frac{1}{2} U_{max} (1-\cos(\Omega t)) & \text{for } 0 \le t \le 2H/V = T \\ 0 & \text{for } t < 0 \; ; \; t > T \end{cases} \qquad (1)$$

$\Omega = \pi V/(k\bar{C})$ can be assumed as a fundamental gust 'frequency'
$T = 2H/V$ = Gust Duration Time

Points j of the A/C structure, having the x-coordinates x_j, measured in the A/C geometric system with origin at the nose, pass the gust front $t_j = x_j/V$ times later than the nose.
These points experience the gust velocity:

$$U(t) = \begin{cases} \frac{1}{2} U_{max} [1-\cos(\Omega(t-t_j))] & \text{for } t_j \le t \le t_j + T \\ 0 & \text{for } t < t_j \; ; \; t_j > t + T \end{cases}$$

This time lag effect is typical in a gust analysis of an A/C with finite dimensions, and which is not idealized to a mathematical point with inertia characteristics. Due to the time lag, gust forces of all aerodynamic surfaces are excited successively, according to the penetration depth into the gust field

In the practical Load Transfer Function analysis the time lag effect of the gust field is considered in the harmonical unit angle-of- attack gust field, with the origin ($t = 0$) at the nose:

$$\begin{aligned} U(t,t_j)/V &= \exp(i\omega(t-t_j)) \\ &= \exp(-i\omega x_j/V) \exp(i\omega t) \qquad (2) \end{aligned}$$

(i = imaginary unit)

The 1-cos gust, (front at the nose), is then applied without time lag, according to Eq. (1).

2.3 *Discrete Gust Parameters and Structural Modelling*

Having previously defined the common Discrete Gust Shape, we will now discuss the differences of the two Discrete Gust variants by comparing US and European/UK requirements. The differences mainly concern the gust parameters U_{max}, H and the Dynamic Modelling.

2.3.1 United States - FAR 25.341/351(b)

- **Maximum Gust Velocity (U_{max})**
  U_{max} = 100% U_{de}, where U_{de} is the derived gust velocity according to the Design Speds V_B, V_C and V_D, defined in FAR 25.341(a).

- **Gust Gradient Distance (H = k $\bar{C}$)**
  The gust gradient distance H is constant with factor k = 12 5

- **Dynamic Modelling of the A/C**
  The Manufacturer has the choice to use a rational analysis method and a full flexible dynamic model or to apply formulae of FAR 25.341(c) for Vertical Load Factors and FAR 25 351(b) for the Vertical Tail Loads.
  In any case, Design Gust Speeds U_{de} of 25.341(a) have to be applied and no Dynamic Reduction Factor is allowed to take into account, if a rational analysis together with a Full Flexible Dynamic Model is used by the Manufacturer.

2.3.2 Continental Europe - JAR 25.341/351(b)

+ Special Condition (SC) for a Reduced U_{de}, applied to Airbus A320

- **Maximum Gust Velocity (U_{max})**

  - U_{max} = 100% U_{de},
    with U_{de}, the derived Gust Velocities, defined in JAR 25.341(a), according to the Design Speeds V_B, V_C and V_D for a QUASI - FLEXIBLE DYNAMIC MODEL of the A/C or if Formulae JAR 25.341(c)/25 351(b) are applied.

  - U_{max} = 90% U_{de}, SC-A320-IM-A 3.8 (AMC)
    to be applied with a FULL FLEXIBLE DYNAMIC MODEL of the A/C, with the justification, that the derived gust velocities U_{de} are based on Pratt- or other simple 1-dof Formulae, used to re-calculate gust speeds from measured load factors with no flexible effects included.

  - ROUND-THE CLOCK Gust Model - JAR 25.427 (b),(2)+(3)
    U_{max} = 100% U_{de} or 90% U_{de}, according to the dynamic modelling.
    The maximum gust velocity vector is required to rotate in the plane vertical to the flight path with variable angle (θ).
    Effective vertical and lateral gust speeds are then obtained by

$$U_V(\theta) = U_{max} \sin(\theta)$$

$$U_L(\theta) = U_{mox} \cos(\theta)$$

The critical angle (θ) or the maximum of the superimposed vertical and lateral loads for components out-off the plane of symmetry has to be determined.

- **Gust Gradient Distance ($H = k \bar{C}$)**
  The gust gradient distance H is constant with k = 12 5

- **Dynamic Modelling of the A/C**

  - FULL FLEXIBLE DYNAMIC MODELL
    A Full Flexible Dynamic Modell has the following characteristics: 2-Vertical or 3-Lateral Rigid Body Modes and m Structural Flexible Modes, where m, the number of structural modes has to be chosen that all significant structural degrees of freedom are accounted for and sufficient convergence of loads at all structural components is achieved. Unsteady Aerodynamics has to be taken into account

  - QUASI - FLEXIBLE DYNAMIC MODEL
    A Quasi - Flexible Dynamic Model has the following characteristics: 2-Vertical or 3-Lateral Rigid Body Modes. Structural Flexibility is taken into account by modifying the aerodynamic coefficients and load distributions due to a statically deformed structure. This procedure is equivalent to the method, where quasi-flexible behaviour is derived directly from the Full Dynamic Model by letting the flexible part of structural accelerations and velocities approach to zero, followed by a subsequent reduction of the Full Dynamic Model to Rigid Body modes only.
    The reduction method is outlined in Chapter "Quasi-Flexible Dynamic Model" on page V-38

2.4 Discrete Tuned Gust Requirement

2.4.1 United Kingdom (UK) - JAR 25.341 G (d) - National Variant

Status: JAR 25 - Change 12
The basic difference of the UK Discrete Tuned Gust and the European Discrete Gust method is the variable Gust Gradient Distance H.
Short Gust Gradients are associated with energy concentration in the high frequency band and vice versa.
Consequently, the Maximum Gust Speed U_{mox} must be shaped by a function of the Gust Gradient Distance due to the physics of turbulence energy distribution.

- **Maximum Gust Velocity $U_{mox}(H)$**
  The maximum gust velocity for the Discrete Tuned Gust is defined as a function of the Gust Gradient Distance H.
  The current 'Shaping Law' below can be used as a Means-of-Compliance, having in mind that

it may change, if better knowledge of Gust Speed distribution versus Gust Gradient is available.

$$U_{max}(H) = \begin{cases} 0.9\, U_{de}\, (H/H_{ref})^{1/3} & \text{for } H \le H_{ref} \\ 0.9\, U_{de} & \text{for } H > H_{ref} \end{cases} \qquad (3)$$

$$\text{with } H_{ref} = 100 \text{ ft}$$

Note: The Shaping Law Eq (3) reflects the Discrete Tuned Gust Requirement status of March '89. Joint international discussions on the subject of Discrete Gust Requirements between Airworthiness Authorities and Manufacturers may lead to a revision of the Shaping Law.

- **ROUND-THE-CLOCK Gust Model - JAR 25.427 (b),(2)+(3)**
  U_{max} = = > $f(H/H_{ref})$, according to Eq. (3)
  The maximum gust velocity vector U_{max} is required to rotate in the plane vertical to the flight path with variable angle (θ).
  Effective vertical and lateral gust speeds are then obtained by

$$U_V(\theta) = U_{max} \sin(\theta)$$
$$U_L(\theta) = U_{max} \cos(\theta)$$

  The critical angle (θ) or the maximum of the superimposed vertical and lateral loads for components out-off the plane of symmetry has to be determined.

- **Gust Gradient Distance (H)**
  The gust gradient distance has to be varied each side of $H = 12.5\, \bar{C}$ and the following range of Gust Gradients may be used as a Means-of-Compliance:

$$30 \text{ ft} \le H \le 350 \text{ ft}$$

- **Dynamic Modelling of the A/C**
  The dynamic model of the A/C to be used with the Discrete Tuned Gust Method is the Full Flexible Dynamic MODEL defined above.

2.5 *Analysis of Discrete Gust Loads*

Discrete Gust Load analysis is performed under the assumption, that a set of Vertical and Lateral Frequency Response Functions $H_i(\omega)$ of Load Quantities $i = 1,L$ for all critical mass and flight conditions is available.

Determination of these Load Frequency Response Functions due to a harmonical gust field, according to Eq. (2) will be provided later in chapter "Determination of Load Frequency Response Functions" on page V-22

From Linear Systems Theory it is known, that the output amplitude spectrum of an interesting system quantity $y(\omega)$ due to an arbitrary input amplitude spectrum $x(\omega)$ is obtained by the convolution product in the Frequency Plane .

$$y(\omega) = H_y(\omega)\, x(\omega)$$

$x(\omega)$ = Fourier Transform of input signal x(t), assumed to exist

$y(\omega)$ = Fourier Transform of output signal y(t)

$H_y(\omega)$ = Frequency Response Function of quantity y.

Introducing Reduced Frequencies k, for which Load Frequency Response Functions are usually provided, and normalised time t':

$$k = \omega L_{ref}/V \quad ; \quad t = V/L_{ref} \cdot t'$$

$$\omega t = k t'$$

e.g. $L_{ref} = c/2$

with c = a reference chord of the wing

Specializing the above relation to the Discrete Gust problem, we obtain the vector of incremental gust load spectra:

$$\Delta L_i(k) = H_i(k)\, U(k)/V$$

$i = 1,L$ Load Quantities

$U(k)/V$ = Fourier Transforms of 1-cos gust angle-of-attack distribution due to the actual Gust Design Speeds, mass and flight conditions.

$$U(k)/V = -(U_{max}/2V)\,(i/k)\,\frac{1 - \exp(-2ikH/L_{ref})}{1 - [\,H/(\pi L_{ref})\,k\,]^2}$$

i = imaginary unit

$H_i(k)$ = Frequency Response Vector of Load Quantities (i) due to a vertical and lateral harmonic field of unit gust angles-of-attack (U/V = 1).

$\Delta L_i(k)$ = incremental Load Spectrum Vector of Quantities (i)

2.6 *Discrete Gust Design Loads*

Converting $\Delta L_i(k)$ to the Time Plane by means of the Inverse Fourier Transform, yields the time history of the incremental Discrete Gust Loads $\Delta L_i(t')$:

$$\Delta L_i(t') = Re\,[\,1/\pi \int_0^{\infty} \Delta L_i(k) \exp(ikt')\, dk\,]$$

Adding the corresponding 1g-Loads, yields the Total Load Time History:

$$L_i(t') = L_{i,1g} + \Delta L_i(t')$$

Envelope Design Loads of quantity (i) are obtained by searching the absolut maximum values, first

in the time history and secondly with respect to the investigated critical load cases (j):

$$L_{i,design} = \max_j [\, \max_t L_i(t') \,]$$
$$i = 1,L \; ; \; j = 1,J$$

2.7 *Round-the-Clock Gust Design Loads*

In order to derive the critical Round-the-Clock Gust Loads, we assume that incremental vertical $\Delta L_{Vi}(t')$ and lateral discrete gust loads $\Delta L_{Li}(t')$ have been previously determined.
Round-the-Clock Gust loads will then be obtained by superposition, according to the following relation:

$$\Delta L_{RC,i}(t',\theta) = \Delta L_{Vi}(t') \sin(\theta) + \Delta L_{Li}(t') \cos(\theta) \qquad (4)$$

Differentiating Eq. (4) with respect to θ and letting the result to be zero, yields the solution of incremental Round-the-Clock Gust loads :

$$\Delta L_{RC,i}(t') = \pm [\, \Delta L^2_{Vi}(t') + \Delta L^2_{Li}(t') \,]^{1/2}$$

Adding the corresponding 1g-Loads yields the Total Load Round-the-Clock Time History :

$$L_{RCi}(t') = L_{i,1g} \pm [\, \Delta L^2_{Vi}(t') + \Delta L^2_{Li}(t') \,]^{1/2}$$

Round-the-Clock Envelope Design Loads of quantity i are obtained by searching the absolute maximum values, first in the time history and secondly with respect to critical load cases j:

$$L_{RC,i,design} = \max_j [\, \max_t L_{RC,i,j}(t') \,]$$
$$i = 1,L \; ; \; j = 1,J$$

2.8 *Future Concepts of Gust Modelling*

Time-plane methods will be increasingly applied in the future for Gust Load analysis of flexible A/C in order to enable adequate modelling of aerodynamic, structural and system non-linearities and to obtain phased loads in natural way.
As a consequence of a more sophisticated modelling of the A/C dynamics, the models of atmospheric turbulence should be reviewed correspondingly
There are two possibilities to create a gust velocity time history representing a patch of severe turbulence more realistically than the current 1-cos shape does.

- Generation of an artificial random gust velocity signal having prescribed statistical characteristics, like probability density distribution, power spectral density function and the associated rms-value of turbulence intensity.

- Definition of a deterministic mathematical function representing more adequately the positive and negative gust speed fluctuations in a short patch of high turbulence energy concentration, having a maximum derived gust velocity U_{de}

Both models should be provided with an appropriate spanwise variation of gust intensities.
The current 1-cos shape with spanwise constant gust velocity distribution is a very simplified approximation of one peak of the patch with maximum gust intensity. Measurements of severe turbulence encounters often show a sequence of peaks with high positive and negative gust speeds.
According to the second deterministic approach above, this type of gust pattern could be modelled by a truncated but multi-periodic sine-function, representing the positive and negative peak alternations.
The amplitudes of the sine-function could be shaped and adjusted relative to a maximum one by appropriate modulating functions. (i e. exponential functions, polynominals) By means of these modulating functions a variety of Discrete Gust models with increasing or decreasing peak amplitude characteristics or a combination of both could be created. The frequency of the sine-function should contain a tuning parameter in order to obtain critical load responses of the various structural components.
The maximum amplitude U_{de} of this new Discrete Gust model must be shaped similar to the current 1-cos Discrete Tuned Gust method by a function of the tuning parameter to take into account the decreasing power density characteristics of the turbulence with increasing frequency.
Finally, a derived maximum gust velocity U_{de} as a function of altitude must be defined for the new model on the basis of operational measurements.
At this point we are faced with a difficult practical problem:
Any proposal for a new gust model and its influence on the structural loads level must be compared with the existing gust models and their parameters in the current requirements, in order to assure that recent safety standards are not eroded or, on the other hand, the improved gust model does not make the requirements over-severe.
For this purpose, a criterion is required to compare existing and new gust models.
A simple criterion to compare two Discrete Gust models might be the ratio of their energy contents represented by the mean-square values of gust intensity.
The maximum gust velocity amplitudes for both models have to be normalized for this comparison
To illustrate the criterion we consider the follwing simple

Example:

Assume it is intended to replace the current 1-cos shape by a truncated sine-shape of the same length.
What is the adequate U_{de} for the sine-gust?

Applying the energy criterion, we have to determine the mean-square values for both gust shapes, yielding:

1-cos shape: ⅜
sine shape: ½

Relating the 1-cos result to the sine result, we obtain the ratio ¾ meaning that the normalized 1-cos gust contains only 75% the energy of the normalized sine-gust or in other words. The normalized sine-gust feeds 33% more energy into the A/C structure than the 1-cos gust model does. Consequently, to obtain the appropriate U_{de} for the sine-gust model with equal total energy content, the 1-cos U_{de} has to be scaled by the square-root of ¾:

$$U_{de,sine} = 0.866\ U_{de,1-cos}$$

Due to the different amplitude spectra (Fourier Transforms) of the normalized truncated sine- and 1-cos gust shapes, the different distributions of the same total energy in the rigid body and flexible modes of the A/C will generate differing load responses, a required effect of the model change

3.0 Continuous Turbulence Analysis for Conventional Aircraft

3.1 Present Concepts of PSD - Random Gust Analysis

The Continuous Turbulence (PSD-) Analysis, recently defined in the US and European Airworthiness Requirements and supplementing the Discrete Gust Methods, consists of the following two variants:

- Design Envelope Analysis
- Mission Analysis

In the Frequency Plane, both methods are based on the relation (9) between the Power Spectra of output and input of a linear dynamic system, exited by random signals.

3.1.1 Turbulence Power-Spectral-Density Function

Similar to the Discrete Gust Analysis, both variants above have a common gust intensity distribution function, the 'Power-Spectral-Density' Function of the atmospheric turbulence.
PSD - Functions represent the distribution of mean-square values of the sinosoidal or harmonical components of a random time-dependent signal of a physical quantity, where the frequency is assumed to vary continuously.
While the Discrete Gust Methods are based on a highly idealized space- or time-dependent gust velocity distribution of 1-cos shape, there is no equivalent random gust time history available or defined in the requirements for Continuous Turbulence Analysis.
Although it is principally possible to generate such samples of artificial time-dependent random gust intensity signals with prescribed statistical characteristics, which would be sometimes preferable for reliable analysis of highly non-linear systems, random processes are usually described by means of statistical parameters and functions, like

- Probability Density Distributions
- Mean- and Mean-Square Values
- Power-Spectral Density Functions, etc.

Power-Spectral-Density Functions are defined in the Frequency Plane and usually derived from sample measurements of time-dependent random signals. An analytical form of the PSD - Function may be found by adapting the parameters of a mathematical PSD - Model by a curve fitting procedure.

3.1.2 The V. Karman Power Spectrum

In both the US-FAR 25 and EUROPEAN-JAR 25 Continuous Turbulence Requirements, the analytical form of the Power-Spectral-Density Function, which has to be used in the above Random Gust Analysis Methods is the V. KARMAN Spectrum:

$$\Phi(\Omega) = \frac{\sigma^2 L}{\pi} \frac{1 + {}^{8}/_{3} (1.339\, \Omega\, L)^2}{[\, 1 + (1.339\, \Omega\, L)^2 \,]^{11/6}} \qquad (5)$$

$\Omega = \omega/V$ (1/ft) = Spatial Frequency
L = 2500 ft = Turbulence Scale Length
σ^2 = Mean Square Value of Turbulence $(ft/s)^2$

3.1.3 Transformation of the v.Karman Spectrum to Other Reduced Frequencies

In the practical analysis, the reduced frequencies of the v Karman Spectrum are usually not compatible with the Reduced Frequencies of the dynamic analysis. This has to be brought in line by transforming the v. Karman-reduced-frequencies to those, used in the Dynamic Gust Analysis:

$$k = \Omega\, L_{ref} \qquad (6)$$

The spatial frequency Ω will be the invariant in this transformation
Differentiating Eq. (6) with respect to k yields

$$d\Omega = 1/L_{ref} \cdot dk \qquad (7)$$

Introducing Eq. (6) and Eq. (7) into the v. Karman Spectrum Eq. (5) and intending to do the integration to obtain the rms-value with respect to k, yields:

$$\Phi(k) = \frac{\sigma^2}{\pi} \frac{L}{L_{ref}} \frac{1 + {}^{8}/_{3} [\, 1.339\, (L/L_{ref})\, k \,]^2}{\{\, 1 + [1.339\, (L/L_{ref})\, k]^2 \,\}^{11/6}} \qquad (8)$$

This form of the v. Karman Spectrum will be applied in the Random Gust Load Analysis, where Load Frequency Responses are provided as functions of k.

3.1.4 The Random Gust Parameters and Structural Modelling

Beside the common v Karman Power Spectrum the other gust parameters defined in the Requirements for Design Envelope Analysis and Mission Analysis are rather different from each other, so that we prefer to discuss them in the context of Random Gust Design Load Analysis
The Dynamic Model of the A/C to be used with the Random Gust Design Load Analysis is the Full Flexible Dynamic Model, already defined in the Discrete Gust Section.

3.2 *Analysis of PSD - Random Gust Design Loads*

3.2.1 Basic Relations

Similar to the Discrete Gust Analysis, Load Frequency Response Functions $H_i(k)$ are also reqired for the Random Gust Analysis methods.

For both PSD-Methods, we will make use of the scalar relation between input and output Power Spectra of a stable linear system, excited by a random input signal having the input Power Spectrum $\Phi(k)$

$$\Phi_y(k) = |H_y(k)|^2 \, \Phi(k) \qquad (9)$$

$\Phi(k)$ = Input Power Spectrum of x(t), v. Karman

$\Phi_y(k)$ = Output Power Spectrum of y(t)

$H_y(k)$ = Frequency Response Function of system quantity y

The above relation can be extended to Transfer Function vectors containing different dynamic load quantities i = 1,L

In this case we write:

$$\Phi_{ik}(k) = H_i(k) \, H_k^{*T}(k) \, \Phi(k) \qquad (10)$$

$$i,k = 1,L$$

With $H^{T*}_i(k)$ the transposed conjugate complex vector of $H_i(k)$ and $\Phi(k)$, the v. Karman Spectrum (8). The resulting complex matrix Φ_{ik} contains the Auto-Power Spectra in the diagonal and the complex Cross-Power Spectra in the off-diagonal elements. The Cross-Power Spectra are later used to determine correlated (phased) loads.

Integrating Eq. (10) with respect to the Reduced Frequency k yields the means square values on the diagonal and $\rho_{ik} \, \sigma_i \, \sigma_k$ in the off-diagonal elements.

$\rho_{ik} = \rho_{ki}$ = Correlation Coefficient between load item i and k

$$\sigma^2_{ik} = \mathrm{Re} \left\{ \int_0^\infty H_i(k) \; H^{*T}_k \, \Phi(k) \, dk \right\}$$

$$i,k = 1,L$$

Assembling the mean-square values on the diagonal in a new vector, taking the square-root and assuming $\sigma^2 = 1$, or $\sigma^2/V^2 = 1$, we obtain the RMS Unit Responses, the 'A-Values'.

$$A_i = \left\{ \int_0^\infty |H_i(k)|^2 \, \Phi(k) \, dk \right\}^{1/2} \qquad (11)$$

The A-Unit load Responses are fundamental quantities to be used with the PSD-Design Methods. For the PSD-Mission Analysis, we need additionally the A-value of the derivative of the Load Quantity i, called here 'Ã-value', to determine the number of zero-level crossings of the i-th Load Quantity per unit time :

$$\tilde{A}_i = \left\{ \int_0^\infty k^2 \, |H_i(k)|^2 \, \Phi(k) \, dk \right\}^{1/2} \qquad (12)$$

Note: If the integral in Eq. (12) does not converge, apply the Houbolt-Break-Off Criterion, also called the 'Knee-Criterion':

Stop the integration of Eq. (12) at that upper frequency limit, where convergence of Eq. (11) is achieved

3.2.2 Design Envelope Analysis Method (DEA)

FAR 25 / Appendix 'G' - (b)
JAR 25 / ACJ 25.305(d) - 2.2

As far as the investigation of critical load cases is concerned, The concept of Design Envelope Analysis is very similar to the Discrete Gust approach.
For a set of critical mass conditions, design loads of all structural components of the A/C are to be determined within the Flight Envelope and on its boundary, according to the Design Speeds V_B, V_C and V_D.
Similar to the Discrete Gust Methods, Design Gust Intensities RMS-values U_σ are provided in the rules and associated to the above Design Speeds dependend on the altitude.

DEA - Design Gust Intensities

Both the US-FAR 25 App G and the EUROPEAN-JAR 25.ACJ 305(d) regulations define two different sets of Design Gust Intensities (U_σ) with different distributions versus altitude.

- U_σ (basic) = 85 ft/s (TAS) at V_C
- U_σ (reduced) = 75 ft/s (TAS) at V_C

The A/C manufacturer is allowed to apply the reduced U_σ = 75 ft/s only under certain conditions, which are also defined in the requirements.
These conditions and their associated Means-of-Compliances are the only item, where FAR 25 and JAR 25 Continuous Turbulence requirements deviate from each other.

FAR 25.App-G (b)(3)(i)(1); U_σ = 75 ft/s - Conditions:
The actual A/C to be certified must be comparable to a similar design with extensive satisfactory service experience
When assessing comparability, the following factors have to be taken into account:

- The typical mission of the new airplane is substantially equivalent to the similar design.
- The transfer function of the new design should exhibit no unusual characteristics as compared to the similar design, which significantly affect response to turbulence
- The similar design should demonstrate the adequacy of the U_σ selected.

JAR 25.ACJ 305 (d) - 75 ft/s Conditions
ACJ 25.305(d) - 2.2.3-a.-ii:
Compared to the previous FAR 25.App G conditions, the corresponding JAR 25 ACJ 305(d) text is kept more general

> U_σ values less than those specified in sub-paragraph (a. i.) may be used where the applicant can show by rational means that the gust velocity selected is adequate for the aeroplane being considered. However, the U_σ values used may not be less than 75 ft/s (22.86 m/s) .....

As 'rational means' European Airworthiness Authorities will accept:

- Extensive satisfactory service experience
  and
- A comparison of design load levels of all structural components due to a 75 ft/s - DESIGN ENVELOPE ANALYSIS
  with
  a MISSION ANALYSIS of typical missions, showing a satisfactory agreement or the 75 ft/s - DEA results to be conservative.

DEA - Design Loads

Similar to the Discrete Gust Analysis, a set of critical load cases of mass and flight conditions must be defined.

By means of the previously derived A-values of interesting Load Quantities, like Shear, Bending and Torque, at a number of structural stations, we may define a vector of A's, containing all critical load cases.

The incremental DEA - Design Loads are then obtained by multiplying the A_i-vector with the U_σ/V-values for V_B, V_C and V_D, according to the requirements :

$$\Delta L_i = A_i \, U_\sigma/V \qquad \text{(RMS)}$$

Total Limit Loads:

$$L_i = L_{i,1g} + \Delta L_i \qquad \text{(RMS)}$$

Envelope Design Loads of the most critical Load Quantities are obtained by searching the maximum of all calculated critical cases j:

$$L_{i,design} = \max_j(L_{i,j}) \qquad \text{(RMS)}$$

$$i = 1,L \; , \; j = 1,J$$

3.2.3 The MISSION ANALYSIS Method (MA)

FAR 25 / Appendix 'G' - (c)
JAR 25 / ACJ 25 305(d) - 2.3

Determination of the Mission Analysis Design Loads is fundamentally different from the Discrete Gust and PSD - Design Envelope Analysis procedures

While the latter ones investigate distinct points within the Flight Envelope and on its boundary, according to the Design Speeds V_B, V_C and V_D for critical mass and c.g. - conditions, ranging from minimum to maximum flying weights, does the PSD - Mission Analysis take into account actual or most probable utilisation of the A/C, considering suitably chosen operational mass conditions.

To comply with the rules, the manufacturer has to investigate different typical missions, varying in total flight times, cruising speeds, altitudes, take-off weights and their associated mass distributions.

Additionally to the Mission Analysis, the manufacturer has to perform a Supplementary Design Envelope Analysis (SDEA) (FAR 25 / Appendix 'G'-d ; JAR 25 / ACJ 25.305(d) - 2.4) with U_σ = 60 ft/s (TAS) at V_C and correspondent gust intensities for the other Design Speeds, to establish a floor level of design loads.

The typical mission can be roughly partitionned into following Flight Phases:

- Take-off and Initial Climb
- Acceleration and Climb to Cruising Altitude
- Cruise
- Descent and Deceleration
- Holding and Final Approach

Dynamic Analysis and calculation of Design Loads is carried out in following steps:

- Sub-divide the Flight Phases of the mission into segments of incremental duration time (t_j ; $j = 1,J$)
- Calculate the normalised incremental duration time of each segment j:

$$t'_j = t_j / T_m$$

$$T = \text{Mission Duration Time}$$

- Assume the mass and flight conditions in a segment as constant.
- Calculate $A_{i,j}$ and $\tilde{A}_{i,j}$-RMS unit-responses of Load Quantity $i = 1,L$ of the segment conditions $j = 1,J$ by means of equations (11) and (12).
- Calculate the number of zero-level crossings per flight hour of Load Quantity i in segment j:

$$N_{0,i,j} = (1800/\pi)\,(V_j/L_{ref})\,\tilde{A}_{i,j}/A_{i,j}$$

$$i = 1,L;\ j = 1,J$$

V_j = Flight Speed in segment j.
$A_{i,j}$ = A_i in flight segment j.
$\tilde{A}_{i,j}$ = $\tilde{A}_i$ in flight segment j.

3.2.4 Mission Analysis Design Loads

Determine PSD - Mission Analysis Design Loads from the Exceedance Rate Formula (13) by solving the non-linear equation for L_i at $N_{i,design} = 2 \cdot 10^{-5}$/h with

$$N(L_i) = \sum_j \{\, t'_j N_{0,i,j} [\, P_{1,j} \exp(-\Delta L_{i,j}/(b_{1,j} A_{i,j})) + P_{2,j} \exp(-\Delta L_{i,j}/(b_{2,j} A_{i,j})) \,] \,\} \qquad (13)$$

and

$$\Delta L_{i,j} = | L_i - L_{i,j,1g} |$$

Most critical Envelope Design Loads of quantities i are obtained by searching the absolute maximum of the individual design loads of M missions:

$$\Delta L_{i,design} = \max_m (L_{i,m})$$

$$m = 1,M$$

Note: Parameters $P_{1,j}$, $P_{2,j}$ and $b_{1,j}$, $b_{2,j}$ for Non-Storm and Storm Turbulence patches as function of flight conditions in segment j have to be taken from the corresponding curves, provided in the rules.

3.3 Design Load Correlation Procedure Applicable to Design Envelope Analysis

The PSD - Random Gust methods as currently defined in the requirements, only say how to derive seperate max. RMS responses for single distinct load quantities like Shear, Bending and Torque at a certain structural component

No information is provided, how to establish correlated or phased loads at other stations or for other associated load quantities.

For Discrete or Deterministic Gust methods, this phasing is automatically provided by means of the time histories.

At a certain time increment $t = t_{x,max}$, where a load item x takes it absolute maximum, all other associated load information is available.

In the PSD - Analysis, where input and output signals of a system are described by means of RMS-values, Power-Spectral-Densities and Joint Probability Density Distributions, phasing information must be derived from the complex-valued Cross-Power-Spectral Density Function of two dynamic quantities.

If additionally the Probability Density Distribution of the random gust field can be assumed as Gaussian, a multi-dimensional Gaussian Joint-Probability-Density Distribution of load quantities can be established. A constant 'Design Probability' then defines a multi-dimensional 'Design Ellipsoid' of Equal Probability, whose radius is equal to U_σ.

Each point on this ellipsoid defines a set of correlated loads.

In the case, where we are interested in getting phased loads only at those points, where the different load quantities take their maximum values A, for $U_\sigma = 1$ or $U_\sigma/V = 1$, a simpler procedure may be applied, without making assumptions for particular gust Probability Density Distributions.

This procedure will now be outlined and shown simultaneously that the so determined set of loads are phased and balanced.

Starting with the equilibrium condition of the dynamic forces $F_i(k)$, obtained from Eq. (32), of a free-free A/C structure, for all Reduced Frequencies k and one critical load case:

$$\Psi_{ri}^{T} F_i(k) = 0 \qquad (14)$$

$$r = 1,R;\ i = 1,N$$

R = Number of Rigid Body Degees-of-freedom

Ψ_{ri}^{T} = Transpose of the Rigid Body Part of the Modal Matrix

N = Number of degrees-of-freedom

In the next step, Eq (14) is post-multiplied by the product of the transposed conjugate-complex force/moment vector $F^{*}{}_{k}{}^{T}(k)$ and the v. KARMAN Spectrum $\Phi(k)$.
Subsequent integration with respect to k yields

$$\Psi_{ri}{}^{T}\ \mathrm{Re}\ \{ \int_{0}^{\infty} F_{i}(k) F^{*}{}_{k}{}^{T}\ \Phi(k)\ dk \} = 0$$

$$i,k = 1,N$$

where the sequence of summation i and integration has been interchanged.
The matrix under the integral sign contains the Cross- Power Spectral Densities in the off-diagonal elements and the Auto-Power Spectra of the forces/moments on the diagonal.
Carrying out the integration, yields

$$\Psi_{ri}{}^{T}\ A^{2}{}_{F,ik} = 0$$

$$i,k = 1,N$$

with

$$A^{2}_{F,ik} = \begin{array}{|c|c|c|} \hline & & \\ F_1^{\,2} & F_2\ F_1\ \rho_{12} & .. \\ \hline F_1\ F_2\ \rho_{21} & F_1^{\,2} & ... \\ \hline F_1\ F_3\ \rho_{31} & F_2\ F_3\ \rho_{32} & F_3^{\,2} \\ \hline \vdots & \vdots & \vdots \\ \hline \end{array}$$

and F_i = A-values of dynamic forces/moments

Decomposition of the matrix $A^{2}{}_{F\,ik}$ into a product of a matrix $A_{\varphi,im}$, containing the phased loads, and a diagonal matrix F_{mk}, containing F-values, and which does not influence the equilibrium condition, yields finally with

$$A^{2}{}_{F\,ik} = A_{\varphi,im}\ F_{mk}$$

$$\Psi^{T}{}_{ri}\ A_{\varphi,im} = 0 \qquad (15)$$

$$k,i,m = 1,N$$

where

$$A_{\varphi,im} = \begin{array}{|c|c|c|c|} \hline & & & \\ F_1 & F_1\,\rho_{12} & F_1\,\rho_{13} & \cdots \\ \hline F_2\,\rho_{12} & F_2 & F_2\rho_{23} & \cdots \\ \hline F_3\,\rho_{13} & F_3\,\rho_{23} & F_3 & \cdots \\ \hline \vdots & \vdots & \vdots & \vdots \\ \hline \end{array}$$

Correlation Coeff. $\rho_{im} = \rho_{mi}$

The columns of matrix $A_{\varphi,im}$ contain the phased loads, associated to $F_1, F_2, F_3, \ldots$ determined by means of the corresponding correlation coefficients ρ_{im}
Simultaneously, it is shown by Eq (15) that the phased loads are balanced.

4.0 Determination of Load Frequency Response Functions

In the previous chapters, Load Frequency Response Functions (or Load Transfer Functions) have been successfully used as a powerful tool to derive design loads for special Discrete Gust shapes and PSD - Random Gusts as well. Due to the fact, that they are fundamental solutions with respect to a harmonic gust field, the same Load Transfer Functions can be applied to derive Discrete or PSD - Gust loads for different other gust shapes or Power Spectra In this section of Gust Analysis the determination of Load Transfer Functions will be outlined

4.1 Dynamic Modelling of the Flexible Aircraft

4.1.1 Co-ordinate Systems

Before the local Design Loads of the A/C structure can be evaluated, the dynamic deformation field under external gust loading must be determined.
In order to set up the corresponding equations of motion, adequate co-ordinate systems for different purposes have to be defined.
Three basic co-ordinate systems must be considered.

- the Inertial Earth-Fixed System
- the A/C - Body-Fixed System
- the Modal Co-ordinate System

The motion of the Body-Fixed co-ordinate system relative to the Inertial System is called 'Rigid

Body Motion', and may have principally six degrees-of-freedom. The dynamic deformation field of the structure is described in the Body-Fixed co-ordinate system, whose origin may be placed at 25%-AMC and not necessarily be attached to the Center-of-Gravity. This choice has the advantage, that the Rigid Body aerodynamic coefficients need not be re-tranformed, if different mass and C.G. positions are to be investigated.

There are principally two alternatives to describe the Rigid Body Motion:

- as small deviations from a steady state reference condition (e.g. Level Flight) in the Inertial Frame. (Structural Dynamics)
- or in the moving (rotating) Body-Fixed axis system. (Flight Mechanics)

In the latter case, translations and rotations of the Body-Fixed co-ordinate system relative to itself have no meaning, therefore the rigid body part of the equations of motion to has be set up in velocity - co-ordinates, as it is normally done for Flight Mechanic studies.

Additionally, caused by the rotating reference frame, apparent centrifugal, gyroscopic and gravitational forces/moments appear, which have to be taken into account in the Dynamic Model.

For the reason of compact and unique presentation of the equations of motion, we will prefer here to use the Inertial Frame version.

It was previouisly mentioned, that the structural deformation field is measured in the Body-Fixed co-ordinate system.

This is not in any case quite correct, because there may be a variety of local or component related systems, offset and rotated against the global Body-Fixed Frame, which might be found more adequate to describe the dynamic deformation field, due to the fact that mass and stiffness properties are often related to those local systems.

We will not go into too much detail here, since it is a well-known fact, that the Aeroelastician is always forced to process large datasets, coming from different sources and referring to different co-ordinate systems Therefore, he is prepared to establish suitable matrices to transform the data into that reference systems, he wishes to work with Also other linear operations, like interpolation or integration can easily handled by such operator matrices.

4.1.2 The Modal Co-ordinate System

Finally, it is necessa to discuss a special co-ordinate system, which has become a classical tool to solve structural dynamic problems: 'The Modal or Generalised Co-ordinate System'

Although initially introduced to solve Partial Differential Equations by reduction to a system of Ordinary Different. l Equations, it is also a powerful method to solve economically high-degree-of-freedom discrete dynamic problems, by expanding the modal displacements in terms of modal deflections

In order to discuss the Modal Co-ordinates, we will introduce the concept of Eigenvectors of a flexible structure already here, although they are formally derived later in the Structural Modelling' chapter.

The Eigenvectors of a conservative free-free flexible structure, including Rigid Body Modes, where all external and damping forces are removed, are distinct dynamic deformation states, moving with their associated Eigenfrequencies. In each of these 'modes', all structural points will oscillate with the same phase.

Since the Eigenvectors are linearly independent of each other, they can be used as basis (unit) vectors of an abstract vector space, the 'Modal Space'.
It can be shown by long experience in structural dynamics, that the dimensions of the Modal Space - number of Eigenvectors used in the analysis - need to be much lower than the original vector space of the physical degrees-of freedom to solve the dynamic problem with sufficient accuracy, if the external force field fulfills certain conditions.
The energy of the external forcing field should be concentrated in the lower frequency band and approach zero with increasing frequency.
To give an idea of the effectiveness of the modal approach, one can state that roughly 1/10 of the number of physical degrees-of-freedom have to be applied for the Modal Space to achieve sufficient accuracy for Vertical and Lateral gust loads
Needless to say that the modal approach is a very economic and efficient method to structural dynamic problems.

4.1.3 Forces and Moments

Two basic types of dynamic forces can be identified for a flexible A/C flying in turbulent atmosphere·

- The external aerodynamic forces, generated by the Gust field, Structural motion and Gravitation.
- The internal forces, as there are Inertia, Elastical, Structural and Artificial Damping forces, as well as Centrifugal and Gyroscopic forces/ moments

The predominant part of all these forces are continuously distributed over the A/C structure.
The objective of the dynamic modelling is to represent this force and deformation field by a finite set of suitably arranged grid points, whose associated degrees- of-freedom should approximate the deformation field in a best way.
External and internal forces are then subsequently condensed or lumped to the grid point's degrees-of-freedom

4.1.4 Structural Modelling

For Structural modelling as understood here, only the mass and stiffness properties of the structure are taken into account. Aerodynamic, structural and artificial damping forces are neglected at this time.
Recently available Finite Element Structural Analysis Software eases the modelling work significantly by providing a variety of nice tools, which can be applied in a flexible manner to different dynamic problems.
The main steps of the Structural Modelling procedure are listed below:

- Select appropriate global and local co-ordinate systems
- Identify symmetry properties of the the structure to reduce the number of degrees-of-freedom (½ A/C).
- Define a set of grid points with associated degrees-of-freedom to approximate the deformation field in an optimal way.
- From an economical point of view use beam-modelling where ever possible

- Take special care of those degrees- of-freedom, who can generate significant aerodynamic and inertia forces.
- Make sure that components like wing and horizontal tailplane with high aspect ratio can perform in-plane motions.
- Model 6-degrees-of-freedom for concentrated masses like engines, APU's, etc.
- Use condensed FE stressing- stiffness matrices for attachement and transition areas of two or more components.
- Generate the global A/C free-free stiffness matrix by coupling the component stiffness matrices.
- Define a set of critical mass and c.g. conditions with varying distributions of payload and fuel, according to the requirements
- Generate the inertia matrices by lumping the distributed structural, payload and fuel masses to the degrees-of-freedom of the grid points.
- Determine the Natural Frequencies and Eigenvectors of the free-free conservative A/C structure for all critical mass conditions.

4.1.5 Determination of Natural Frequencies and Eigenvectors

In a conservative dynamic problem the sum of inertia and elastical forces is equated to zero.

$$m_{ij}\ddot{v}_j + k^s_{ij}v_j = 0 \qquad (16)$$

$$i,j = 1,N$$

v_j = N-dimensional deformation vector, containing grid points implicitly. Ordering of d.o.f may be due to practical conciderations.

m_{ij} = N·N-dimensional mass matrix

k^s_{ij} = N·N-dimensional free-free (singular) stiffness matrix. Singularity is of order R, according to the number of Rigid Body Modes, including control surface motions.

In order to solve the homogeneous differential equation (16), we try a harmonic solution .

$$v_j(t) = \psi_j \exp(i\Omega t) \qquad (17)$$

Introduction of Eq. (17) in Eq. (16), yields the associated algebraic eigen-value problem:

$$[-\Omega^2 m_{ij} + k^s_{ij}]\psi_j = 0 \qquad (18)$$

With the new unknowns Ω, the Eigenfrequencies and ψ_j, their associated Eigenvectors FE-Structural Analysis Software (i.e. NASTRAN) contains effective solvers also for singular Eigenvalue problems like Eq. (18), which are able to extract all theoretically possible N solutions

It was already mentioned, that we intend to use the M lower as modal space co-ordinates to solve the dynamic gust problem.

For this purpose, the M Eigenvectors are assembled in a N·M-Modal Matrix Ψ_{jm} and the Eigenfrequencies in a M·M diagonal Eigenfrequency Matrix Ω^2_{km}.

The Eigenvectors are assumed to be normalised by the Maximum-Norm.

For later reference, we need some identities, obtainable by re-substitution of Modal and Eigenfrequency Matrix into Eq. (18):

$$m_{ij}\,\Psi_{jk}\,\Omega^2_{km} = k_{ij}\,\Psi_{jm} \qquad (19)$$

$$k,m = 1,M$$

The second identity is obtained by pre-multiplication of Eq. (19) with the transpose of the Modal Matrix:

$$M_{nk}\,\Omega^2_{km} = K^s_{nm}$$

$$n,k,m = 1,M$$

$$M_{nk} = \Psi^T_{ni}\,m_{ij}\,\Psi_{jk} = \text{Generalised Mass Matrix}$$

$$K_{nm} = \Psi^T_{ni}\,k_{ij}\,\Psi_{jm} = \text{General. Stiffness Matrix}$$

Since the Eigenvectors are orthogonal in pairs with respect to the mass matrix m_{ij}, the Generalised Mass and Stiffness Matrices are diagonal.

A particular problem has to be considered for the R Rigid Body Modes.

The enfrequencies are all zero and consequently the modes can be arbitrarily chosen with the constraint to be linearly independent of each other.

Rigid Body Modes, generated by the FE - Eigenvalue solvers do normally refer to the Principal Axis System of the rigid structure.

This is often inconvenient for A/C dynamic problems Usually it is more appropriate to have the Rigid Body Modes referred to the Non-Principal Body-Fixed Axis system

In this case, the Eigenvectors produced by the FE-solver have to be subsequently transformed

The resulting R·R block-diagonal sub-matrix of M_{nk} will become non-diagonal.

4.1.6 Damping Modelling

In this chapter of Dynamic Modelling, forces and moments are considered, which are proportional to translational and rotational velocities of the structural grid points.

The following effects may belong to that category.

- Structural Damping Forces/Moments
- Artificial Damping Forces/Moments, due to control surface flutter prevention measures
- Gyroscopic Forces/Moments, produced by rotating machinery in dynamically moving bearings
- Centrifugal Forces/Moments, occuring if Rigid-Body Dynamics are modelled in rotating Body-Fixed Co-ordinates (Flight Mechanics System)

Structural damping coefficients usually cannot be specified in physical co-ordinates as factors on the

velocity differences of two adjacent grid points.

They can be defined only in a more global form for each flexible mode of the structure, being proportional to its Generalised Stiffness and determined by Ground Vibration Tests (GVT)

(Modal Damping)

If GVT results are not available in an early design phase, structural damping coefficients may be assessed as 1 - 2% of the theoretical Generalised Stiffnesses.

Re-distribution of the Modal Damping coefficients to the physical degrees-of-freedom in order to avoid load balancing problems is not necessary as we will see later

Assembling the damping coefficients due to the above sources, except the unknown structural damping, in the matrix $b_{i,j}$, the damping force vector $f_{b,i}$ is defined as follows :

$$f_{b,i} = b_{i,j} \dot{w}_j$$

$$i,j = 1,N$$

4.1.7 Aerodynamic Modelling

The physical nature of the Dynamic Gust problem is characterised by rapid flexible structural motions and rapid changes of gust angles-of-attack, which does no longer allow to consider the aerodynamic pressure build up as quasi-steady.

Consequently, unsteady aerodynamic methods for compressible flow have to be applied to derive the aerodynamic forces/moments due to structural motion and the gust field.

Unsteady 3-dimensional compressible flow methods for harmonically oscillating lifting surfaces, applied to derive an unknown pressure field from a given down-wash field are based on Kuessners-Integral Equation, using the numerically suited Kernels of Watkins/Runyan/Woolston in the Frequency Plane

According to the kind of numerical solution of the integral equation, we may be faced with two basic methods:

- The Kernel Function Methods
- The Doublet Lattice Methods

Due to the fact that the Doublet Lattice Method is well suited to Finite Element modelling of the structure and integrated in the NASTRAN- Aeroelastic Supplement, where it can be used in combination with the 'Slender Body Theory' for fuselages and other slender bodies, we prefer to describe the Aerodynamic Modelling on the basis of this method.

The idea of Doublet Lattice modelling is to sub-divide the lifting surface into a number of small rectangular or trapezoidal panels, whose side edges are parallel to the flow and should coincide with lines, where surface discontinuities occur (control surfaces edges, etc.).

Singularity problems, which are always present in the Kernel Function Methods are inherently avoided in the Doublet Lattice approach, because the down-wash and pressure reference points can never coincide.

The unknown pressure on a single panel is assumed as constant and to acts on the ¼-line of the panel chord in panel mid-span.

The down-wash reference point is located on the ¾-line also in panel mid-span.

This latter assumption automatically fulfills the Kutta-Condition of the flow at the surface trailing edge, which was found empirically

Number and arrangement of panels, chord- and span-wise, depend on the following conditions:

- Largest Reduced Frequency
- Mach Number
- Pressure Gradient

The Doublet Lattice method recommends to keep the panel's aspect ratio approx. unity, causing a dependency of chord-wise and span-wise number of panels

In areas of high pressure gradients, e.g at the leading edge of lifting and control surfaces or in the outer span region, the panel density should be higher than in the other areas. For high Mach Numbers and Reduced Frequencies the number of panels should also be increased.

Having established the aerodynamic model by panelling the total A/C surface and run the Doublet Lattice Method for different Mach Numbers and Reduced Frequencies, we obtain the complex-valued Aerodynamic Influence Matrix $K_{sr}(M,k)$.

The Down-wash/Pressure - Integral Equation is reduced to the following complex-valued linear algebraic equation :

$$\alpha_s(k) = K_{sr}(M,k)\,\Delta c_{p,r}(M,k) \qquad (20)$$

$$r,s = 1,P$$

$\alpha_s(k)$ = Complex Down-wash angle-of-attack at the ¾-point of the s-th panel

$\Delta c_{pr}(k)$ = Complex unknown pressure difference at the ¼point of the r-th panel

M = Mach Number

P = Number of Panels

k = reduced Frequency

Solving Eq (20) by inversion, we obtain the pressure-difference vector.

$$\Delta c_{p,r}(M,k) = A_{rs}(M,k)\,\alpha_s(k) \qquad (21)$$

$$r,s = 1,P$$

Calculation of Structural Motion Angles-of-Attack

In order to determine aerodynamic forces/moments due to structural motion from Eq (21), the nodal velocities and deformations have to be converted to angles-of-attack and related to the ¾-points of the panels.

Dimensions and geometrical reference points of the pressure and angle-of-attack vector are normally not compatible with those of the deformations vector w_j. Therefore, an interpolation step is necessary

Angles-of-attack due to structural motion are generated by the velocity components of the nodal points vertical to the aerodynamic surface and by the rotational degrees-of-freedom having in-plane components vertical to the flow direction.

By means of appropriately chosen operator matrices TV_{sj} and TR_{sj}, containing all the properties

to transform the nodal velocity and deformation field to the ¼-points of the panels, the angle-of-attack vector in Frequency Plane term reads as follows :

$$\alpha_{M,s}(k) = (-ik/L_{ref}TV_{sj} + TR_{sj})\ w_j(k) \qquad (22)$$

$$j = 1,N\ ;\ s = 1,P$$

The operator matrices (TV_{sj} and TR_{sj}) provide the following features

- Geometric Transformation
- Interpolation
- Co-ordinate Transformation
- Selecting elements from the deformation vector

A more detailed description of the operator matrices is not possible, because their elements must be determined appropriately to the specific A/C's structural and aerodynamic modelling characteristics.

Calculation of Gust Angles-of-Attack

The angles-of-attack at the ¼-points of the panels due to a vertical or lateral harmonic gust field of unit amplitude, fixed in space and passed by the A/C with speed V, can be determined from the following relation :

$$\alpha_{G,s}(k) = TG_{sk} \exp(-ik\Delta x_k/L_{ref}) \qquad (23)$$

$$s,k = 1,P$$

$\alpha_{G,s}$ = Angle-of-attack vector due to a harmonic gust field

TG_{sk} = Diagonal Transformation Matrix to convert gust velocities from the Earth-Fixed System into the panel system ¼-points

exp (..) = Time lag vector

$\Delta x_k/L_{ref}$ = Normalised x-distance from the gust front to the ¼-point of the k-th panel

Calculation of Aerodynamic Forces/Moments

By means of the previously defined discrete pressure-differences, aerodynamic forces/moments acting in the degrees- of-freedom of the structural grid points, can now be determined from the panel pressures surrounding these grid points.

For this purpose, another operator matrix TF_{ir} will be established, performing the following tasks

- Multiplication with panel areas
- Calculation of moments
- Summation
- Co-ordinate Transformation
- Correction of theoreticaly calculated panel pressures, in order to match steady windtunnel measured span-wise load distributions at k = 0

Pre-multiplication of Eq. (21) with the operator matrix yields the aerodynamic force/moment vector:

$$f_{a,i}(M,k) = Q\ TF_{ir}\ \Delta c_{p,r}(M,k) \qquad (24)$$

$$i = 1,N\ ;\ r = 1,P$$

Substitution of the angles-of-attack (22) and (23) in Eq. (21) and subsequentiy the results in Eq. (24), yields the aerodynamic forces/moments with respect to structural motion and the gust field:

Forces/Moments due to Structural Motion:

$$f_{M,i}(M,k) = Q \left[ikd_{ij}(M,k)/L_{ref} + c_{ij}(M,k) \right] w_j(k)$$

$w_j(k)$ = Deflection vector of nodal point degrees-of-freedom in the Frequency Plane

$d_{ij}(M,k) = -TF_{ir}\ A_{rs}(M,k)\ TV_{sj}$

$c_{ij}(M,k) = TF_{ir}\ A_{rs}(M,k)\ TR_{sj}$

Q = Dynamic Pressure

i,j = $1,N$ = Number of Nodal Degrees of Freedom

Forces/Moments due to a Harmonic Gust Field:

$$g_i(M,k) = TF_{ir}\ A_{rs}(Ma,k)\ TG_{sk} \exp(-ik\Delta x_k/L_{ref})$$

$i = 1,N$; $r,s,k = 1,P$ = Number of Panels

Transformation of Unsteady Aerodynamic Forces/Moments to the Time Plane

The behaviour of the unsteady aerodynamic forces/moments in the Frequency Plane does not allow to apply numerical Inverse Fourier Transform for conversion to Time Plane. For flutter analysis in the Time Plane, Pade-Approximants, consisting of a complex-valued polynominal in k and a rational function part, have been proposed to approximate the elements of the Generalised Aerodynamic Force Matrices in the Frequency Plane

In the Dynamic Gust Load Analysis, we have to approximate the 'Modalised' Aerodynamic Force Matrices due to structural motion $d_{q,im}(k)$ and $c_{q,im}(k)$ of Eq. (29).

The number of approximants in this case is significantly larger than those of the Generalised Forces, but guarantees balancing of forces/moments.

The unsteady gust forces/moments due to a gust of specified shape can be transformed to the Time Plane by numerical Inverse Fourier Transform, if the Fourier Transform of this gust field vanishes with sufficient order for large k. At least symbolically, we may apply the Inverse Fourier Transform of $f_{M,i}(k)$ to understand, how the Time Plane form should look like:

$$f_{M,i}(t') = Q/\pi \cdot \mathrm{Re} \left\{ \int_0^\infty d_{ij}(M,k)\ ik\ w_j(k) \exp(ikt')/L_{ref}\ dk + \int_0^\infty c_{ij}(M,k)\ w_j(k) \exp(ikt')\ dk \right\}$$

The Inverse Fourier Transform of the Frequency Plane products under the integral signs can be identified as Convolution Integrals in the time plane, yielding for Structural Motion.

$$f_{M,i}(t') = Q \left\{ \int_0^t d_{ij}(M,t'-t'')\ w_j(t'')/L_{ref}\ dt'' + \int_0^t c_{ij}(M,t'-t'')\ w_j(t'')\ dt'' \right\}$$

$i,j = 1,N$

t', t'' = Normalised Time

t' = $V \cdot t/L_{ref}$

A dot on the variable therefore means differentiation with respect to t' or t".

For a Gust Field of Specified Shape U(t') we obtain

$$f_{U,i}(t') = Q/\pi \, Re\{ \int_0^\infty g_i(M,k) \; U(k)/V \exp(ikt') \, dk \}$$

$$f_{U,i}(t') = Q \int_0^t g_i(M,t'-t'') \; U(t'')/V \, dt'' \}$$

$$i = 1,N$$

4.2 *Time Plane Gust Analysis*

In the previous chapters we have introduced all dynamic forces/moments appearing in a Dynamic Gust Problem of an A/C with significant flexible structure
Equilibrating internal and external forces/moments, yields the Equation of Motion in the Time Plane, written in terms of normalised time t'.

$$V^2/L^2_{ref} \, m_{ij} \ddot{w}_j + V/L_{ref} \, b'_{ij} \dot{w}_j + k^s_{ij} \, w_j + Q/L_{ref} \int_0^t d_{ij}(M,t'-t'') \, \dot{w}_j(t'') \, dt'' +$$

$$+ Q \int_0^t c_{ij}(M,t'-t'') \, w_j(t'') \, dt'' = Q \int_0^t g_i(M,t'-t'') \; U(t'')/V \, dt''$$

$$i,j = 1,N \qquad (25)$$

Explanations:

$w_j(t')$	=	Deflection Vector of Grid Points, containing Rigid Body Motion and Control Surface Motion
$\dot{w}_j$, $\ddot{w}_j$	=	Derivatives of $w_j(t')$ with respect to normalisedTime
m_{ij}	=	Mass Matrix, containing masses, mass moments and moments-of-inertia
b'_{ij}	=	Damping Matrix, containing artificial, centrifugal and gyroscopic damping coefficients. No structural damping specified here.
k^s_{ij}	=	Singular Structural Stiffness Matrix Singularity is of order (R), according to the number of Rigid Body Modes and Control Surface Deflections
$c_{ij}(t')$, $d_{ij}(t')$	=	Unsteady Aerodynamic Force/MomentDelta-Pulse response matrices due to nodal velocities and rotations
$g_i(t')$	=	Convolution Kernel Vector of Unsteady Aerodynamic Gust Force Delta-Pulse responses.
$U(t')/V$	=	Gust Angle-of-Attack of an arbitrary, but specified Gust Field in normalised time t'.
Q	=	Dyamic Pressure
ρ	=	Air Density
V	=	Flight Speed
l_{ref}	=	Reference Length to normalise time and frequency
t', t"	=	Normalised Times

4.2.1 Transformation to Modal Co-ordinates

Although equation (25) is in most cases not a practical working form, it can be taken as a basis to derive all the other variants, which are more appropriate for Dynamic Gust Analysis.

In a first step, Modal Co-ordinates will be introduced to reduce the number of degree-of-freedom in the analysis

For this purpose, the deformation vector w_j will be expanded in terms of Eigenvectors of the conservative dynamic problem, assembled in the Modal Matrix Ψ_{jm} as column vectors:

$$w_j(t') = \Psi_{jm}\, q_m(t') \qquad (26)$$

In Eq. (26), the Generalised Co-ordinate vector q_m replaces w_j, and takes the role of the new unknown in the Modal System.

Introduction of Eq. (26) in Eq. (25), yields the 'Modalised Equation' of motion, which is an incomplete Modal Transformation, where the deformation vector is replaced by Eq (26) and the force/moment vector remains untransformed.

The Modalised Equation is the appropriate form to calculate the dynamic forces/moments from, once the Generalised Co-ordinate vector q_m has been determined from the Generalised Equation of motion. In order to compress the number of intermediate steps to derive the final form of the working equations, the following operations will be additionally applied to Eq (25)

- Multiplication with $(L_{ref}/V)^2$
- Putting remaining factors of the different dynamic terms inside the matrices, without renaming
- Introduction of Modal Damping Coefficients in

  $$b'_{q,im} = b_{ij}\, \Psi_{jm}$$

  by superimposing a Modalised Damping Matrix, $b_{s,im}$ defined as follows:

  $$b_{s,im} = m_{ik}\, \Psi_{ks}\, \Omega^2_{sr}\, \beta_{rm}$$

  β_{rm} = Diagonal Matrix of Modal Damping Coefficients as fractions of the Generalised Stiffness.

  The completed modalised damping matrix subsequently used is defined as follows:

  $$b_{q,im} = b'_{q,im}\, L_{ref}/V + b_{s,im}$$

Having carried out the above measures, we obtain the Modalised Equation of Motion:

4.2.2 The Modalised Equation of Motion

$$m_{q,im}\, \ddot{q}_m + b_{q,im}\, \dot{q}_m + m_{q,ik}\, K_e^2{}_{km}\, q_m + \rho \int_0^t d_{q,im}(M,t'-t'')\dot{q}(t'')\, dt'' +$$

$$+ \rho \int_0^t c_{q,im}(M,t'-t'')q(t'')\, dt'' = \rho \int_0^t g_i(M,t'-t'')\, U(t'')/V\, dt'' \qquad (27)$$

$$i = 1,N\ ;\ m = 1,M << N$$

Explanations:

$m_{q,im} = m_{ij}\, \Psi_{jm}$ = Modalised Mass Matrix

$b_{q,im} = b_{ij}\, \Psi_{jm}$ = Modalised Damping Matrix, Structural Damping included

$K^2_{e,km} = \Omega^2_{km} (L_{ref}/V)^2$ = Diagonal Matrix of Normalised Eigenfrequencies (28)

$d_{q,im}(t')$, $c_{q,im}(t')$ = Modalised Convolution Kernel Matrices of Unsteady Aerodynamic Delta-Pulse responses.

$k^s_{q,im} = k^s_{ij} \Psi_{jm} = m_{ij} \Psi_{jk} \Omega^2_{km} = m_{q,ik} \Omega^2_{km}$ = Modalised Stiffnes Matrix = Identity (see Eq. 19)

All matrices have N·M dimensions

4.2.3 The Generalised Equation of Motion

Multiplication of Eq. (27) with the transpose of the Modal Matrix (Ψ^T_{ni} , n = 1,M) completes the Modal Transformation of (25), obtaining the Modal (Generalised) Equation of Motion in the Time Plane:

$$M_{nm}\ddot{q}_m + B_{nm}\dot{q}_m + M_{nk}K^2_{e,km}q_m + \rho \int_0^t D_{nm}(M,t'-t'')\dot{q}_m(t'')\,dt'' +$$

$$+ \rho \int_0^t C_{nm}(M,t'-t'')q_m(t'')\,dt'' = \rho \int_0^t G_n(M,t'-t'')U(t'')/V\,dt''$$

$$n,m = 1,M << N$$

Explanations:

$M_{nm} = \Psi^T_{ni} m_{ij} \Psi_{jm}$ = Generalised Mass Matrix

$B_{nm} = \Psi^T_{ni} b_{ij} \Psi_{jm}$ = Generalised Damping Matrix, including Structural Damping

$D_{nm}(t')$, $C_{nm}(t')$ = Generalised Convolution Kernel Marices of Unsteady Aerodynamic Forces, due to structural motion

$= \Psi^T_{ni}(d_{ij},c_{ij})\Psi_{jm}$

$G_n(t') = \Psi^T_{ni} g_i(t')$ = Generalised Convolution Kernel Vector of Unsteady Aerodynamic Forces, due to a harmonical Gust Field

All matrices have MxM - dimensions

Readers, who want to do the Dynamic Gust Analysis in the Time Plane, because several strong non-linearities have to be modelled and who want to take into account 3-dim Unsteady Aerodynamics, are recommended to decompose the complex Modalised Aerodynamic Force/Moment Matrices $d_{q,im}(k)$ and $c_{q,im}(k)$ of Eq. (29) by Pade-approximants.

Subsequent re-transformation to the Time Plane yields the Modalised Convolution Kernels and additional terms, which can be superimposed to Modalised Mass, Damping and Stiffness Matrices appropriately

Due to the properties of the Pade Approximants, the resulting convolution kernels consist of exponential function terms exp(-const·(t'-t''), which degenerate to a product of two exponentials, causing the Integro- Differental Equation (27) to be convertible into an Ordinary Differential Equation with constant coefficient matrices and augmented Modal State Vector (q_m , m = 1,M + X). These Differential Equations, are obtained by successive differentiation and elimination.

Subsequent pre-multiplication of the resulting Differential Equation with the transpose of the appropriately extended Modal Matrix (Ψ^T_{ni}, n = 1,M + X) yields the Dynamic Gust Differential

Equation in extended Modal Co-ordinates. Although the number of Pade Approximants for the Modalised Aerodynamic Matrices is considerably high, the procedure guarantees that Modalised and Generalised equations are compatible and resulting gust loads are balanced.

As far as Time Plane transformation of 3-dim. Unsteady Gust forces is concerned, there is no need for a Pade - Approximation, if the Gust Shape is specified and its Fourier Transform decreases with sufficient order for increasing Reduced Frequency k.

In this case the product $g_i(M,k) \cdot U(k)/V$ of Eq. (29) can be numerically transformed to the Time Plane by Inverse Fourier Transform.

4.3 *Determination of Load Transfer Functions*

4.3.1 The Modalised Dynamic Gust Equation

In order to follow the objective to derive Gust Load Transfer Functions, we will now turn to the Frequency Plane analysis.

The Frequency Plane form of Eq (27) will be obtained by Fourier Transformation with respect to t'.

Splitting the resulting complex aerodynamic matrices in real and imaginary parts on the left side and after suitable re-ordering, we obtain the following final form of the Modalised Gust Equation in the Frequency Plane with real matrices $d_{q,im}(k)$ and $c_{q,im}(k)$:

$$\{ m_{q,ik}(K^2_{e,km} - k^2 I_{km}) + ik[b_{q,im} + \rho d_{q,im}(k)] + \rho c_{q,im}(k) \} q_m(k) = \rho g_i(k)\, U(k)/V \qquad (29)$$

$$i = 1,N \; ; \; m,k = 1,M << N$$

Equation (29) will become the basis of the Load Transfer Functions to be derived later, since the Modal Co-ordinates have been determined from the Generalised Equations (30).

4.3.2 The Generalised Equations of Motion

Completing the Modal Transformation by pre-multiplying Eq. (29) with the transposed Modal Matrix, we obtain:

$$\{ M_{nr} (K^2_{e,rm} - k^2 I_{rm}) + ik[B_{nm} + \rho D_{nm}(k)] + \rho C_{nm}(k) \} q_m(k) = \rho \cdot G_n(k)\, U(k)/V \qquad (30)$$

$$n,m = 1,M << N$$

Explanations:

B_{nm} = Generalised real-valued Structural damping matrix

$D_{nm}(k)$, $C_{nm}(k)$ = Generalised real-valued Aerodynamic Damping and Aerodynamig Stiffness Matrices

$G_n(k)$ = Generalised complex-valued Aerodynamic Force Vector due to a harmonical Gust Field of unit angle-of-attack

4.3.3 Determination of Modal Co-ordinates

Abbreviation of Eq. (30) by

$$A_{nm}(k,M,\rho,V,\text{mass})\ q_m(k) = \rho\ G_n(k) \qquad (31)$$

yields a complex-valued system of linear equations for the unknown $q_m(k)$ with $U(k)/V = 1$, for determining Load Transfer Functions.

Solving equation (31) for $q_m(k)$ and an appropriate number of discrete Reduced Frequencies, the calculation of Load Transfer Functions will be performed by introducing the solution $q_m(k)$ in Eq (29).

4.3.4 The Dynamic Force/Moment Vector

Identifying in Eq. (29) the term $m_{q_j,ik}\ K^2_{e,km}\ q_m(k)$ by means of the identity (19) and Eq. (28) as the dynamic internal force vector

$$F_i(k) = m_{ij}\ \Psi_{jk}\ K^2_{e,km}\ (V/L_{ref})^2\ q_m(k)$$

and solving Eq (29) with respect to this term, we obtain the internal dynamic force vector due to a Harmonical Gust Field by letting $U(k)/V = 1$

$$F_i(k) = (V/L_{ref})^2\ \{\ \rho g_i(k) + [\ k^2 m_{q_j,im} - ik(b_{q_j,im} + \rho d_{q_j,im}(k)) - \rho c_{q_j,im}(k)\ ]\ q_m(k)\ \} \qquad (32)$$

By means of an appropriately chosen Operator Matrix (TL_{si}), linear combinations of the nodal forces/moments like Shear, Bending Moments and Torques can be generated for beam-like structural components,

$$H_s(k) = T_{si}\ F_i(k)$$

$$s = 1,L$$

yielding the required Transfer Function Vector of interesting structural Gust Load Quantities $s = 1,L$

4.3.5 Transfer Functions for Other Dynamic Quantities

Furthermore, the Modal Co-ordinate solutions $q_m(k)$ in combination with the expansion (26) may be used to derive other interesting dynamic quantities, like accelerations, tank pressures, control signals, etc. , representable by a linear combination of Modal Co-ordinates $q_m(k)$ or the nodal displacement vector $w_j(k)$ and its derivatives

The linear combination is performed by appropriately chosen Operator Matrices (TA_{rm}, TB_{rm}, TC_{rm})

$$H_r(k) = (\ -k^2 TA_{rm} + ikTB_{rm} + TC_{rm}\ )\ q_m(k)$$

$$r = 1,Q\ ;\ m = 1,M$$

Q = Number of Interesting Quantities

$H_r(k)$ = Transfer Function of Interesting Quantity (r)

If $H_r(k)$ has to be related to the displacement vector $w_j(k)$, the Operator Matrices must additionally contain the appropriate parts of the Modal Matrix Ψ_{jm}

4.4 *Quasi-Flexible Dynamic Model*

The so-called Quasi-Flexible dynamic model mentioned in "Discrete Gust Parameters and Structural Modelling" on page V-4 can be derived consistently from the Full Dynamic Model by letting the flexible part of structural accelerations and velocities approach zero

Only the static (rotational) displacement field and its influence on the aerodynamic pressure distribution will be maintained

Unsteady aerodynamic effects due to the Rigid Body Motion also remain included in the Quasi-Flex model.

In order to derive the corresponding equation of motion, the Generalised Dynamic Gust Equation (30) is partitioned in a Rigid Body part R and a Flexible part E.

Partitioning of Eq. (30) yields:

$$\left[\begin{array}{c|c} M_{RR} & M_{RE} \\ \hline M_{ER} & M_{EE} \end{array}\right] \cdot \left[\begin{array}{c|c} 0 & 0 \\ \hline 0 & K^2_{eEE} \end{array}\right] \cdot k^2 \left[\begin{array}{c|c} I_{RR} & 0 \\ \hline 0 & I_{EE} \end{array}\right] + i\cdot k \cdot \left[\begin{array}{c|c} B_{RR} & B_{RE} \\ \hline B_{ER} & B_{EE} \end{array}\right] + \rho \cdot \left[\begin{array}{c|c} D_{RR}(k) & D_{RE}(k) \\ \hline D_{ER}(k) & D_{EE}(k) \end{array}\right]$$

$$+ \rho \left[\begin{array}{c|c} C_{RR}(k) & C_{RE}(\ ) \\ \hline C_{ER}(k) & C_{EE}(k) \end{array}\right] \cdot \left[\begin{array}{c} q_R \\ \hline q_E \end{array}\right] = \rho \left[\begin{array}{c} G_R(k) \\ \hline G_E(k) \end{array}\right] \cdot U(k)/V$$

(33)

Explanations:

I = Identity Matrix

R = Number of Rigid Body Modes

E = M-R = Number of Flexible Modes

M = Total Number of Modal Co-ordinates

and $M_{RE} = M_{ER} = 0$, due to Orthogonality of Rigid Body and Flexible Modes.

Separating Eq. (33) in

Rigid Body Motion:

$$\{ -k^2 M_{RR} + ik[B_{RR} + \rho D_{RR}(k)] + \rho C_{RR}(k) \}\ q_R$$

$$+ \{ ik[B_{RE} + \rho D_{RE}(k)] + \rho \cdot C_{RE}(k) \}\ q_E = \rho G_R(k) U(k)/V \qquad (34)$$

and Flexible Motion:

$$-k^2 M_{EE} q_E + \{ ik(B_{ER} + \rho D_{ER}(k)] + \rho C_{ER}(k) \} q_R$$
$$+ \{ M_{EE} K^2_{\bullet,EE} + ik[B_{EE} + \rho D_{EE}(k)] + \rho C_{EE}(k) \} q_E = \rho G_E(k) U(k)/V \qquad (35)$$

Letting in Eqs. (34) and (35) the terms $ik[B_{RE} + \rho D_{RE}(k)]q_E$, $-k^2 M_{EE} q_E$ and $ik[B_{EF} + \rho D_{EE}(k)]q_E$ approach zero and solving Eq. (35) subsequently for $q_E(k)$, we obtain:

$$q_E(k) = L^{-1}_{EE}(k) \{ \rho G_E(k) U(k)/V - [ik(B_{ER} + \rho D_{ER}(k)) - \rho C_{ER}(k)] q_R \} \qquad (36)$$

where now the flexible part of the modal co-ordinate vector has been expressed in terms of the Rigid Body part,

with $$L_{EE}(k) = \rho C_{EE}(k) + M_{EE} K^2_{\bullet,EE}$$

4.4.1 The Generalised Quasi-Flex. Equation of Motion

The divergence matrix $I_{FF}(k)$ will become singular, if the dynamic pressure approaches its critical value and consequently the Quasi-Flex dynamic equation has no solution, similar to the situation, if the flight speed in the Full Dynamic equation approaches a critical flutter speed. Substitution of Eq (36) in Eq (34), the Rigid Body part, subsequent re-ordering left and right side and definition of new matrices, yields the reduced Generalised Quasi-Flex Equation of Motion

$$\{ -k^2 M_{RR} + ik[B'_{RR} + \rho D'_{RR}(k)] + \rho C'_{RR}(k) \} q_R = \rho G'_R(k) U(k)/V$$

Dynamic Pressure $Q \neq Q_{div}$

Explanations:

$$B'_{RR}(k) = B_{RR} - \rho C_{RE}(k) L^{-1}_{EE}(k) B_{ER}(k)$$
$$D'_{RR}(k) = D_{RR} - \rho C_{RE}(k) L^{-1}_{EE}(k) D_{ER}(k)$$
$$C'_{RR}(k) = C_{RR} - \rho C_{RE}(k) L^{-1}_{EE}(k) C_{FR}(k)$$
$$G'_R(k) = G_R(k) - \rho C_{RE}(k) L^{-1}_{EE}(k) G_E(k)$$

Note: In the Quasi-Flexible Dynamic Model, the number of flexible modes to approximate the stationary displacement field has to be increased significantly, compared to the Full Dynamic Model, in order to obtain sufficient convergence for the loads at all aircraft components.

4.4.2 The Modalised Quasi-Flex. Equation of Motion

The Modalised Dynamic Gust Equation (29) has to be partitionned and modified in a similar way to obtain the dynamic force vector of the Quasi-Flex Model.

Here we give directly the result.

$$\{ -k^2 m_{q,iR} + ik[b'_{q,iR} + \rho d_{q,iR}(k)] + \rho c_{q,iR}(k) \} q_R(k) + m_{q,iE} K^2_{e,FE} q_E = \rho g_i(k) U(k)/V \qquad (37)$$

where $m_{q,iE} K^2_{e,EE}\, q_E = F'(k)$ is the dynamic force vector of the Quasi-flex. Model.

4.4.3 The Quasi-Flex. Dynamic Force/Moments:

Solving Eq. (37) for $F'_i(k)$ yields:

$$F'_i(k) = \rho g'_i(k) U(k)/V + \{ k^2 m_{q,iR} - ik[b'_{q,iR} + \rho d'_{q,iR}(k)] + \rho c'_{q,iR} \}\, q_R(k)$$

$$i = 1,N$$

Explanations:

$$b'_{q,iR}(k) = b_{q,iR} - \rho\, c_{q,iE}\, L^{-1}_{EF}(k)\, B_{ER}(k)$$

$$d'_{q,iR}(k) = d_{q,iR} - \rho\, c_{q,iE}\, L^{-1}_{EF}(k)\, D_{ER}(k)$$

$$c'_{q,iR}(k) = c_{q,iR} - \rho\, c_{q,iE}\, L^{-1}_{EE}(k)\, C_{ER}(k)$$

$$g'_i(k) = g_i - \rho\, c_{q,iE}\, L^{-1}_{EE}(k)\, G_E(k)$$

5.0 The Influence of Electrical Flight Control Systems on Gust Load Analysis

Modern civil an military aircraft have a variety of (electrical) control systems, designed to perform one or more of the following tasks:

- Auto-Pilot Function (AP)
- Stability Augmentation (SAS)
- Maneuvrability Enhancement (ME)
- Gust / Maneuver Load Alleviation (G/MLA)
- Protected Flight Control (EFCS)
- Flexible Mode Control (FMCS)
- Ride Comfort Enhancement (RCES)
- Flutter Margin Augmentation (FMAS)
- etc.

The influence of these control systems, including their failed or degraded states, on structural loads due to gusts, maneuvers and on dynamic stability (flutter) has to be investigated.
Systems, which are not intentionally designed to alleviate loads, may possibly increase the loads, compared to an aircraft without such control systems.

5.1 *Analysis (Frequency Plane)*

The diagrams below show a comparison of an uncontrolled and an (automatically) controlled aircraft, flying in discrete or random turbulence.

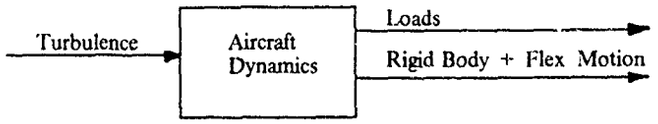

Figure 1. The Uncontrolled Aircraft (Open-Loop System)

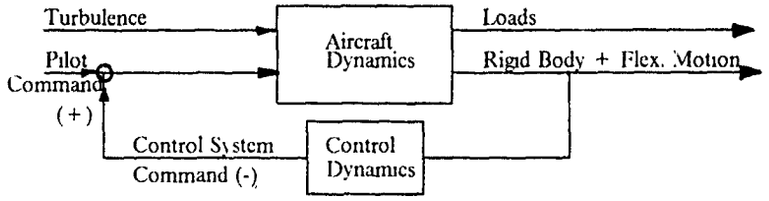

Figure 2. The Automatically Controlled Aircraft (Closed-Loop System)

In terms of Control Theory, the uncontrolled aircraft disturbed by the turbulence field, is an Open-Loop system, where the output quantities, Loads and Structural motion, are direct and only reactions of the flexible aircraft on aerodynamic forces generated by the turbulence field.

The automatically controlled aircraft is a Closed Loop system, where selected quantities of the aircraft's velocity and acceleration field are measured, filtered, linearly combined, amplified and phased by the Control Dynamics block, and after further signal conditioning by adequate non-linearities, like limiters, thresholds, etc , fed back into the servo-actuators of the aircraft's classical control surfaces or additional new control devices, in order to achieve the desired control objective In this case, the aircaft responses are functions of turbulence *and* control system commands.

The original open-loop aircraft dynamics are altered by introduction of the control system, and consequently the original open-loop load transfer functions will also change, causing the resulting aircraft component loads to be lower or higher, dependent on the parameters and dynamics of the control system.

The parameters of the control system are derived systematically by theoretical optimisation methods provided by Control Theory, making a control objective function to a maximum or minimum, followed by a later fine-tuning during flight testing.

In order to show the influence of the control system on the open-loop load transfer functions, we will assume that the control system parameters have already been determined and the control system dynamics are fully defined.

5.2 *The Linear Aircraft and Control System*

In a first step, the control system and the aircraft dynamics are assumed as linear. Signals and transfer functions of the closed-loop system, Aircraft + Control Dynamics, necessary to derive the modified Load Transfer Functions, are outlined in the signal flow diagram below :

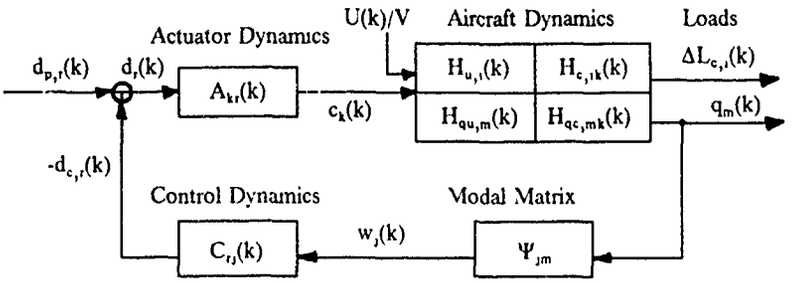

Figure 3. Linear Control Dynamics

The Pilot Command $d_{p,r}(k)$ is zero for Dynamic Gust Analysis.

Explanations:

Signals.

k = $\omega L_{ref}/V$ = Reduced Frequency

$U(k)/V$ = Discrete or Random Turbulence Amplitude Spectrum

$q_m(k)$ = Modal Response Vector of the Aircraft Rigid Body and Flexible Motion (m = 1,M)

$\Delta L_{c,i}(k)$ = Controlled Aircraft Loads Amplitude Spectrum Vector. (i = 1,L)

$w_j(k)$ = Structural Displacement Vector, incl. Rigid Body Motion Only Time-derivatives of the Displacement Vector can be directly measured by gyros or accelerometers.(j = 1,N)

$c_k(k)$ = Control Surface Deflection Vector. (k = 1,K)

$d_{p,r}(k)$ = Pilot Command Signals for r = 1,K Control Surfaces.

$d_{c,r}(k)$ = Control System Command Signals for r = 1,KControl Surfaces

$d_r(k)$ = $d_{p,r}(k) - d_{c,r}(k)$
= Difference Signal of Pilot Command and Control System Command

Transfer Function Vectors/Matrices :

$H_{u,i}(k)$ = Open-Loop Aircraft Load Transfer FunctionVector, due to a harmonic Gust Field, for $q_{c,k}(k) = 0$

$H_{c,ik}(k)$ = Open-Loop Aircraft Load Transfer FunctionMatrix of Quantities i, due to the k-th harmonically moving Control Surface, for $U(k)/V = 0$.

$H_{qu,m}(k)$ = Open-Loop Modal Response Transfer FunctionVector, including Rigid Body Motion, due to a harmonic Gust Field, for $q_{c,k}(k) = 0$ (m = 1,M)

$H_{qc,mk}(k)$ = Open-Loop Modal Response Transfer Function Matrix Matrix, including Rigid body Motion, due to the k-th harmonically moving Control Surface, for $U(k)/V = 0$.

$A_{kr}(k)$ = Diagonal Matrix of Control Surface's ActuatorTransfer Functions.

$C_{rj}(k)$ = Control System Dynamics (Control Law) Transfer Function Matrix, performing additionally Differentiation and Element Selection on the Physical Displacement Vector $w_j(k)$. r = 1,K ; j = 1,N

Ψ_{jm} = Modal Matrix (Chapt. 3), only used for theoretical Dynamic Gust Load analysis to generate Nodal Velocities and Accelerations Measurements from the Modal Simulation Model.

$q_m(k)$ = Modal State Vector

Indices:

N = Number of Nodal Degrees-of-Freedom

M = Number of Modal Co-ordinates, including Rigid Body Motion.

K = Number of actuated Control Surfaces.
L = Number of Interesting Load Quantities.

By means of the open-loop transfer functions of the aircraft, control system and the servo-actuators, the following input/output relations can be derived from Figure 3 on page V-43. to determine closed loop Load Transfer Functions:

- Loads. $$L_{c,l}(k) = H_{u,l}(k)\, U(k)/V + H_{c,k}(k)c_k(k) \qquad (38)$$

- Modal State Vector $$q_m(k) = H_{qu,m}(k)\, U(k)/V + H_{qc,mk}(k)c_k(k) \qquad (39)$$

- Actuator Dynamics. $$c_k(k) = A_{kr}(k)d_r(k) = A_{kr}(k)[\, d_{p,r}(k) - d_{c,r}(k)\,]$$

  With the pilot's command amplitude spectrum, $d_{p,r}(k) = 0$, for Gust Load Analysis:
  $$c_k(k) = -A_{kr}(k)d_{c,r}(k) \qquad (40)$$

- Control Dynamics $$d_{c,r}(k) = C_{rj}(k)\Psi_{js}q_s(k) \qquad (41)$$

For theoretical analysis, time-derivatives of $w_j(k)$) are generated within $C_{rj}(k)$

5.2.1 Determination of the Closed Loop Load Transfer Functions :

In order to derive the Closed-Loop Load Transfer Functions, Eq. (41) is introduced in Eq. (40) and subsequently the result in Eq. (39).

$$q_m(k) = H_{qu,m}(k)\, U(k)/V - H_{qc,mk}(k)A_{kr}(k)C_{rj}\Psi_{js}q_s(k)$$

Letting $$q_m(k) = I_{ms}q_s(k) \quad ;\ m,s = 1,M$$

and $$E_{ks}(k) = A_{kr}(k)C_{rj}(k)\Psi_{js}$$

we obtain:

$$[\, I_{ms} + H_{qc,mk}(k)E_{ks}(k)\,]\, q_s(k) = H_{qu,m}(k)\, U(k)/V$$

Abbreviating $$G_{ms}(k) = I_{ms} + H_{qc,mk}(k)E_{ks}(k)$$

yields. $$G_{ms}(k)q_s(k) = H_{qu,m}(k)\, U(k)/V \qquad (42)$$

Pre-multiplying Eq (42) with the inverse of $G_{ms}(k)$, yields:

$$G^{-1}{}_{nm}(k)G_{ms}(k)q_s(k) = G^{-1}{}_{nm}(k)H_{qu,m}(k)\, U(k)/V$$

$$I_{ns}q_s(k) = q_n(k) = G^{-1}{}_{nm}(k)H_{qu}(k)\, U(k)/V \qquad (43)$$

Renaming the free index n of Eq (43) with s yields the Modal State Vector of the Controlled Aircraft due to the turbulence amplitude spectrum U(k)/V:

$$q_s(k) = G^{-1}{}_{sm}(k)H_{qu,m}(k)\, U(k)/V \qquad (44)$$

Introduction of (44) in (41), (41) in (40) and subsequently applying the result in the load equation (38), yields the incremental Loads Amplitude Spectrum Vector of the controlled aircraft:

$$\Delta L_{c_{j,t}}(k) = [\, H_{u_{j,t}}(k) - H_{c_{j,tk}}(k)\, E_{ks}(k) G^{-1}{}_{sm}(k) H_{qu_{j,m}}(k) \,]\, U(k)/V$$

With

$$H_{cu_{j,t}}(k) = H_{u_{j,t}}(k) - H_{c_{j,tk}}(k) E_{ks}(k) G^{-1}{}_{sm}(k) H_{qu_{j,m}}(k)$$

$$i = 1,L \; ; \; k = 1,K \; ; \; s,m = 1,M$$

the required Closed Loop Load Transfer Function Vector.

For $E_{ks}(k) = 0$, (i.e. no control), we obtain the original Open-Loop Load Transfer Function $H_{u_{j,t}}(k)$ of the uncontrolled aircraft.

5.3 *The Non-Linear Control System*

Practical control system designs normally contain different types of non-linearities for signal conditioning, i.e. limiters to avoid over-powering the servo-valves of control surface actuators.
In this case, transfer functions of the control system do not exist in the classical linear sense and the superposition principle does no longer hold.
The dynamicist, who is faced with such non-linear systems in the Gust Load Analysis work is recommended to apply time-plane methods here wherever possible and practical, in order to avoid discussions about the applicability of the Quasi-Linearisation Methods outlined below

5.3.1 Quasi-Linearisation Methods of Non-Linear Elements

Quasi-Linearisation methods , which are not re stricted to small deviations from a steady or dynamic reference state, have been developed very early in the practice of dynamic systems analysis to solve non-linear control system stability analysis.
In the literature of Control System Design these linearisation methods are known as:

- The Describing Function Method (Harmonic Balance) for *sinosoidal* signals
- The Equivalent Gain Method for *random* signals

5.3.2 The Describing Function Method

The basic idea of the Describing Function Concept is to replace the non-linear system element by a simple gain block, where the gain itself may be real- or complex-valued. depending on the type of non-linearity being considered. For this pupose the non-linearity is fed with a sinosoidal signal $x = a\cos(\omega t)$ or $x = a\sin(\omega t)$.
The non-linear element may be assumed as non-dynamic, $y \neq f(x, dx/dt)$ and anti-symmetric, having the following general static or quasi-static characteristics:

- $y = f(x) = -f(-x)$ ==> Static Non-Linearity

- $y = f(dx/dt) = -f(-dx/dt) = = >$ Static Non-Linearity

- $y = f(x,\text{sign}(dx/dt)) = = >$ Hysteresis-Type Non-Linearity
  $= -f(-x,\text{sign}(dx/dt))$

The output signal is expanded in a Fourier Series, where only the fundamental harmonics (the linear part) are maintained for further analysis :

$$y = A\cos(\omega t) + B\sin(\omega t)$$

The coefficients A and B are functions of the input signal amplitude and the particular non-linearity considered. They are not frequency dependent, if the non-linearity is non-dynamic.
The Fourier Coefficients A and B can be calculated from the following relations:

$$A = 1/\pi \int_0^{2\pi} [\, f(x, \text{sign}(dx/du)\,] \cos(u)du$$
$$B = 1/\pi \int_0^{2\pi} [\, f(x, \text{sign}(dx/du)\,] \sin(u)du \qquad (45)$$

with:

$$u = \omega t\ ;\ x = a\cos(u)\ ;\ dx/du = -a\sin(u)$$

5.3.3 Alternative Describing Function Approach

In order to show the close relations between the Describing Function for harmonical input signals and the Equivalent Gain Concept for random signals, equations (45) will now be derived more formally, but perhaps with more physical insight, allowing furthermore the input signals to be complex-valued

$$x = a\exp(i\omega t)$$
$$dx/dt = i\,\omega\, a\exp(i\omega t)$$

For this pupose, we consider the following diagram:

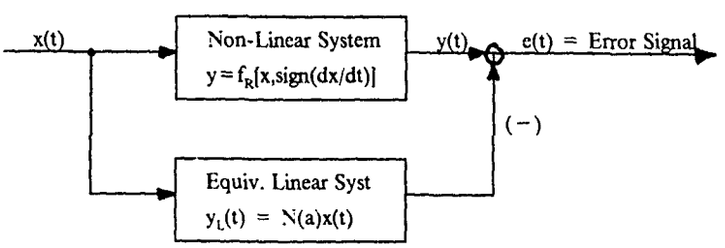

Figure 4. Describing Function Approach

Explanations

x	$= a\exp(+i\omega t)$	= The Complex Input Signal
x^*	$= a\exp(-i\omega t)$	= Complex-Conjugate of x
y	$= 2f_R(x, \text{sign}(dx/dt))$	= Distorted Output Signal of the Non-Linearity. (Real Parts twice to avoid handling of the redundant Information, of the complex-conjugate input signal to the Non-Linearity)

f_R	$= f\{Re(x), sign[Re(dx/dt)]\}$	
$y_L(t)$	$= N(a)\,x(t)$	= Equivalent Linear System Response (Fundamental Harmonics) with Complex Gain, N(a)
$e(t)$	$= y - N(a)x$	= Error Signal, Higher Harmonics of y(t)
$e^*(t)$	$= y - N^*(a)x^*$	= Complex-Conjugate of the Error Signal
$N(a)$	$= N_R(a) + iN_I(a)$	= Real and Imaginary Parts of N(a).

The complex gain N(a), the Describing Function, is determined by minimizing the variance of the error signal, (energy contained in the higher harmonics of (y(t)) with respect to the real and imaginary parts of N(a):

$$\text{var}[e(t)] = 1/T \int_0^T e(t)e^*(t)\,dt = => \min \qquad (46)$$

$$T = \text{Time Interval} = 2\pi/\omega$$

leading to the following conditions to be fulfilled·

$$d\{\text{var}[e(t)]\} / dN_R = 0 \;,\; d\{\text{var}[e(t)]\} / dN_I = 0$$

or $$1/T\int_0^T d(ee^*)/dN_R\,dt = 0 \quad ; \; 1/T\int_0^T d(ee^*)/dN_I\,dt = 0$$

To constitute a minimum, the second derivatives of Eq (46) must be positive.

Carrying out the differentiation under the integral sign yields the form :

$$\begin{aligned} 1/T\int_0^T ede^*/dN_R + e^*de/dN_R\,]\,dt &= 0 \\ 1/T\int_0^T ede^*/dN_I + e^*de/dN_I\,dt &= 0 \end{aligned} \qquad (47)$$

and after some algebraics Eq. (47) yields

$$1/T \int_0^T [\,-2yacos(\omega t) + 2N_R xx^*\,]\,dt = 0$$

$$1/T \int_0^T 2yacos(\omega t) + 2N_I xx^*\,]\,dt = 0$$

with $$1/T \int_0^T (\,xx^*\,)\,dt = a^2 \quad ; \omega t = u$$

$$y = 2\,f_R = 2\,f\,[acos(u),-sign(sin(u))]$$

$$N_R(a) = 1/(\pi a) \int_0^{2\pi} f[acos(u),-sign(sin(u))]cos(u)\,du$$

$$N_I(a) = -1/(\pi a) \int_0^{2\pi} f[acos(u),-sign(sin(u))]sin(u)\,du$$

or in complex notation:

$$N(a) = 1/(\pi a) \int_0^{2\pi} \{ f[\text{acos}(u),-\text{sign}(\sin(u))]\exp(-iu) \}\, du$$

For a static non-linearity $y = f(x)$ or $y = f(dx/dt)$, the imaginary part of N(a) is zero.

5.4 *Non-Linearity in a Closed Loop System*

In order to study the behaviour of a non-linear element in a Closed Loop, we consider the following Control System disturbed by a steady state sinosoidal input signal. The dynamic quantity y(a,k) is measured, gained and phased by C(k), yielding the non-linearity input signal x(a,k). The non-linearity is replaced by its Describing Function N(a), which may be complex-valued, input-amplitude-dependent but not frequency dependent.

The output signal of the Describing Function block $d_n(a,k)$, (the control signal), is fed back into the system to be controlled. The repercussions of the quasi-linearised non-linear element on the control system dynamics will be shown by deriving the transfer function x(a,k) as a function of the input signal amplitude A and the control signal $d_n(a,k)$.

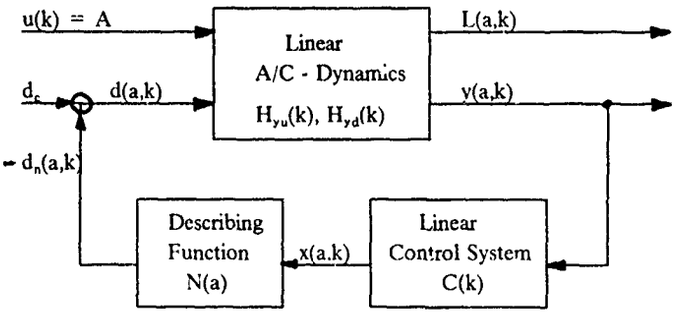

Figure 5. Non-Linear Control Dynamics

Explanations

u(k)	= A	= Steady State Sinosoidal Input Signal with Amplitude (A).
u(t')	= Aexp(ikt')	
y(a,k)		= Measurment Signal
L(a,k)		= i.e., Loads Quantity Signal
$d_n(a,k)$		= Control Command Signal
$d_c(k)$		= Guidance Signal = 0 for Gust Load Analysis
d(a,k)	$= d_c - d_n$	= Difference Signal
$H_{yu}(k)$, $H_{yd}(k)$		= A/C - Transfer Functions
x(a,k)	= a(k)exp(ib(a,k))	= Non-Linearity Input Signal with Phase Angle b(a,k) and Amplitude a(k).

From Figure 5 we can derive the following equations:

$$y(a,k) = AH_{yu}(k) + H_{yd}(k)d(a,k)$$

$$d(a,k) = - N(a)\, x(a,k), \quad (d_c = 0)$$

$$x(a,k) = C(k)\, y(a,k)$$

$$= C(k)[\, A H_{yu}(k) - H_{yd}(k) N(a) x(a,k)\,]$$

With $$G(a,k) = C(k)\, H_{yd}(k)\, N(a)$$

$$[1 + G(a,k)]\, x(a,k) = A\, C(k)\, H_{yu}(k) \qquad (48)$$

$$x(a,k) = A\, C(k)\, H_{yu}(k)/[1 + G(a,k)] = a(k)\exp[jb(a,k)]$$

Taking the (squared) absolute value of x(a,k), we obtain:

$$a^2(k) = x(a,k)\, x^*(a,k)$$

$$a^2(k) = A^2 C C^* H_{yu} H^*_{yu}/\{[1 + G(a)][1 + G^*(a)]\} \qquad (49)$$

From equation (49) we can conclude, that in a Closed-Loop system the input amplitude (a) of the non-linearity is itself a function of the non-linearity's Describing Function N(a) and the system input amplitude A, caused by the feed-back dynamics

Eq. (49) is a non-linear equation for the unknown amplitude (a) with Reduced Frequency k as a parameter The solutions of Eq. (49) and the corresponding other "frequency response" functions, like Loads L(a,k), are valid only for the specific system input amplitude A Therefore, due to the missing more general characteristics of a linear system, where the dynamic behaviour can be completely determined by applying a Unit Amplitude input, the Superposition Principle does not hold here and solutions for others than sinosoidal system input signals cannot be generated

5.4.1 Stability Analysis

The stability of the closed-loop control system or possible Limit Cycles with critical amplitudes a' and frequencies k' can be determined by means of equation (48) with the sinosoidal system input set to zero (A = 0), leading to the condition:

$$1 + G(a',k') = 0$$

The Describing Function Method is applicable in this case, because at the stability limits, a sinosoidal signal is circulating in the system, if its linear parts have sufficient low-pass characteristics to suppress the higher harmonics generated by the non-linearity

Under these conditions the system is in "Harmonic Balance".

5.4.2 The Jumping Phenomenon

For a certain range of Reduced Frequencies ($k_{j,1} \le k \le k_{j,2}$), equation (49) may have more than one single solution, and one of these solutions can be unstable.

In this case, the non-linear "frequency responses" are ambiguous, depending on the direction of

frequency variation (increasing or decreasing k) The following figure may help to understand the phenomenon .

Let the right-(or left-)hand-side distorted "frequency response" curve be the graph of the solution of Eq. (49 <). With increasing k, ($0 \leq k \leq = k_{max}$), the amplitude a(A,k) increases up to point "C", where the resonance curve has a vertical tangent. With further increasing k the amplitude drops to point "D" at $k = k_{j,2}$. Beyond $k = k_{j,2}$ the solutions are again unique and the amplitude decreases continuously up to $k = k_{max}$.
Starting at $k = k_{max}$, with decreasing frequencies k the amplitude increases up to point "B", where the resonance curve has another vertical tangent at $k = k_{j,1}$. With further decreasing k, the amplitude jumps to the higher value at point "A" and subsequently decreases continuously to the value at k = 0, because the solutions of Eq. (49) are again unique below $k = k_{j,1}$. Between $k_{j,1}$ and $k_{j,2}$ the solutions of Eq. (49) are not unique and the branch (B-C) of the resonance curve is unstable.

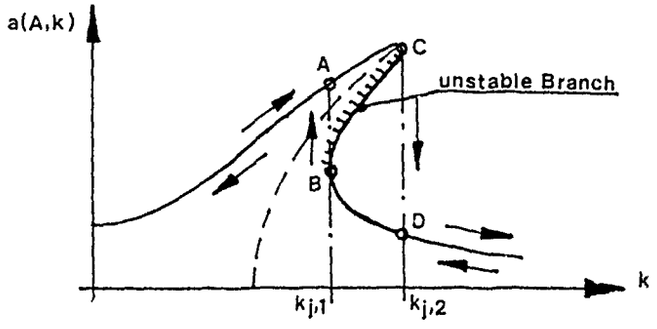

Figure 6. The Jumping Phenomenon

5.4.3 Applicability Conditions of the Describing Function Method

Although the general concept of the Describing Function Method looks very attractive on a first glance, it must be stated that the applicability conditions for Discrete Gust Load analysis are very restrictive.
The method is applicable only under the following conditions:

- Wherever the non-linear element is placed in the control system circuit, the input signal to the non-linearity must be definitely sinosoidal, otherwise the Quasi-Linearisation conditions are not fulfilled.

- The linear parts of the dynamic system + control system must have sufficient low-pass characteristics relative to the fundamental frequency of the driving signal or to the frequency of a possible Limit Cycle in order to be able to suppress the higher harmonics generated by the non-linear element.

- External exiting signals are restricted to either steady state sinosoidal ones (ideal) or to more general steady state non-sinosoidal but periodic signals.

- If the dynamic system is near or at its stability boundaries (Limit Cycles), the applicability conditions of the Describing Function Method are fulfilled, because in this case a harmonic signal is circulating in the control system.
  The system is in a "Harmonic Balance".

- The non-linear system should be anti-symmetric $y = f(x) = -f(-x)$ to avoid generation of a constant bias signal, which would be in conflict with the first criterion

5.4.4 Discrete Gust Load Analysis (Non-) Applicability

As a consequence of that what has previously been outlined, it must be stated that the Describing Function Method is *not* applicable for recent Discrete Gust input signals, due to their non-steady state, aperiodic , 1-cos characteristics.
For such aperiodic, non-steady state input signals the Describing Function is not defined and the Discrete Gust Load analysis should be done in the time-plane.

Despite of non-applicability of the Describing Function Method with recent Discrete Gust Models, the essentials of the method were outlined here in detail, in order to extend the tool-box of Frequency Plane analysis methods also for non-linear systems, and to enable load studies with Sinosoidal Discrete Gust inputs, although recently not supported by the requirements.

5.4.5 The Eqivalent Gain Method

The Quasi-Linearisation approach for non-linear system elements exited by random input signals is known as 'The Eqivalent Gain Method'.
The following assumptions and restrictions for random input signals and system characteristics are made before the basic equation to determine Equivalent Gains for specific types of non-linear elements will be derived.

The random input signal should be stationary and ergodic, having a Gaussian probability density distribution with zero mean-value The gaussian distribution is required to use the linearized element in a closed-loop control system. Furthermore, it is assumed that the distorsions in the output signal generated by the non-linearity are not correlated with the input signal.
The non-linearity is assumed static and anti-symmetric, $y = f(x) = -f(-x)$, causing the Equivalent Gain to be real-valued and the output signal bias-free
For hysteresis-type non-linearities a 90-degree phase-shifted or an orthogonal signal to the input signal x(t) would be additionally required to establish the imaginary part of the Equivalent Gain. This more complicated case will not be considered.

5.4.6 Determination of the Equivalent Gain

In order to derive the fundamental equation to determine Equivalent Gains for specific non-linearities of the above class, we refer to Figure 4 on page V-47.
The input signal x(t) will now be assumed as a random function and the designation N(a) for a

complex Describing Function is renamed by k_e, the real Equivalent Gain, yielding the new random error signal:

$$e(t,k_e) = f[x(t)] - k_e x(t)$$

Following the same approach applied to derive the Describing Function for a sinosoidal input signal, the variance of the error signal is minimized with respect to k_e:

$$\text{var}[e(t)] = \lim_{T\to\infty} 1/2T \int_{-T}^{T} e^2(t,k_e)\, dt = = > \min$$

or applying equivalent sample integration for ergodic signals:

$$\text{var}[e(x)] = \int_{-\infty}^{\infty} e^2(x,k_e)p(x)\, dx = = > \min$$

Where $p(x)$ is the probability density distribution of the input signal.
Differentiating the variance of the error signal with respect to k_e, yields:

$$\text{dvar}[(e(x)]/dk_e = \int_{-\infty}^{\infty} 2\ e(x,k_e)\ d[e(x,k_e)]/dk_e p(x)\, dx = 0$$

$$= \int_{-\infty}^{\infty} [\ -xf(x) + k_e x^2\ ]\ p(x)\, dx = 0$$

With $$\sigma_x^2 = \int_{-\infty}^{\infty} x^2\ p(x)\, dx\ ,$$

the mean-square value of $x(t)$, we obtain the required basic relation to determine the Equivalent Gain:

$$k_e = 2/\sigma_x^2 \int_{0}^{\infty} x\, f(x)\, p(x)\, dx \qquad (50)$$

The lower integration limit can be zero, because due to the previous assumptions, the expression under the integral sign is a symmetric function.
For Gaussian probability density distributions, the following formula may be alternatively used:

$$k_e = 2/(\sqrt{2\pi}\sigma_x) \int_{0}^{\infty} f'(x)\exp[-x^2/(2\sigma_x^2)]\, dx \qquad (51)$$

where $f'(x)$ is the derivative of $f(x)$ with respect to x.
Formulae (50/51) show that the Equivalent Gain is a function of the mean-square or rms-value of the input signal $x(t)$ In the random case the rms-value takes the role the amplitude has in the Describing Function analysis.
If the non-linear element is part of a closed-loop control system, we get the same relations already found in the Describing Function method: The input signal rms-value of the non-linearity becomes itself dependent on the unknown k_e, yielding the general non-linear equation to determine the Equivalent Gain:

$$k_e = f[\sigma_x(k_e)]$$

For application of the Equivalent Gain in a closed-loop system, the theoretical approach and the system arrangement outlined for the Describing Function method can be analogously used, if N(a) is renamed by k_e and the signals are considered as random functions described by their power spectral densities and associated rms-values.

Instead of Eq. (49), the eqivalent equation for the mean-square value of x(t) due to a random exiting signal u(t) reads:

$$\sigma_x^2(k_e) = \int_0^\infty |H_x(k,k_e)|^2 \Phi(k)\, dk$$

$\sigma_x^2(k_e)$ = Mean-square value of the non-linearity input signal x(t) in a closed-loop.

$H_x(k,k_e) = C(k)H_{yu}(k)/[1 + G(k,k_e)]$ Transfer Function of x(t), A = 1 in Eq. (48)

$G(k,k_e) = C(k)H_{yd}k_e$

$\Phi(k)$ = Power Spectrum (v.Karman) of the random exiting signal u(t) with rms-value σ.

Examples:

Limiter:

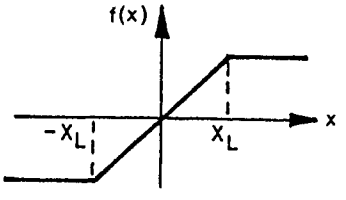

$$f(x) = \begin{cases} x & \text{for } |x| \le X_L \\ X_L & \text{for } |x| > X_L \end{cases}$$

$$f'(x) = \begin{cases} 1 & \text{for } |x| \le X_L \\ 0 & \text{for } |x| > X_L \end{cases}$$

Applying formula (51) for gaussian input signals, we obtain:

$$k_{e,L} = f_0 \int_0^{X_L} \exp[-x^2/(2\sigma_x^2)]\, dx$$

$$f_0 = 2/(\sqrt{(2\pi)}\sigma_x)$$

Normalizing the integral with $x = \sqrt{2}\sigma_x u$ $dx = \sqrt{2}\sigma_x du$ and $U_L = X_L/(\sqrt{2}\sigma_x)$, yields

$$k_{e,L} = 2/\sqrt{\pi} \int_0^{U_L} \exp(-u^2)\, du$$

$$k_{e,L} = \text{erf}(U_L) = \text{erf}[X_L/(\sqrt{2}\sigma_x)]$$

erf(.) = Error Function

Quadratic Damping:

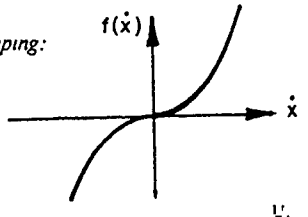

$$f(\dot{x}) = d\,\dot{x}^2 \text{sign}(\dot{x})$$

$$f'(x) = 2\,d\,|\dot{x}|$$

By means of Eq. (51): $$k_{e,Q} = d_0 \int_0^{U_L} \exp[-\dot{x}^2/(2\sigma_{\dot{x}}^2)\dot{x}]\, d\dot{x}$$

$$d_0 = 4d/(\sqrt{2\pi}\sigma_{\dot{x}})$$

Normalizing the integral by $u = \dot{x}^2/(2\sigma_{\dot{x}}^2)$ and $\sigma_{\dot{x}}^2\ du = \dot{x}\ d\dot{x}$, yields:

$$k_{e,Q} = 4d/\sqrt{2\pi}\ \sigma_{\dot{x}} \int_0^\infty \exp(-u)\ du$$

and finally

$$k_{e,Q} = 4d/\sqrt{2\pi}\sigma_{\dot{x}}$$

Dead Zone:

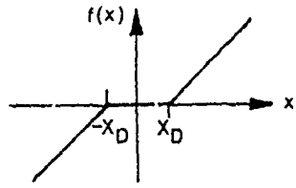

$$f_D(x) = \begin{cases} 0 & \text{for } |x| \le X_D \\ x & \text{for } |x| > X_D \end{cases}$$

The Dead Zone function can be represented by the difference of a linear function $f(x) = x$ and a Limiter function $f_L(x)$ with $X_L = X_D$.

$$f_D(x) = x - f_L(x)$$

$$f'_D(x) = 1 - f'_L(x)$$

Applying Eq (51) and using the result of the Limiter function with $X_L = X_D$, yields

$$k_{e,D} = f_0 \cdot \int_0^\infty \exp(-x^2/(2\sigma_x^2))\ dx \cdot \mathrm{erf}[X_D/(\sqrt{2}\cdot\sigma_x)$$

and finally

$$k_{e,D} = 1 - \mathrm{erf}\,[\,X_D/(\sqrt{2}\sigma_x)\,]$$

5.4.7 Applicability of the Equivalent Gain Concept

In a closed-loop system, most of the general applicability conditions remain valid also for the Equivalent Gain Method, when in "Applicability Conditions of the Describing Function Method" on page V-51 the term 'Sinosoidal Signal' is replaced by 'Gaussian Signal'

Low-pass filtering of the higher harmonics is considered as equivalent to low-pass filtering the non-gaussian disturbances generated by the non-linear element in order to maintain gaussian signal characteristics in the control system.

The Equivalent Gain is applicable for the PSD-DESIGN ENVELOPE ANALYSIS method due to its close relation to the rms-value of a random signal.

It is *not* applicable for the PSD-MISSION ANALYSIS method, because the number-of-exceedances of *peak* load levels are under-estimated with the classical Equivalent Gain Concept.

For the PSD-MISSION ANALYSIS case, R. NOBACK/C BLAAUBOER propose to determine the Equivalent Gain by minimizing the variance of the *energy-error* signal, instead of minimizing the variance of the error signal itself:

$$\mathrm{var}(\,e_{EN}\,) = \mathrm{var}(\,f^2(x) - k_e^2 x^2\,) = => \min$$

The resulting Equivalent Gain is more appropriate for PSD-MISSION ANALYSIS application due to the squaring effect, which puts more weight on the amplitude *peaks* of the signals leaving the non-linearity and the linear Equvalent Gain block.

6.0 References

1. R.L. Bisplinghoff, H. Ashley and R.L. Halfman
AEROELASTICITY
Addison-Wesley Publishing Company, 1957

2. H.W. Foersching
GRUNDLAGEN DER AEROELASTIK
Springer Verlag; Berlin, Heidelberg, New York

3. J.C. Houbolt, R. Steiner and K.G Pratt
Langley Research Center, Langley Station, Hampton, Virginia
DYNAMIC RESPONSE OF AIRPLANES TO ATMOSPHERIC TURBULENCE INCLUDING FLIGHT DATA ON INPUT AND RESPONSE
NASA Technical Report TR R-199, June 1964

4. F M. Hoblit, Neil Paul, J.D. Shelton and F.E. Ashford
DEVELOPEMENT OF A POWER-SPECTRAL GUST DESIGN PROCEDURE FOR CIVIL AIRCRAFT
LOCKHEED-California, Burbank, California
Technical Report ADS 53, January 1966 ; prepared for The FEDERAL AVIATION AGENCY

5. R. Fuller, L.D. Richmond, C.D. Larkins and S.W. Russell
The Boeing Company, Renton, Washington
CONTRIBUTIONS TO THE DEVELOPEMENT OF A POWER-SPECTRAL GUST DESIGN PROCEDURE FOR CIVIL AIRCRAFT
Technical Report ADS 54, January 1966 ; prepared for THE FEDERAL AVIATION AGENCY, Aircraft Developement Service

6. J.C. Houbolt
Aeronautical Research Associates of Princeton Inc., Princeton, New Jersey
EXCEEDANCES OF STRUCTURAL BOUNDARIES FOR RANDOM EXCITATION
AIAA Paper 68-140, January 1968

7. J.C. Houbolt
ON TURBULENCE ENVIRONMENT AND DESIGN CRITERIA
prepared for AGARD Flight Mechanics Panel Symposium, Woburn Abbey, Bedford, Bedfordshire, United Kingdom, 17-18 May 1973

8. J.R. Fuller
The Boeing Company, Seattle, Washington
BOUNDARY EXCURSIONS FOR COMBINED RANDOM LOADS
AIAA-Journal Vol. 20, No. 9, January 1982

9. H.N. Murrow, K.G. Pratt, and J.C. Houbolt
NASA Langley Research Center, Hampton, Virginia 23665-5225
NACA/NASA RESEARCH RELATED TO EVOLUTION OF U.S. GUST DESIGN CRITERIA
89-1373-CP

10. H. Schlitt
STOCHASTISCHE VORGAENGE IN LINEAREN UND NICHTLINEAREN REGELKREISEN
Stochastic Processes in Linear and Non-linear Control Systems
Verlag Friedr. Vieweg & Sohn, Braunschweig, 1968

11. Ranjan Vepa
NASA Langley Research Center Hampton, Virginia
ON THE USE OF PADE APPROXIMANTS TO REPRESENT UNSTEADY AERODYNAMIC LOADS FOR ARBITRARY SMALL MOTIONS OF WINGS
AIAA-Journal 1976

12. R. Noback and C. Blaauboer
Nationaal Lucht- en Ruimtevaart Laboratorium
THE DETERMINATION OF GUST LOADS ON NON-LINEAR AIRCRAFT USING A POWER-SPECTRAL DENSITY APPROACH
National Aerospace Laboratory NLR, The Netherlands, Dec 1980

13 MSC / NASTRAN
- HANDBOOK OF DYNAMIC ANALYSIS
- AEROELASTIC SUPPLEMENT
The MacNeal Schwendler Corporation

14. Federal Aviation Regulations FAR, Part 25
Airworthiness Standards, Transport Airplanes Category

15. Joint Aviation Requirements, JAR, Part 25 : Large Aeroplanes
Joint Airworthiness Authorities

CHAPTER VI
ANALYSIS BY THE STATISTICAL DISCRETE GUST METHOD

by

John Glaser
Boeing Canada, de Havilland Division
Garratt Blvd., Downsview
Ontario M3K 1Y5
Canada

CONTENTS

ABSTRACT

The general formulation of the Statistical Discrete Gust (SDG) model for atmospheric turbulence proposed by J.Glynn Jones for the von Karman spectrum in its higher frequency range is defined and illustrative results are presented. The equivalence of the two models, SDG and PSD, is confirmed by showing that the dynamic response ratios, $\bar{\eta}/\bar{A}$, for both rigid and elastic aircraft loads are reasonably constant and approximately equal to the expected value of 10.4 ft.$^{1/3}$. Although the SDG method is more complex to implement and more costly to run than the PSD method of FAR/JAR 25, its implementation for routine calculations of linear aircraft structures is confirmed by the present study. The SDG model offers an alternative time domain analysis method for calculating response loads to continuous turbulence for both linear and non-linear aircraft structures (active controls). In addition, the SDG method can potentially provide a more representative model for extreme gust processes, but this requires further development.

NOTATION

$\bar{A}$ PSD dynamic response for unit gust velocity ($U_\sigma = 1$)
H gust gradient length
I_n fractional gradient energy for gust with n ramps
L integral scale of turbulence
n number of component gust ramps
$\bar{n}$ number of component gust ramps in the critical gust pattern
Δn aircraft cg vertical acceleration factor
P_n gust amplitude factor for gust with n ramps
U_o design gust velocity, SDG method
U_σ design gust velocity, PSD method
w component (1-cos) ramp hold gust velocity
W_n gust velocity pattern made up of n component gust ramps
x spatial coordinate
γ SDG dynamic response for a tuned gust pattern and unit gust velocity (U_σ=1)
$\bar{\gamma}$ SDG dynamic response for the critical gust pattern and unit gust velocity (U_o=1)
$\Delta\dot{\theta}$ aircraft cg pitch velocity
$\Gamma(\ )$ gamma function

1. INTRODUCTION

The assumption underlying the Statistical Discrete Gust (SDG) model of atmospheric turbulence is that the turbulent flow field, even when apparently continuous, contains coherent structures which in some cases may be more appropriately represented by spatial velocity distributions than by a frequency or spectral form (Reference 1). For one-dimensional turbulence models, the coherent structure may be expressed by simple, discrete, (1-cos) ramp-hold components, having random gradient distances, H, and amplitudes, w, randomly distributed in space, x, (Figures 1 and 2).

Various models of atmospheric turbulence can be simulated using the (1-cos) ramp gust as a building block. For example, it is evident that measured extreme gust patterns, as shown in Figure 3 (from Reference 2) may be approximated with 1, 2 or more components. For these extreme gusts, there is sufficient evidence to indicate that the following relationship holds between gust intensity, w, and gust gradient distance, H:

$$w \propto H^{1/6}$$

However, further data analysis is required to establish the statistical weighting factors or amplitude factors needed to complete an SDG model for these extreme gust conditions. Presently, the versed sine gust shape of FAR/JAR 25.341, is used to determine aircraft design loads for extreme gust encounters. This gust pattern will be recognized as a special, two-ramp case with $H_1 = H_2$, $w_1 = w_2$ and $H_s = 0$, in Figure 1b.

For continuous random processes such as Dryden or von Karman, SDG models have been proposed using the discrete-

element technique of Reference 3. For the von Karman Power Spectral Density (PSD) model, the relationship between gust intensity and gust gradient distance is:

$$W \propto H^{1/3}$$

for values of frequency ω in the $\omega^{-5/3}$ range. The family of (1-cos) gust components forming this gust model is illustrated in Figure 4 and the example gust patterns shown in Figures 1 and 2 reflect the $H^{1/3}$ gust intensity relationship.

This proposed SDG approach has been the subject of some study by an ad hoc committee of international gust specialists. One objective of that study was to determine if the two models, SDG and PSD, were in fact equivalent in terms of aircraft responses; ie., whether there was a so-called "overlap" of the SDG time domain and the PSD frequency domain models. The present report stems from that activity. See also Reference 4.

In the course of its development, a number of SDG formulations have been proposed for this region of "overlap". They are characterized by the complexity of the gust patterns producing maximum responses and by the related methods used to calculate the amplitude factors. They are identified as Methods 1, 1a, 2 and 3 in Reference 1 where Method 3 is the most general. For the present report, Method 2 was selected because it imposed no restrictions on gust pattern and because the approximation made in calculating the amplitude factors introduced little error in dynamic response values (4% at most) while reducing computer costs. The application of this simpler method thus permitted an assessment on the practicality of implementing the SDG method (Methods 2 or 3) for routine aircraft design computations.

The report begins by defining the SDG method employed in the present study. Illustrative results are then presented for an aircraft with linear structural dynamic properties from which an assessment on "overlap" can be made. The results presented have been scaled by an arbitrary factor and can be treated as dimensionless; absolute magnitudes are not important to this report.

2. THE SDG GUST MODEL

An expression for a general gust pattern made up of n, (1-cos), ramp-hold gust components may be written as follows:

$$W_n(x) = U_o P_n \sum_{1}^{n} (sgn)_i \, \Delta W_i(x-x_i) \qquad (1)$$

where

$$\Delta W_i(x-x_i) = 0 \qquad (x-x_i) < 0$$

$$\Delta W_i(x-x_i) = \frac{1}{2} H_i^{1/3} \left(1-\cos \frac{\pi(x-x_i)}{H_i}\right) \qquad 0 \le (x-x_i) \le H_i$$

$$\Delta W_i(x-x_i) = H_i^{1/3} \qquad H_i < (x-x_i)$$

Consistent with the von Karman gust spectrum of FAR/JAR 25 for the $\omega^{-5/3}$ frequency range, the (1-cos) ramp hold components have been given magnitudes, w_i, proportional to $H_i^{1/3}$ where H_i is the gust gradient distance for component i. Also, H_i is restricted in magnitude to a maximum of 2500 feet, the integral scale of turbulence, L , specified for the FAR/JAR 25 PSD model. The term, $(sgn)_i$, is used to represent the "+" or "-" sign for each component gust. Note that the i^{th} gust component starts at x_i and that x_1 is taken to be zero (Figure 2).

Equation 1 includes a statistical weighting or amplitude factor, P_n, which is used to place the intensities of each gust pattern on an equal probability basis. These P_n factors have the values:

$$P_1 = 1$$

$$P_n = \frac{1}{.88\sqrt{I_n/I_1}} \qquad n > 1 \qquad (2)$$

where n is the number of ramp gust components forming the pattern and where I_n is the fractional gradient energy (FGE) given by

$$I_n = \int_0^{x_{max}} \left(\frac{d^{5/6} W_n(x)}{dx^{5/6}}\right)^2 dx \qquad (3)$$

where the upper limit of integration, x_{max}, corresponds to the end of the final ramp (Figure 2). It is at this point where Method 3 differs from Method 2 because in Method 3 the integration is taken to infinity, or at least to convergence.

The fractional derivative forming the integrand has the analytical expression (References 5 and 6):

$$\frac{d^{5/6} W_n(x)}{dx^{5/6}} = D^{5/6} W_n(x) - \frac{d}{dx}\left(\frac{1}{\Gamma(1/6)} \int_0^x (x-t)^{-5/6} W_n(t)dt\right) \qquad (4)$$

and may be evaluated numerically by dividing the range 0 to x by N + 1 equally spaced points as follows:

$$D^{5/6} W_n(x) = \frac{(\Delta x)^{-5/6}}{\Gamma(7/6)} (A_o \delta w_o + A_1 \delta w_1 \ldots + A_{N-1} \delta w_{N-1}) \qquad (5)$$

where

$$\Delta x = x/N$$
$$A_o = 1$$
$$A_j = (j + 1)^{1/6} - j^{1/6}$$

and where

$$\delta w_j = w_j - w_{j+1}$$

A peculiar characteristic of the fractional derivative is that its value depends on the prior behavior of the gust pattern and not just on its properties at the evaluation point. This is apparent from the expression for the fractional derivative (Equation 4) because it involves integration. The implication is that the fractional derivative is not zero at and beyond the end of the final ramp, x_{max}, (as it would be for a first derivative), but it converges asymptotically to that value as x tends to infinity. As a result the value for the fractional gradient energy, I_n, is underestimated by truncating the integration at x_{max}. The magnitude of this underestimation was determined for various gust patterns and varied from 1% for a versed sine gust to a maximum of about 8%. The influence on amplitude factor, P_n, however, was only ±4% because of the square root effect (Equation 2).

Before proceeding further, it might be helpful to know that for gust patterns with non-overlapping components (Method 1 of Reference 1) the amplitude factors, P_n, are reasonably well approximated by

$$P_1 = 1$$

$$P_n = \frac{1}{.88\sqrt{n}} \qquad n > 1 \qquad (6)$$

This approximation makes clear the general trend that for equal probability, the amplitude factors decrease as the number of component ramps increase. While this approximation may be useful for qualitative assessments, for routine calculations it is recommended that the P_n factors be calculated using the fractional gradient energy expressions.

Finally in Equation 1, U_o is the design gust velocity paralleling the parameter U in the PSD gust model. For

now, U_o will be taken equal to 1 ft/sec/ $ft^{1/3}$. The peculiar dimension for U_o should be noted.

3. ESTABLISHING CRITICAL GUST PATTERNS

The critical gust pattern is defined as the tuned gust pattern (with $U_o = 1.$) giving the largest response magnitude from the set of tuned patterns made up of one, two, three ... etc. ramp components with the appropriate amplitude factor, P_n, applied. In general, the critical gust pattern for each response parameter (normal acceleration, wing root bending moment, etc) will be different. With reference to Equation 1, the search for the critical gust pattern involves determining values for:

$\bar{n}$ = the number of component ramps making up the critical gust pattern
H_i = the gust gradient length for each ramp (recall w is proportional to $H^{1/3}$)
$(sgn)_i$ = the gust direction for each ramp (up or down for a vertical gust field)

and

x_i = the spatial starting points for each ramp assuming $x_1 = 0$.

For linear systems, tuned gust patterns are efficiently established by applying the superposition principle in the manner detailed in steps (a) through (f) below. This procedure must be repeated for each response parameter of interest.

(a) Calculate the time history response for a number of single ramp components of varying gust gradient length, H, defined by Equation 1. Sample time histories for vertical shear (NSV) at fuselage station (FS) 424 are shown in Figure 5 for four different vertical gust lengths.

(b) From the time history response for each H, determine the largest absolute response value between each pair of zero crossings of the time history and plot these peak values vs. H. The resultant graph which makes use of data from Figure 5 is given in Figure 6. Reference 7 provides a Fortran computer routine for sorting the peak response data and removing the unnecessary discontinuities that often appear in these plots. The routine does this by tracking and removing discontinuities in the better behaved, peak time vs. H data.

(c) Determine the stationary (zero slope) response values for each peak response curve and mark them in order of decreasing magnitude. Denote these values M_j. Associate with each M_j, the gust gradient length H_j. Figure 6 illustrates for M_3 and H_3.

(d) Construct the set of tuned gust patterns using H_1, H_1+H_2, $H_1+H_2+H_3$, ... gust ramps as illustrated in Figure 7. The suggested set of patterns made up of 1, 2, 4, 8,....ramps, (References 1 and 2) was not

adopted because there was no assurance that the largest response would be obtained. Indeed, the results presented in Tables 1 and 2 which gives the critical number of ramps for each response parameter confirm that the full set should be considered.

(e) Calculate P_n for each pattern using equation (2) and the expressions for fractional gradient energy.

(f) Calculate the peak response magnitudes for each tuned gust sequence by applying superposition as follows:

$$\begin{aligned}
\gamma_1 &= P_1 M_1 \\
\gamma_2 &= P_2(M_1 + M_2) \\
\gamma_3 &= P_3(M_1 + M_2 + M_3) \\
&\cdot \\
&\cdot \\
&\cdot \\
&\cdot \\
\gamma_n &= P_n(M_1 + M_2 + \ldots M_n) \qquad \text{for all } n
\end{aligned} \tag{7}$$

The gust pattern producing the largest value of γ_i, denoted as $\bar{\gamma}$, is called the critical gust pattern for the particular response parameter under consideration.

As an example, the critical gust pattern for vertical shear at fuselage station 424, determined by the above procedure, is illustrated in Figure 8. Also shown in Figure 8 is the corresponding response time history. Note that the peak time history response value, $\bar{\gamma}$, will be the same as the maximum value obtained in step (f).

Once the critical gust pattern has been established for a particular parameter of interest, the time correlated responses for all parameters can be calculated using that pattern (and associated amplitude factor, P_n).

4. ASSESSING THE "OVERLAP"

Having established the critical gust pattern (for $U_o = 1$) for a particular load of interest, design limit loads are given by:

$$L_{Limit} = L_{Static} \pm U_o \bar{\gamma} \tag{8}$$

Design values for U_o have not yet been established; however, on an individual load basis, values may be determined by applying the following expression relating SDG and PSD dynamic results.

$$U_o \bar{\gamma} = U_\sigma \bar{A}$$

or, equivalently;

$$\bar{\gamma}/\bar{A} = U_\sigma/U_o \tag{9}$$

Since U_ρ and U_o are taken to be constants, the determination of equivalence or whether the two gust models "overlap" requires that the SDG to PSD dynamic ratio, $\bar{\gamma}/\bar{A}$, be a constant as well, independent of the aircraft or load under consideration. This ratio was estimated in Reference 3, on the basis of a single degree of freedom system, to have a value of approximately 10.4 ft.$^{1/3}$. Note that the ratio, $\bar{\gamma}/\bar{A}$, is dimensional and therefore its value will depend on the system of units used. The values obtained for $\bar{\gamma}/\bar{A}$ from the present analysis for both rigid and flexible aircraft models are given in the following section.

5. ILLUSTRATIVE RESULTS

When applying the SDG method as formulated in Equation 1, it first must be confirmed that flight stability and structural frequencies do in fact lie in the higher frequency range of the von Karman spectrum for which the present SDG model was designed. Specifically, Perry shows in Reference 4 for a rigid aircraft that the short period frequency must be at least ten (10) times greater than the frequency corresponding to the point of maximum intensity, F^*, of the spectrum (Figure 9). With this condition satisfied, Perry found that the SDG-to-PSD dynamic response ratio, $\bar{\gamma}/\bar{A}$, was well approximated by 10.4 ft.$^{1/3}$ as expected from the results of Reference 3. He also found that when the short period frequency fell in the range F^* to $10F^*$ the $\bar{\gamma}/\bar{A}$ ratio deviated from 10.4 by almost 20%.

For the present analysis, as indicated in Figure 9, Perry's requirement on frequency is satisfied and therefore the value expected for $\bar{\gamma}/\bar{A}$ is 10.4 ft.$^{1/3}$. The cg response results for vertical acceleration, Δn, and pitch velocity, $\Delta\dot{\theta}$, presented in Table 1 for a rigid aircraft subject to single point excitation, support to within 2% that expectation for both nominal and 50% nominal short period damping.

When wing and tail spatial excitation effects are included, the maximum deviation from 10.4 ft.$^{1/3}$ approaches 7% for both the rigid and the flexible aircraft case with nominal short period damping.

Table 2 presents uncorrelated dynamic response ratios for a number of wing, horizontal tail and fuselage loads and compares them with the expected value of 10.4 ft.$^{1/3}$. While the values range from 7.9 (ie, 24% low) to 12.1 (ie, 16% high) the mean value obtained for $\bar{\gamma}/\bar{A}$ is 10.6 ft.$^{1/3}$ with a standard deviation of 0.88.

Figures 10 and 12, present SDG and PSD correlated vertical shear distributions for the fuselage matched at stations 424 and 711, respectively. Figures 11 and 13 present the corresponding correlated vertical bending moment distributions. The dynamic ratios, $\bar{\gamma}/\bar{A}$, required to match SDG and PSD results at these stations are shown in the figures and are the same as those given in Table 2. The largest difference in these results is approximately 13% and occurs in the vertical shear load at the wing front spar station (Figure 12).

6. CONCLUDING REMARKS

The general formulation (Method 2 of Reference 1) of the Statistical Discrete Gust (SDG) model proposed by J. Glynn Jones for the von Karman spectrum in its higher frequency range was defined and illustrative results were presented .

The equivalence of the two models, SDG and PSD, was assessed by comparing the dynamic response ratios, $\bar{\eta}/\bar{A}$, for both rigid and elastic aircraft cg responses and for a variety of elastic aircraft loads. Although there is some variation in the results, the values obtained for $\bar{\eta}/\bar{A}$ are sufficiently consistent to conclude that there is adequate equivalence or "overlap" between the two models. Based on 34 elastic aircraft loads results, the mean value for $\bar{\eta}/\bar{A}$ was 10.6 $ft.^{1/3}$ (ie., 2% higher than the expected value of 10.4) with a standard deviation of 0.88.

The implementation of the proposed SDG method for routine calculations of linear aircraft structures has been confirmed as a consequence of the present study. However, the SDG method is more complex to implement than the PSD gust method of FAR/JAR 25 and it is more computer costly to run.

The SDG model offers an alternative time domain analysis method for determining response loads to continuous turbulence for linear and non-linear aircraft structures (active controls). In addition, the SDG method can potentially provide a more representative model for extreme gust processes. In light of these potential advantages it is recommended that development of the SDG method should continue.

7. ACKNOWLEDGEMENTS

To J. Glynn Jones who saw order in disorder for his pioneering work in the SDG method. To Jack Grabowski, Duan Qian and Mark Wajda for developing the computational methods and for preparing the results.

8. REFERENCES

1) Jones, J.G. **"The Statistical Discrete Gust (SDG) Method in its Developed Form"**, presented at the 30th AIAA Structures, Dynamics and Materials Conference, Mobile Alabama, AIAA 89-1375-CP, April 1989

2) Jones, J.G. **"On the Formulation of Gust-Load Requirements in Terms of the Statistical Discrete - Gust Method"**, RAE TM FS 208, October 1978.

3) Jones, J.G. **"On the Implementation of Power - Spectral Procedures by the Method of Equivalent Deterministic Variables, Part 2, Discrete - Element Technique"**, RAE TM Space 335, May 1984.

4) Perry III, B. Pototzky, A. Woods, J. **"An Investigation of the "Overlap" Between the Statistical-Discrete-Gust and the Power-Spectral-Density Analysis Methods"**, presented at the 30th AIAA Structures, Dynamics and Materials Conference, Mobile Alabama, AIAA 89-1376-CP, April 1989

5) Courant, R. **Differential and Integral Calculus, Vol. II**, Blackie and Sons, 1936.

6) Oldham, K.B. Spanier, J. **The Fractional Calculus**, Academic Press Inc., 1974.

7) Glaser, J.J. Qian, D. **"Method for Smoothing Discontinuities in Peak Tracking Curves Employed in The Statistical Discrete Gust Method"**, presented at the Gust Specialists' Meeting, Mobile, Alabama, April 6, 1989.

TABLE 1

Uncorrelated Aircraft CG Response Ratios $\bar{\gamma}/\bar{A}$

and Comparison with 10.4 Feet$^{1/3}$

Vertical Gust Excitation	Aircraft Model		Response Parameter	Dynamic Ratio $\bar{\gamma}/\bar{A} = U_\sigma/U_o$		No. of Ramps in Critical Pattern $\bar{n}$
	Modes Included*	Short Period Damping		Value Feet$^{1/3}$	Compared to 10.4 (%)	
single point	short period, no elastic	nominal	Δn $\Delta \dot{\theta}$	10.30 10.35	-1.0 -0.5	1 1
single point	short period, no elastic	50% nominal	Δn $\Delta \dot{\theta}$	10.32 10.20	-0.8 -2.0	2 4
distributed over aircraft	short period, no elastic	nominal	Δn $\Delta \dot{\theta}$	11.10 10.60	+6.7 +1.9	2 2
distributed over aircraft	short period, +50 elastic	nominal	Δn $\Delta \dot{\theta}$	11.10 10.50	+6.7 +1.0	2 2

* Short Period Frequency = 0.45 Hz

Δn = Vertical Acceleration of CG

$\Delta \dot{\theta}$ = Pitch Velocity about CG

TABLE 2

Uncorrelated Dynamic Response Ratios Results $\bar{\gamma}/\bar{A}$

and Comparison with 10.4 Feet$^{1/3}$

Aircraft Component	Response Parameter	Location % Semi-Span	Dynamic Ratio Value ft$^{1/3}$	Dynamic Ratio Compared to 10.4 %	Number of Ramps $\bar{n}$
Wing	Vertical Shear	8	11.1	+7	3
		32	11.2	+8	3
		59	11.3	+9	3
		86	10.5	+1	2
	Vertical Bending Moment	8	11.2	+8	3
		32	11.4	+10	2
		59	11.7	+13	3
		86	11.2	+8	3
	Torsion	8	9.0	-13	8
		32	9.8	-6	4
		59	9.0	-13	4
		86	10.3	-1	4
Horizontal Tail	Vertical Shear	4	11.1	+7	2
		58	10.5	+1	2
	Vertical Bending Moment	4	10.8	+4	2
		58	9.7	-7	2
	Torsion	4	9.5	-9	5
		58	7.9	-24	5

Aircraft Component	Response Parameter	Station	Dynamic Ratio Value ft$^{1/3}$	Dynamic Ratio Compared to 10.4 %	Number of Ramps $\bar{n}$
Fuselage	Vertical Shear	192	10.8	+4	4
		312	10.5	+1	6
		387	11.3	+9	3
		424	11.4	+10	3
		531	11.1	+7	3
		607	11.2	+8	3
		711	10.7	+3	6
		822	11.6	+12	3
	Vertical Bending Moment	192	10.7	+3	4
		312	10.7	+3	4
		387	10.8	+4	4
		424	10.3	-1	5
		531	10.6	+2	3
		607	9.6	-8	6
		711	11.0	+6	3
		822	12.1	+16	3

$(\bar{\gamma}/\bar{A})_{mean}$ = 10.6

Std. Deviation = 0.88

Typical Ramp Gust Patterns

(a) Discrete-Ramp Gust

(b) Pattern Comprising a Pair of Ramp Gusts

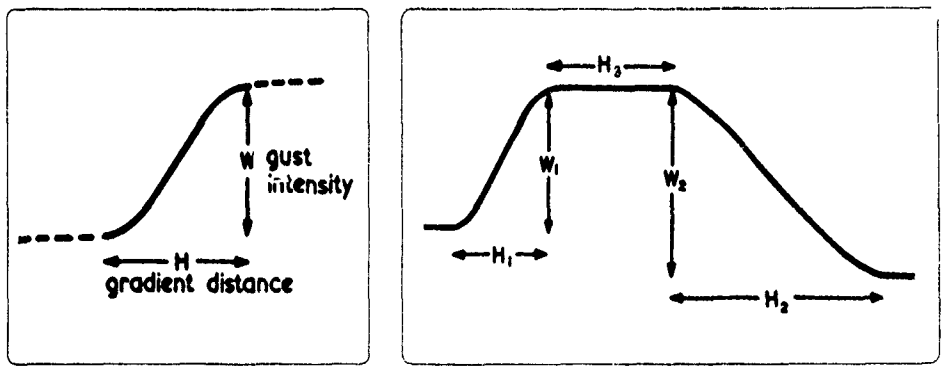

(sketches from reference 2)

FIGURE 1

Example Gust Patterns

Ramps without Overlaps

Ramps with Overlaps

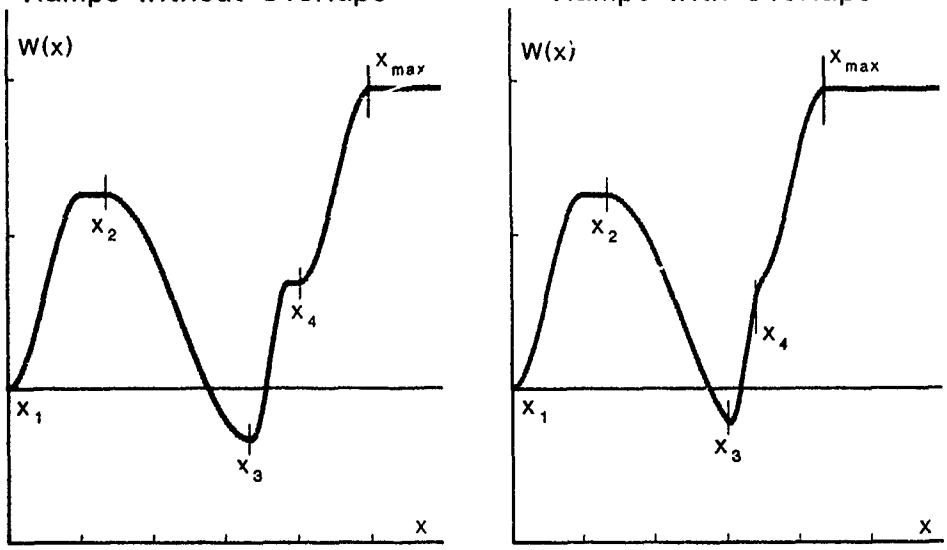

FIGURE 2

Examples of Relatively Isolated Gusts from U.S. High Intensity Gust Investigation

(F-106A Aircraft in Thunderstorms - from reference 2)

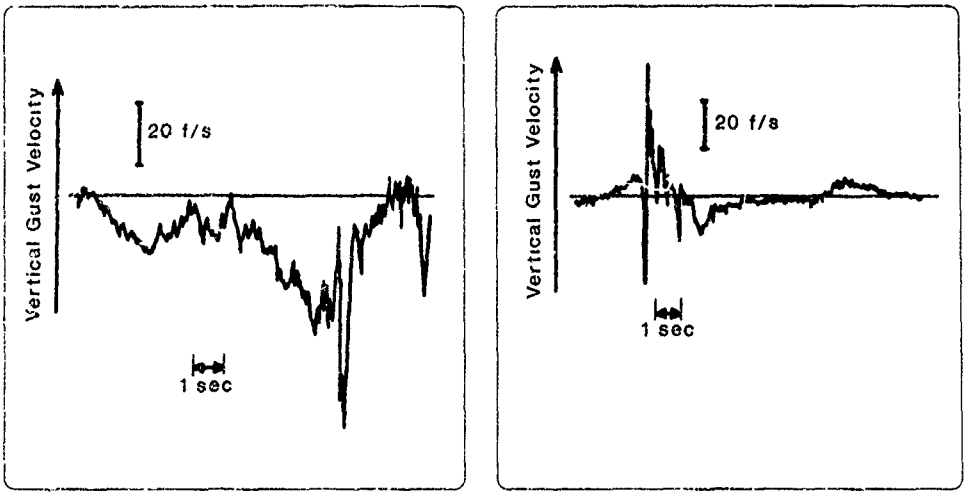

FIGURE 3

Family of Equiprobable Ramp Gusts Defined for H ≪ L

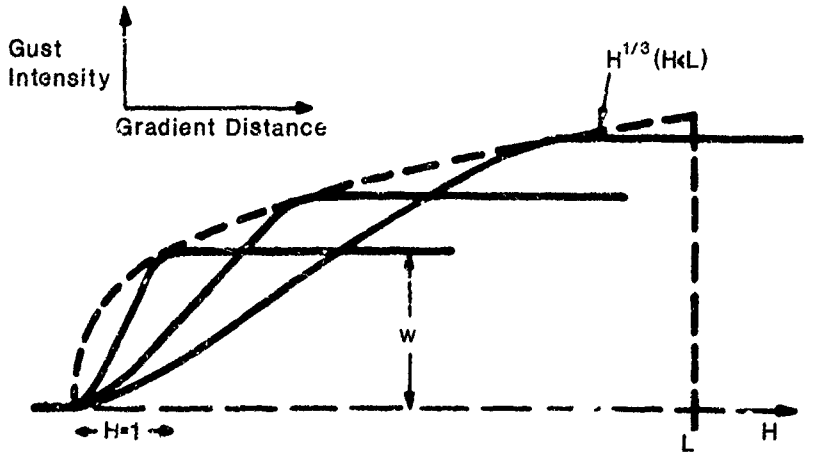

(sketch from reference 2)

FIGURE 4

Response to Selected Ramps

Vertical Shear (NSV), Fuselage Station (FS) 424

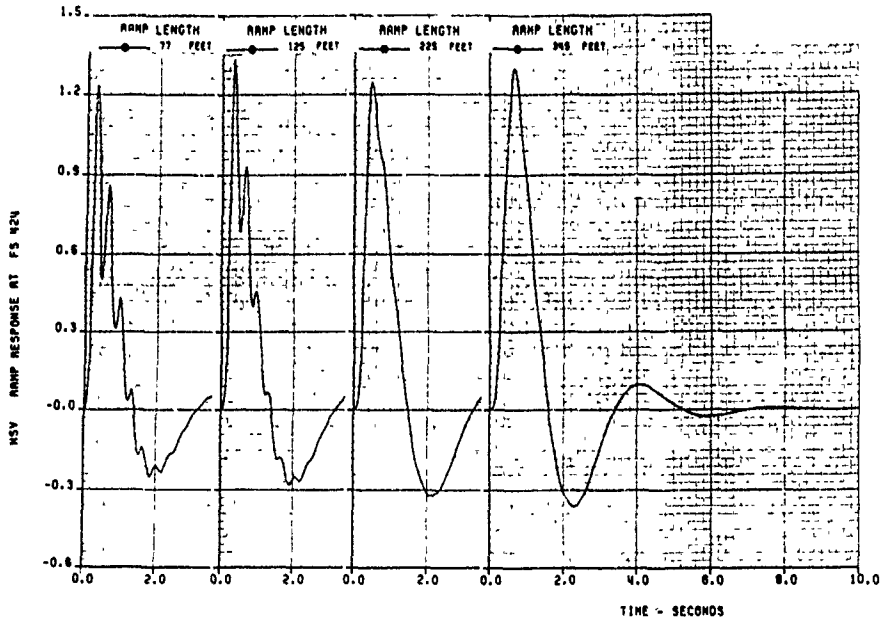

FIGURE 5

Variation in Peak Response with Ramp Length

Vertical Shear (NSV),

Fuselage Station (FS) 424

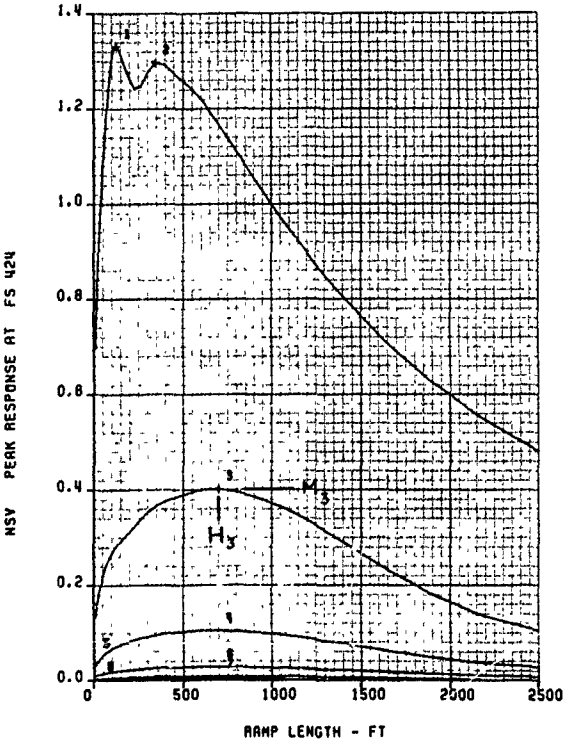

FIGURE 6

The SDG Tuning Process

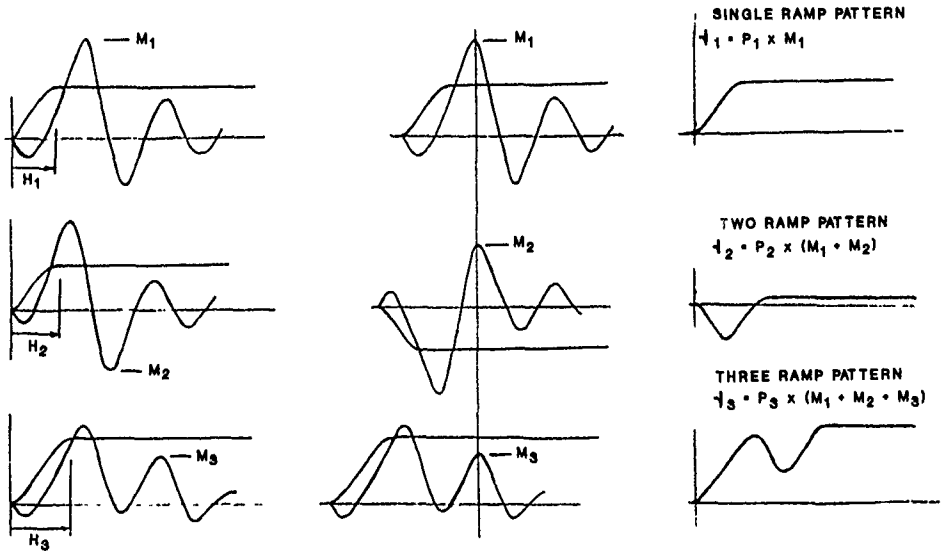

FIGURE 7

Critical Gust Pattern and Corresponding Response Time History

Vertical Shear (NSV), Fuselage Station (FS) 424

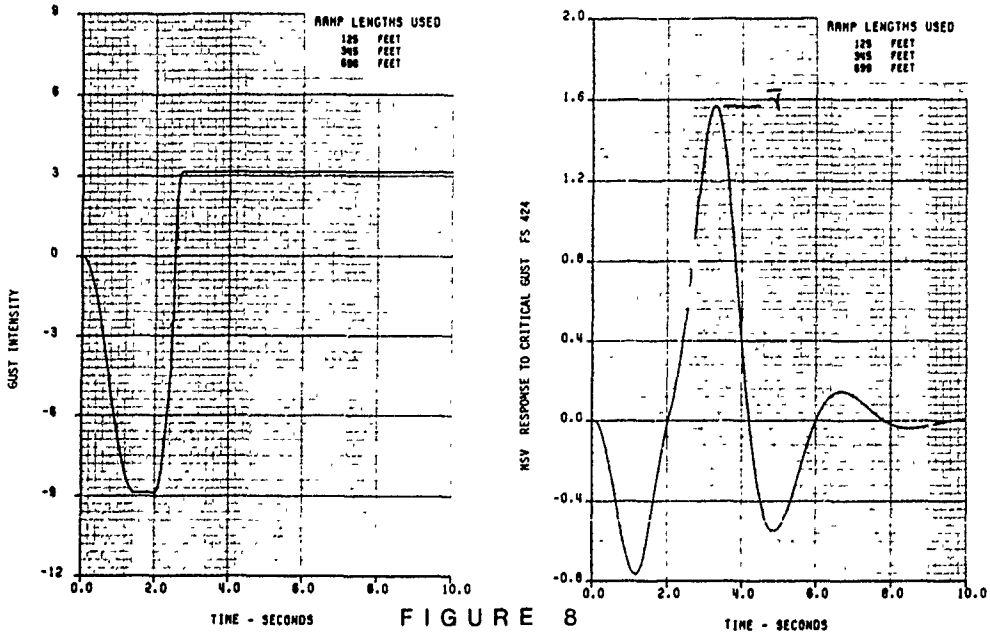

FIGURE 8

Von Karman Turbulence Model

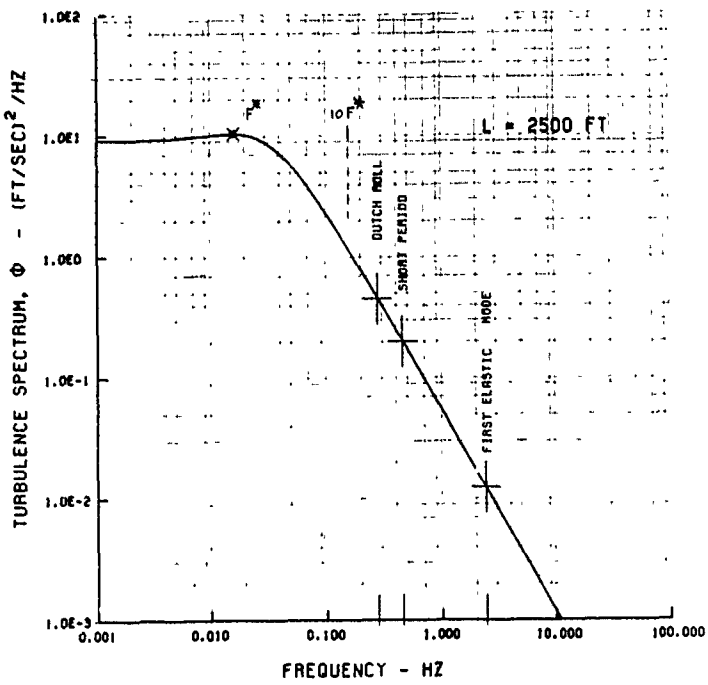

FIGURE 9

Fuselage Vertical Shear Distributions Due to Various Gust Models

Results Matched to Uncorrelated Shear at FS 424

FLEXIBLE AIRCRAFT DESIGN ENVELOPE METHOD

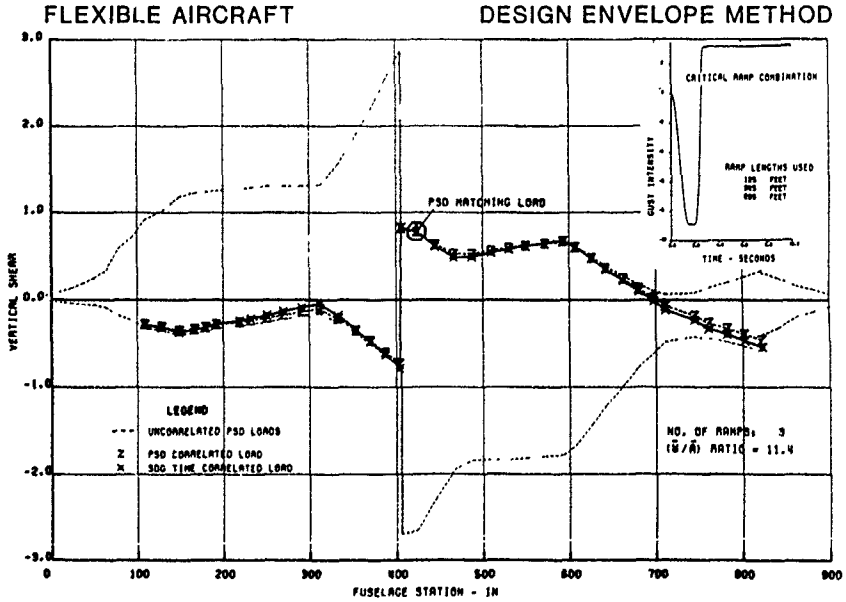

FIGURE 10

Fuselage Vertical Bending Moment Distributions Due to Various Gust Models

Results Matched to Uncorrelated Shear at FS 424

FLEXIBLE AIRCRAFT DESIGN ENVELOPE METHOD

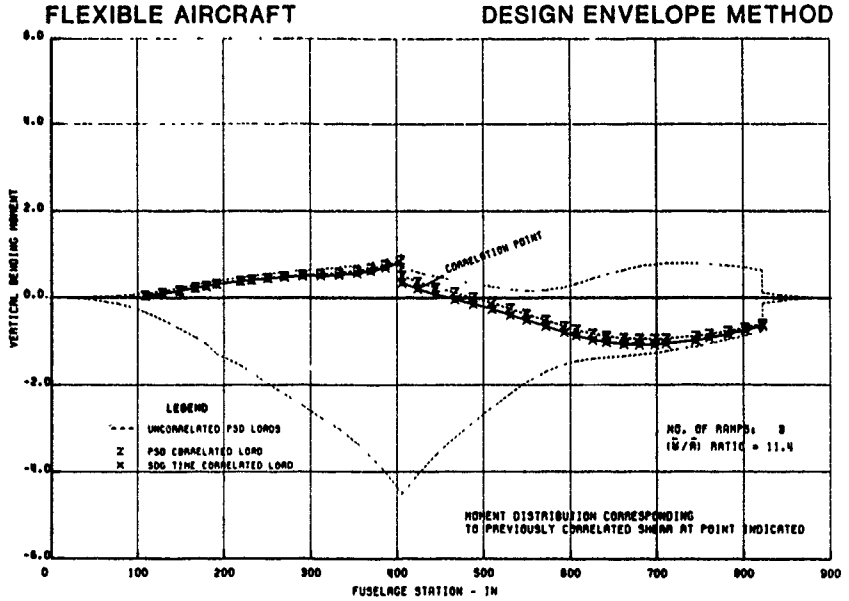

FIGURE 11

Fuselage Vertical Shear Distributions Due to Various Gust Models

Results Matched to Uncorrelated PSD at FS 711

FLEXIBLE AIRCRAFT DESIGN ENVELOPE METHOD

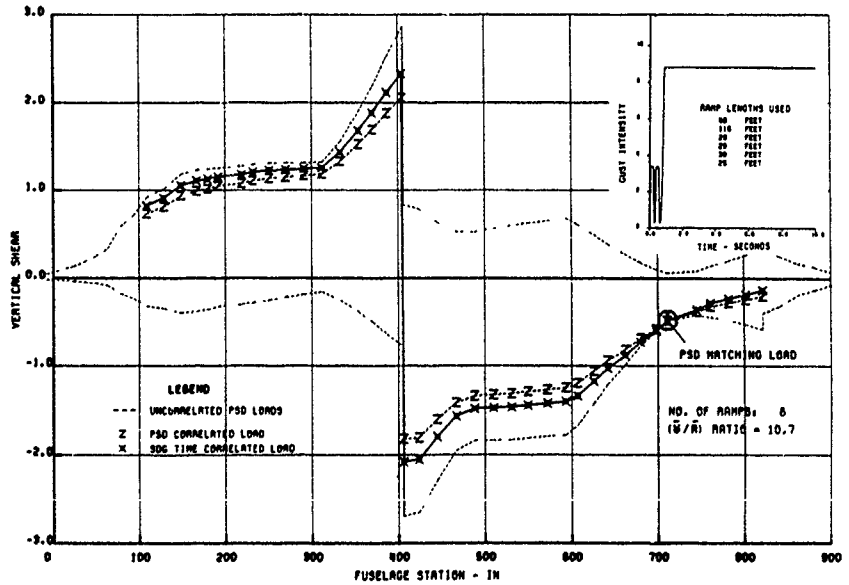

FIGURE 12

Fuselage Vertical Bending Moment Distributions Due to Various Gust Models

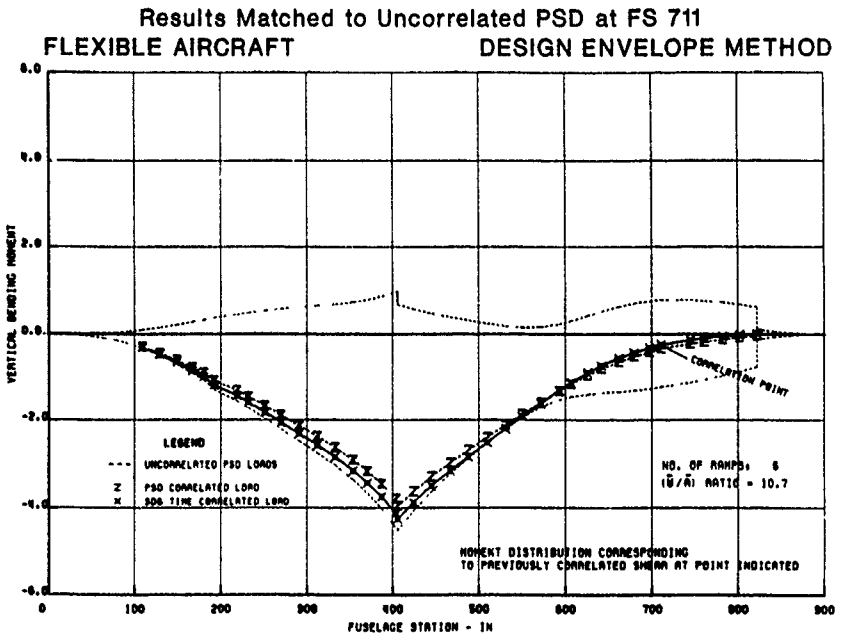

FIGURE 13

CHAPTER VII
MATCHING OF P.S.D.-DESIGN LOADS

by

Roel Noback
National Aerospace Laboratory — NLR
P.O. Box 90502
1006 BM Amsterdam
The Netherlands

CONTENTS

1. INTRODUCTION

The P.S.D.-method as described in the requirements produces the design loads, however not the mutual relation or phasing. For stressing purposes and also for testing, realistic load combinations or design load conditions are needed.

In the discrete gust case design load conditions almost naturally consist of the loads occurring at the same time, usually at the time that one of the loads reaches its maximum value.

The P.S.D.-method is based on statistical considerations and P.S.D.-design load conditions should have the same basis. A method to generate design load conditions or to match design loads, obtained with the Design Envelope Analysis of the P.S.D.-method will be described in the following paragraphs. The method is based on the statistical correlation between outputs -loads- of a linear system, the aircraft, to a common input, atmospheric turbulence. For design loads obtained with the mission analysis such a direct relation does not exist and the generation of design load conditions is more involved and will not be treated here. An approximate method is proposed in reference 1.

A design load condition should be in equilibrium, that is the equations of equilibrium should be valid for these loads. This will be proven for the design load conditions as generated with the described method.

The derivation of the design load conditions will be given for the case that only two loads are involved. The derivation for the general case with N loads is given in reference 1. Only the results will be presented here.

2. CORRELATION AND EQUAL PROBABILITY

For the derivation of design load conditions with equal probability it will be assumed that atmospheric turbulence is a quasi-stationary random process, with Gaussian probability-density function (p.d.f) and with normalized power spectrum ϕ_w^n and standard deviation σ_w. This random process acts as input to a linear system, the aircraft. The outputs, loads and stresses, also are Gaussian.

The power spectrum of the output y_i is

$$\phi_{yi}(\omega) = \sigma_w^2 |H_{iw}(\omega)|^2 \phi_w^n(\omega) \qquad (1)$$

$H_{iw}(\omega)$ is the transferfunction of output y_i

The ratio of the standard deviations of output y_i and input w is

$$\bar{A}_i = \frac{\sigma_i}{\sigma_w} = \left[\int_0^\infty |H_{iw}(\omega)|^2 \, \phi_w^n(\omega) d\omega \right]^{\frac{1}{2}} \qquad (2)$$

According to the requirements the design load has to be calculated with

$$y_{id} = \bar{A}_i U_\sigma = \sigma_i \frac{U_\sigma}{\sigma_w} \qquad (3)$$

U_σ is a design value and is prescribed in the requirements.

The outputs y_i and input w are correlated. The correlation coefficient between outputs y_1 and y_2 is

$$\rho_{12} = \frac{1}{2\sigma_1\sigma_2} \int_0^\infty \{H_{1w}(j\omega)\, H_{2w}^*(j\omega) + H_{1w}^*(j\omega)\, H_{2w}(j\omega)\}\, \phi_w^n(\omega)\, d\omega$$

$$= \frac{1}{\sigma_1\sigma_2} \int_0^\infty \{HRE_1(\omega) \cdot HRE_2(\omega) + HIM_1(\omega) \cdot HIM_2(\omega)\}\, \phi_w^n(\omega)\, d\omega \qquad (4)$$

where $H_{iw}^*(j\omega)$ is the complex conjugate of $H_{iw}(j\omega)$. $HRE_i(\omega)$ and $HIM_i(\omega)$ are the real and imaginary parts of $H_{iw}(j\omega)$.

The joint probability density function of two loads y_1 and y_2 with correlation coefficient ρ_{12} is

$$p_{12}(y_1,y_2) = \frac{1}{2\pi\sigma_1\sigma_2\sqrt{1-\rho_{12}^2}} * \exp - \frac{\frac{y_1^2}{\sigma_1^2} - \frac{2\rho_{12}\, y_1\, y_2}{\sigma_1\sigma_2} + \frac{y_2^2}{\sigma_2^2}}{2(1-\rho_{12}^2)} \qquad (5)$$

Any combination of loads y_1 and y_2 such that

$$\frac{y_1^2}{\sigma_1^2} - \frac{2\rho_{12}\, y_1\, y_2}{\sigma_1\sigma_2} + \frac{y_2^2}{\sigma_2^2} = \frac{U^2}{\sigma_w^2}(1-\rho_{12}^2) \qquad (6)$$

has the same probability density, namely

$$p_{12}(y_1,y_2) = \frac{1}{2\pi\sigma_1\sigma_2\sqrt{1-\rho_{12}^2}} \exp\left\{-\frac{U^2}{2\sigma_w^2}\right\} \qquad (7)$$

It should be noted that Eq. (6) represents an ellipse.

3. DESIGN STRESS AS FUNCTION OF TWO LOADS

It will now be assumed that stress q is a linear function of loads y_1 and y_2.

$$q = a_1\, y_1 + a_2\, y_2 \qquad (8)$$

The coefficients a_1 and a_2 depend on the dimensions of the structure.
The design value for the stress q can be calculated with

$$q_d = \bar{A}_q\, U_\sigma \qquad (9)$$

in which $\bar{A}_q$ can be expressed as

$$\bar{A}_q = \frac{\sigma_q}{\sigma_w} = \left[\int_0^\infty H_{qw}(j\omega) H_{qw}^*(j\omega) \phi_w^n(\omega)\, d\omega\right]^{\frac{1}{2}}$$

$$= \left[\int_0^\infty |H_{qw}(\omega)|^2\, \phi_w^n(\omega)\, d\omega\right]^{\frac{1}{2}} \qquad (10)$$

From Eq. (8) follows

$$H_{qw}(j\omega) = a_1\, H_{1w}(j\omega) + a_2\, H_{2w}(j\omega) \qquad (11)$$

This gives with Eqs. (4) and (10)

$$\bar{A}_q^2 = \frac{\sigma_q^2}{\sigma_w^2} = \int_0^\infty \{a_1^2\, H_{1w}(j\omega) H_{1w}^*(j\omega) + a_1\, a_2\, H_{1w}(j\omega) H_{2w}^*(j\omega) +$$

$$+ a_1\, a_2\, H_{1w}^*(j\omega) H_{2w}(j\omega) + a_2^2\, H_{2w}(j\omega) H_{2w}^*(j\omega)\} \phi_w^n(\omega)\, d\omega$$

$$= \{a_1^2\, \sigma_1^2 + 2a_1\, a_2\, \rho_{12}\, \sigma_1\, \sigma_2 + a_2^2\, \sigma_2^2\}/\sigma_w^2 \qquad (12)$$

It should be noted that stress q is a linear function of the Gaussian processes y_i. This implies that q also is a Gaussian process.
Loads y_1, y_2 and stress q are correlated. The correlation coefficient ρ_{1q} between load y_1 and stress q follows from Eq. (4) and (11).

$$\rho_{1q} = \frac{1}{2\,\sigma_1\sigma_q}\int_0^\infty (H_{1w}(j\omega)\,H^*_{qw}(j\omega) + H^*_{1w}(j\omega)\,H_{qw}(j\omega))\phi^n_w(\omega)\,d\omega$$

$$= \frac{a_1\sigma_1 + \rho_{12}\,a_2\sigma_2}{\sigma_q} \qquad (13a)$$

Similarly,

$$\rho_{2q} = \frac{\rho_{12}\,a_1\sigma_1 + a_2\sigma_2}{\sigma_q} \qquad (13b)$$

The p.d.f. of load y_1 under the condition that stress q is equal to its design value q_d, is

$$p_1(y_1|q = q_d) = \left\{\frac{p_{1,q}(y_1,q)}{p_q(q)}\right\} q = q_d$$

$$= \frac{1}{\sqrt{2\pi}\,\sigma_1\sqrt{1-\rho^2_{1q}}}\exp\left\{-\frac{\left(y_1 - \rho_{1q}\,\sigma_1\frac{q_d}{\sigma_q}\right)^2}{2\,\sigma_1^2\,(1-\rho^2_{1q})}\right\} \qquad (14)$$

This is a Gaussian p.d.f. with mean

$$\bar{y}_1 = \rho_{1q}\,\sigma_1\frac{q_d}{\sigma_q} = \rho_{1q}\,\sigma_1\frac{U_\sigma}{\sigma_w} = \rho_{1q}\,y_{1d} \qquad (15)$$

The design load condition, having the highest probability under the condition that q is equal to q_d, is

$$\bar{y}_1 = \rho_{1q}\,y_{1d} \text{ and } \bar{y}_2 = \rho_{2q}\,y_{2d} \qquad (16)$$

The locus of the loads $\bar{y}_1$ and $\bar{y}_2$ will now be determined, using non-dimensional loads x_1 and x_2

$$x_1 = \frac{y_1}{y_{1d}} \qquad x_2 = \frac{y_2}{y_{2d}} \qquad (17)$$

The non-dimensional design loads are

$$\bar{x}_1 = \frac{\bar{y}_1}{y_{1d}} = \rho_{1q} = \frac{n_1 + \rho_{12}\,n_2}{\sigma_q}$$

$$\bar{x}_2 = \frac{\bar{y}_2}{y_{2d}} = \rho_{2q} = \frac{\rho_{12}\,n_1 + n_2}{\sigma_q} \qquad (18)$$

in which $n_i = a_i\,\sigma_i$

and (see Eq. 12)

$$\sigma^2_q = n_1^2 + 2\rho_{12}\,n_1\,n_2 + n_2^2 \qquad (19)$$

Loads y_1 and y_2 giving design stress q_d can have all values satisfying (Eq. 8)

$$a_1y_1 + a_2y_2 = q_d \qquad (20)$$

or

$$n_1x_1 + n_2x_2 = \sigma_q$$

Solving Eq. (18) for n_1 and n_2 and inserting the result in Eq. (20) gives the relation between $\bar{x}_1$ and $\bar{x}_2$. The locus of the points $(\bar{x}_1, \bar{x}_2)$ is the ellipse

$$x_1^2 - 2\rho_{12}\,x_1\,x_2 + x_2^2 = 1 - \rho^2_{12} \qquad (21)$$

This equation represents the same ellipse as Eq. (6).
An example is given in figure 1.

Eq. (20) represents the tangent to the ellipse in point $(\bar{x}_1, \bar{x}_2)$. This point represents the optimal design load condition (Eq. 16 and 18), with parameters n_1 and n_2.
The distance from the centre of the ellipse to this tangent is

$$D(n_1, n_2) = \frac{\sigma_q}{\sqrt{n_1^2 + n_2^2}} \tag{22}$$

The coefficients a_1 and a_2, and thus n_1 and n_2 are not known in the design stage. Besides that, for various parts of the structure different values of a_1 and a_2 are valid.

Suppose that another design load condition is chosen for the calculation of stress q, for example with parameters k_1 and k_2 instead of n_1 and n_2 (see Fig. 1).

$$\tilde{x}_1 = \frac{k_1 + \rho_{12} k_2}{\sigma_k} \quad \text{or} \quad \tilde{y}_1 = \frac{k_1 + \rho_{12} k_2}{\sigma_k} \sigma_1 \frac{U_\sigma}{\sigma_w}$$

$$\tilde{x}_2 = \frac{\rho_{12} k_1 + k_2}{\sigma_k} \quad \text{or} \quad \tilde{y}_2 = \frac{\rho_{12} k_1 + k_2}{\sigma_k} \sigma_2 \frac{U_\sigma}{\sigma_w} \tag{23}$$

with

$$\sigma_k^2 = k_1^2 + 2 \rho_{12} k_1 k_2 + k_2^2 \tag{24}$$

The stress that will be obtained with these values of the design load condition is

$$\begin{aligned} q_e &= a_1 \tilde{y}_1 + a_2 \tilde{y}_2 \\ &= \frac{n_1(k_1 + \rho_{12} k_2) + n_2(\rho_{12} k_1 + k_2)}{\sigma_k} \frac{U_\sigma}{\sigma_w} \\ &= \sigma_{qe} \frac{U_\sigma}{\sigma_w} \end{aligned} \tag{25}$$

The line through the point $(\tilde{x}_1, \tilde{x}_2)$ as defined with the parameter values k_1 and k_2, and parallel to the tangent as given in Eq. (20) is (see Fig. 1)

$$n_1 x_1 + n_2 x_2 = \sigma_{qe} \tag{26}$$

The distance from the centre of the ellipse to this line is

$$D(k_1, k_2) = \frac{\sigma_{qe}}{\sqrt{n_1^2 + n_2^2}} \tag{27}$$

It can be shown for $N \geq 3$ (Ref. 1) and it is easily visible in figure 1, that the estimate σ_{qe} is always smaller than or equal to σ_q, or $q_{de} \leq q_d$.

From the foregoing can be concluded that combinations of loads y_1 and y_2 can be defined that have an equal probability density. The locus of these design load conditions is an ellipse, that has as a tangent the line representing the relation between the design stress q_d and the loads y_1 and y_2. Each combination of parameters k_1 and k_2 defines a point on the ellipse and each point on the ellipse defines an estimate $q_e \leq q_d$. One point on the ellipse (the point of contact with the tangent) gives the exact value of q_d.

The locus in the case of N loads is an N-dimensional second order surface, for N = 3 an ellipsoid.

4. DESIGN LOAD CONDITIONS

4.1 Introduction

As shown in the previous paragraph any point on the ellipse can be chosen to represent an equal probability design load condition. As in the case of the discrete gust design load conditions, care must be taken to choose meaningful conditions (for example in the discrete gust case, those conditions for which one of the loads attains its maximum or minimum value).

The correlation coefficients ρ_{ij} between N loads can be represented in the symmetric matrix R of order N*N. Any vector k of order N can be used to generate a design load condition, which implies that any matrix K of order N*N can be used to generate N design load conditions, each with N loads.

Two sets of design load conditions will be proposed for practical use. The first one, the correlated design load condition is comparable to the discrete gust case, where maximum loads are combined with the loads occurring at the same time. The design load conditions in the discrete gust case will produce relatively low estimates of the design stress if the phase differences between the loads are large. The same will be true for the correlated design load conditions if the correlation coefficients are small. Therefore a second set of design load conditions, the "eigen-vector" loads is proposed.

A third set of design load conditions produces a conservative estimate of the stress and can be used to establish a range for q_d.

4.2 Correlated design load conditions

Each design load condition consists of one design load plus the correlated values of the other loads. This is analogous to the discrete gust case, where each design load condition is composed of one design load plus the values of the other loads at the same time that the first load reaches its maximum value.
The design load conditions can be generated with the unity matrix. This gives for the case N=2:

	condition 1	condition 2
k_1	1	0
k_2	0	1

(28)

The result is

$$\bar{y}_{11} = y_{1d} \qquad \bar{y}_{21} = \rho_{12}\, y_{1d}$$
$$\bar{y}_{12} = \rho_{12}\, y_{2d} \qquad \bar{y}_{22} = y_{2d} \tag{29}$$

The correlated design load conditions for N loads are

$$\bar{Y} = \begin{array}{c|cccc} \text{condition} & 1 & 2 & 3 & \ldots\ldots N \\ \hline & y_{1d} & \rho_{12}\, y_{1d} & \rho_{13}\, y_{1d} & \cdots\cdots \\ & \rho_{12}\, y_{2d} & y_{2d} & \rho_{23}\, y_{2d} & \cdots\cdots \\ & \rho_{13}\, y_{3d} & \rho_{23}\, y_{3d} & y_{3d} & \cdots\cdots \\ & \rho_{14}\, y_{4d} & \cdots\cdots & & \\ & \rho_{1N}\, y_{Nd} & \rho_{2N}\, y_{Nd} & \cdots\cdots & y_{Nd} \end{array} \tag{30}$$

4.3 Eigen-vector design load conditions

The second set of design load conditions will be defined as the loads that are represented by the end points of the main axes of the N-dimensional second order surface.
These points can be determined using eigen-values and eigen-vectors of the matrix R with the correlation coefficients. This will be shown for the 2-dimensional case.
The eigen-vector κ_i is defined with the set of equations

$$\begin{aligned} \kappa_1 + \rho_{12}\kappa_2 + \cdots &= \lambda\kappa_1 \\ \rho_{12} + \kappa_2 + \cdots &= \lambda\kappa_2 \end{aligned} \tag{31}$$

The values of κ define the direction of the main axes.
λ is a scale factor.
This set of equations has a solution only if the determinant is equal to zero.

$$\begin{vmatrix} 1-\lambda & \rho_{12} & \cdots \\ \rho_{12} & 1-\lambda & \cdots \\ \cdots & \cdots & \end{vmatrix} = 0 \tag{32}$$

This is an N^{th} order equation in λ, giving N roots or eigen-values λ_i. For N = 2 follows

$$\lambda_1 = 1 + \rho_{12} \qquad \lambda_2 = 1 - \rho_{12} \tag{33}$$

Inserting these solutions in Eq. (31) gives

$$\begin{aligned} &\text{for } \lambda_1 : \ \kappa_{11} = \kappa_{12} \\ &\text{for } \lambda_2 : \ \kappa_{21} = -\kappa_{22} \end{aligned} \tag{34}$$

The normalised eigen-vectors will now be used to define the design load

$$k_{11} = \frac{\kappa_{11}}{\sqrt{\kappa_{11}^2 + \kappa_{12}^2}} = \frac{1}{\sqrt{2}} \qquad k_{21} = \frac{\kappa_{21}}{\sqrt{\kappa_{21}^2 + \kappa_{22}^2}} = -\frac{1}{\sqrt{2}}$$
$$k_{12} = \frac{\kappa_{12}}{\sqrt{\kappa_{11}^2 + \kappa_{12}^2}} = \frac{1}{\sqrt{2}} \qquad k_{22} = \frac{\kappa_{22}}{\sqrt{\kappa_{21}^2 + \kappa_{22}^2}} = \frac{1}{\sqrt{2}} \tag{35}$$

The design load conditions become (see Eq. 23)

$$\bar{y}_{11} = \frac{k_{11} + \rho_{12}\, k_{12}}{q_{k1}}\, y_{1d} \qquad \bar{y}_{21} = \frac{k_{21} + \rho_{12}\, k_{22}}{q_{k2}}\, y_{1d}$$

$$\bar{y}_{12} = \frac{\rho_{12}\, k_{11} + k_{12}}{q_{k1}}\, y_{2d} \qquad \bar{y}_{22} = \frac{\rho_{12}\, k_{21} + k_{22}}{q_{k2}}\, y_{2d} \tag{36}$$

It can be proven that $q_{ki}^2 = \lambda_i$ (Ref. 1).
For the 2 dimensional case:

$$q_{k1}^2 = k_{11}^2 + 2\,\rho_{12}\, k_{11}\, k_{12} + k_{12}^2 = 1 + \rho_{12}\ (= \lambda_1)$$

$$q_{k2}^2 = k_{21}^2 + 2\,\rho_{12}\, k_{21}\, k_{22} + k_{22}^2 = 1 - \rho_{12}\ (= \lambda_2) \tag{37}$$

From equations (31) follows

$$k_{11} + \rho_{12}\, k_{12} = \lambda_1\, k_{11} \qquad k_{21} + \rho_{12}\, k_{22} = \lambda_2\, k_{21}$$

$$\rho_{12}\, k_{11} + k_{12} = \lambda_1\, k_{12} \qquad \rho_{12}\, k_{21} + k_{22} = \lambda_2\, k_{22} \tag{38}$$

These results inserted in Eq. (36) gives

$$\bar{y}_{11} = \sqrt{\lambda_1}\, k_{11}\, y_{1d} \qquad \bar{y}_{21} = \sqrt{\lambda_2}\, k_{21}\, y_{1d}$$

$$\bar{y}_{12} = \sqrt{\lambda_1}\, k_{12}\, y_{2d} \qquad \bar{y}_{22} = \sqrt{\lambda_2}\, k_{22}\, y_{2d} \tag{39}$$

or

$$\bar{y}_{11} = \sqrt{\frac{1+\rho_{12}}{2}}\, y_{1d} \qquad \bar{y}_{21} = -\sqrt{\frac{1-\rho_{12}}{2}}\, y_{1d}$$

$$\bar{y}_{12} = \sqrt{\frac{1+\rho_{12}}{2}}\, y_{2d} \qquad \bar{y}_{22} = \sqrt{\frac{1-\rho_{12}}{2}}\, y_{2d} \tag{40}$$

The eigen-vector design load conditions for N loads are:

$$\bar{Y} = \begin{array}{c|cccc} \text{condition} & 1 & 2 & & N \\ & \sqrt{\lambda_1}\, k_{11}\, y_{1d} & \sqrt{\lambda_2}\, k_{21}\, y_{1d} & \cdots\cdots & \sqrt{\lambda_N}\, k_{N1}\, y_{1d} \\ & \sqrt{\lambda_1}\, k_{12}\, y_{2d} & \sqrt{\lambda_2}\, k_{22}\, y_{2d} & \cdots\cdots & \sqrt{\lambda_N}\, k_{N2}\, y_{2d} \\ & \sqrt{\lambda_1}\, k_{13}\, y_{3d} & \sqrt{\lambda_2}\, k_{23}\, y_{3d} & \cdots\cdots & \sqrt{\lambda_N}\, k_{N3}\, y_{3d} \\ & \cdots\cdots & \cdots\cdots & \cdots\cdots & \cdots\cdots \\ & \sqrt{\lambda_1}\, k_{1N}\, y_{Nd} & \sqrt{\lambda_2}\, k_{2N}\, y_{Nd} & \cdots\cdots & \sqrt{\lambda_N}\, k_{NN}\, y_{Nd} \end{array} \tag{41}$$

k_{ij} is the j-th element of the normalized eigen-vector k_i.
The design load conditions for N=2 are presented in figure 2. The points opposite to the ones defined above produce the same design load conditions, however with opposite sign.

4.4 Special properties

The design load conditions as defined have special properties. When the design is finished and the dimensions have been defined it is then possible to calculate the correct value of the stress $q = q_d$. Of course the correct value can be calculated also with Eq. (12), using the σ_i and ρ_{ij} values. Assuming, however, that only the design load conditions are available to the stress office, the design-stresses can be calculated with the following rules.

a. Using the estimates q_{ei} of the stress as calculated with the correlated design load conditions. The square of the design-stress q_d is equal to the sum of the products of the i-th estimate and the stress due to the i-th design-load.

$$q_d^2 = \Sigma\, a_i\, y_{id}\, q_{ei} \tag{42}$$

The estimates q_{ei} in the 2-dimensional case are

$$\begin{aligned} q_{e1} &= a_1 y_{1d} + a_2 \rho_{12} y_{2d} \\ q_{e2} &= a_1 \rho_{12} y_{1d} + a_2 y_{2d} \end{aligned} \tag{43}$$

Inserting this in Eq. (42) and using Eqs. (3), (9) and (12) proves the rule for the 2-dimensional case.

b. Using the estimates of the stress as calculated with the eigen-vector design load conditions
The square of the stress q_d is equal to the sum of the squares of the estimates

$$q_d^2 = \Sigma\, q_{ei}^2 \tag{44}$$

The estimates q_{ei} in the 2-dimensional case are

$$\begin{aligned} q_{e1} &= a_1 \sqrt{\frac{1+\rho_{12}}{2}} y_{1d} + a_2 \sqrt{\frac{1+\rho_{12}}{2}} y_{2d} \\ q_{e2} &= -a_1 \sqrt{\frac{1-\rho_{12}}{2}} y_{1d} + a_2 \sqrt{\frac{1-\rho_{12}}{2}} y_{2d} \end{aligned} \tag{45}$$

Inserting this in Eq. (44) and using Eqs. (3), (9) and (12) proves the rule for the 2-dimensional case.
Proofs for these rules for the N-dimensional case are given in reference 1.

4.5 Conservative design load conditions

The correlated and eigen-vector design load conditions (d.l.c.) produce estimates of the stress that are lower than the design value q_d. It is possible to define design load conditions that produce at least one conservative estimate of the stress.

The proposed conservative d.l.c. are based on the eigen-vector d.l.c. In the case of N loads also N eigen-vector d.l.c. are defined. The conservative d.l.c. in this case consists of N sets, each consisting of 2^{N-1} d.l.c. The m-th set is equal to the m-th eigen-vector d.l.c. plus or minus a fraction c of each of the other eigen-vector d.l.c. The ℓ-th d.l.c. of this set can be presented in vector notation with $\bar{y}_j$ as the j-th eigen-vector d.l.c., as

$$\hat{y}_{m\ell} = c \sum_{j=1}^{m-1} \pm \bar{y}_j + \bar{y}_m + c \sum_{j=m+1}^{N} \pm \bar{y}_j \tag{46}$$

The conservative d.l.c. are in the case that N=2:

$$\begin{aligned} \hat{y}_{11} &= \begin{vmatrix} y_{11} + c\, y_{21} \\ y_{12} + c\, y_{22} \end{vmatrix} & \hat{y}_{12} &= \begin{vmatrix} y_{11} - c\, y_{21} \\ y_{12} - c\, y_{22} \end{vmatrix} \\ \hat{y}_{21} &= \begin{vmatrix} c\, y_{11} + y_{21} \\ c\, y_{12} + y_{22} \end{vmatrix} & \hat{y}_{22} &= \begin{vmatrix} -c\, y_{11} + y_{21} \\ -c\, y_{12} + y_{22} \end{vmatrix} \end{aligned} \tag{47}$$

in which y_{ij} is the j-th element of the i-th eigen-vector d.l.c.
Rewriting this in non-dimensional units $x_{ij} = y_{ij}/y_{1d}$, gives

$$\begin{aligned} \hat{x}_{11} &= \bar{x}_1 + c\, \bar{x}_2 & \hat{x}_{12} &= \bar{x}_1 - c\, \bar{x}_2 \\ \hat{x}_{21} &= c\, \bar{x}_1 + \bar{x}_2 & \hat{x}_{22} &= -c\, \bar{x}_1 + \bar{x}_2 \end{aligned} \tag{48}$$

In reference 2 has been shown that one conservative d.l.c. will produce an estimate $\hat{q}_e$ of the stress that will be higher than the design value q_d if c is chosen equal to $\sqrt{2}-1 = 0.4142$.
The conservative d.l.c. are represented in figure 3 with the points indicated as upper limit d.l.c.
It also has been shown in reference 2 that

$$q_d \leq \hat{q}_e \leq q_d \sqrt{1+F} \tag{49}$$

with $F = (N-1)\, c^2$. (50)

From Eq. (49) follows the lower limit for the design stress

$$\check{q}_e = \frac{q_e}{\sqrt{1+F}} \leq q_d \tag{51}$$

and thus

$$\check{q}_e = \frac{\hat{q}_e}{\sqrt{1+F}} \leq q_d \leq \hat{q}_e \tag{52}$$

The lower limit $\check{q}_e$ for q_d can be obtained with the lower limit d.l.c. (see Eq. (46))

$$\check{y}_{m\ell} = \frac{1}{\sqrt{1+F}}\ \hat{y}_{m\ell} \tag{53}$$

The lower limit d.l.c. are presented in figure 3. The points representing this d.l.c. are located on the ellipse.

5. EQUILIBRIUM OF A P.S.D.-DESIGN LOAD CONDITION

The internal loads (shears, bending moments) and the external loads (aerodynamic loads, inertia loads) acting on a part of a structure are in equilibrium. The design load conditions in the discrete gust case are in equilibrium, because the loads of such a condition are defined as a set of loads, occurring at the same time. It can not be assumed a priori that the loads of a P.S.D.-design load condition have the same property. In the following will be shown that they also are in equilibrium.

Suppose that N_i internal and N_e external loads act on a structure. The N_e equations of equilibrium have the shape

$$c_1 y_1 + c_2 y_2 + \ldots\ldots = 0 \tag{54}$$

or

$$\sum_{n=1}^{N} c_n\, y_n = 0$$

with $N = N_i + N_e$.
y_n is the n-th internal or external load.

The steady state response of load y_n to a sinusoidal input $w(j\omega)$ is

$$y_n(j\omega) = H_{nw}(j\omega)\ w(j\omega)$$

and it follows that

$$w(j\omega) \sum_{n=1}^{N} c_n\, H_{nw}(j\omega) = \sum_{n=1}^{N} c_n\, y_n(j\omega) = 0$$

or

$$\sum_{n=1}^{N} c_n\, H_{nw}(j\omega) = 0 \tag{55}$$

The P.S.D.-design load conditions are based on the correlation coefficients (Eq. (4)).

$$\rho_{mn} = \frac{1}{2\sigma_m \sigma_n} \int_0^{\infty} \{H_m(j\omega)\ H_n^*(j\omega) + H_m^*(j\omega)\ H_n(j\omega)\}\phi_w^n(\omega)\,d\omega \tag{56}$$

and it follows that

$$2 \sum_{n=1}^{N} c_n \sigma_m \sigma_n \rho_{mn} =$$

$$= \int_0^{\infty} \{H_m(j\omega) \sum_{n=1}^{N} c_n\, H_n^*(j\omega) + H_m^*(j\omega) \sum_{n=1}^{N} c_n\, H_n(j\omega)\}\phi_w^n(\omega)\,d\omega \tag{57}$$

With Eq.(55) follows

$$\sum_{n=1}^{N} c_n\, \sigma_n\, \rho_{mn} = 0 \tag{58}$$

note that $\rho_{mn} = \rho_{nm}$ and $\rho_{nn} = 1$.

The n-th load of a design load condition can be written as (see Eq. (23))

$$\bar{y}_n = \frac{U_\sigma}{\sigma_k}\ \sigma_n \sum_{m=1}^{N} \rho_{nm}\, k_m \tag{59}$$

The loads of a design load condition inserted in one of the equations of equilibrium gives:

$$\sum_{n=1}^{N} c_n \bar{y}_n = \frac{\sigma}{\sigma_k} \sum_{n=1}^{N} c_n \sigma_n \sum_{m=1}^{N} \rho_{nm} k_m$$

$$= \frac{\sigma}{\sigma_k} \sum_{m=1}^{N} k_m \sum_{n=1}^{N} c_n \sigma_n \rho_{nm} \qquad (60)$$

With equation (58) follows that this sum is equal to zero, which implies that the loads of a design load condition are in equilibrium.

There is no need to calculate design load conditions, including the external loads. If they are needed they can be calculated with the equations of equilibrium, using the internal loads of the design load condition.

6. DISCUSSION AND CONCLUSIONS

It has been shown that it is possible to generate equal probability design load conditions using P.S.D.-design loads obtained with the Design Envelope criterion, and the correlation coefficients between these loads. The correlation coefficients can be calculated easily together with the $\bar{A}$-values.

The matrix of correlation coefficients can be used to define an N-dimensional surface. For the 2-dimensional case this surface reduces to an ellipse. Each point on the surface defines an equal probability design load condition. It has been shown that such a condition is in equilibrium.

Each design load condition can be used to calculate an estimate for the stress in a point of the structure. Each estimate is lower than the correct value. Only one point on the N-dimensional surface represents a design load condition, that will give the correct value of the stress.

Two sets of N design load conditions are proposed for practical use. They have been chosen such that it can be expected that at least one of the estimates will deviate not too much from the correct value. This however can not be guaranteed. Fortunately the chosen sets of design load conditions both have the proper that the correct value of the stress can be calculated, using the esti es. This knowledge can then used to redefine the dimensions. Note that with the discrete gust me od such a check is not possible.

A third set consisting of $N.2^{N-1}$ design load conditions produces a conservative estimate of the design value of the stress. The same set can be used to define an upper and a lower limit for the design value of the stress.

The method also can be used to generate design load conditions for the complete structure, for example the wing. A problem arises if stresses have to be calculated for a section of the structure for which the design values of the loads and the correlation coefficients have not been calculated. It then seems a logical approach to interpolate within a design load condition. This however leads to inconsistent values of both loads and stresses in that section. The same problem arises in a discrete gust analysis if the design load conditions are defined as the loads occurring at the same time. This problem is discussed in more detail in reference 1. A possible solution is to interpolate between the corresponding design loads and correlation coefficients of the adjoining sections.

The methods for the determination of equal probability design load conditions can not be used if the loads are obtained with the Mission Analysis. The correlation coefficients in that case are not defined. However it is possible to approximate the equal probability design load conditions. The correlated design load conditions in that case consist of the median value of the loads under the condition that one of the loads exceeds its design value. The derivation and also the application is rather involved. A description is given in reference 1.

7. EXAMPLE

The method as given in the previous chapters will be illustrated with an example.
The transfer functions of shear, bending moment and torsion in various wingstations of a transport airplane for one of the design envelope conditions have been determined for a number of reduced frequencies ω_r. The $\bar{A}$-values and the correlation coefficients between shear, bending and torsion can be calculated with equations (2) and (4).
The output spectra $\phi_y(\omega_r) = |H_y(\omega_r)|^2 \phi_w(\omega_r)$ for the loads in wingstation m are given in figure 5.

The $\bar{A}$-values, the design values with U_σ = 25 m/s and the correlation coefficients in wingstation m are

	$\bar{A}$	Y_d		correlation coefficients		
shear	31241.48	781037	[N]	1.0	0.0283366	0.635032
bending	200616.60	5015415	[Nm]	0.0283366	1.0	-0.0968185
torsion	144092.92	3602323	[Nm]	0.635032	-0.0968185	1.0

The eigenvalues and eigenvectors of the matrix of correlation coefficients for three loads can be calculated with

$$\lambda_1 = 1 - C.\cos\alpha_1 \qquad \alpha_1 = \varphi/3$$
$$\lambda_2 = 1 + C.\cos\alpha_2 \qquad \alpha_2 = (\pi+\varphi)/3$$
$$\lambda_3 = 1 + C.\cos\alpha_3 \qquad \alpha_3 = (\pi-\varphi)/3$$

with $\varphi = \arccos\left(\frac{|Q|}{P\sqrt{P}}\right)$ rad and $C = \frac{2Q\sqrt{P}}{|Q|}$

in which $P = (\rho_{12}^2 + \rho_{13}^2 + \rho_{23}^2)/3$ and $Q = -\rho_{12}\,\rho_{13}\,\rho_{23}$

The components of the eigenvectors follow from

$$(1-\lambda_i)\,x_{i1} + \rho_{12}\,x_{i2} + \rho_{13}\,x_{i3} = 0$$

$$\rho_{12}\,x_{i1} + (1-\lambda_i)\,x_{i2} + \rho_{23}\,x_{i3} = 0$$

$$x_{i3} = +1 \text{ or } -1$$

The eigenvalues and normalized eigenvectors of the matrix of correlation coefficients are then

λ_i	0.3528321	1.008429	1.638739
k_{i1}	-0.696913	0.150041	0.701285
k_{i2}	0.135861	0.987784	-0.0763244
k_{i3}	0.704169	-0.0420856	0.708784

The design load conditions can now be established.

A. Correlated designload conditions

condition	1	2	3	1	2	3
shear [N]	Y_{sd}	$\rho_{12}\,Y_{sd}$	$\rho_{13}\,Y_{sd}$	781037.0	22131.96	495983.3
bending [Nm]	$\rho_{12}\,Y_{bd}$	Y_{bd}	$\rho_{23}\,Y_{bd}$	142120.0	5015415	-485585.0
torsion [Nm]	$\rho_{13}\,Y_{td}$	$\rho_{23}\,Y_{td}$	Y_{td}	228758.9	-348771.5	360232.3

B. Eigenvector design load conditions

condition	1	2	3	1	2	3
shear [N]	$\sqrt{\lambda_1}\,k_{11}\,Y_{sd}$	$\sqrt{\lambda_2}\,k_{21}\,Y_{sd}$	$\sqrt{\lambda_3}\,k_{31}\,Y_{sd}$	-323321.2	117680.7	701165.8
bending [Nm]	$\sqrt{\lambda_1}\,k_{12}\,Y_{bd}$	$\sqrt{\lambda_2}\,k_{22}\,Y_{bd}$	$\sqrt{\lambda_3}\,k_{32}\,Y_{bd}$	404748.4	4974980	-490032.9
torsion [Nm]	$\sqrt{\lambda_1}\,k_{13}\,Y_{bd}$	$\sqrt{\lambda_2}\,k_{23}\,Y_{td}$	$\sqrt{\lambda_3}\,k_{33}\,Y_{td}$	1506795	-152243.6	3268521

C. Conservative design load conditions
The 12 conservative design load conditions are derived from the eigenvector design load conditions. They are presented in table 1.

The design load conditions are used to design the tapered wingbox at wingstation w. The shape is simplified to a rectangle with center spar (Fig. 4).

It is now assumed that the given design load conditions and probably those pertaining to other design envelope conditions have been used to establish (provisional) dimensions of the structure. The shear stresses in the points 1, 2 and 3 and the normal stress in the lower skin (point 4) can now be expressed as linear functions of the loads.

$$q_i = a_{is}\,S + a_{ib}\,B + a_{it}\,T$$

Based on simple theory the coefficients have been calculated with the following results

$$q_1 = -32.40836\,S + 2.457209\,B + 19.30623\,T$$
$$q_2 = 47.29934\,S - 3.305001\,B + 0.0\,T$$
$$q_3 = 37.92407\,S - 2.457209\,B + 19.30623\,T$$
$$q_4 = 0.0\,S + 33.30495\,B + 0.0\,T$$

Note that q_4 depends on one load and q_2 depends on two loads.

These stresses will now be determined for the various design load conditions (1 MPa = 10^6 N/m^2)

A. Correlated design load conditions

Condition	1	2	3	equation (42)
q_1 [MPa]	19.20182	4.873200	<u>52.28008</u>	56.65647
q_2 [MPa]	<u>36.47283</u>	-15.52912	25.06454	40.06006
q_3 [MPa]	73.43561	-18.21805	89.55016	92.88519
q_4 [MPa]	4.733297	<u>167.0381</u>	-16.17238	167.0381

The stresses due to the design load conditions can be used to calculate the exact values of the stresses with equation (42). These values can be calculated also using the equivalent of equation (12) for three loads. However, it is assumed that $\bar{A}$-values and correlation coefficients are not available in the stress office.

B. Eigenvector design load conditions

Condition	1	2	3	equation (44)
q_1 [MPa]	40.56269	5.471479	39.17507	56.65647
q_2 [MPa]	-16.63057	-10.87610	34.78424	40.06006
q_3 [MPa]	15.83362	-10.70089	90.89799	92.88518
q_4 [MPa]	13.48013	165.6915	-16.32052	167.0382

The stresses due to the design load conditions can be used to calculate the exact values of the stress with equation (44).

As is to be expected, the estimates of the stresses based on design load conditions are lower than the exact value of the stresses. However, contrary to the discrete gust case the exact values of the stresses can be derived from the estimates.

C. Conservative design load conditions

The stresses due to the conservative design load conditions are presented in table 1.
The exact value of the stress will be lower than the maximum value of these estimates, and it will be higher than this maximum value divided by $\sqrt{1 + F}$, with $F = (N-1)c^2 = 2 * 0.4142^2 = 0.343146$, and thus $\sqrt{1 + F} = 1.15894$.

stress	upper limit (maximum from table 1)	lower limit = upper limit divided by $\sqrt{1 + F}$	exact	maximum estimate correlated + eigen vector
q_1	59.0566	50.9574	56.6565	52.2801
q_2	46.1779	39.8449	40.0601	36.4728
q_3	101.8892	87.9157	92.8852	90.8980
q_4	178.0353	153.6189	167.038	167.038

8. REFERENCES

1. Noback, R., The generation of equal probability design load conditions, using P.S.D.-techniques, NLR TR 85014 U, 23-I-1985.

2. Noback, R., Matching P.S.D.-design loads, AGARD-R-734 addendum, June 1988.

TABLE 1
Conservative design load conditions

	$\bar{y}_1$ +				$\bar{y}_2$ +				$\bar{y}_3$ +			
	$c\bar{y}_2 + c\bar{y}_3$	$c\bar{y}_2 - c\bar{y}_3$	$-c\bar{y}_2 + c\bar{y}_3$	$-c\bar{y}_2 - c\bar{y}_3$	$c\bar{y}_3 + c\bar{y}_1$	$+c\bar{y}_3 - c\bar{y}_1$	$-c\bar{y}_3 + c\bar{y}_1$	$-c\bar{y}_3 - c\bar{y}_1$	$+c\bar{y}_1 + c\bar{y}_2$	$+c\bar{y}_1 - c\bar{y}_2$	$-c\bar{y}_1 + c\bar{y}_2$	$-c\bar{y}_1 - c\bar{y}_2$
SHEAR [N]	15856.1	-565008.6	-81633.8	-66.498.5	274189.1	542037.1	-306675.7	-38827.7	615986.7	518496.8	883834.8	786344.9
bending [Nm]	2262474.3	2668430.9	-1858934.1	-1452977.5	4939654.0	4604349.5	5345t'9.5	5010306.0	1738323.6	-2383084.8	1403019.0	-2718389.4
torsion [Nm]	2797599.4	89867.9	2923722.1	215990.6	1825757.1	577487.2	-881974.4	-2130244.3	3829594.6	3955717.3	2581324.7	2707447.4
q_1 [MPa]	59.0566	26.6029	54.5239	22.0702	38.5002	4.8964	6.0465	-27.5573	58.2433	53.7106	24.6395	20.1068
q_2 [MPa]	-6.7275	-35.5437	2.2826	-26.5337	-3.3566	10.4206	-32.1728	-18.3956	23.3906	32.4007	37.1678	46.1779
q_3 [MPa]	49.0531	-26.2493	57.9180	-17.3844	33.5091	20.3915	-41.7933	-54.9109	93.0243	101.8892	79.9067	88.7717
q_4 [MPa]	75.3516	88.8720	-61.9117	-48.391ɔ	164.5149	153.3476	178.0353	166.8680	57.8948	-79.3685	46.7275	-90.5358

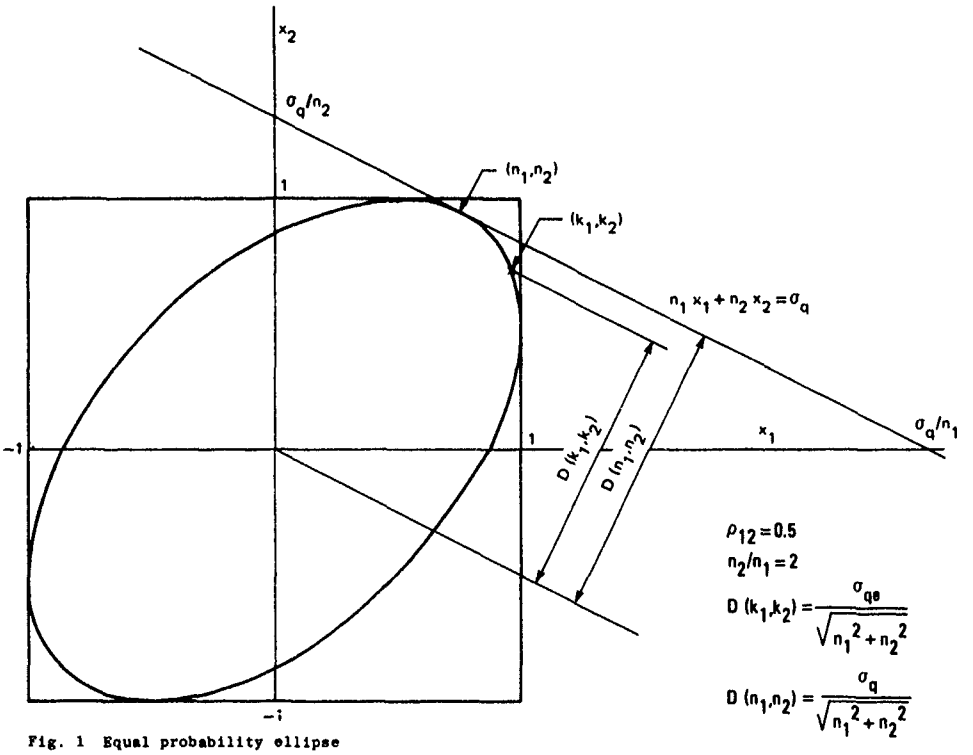

Fig. 1 Equal probability ellipse

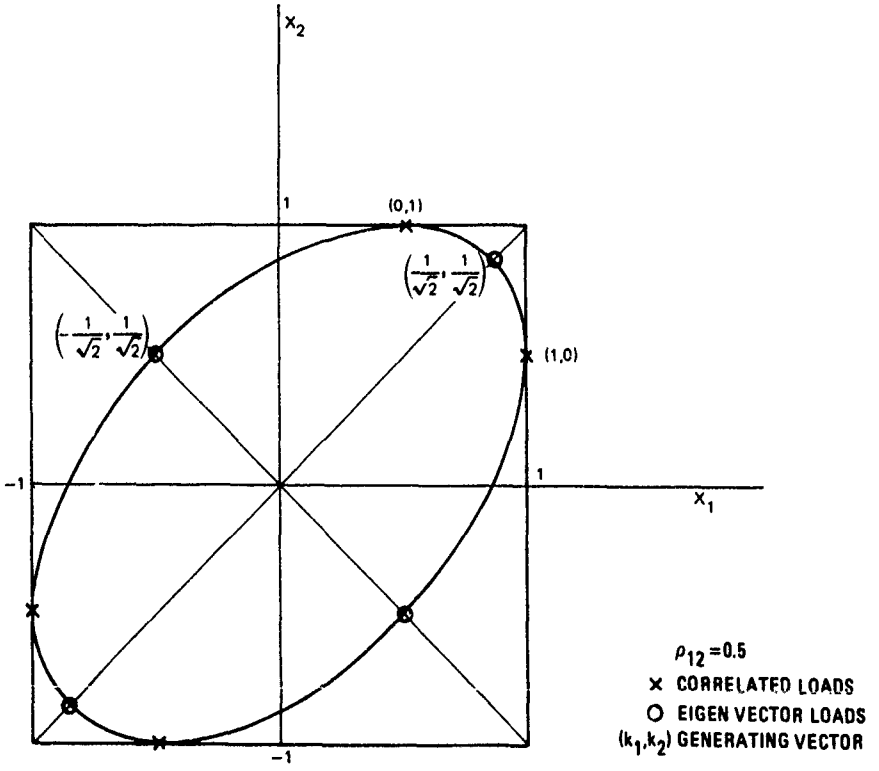

Fig. 2 Design load conditions

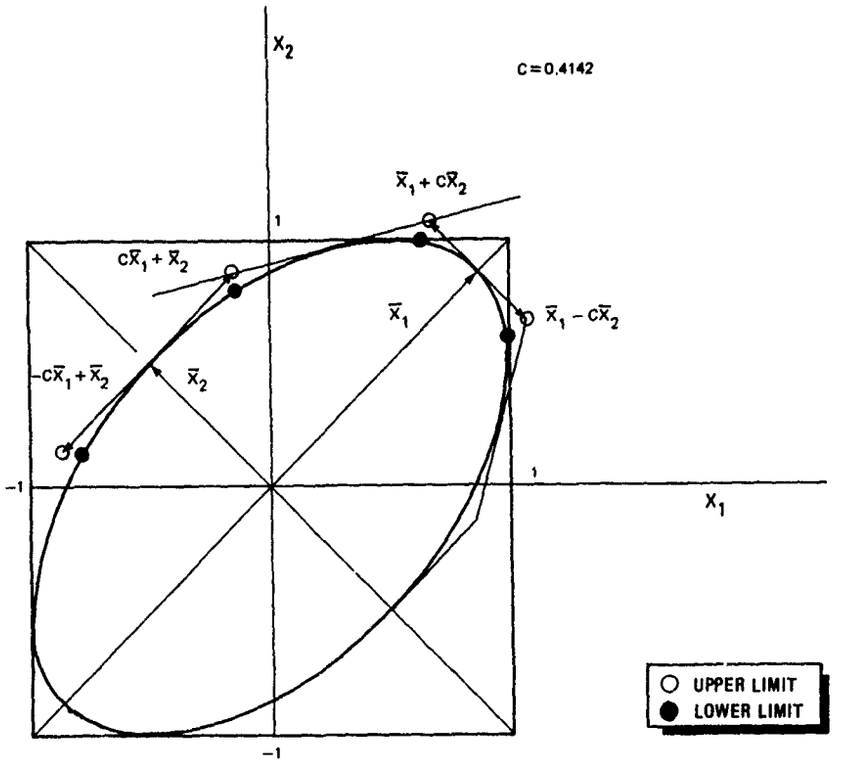

Fig. 3 Upper and lower limit design load conditions

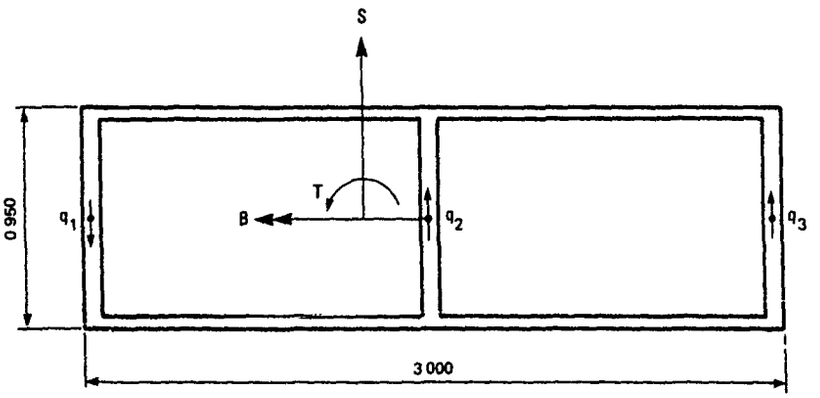

Fig. 4 Wingbox

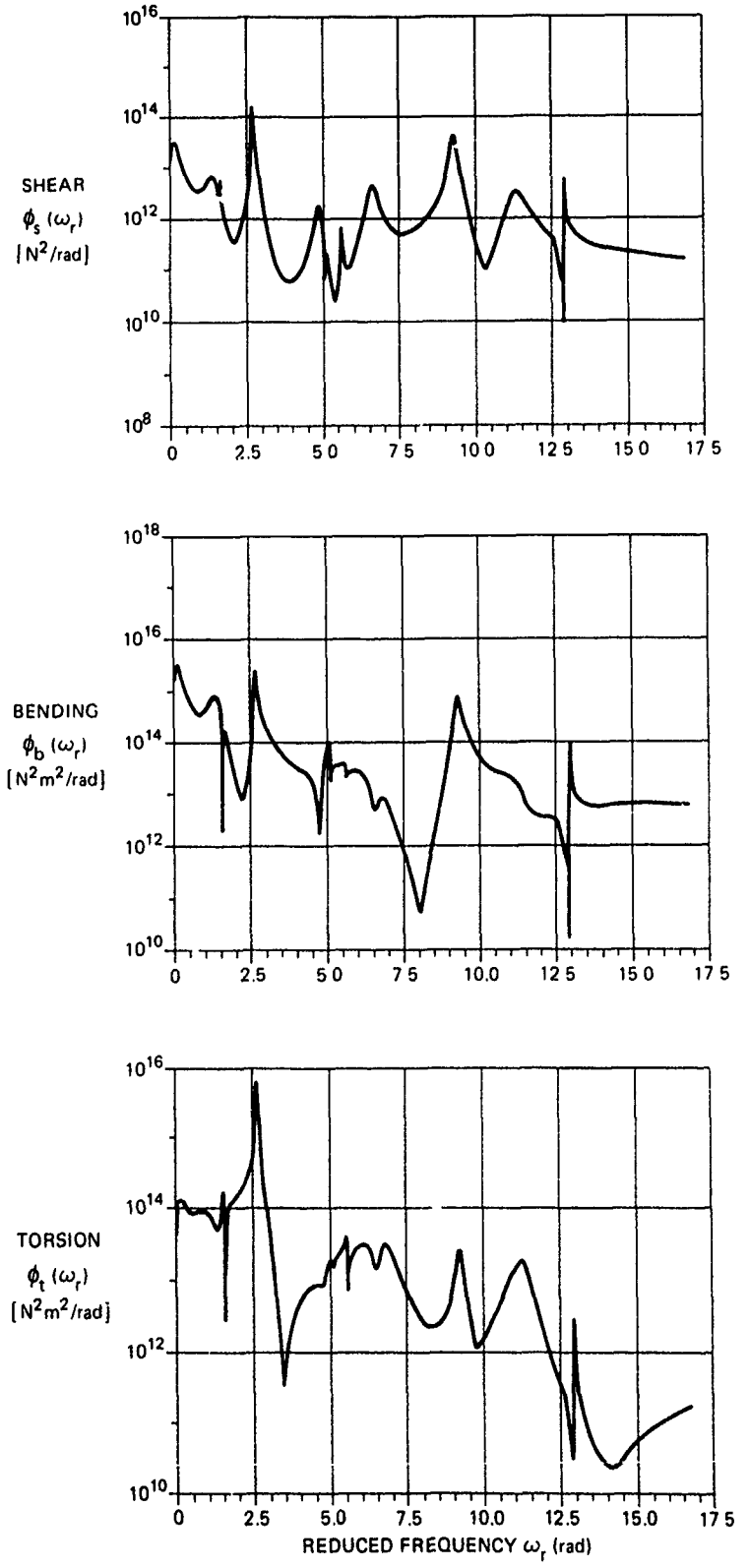

Fig. 5 Power spectra

CHAPTER VIII
TRENDS IN CERTIFICATION PROCEDURES AND DESIGN ANALYSIS

by

Vic Card
CAA
Brabazon House
Redhill, Surrey RH1 1SQ
United Kingdom

and

Terence J.Barnes
FAA
United States

CONTENTS

1. DISCUSSION OF REQUIREMENTS (V. Card, CAA)

In the past various gust load formulas have been developed for the calculation of design gust loads on aircraft. Since the time it was first published in 1954 (Reference 1), the alleviation factor approach of Pratt and Walker has gained almost universal acceptance and, for many years, it has been a familiar part of the airworthiness requirements for both civil and military aircraft.

The original concept of the "Pratt Formula" was to predict the peak accelerations due to discrete gusts on a given aircraft from the peak acceleration measured on another aircraft for flight through a discrete gust of the same shape and amplitude. Thus the derived gust velocity is not so much an absolute physical quantity but is rather more a gust load transfer factor defined within the terms of the formula. As such the method is most accurate when restricted to use on aircraft with very similar gust response characteristics. Less confidence must be attached to predicted gust loads on aircraft which are unconventional when compared to the data collecting aircraft.

Fortunately, as in many other fields of aeronautical science, the methods of calculating design gust loads have been constantly improved over the past 30 years. Rational and accurate analysis procedures are now common amongst all the major aircraft manufacturers. These have allowed all the important features of new aircraft designs to be modelled and thus have ensured that differences in gust response characteristics can be fully accounted for in the design process. This is fully in accord with a fundamental principle of airworthiness requirements which demands that load intensities and distributions should closely represent actual conditions, or else they must be shown to be conservative. In general, however, only one set of design gust velocities is prescribed and these are based upon equivalent values derived using the simple formula.

This would be reasonable if all the elements of the modern gust analysis were only applicable to modern aircraft and if the effects on the previous generation of aircraft were insignificant. However, this is patently not the case. The alleviation factor approach leans heavily on many simplifying assumptions which were introduced purely to facilitate the solution of the equations of motion. That is not to say that all the elements of the

equations of motion which were eliminated by Pratt and Walter and other researchers were negligible but, rather, that their inclusion would have led to an overly arduous analysis task.

The present gust load requirements for transport aircraft have evolved largely through experience with past successful aircraft and their modes of operation. Therefore, in a statistical sense, they imply an acceptable level of risk associated with exceeding limit load.

Obviously there will always be a calculated, but remote, risk of structural failure due to gusts and turbulence and the determination of this risk level, must be based upon carefully analyzed statistical load measurements made over many years of routine transport operations. Careful analysis of such statistical data must be subject to continuing interpretation in formulating new design criteria.

Continuous turbulence response loads have formed an important part of the design process for new large transport aircraft since the introduction of Amendment 25-54 of FAR 25 which introduced the Appendix G criteria. During that period aircraft manufacturers have worked steadily towards overcoming many of the problems associated with the basic procedures in order to develop a useable design tool. These problems exist in the following area:

(1) The basic PSD procedure produces design load values of equal probability at various points on the structure. Normal stress analysis requires design loads to be defined as they will exist on the whole structure at any given time. Otherwise static equilibrium will not be achieved. PSD loads, as defined by either design envelope (as ABAR times Usigma), or mission analysis (as the load level exceeded at the design probability of exceedance), are necessarily uncorrelated. If all combinations of the maximum positive and negative values of these loads are used to calculate a stress which is dependant upon more than one load then the design stress will usually be overestimated. To avoid this possibility methods to establish correlated, or phased design PSD loads have been developed.

(2) The basic assumptions behind the PSD procedure are that the atmosphere can be described as a stationary guassian process and that the aircraft can be described by means of a linear transfer function. This means that the response loads will themselves be guassian. For most modern aircraft the equations of motion are not exactly linear. This is because of non-linearities in the aerodynamics at high angles of attack, variation of lift curve slope for positive and negative angles of attack, or addition of non-linear systems such as yaw-dampers and longitudinal stability augmentation systems. These non-linearities require special handling in the context of a continuous turbulence response.

Originally, the PSD criteria were introduced in an attempt to provide a more realistic description of the random nature of gust loading on aircraft through its use of a statistical formulation allied with power spectral density (PSD) techniques of analysis. However, in spite of the intended improvements, the continuous turbulence analysis has not been allowed to supercede the more artificial, but well proven discrete gust requirements. In part, this probably reflects concerns over the wisdom of relying totally on the PSD method for the prediction of design loads.

In support of this view it is often noted from measured flight data that the larger disturbances often stand out as discrete events above a background of more moderate atmospheric fluctuation. In particular, it is noted that the majority of gust load accidents involving loss of aircraft have been related to "sudden events", rather than to continuous turbulence. It has also been noted that a significant proportion of high load turbulence encounter events detected during the monitoring of civil transport operations, and a

significant proportion of occurrences involving passenger injury, occur in events which are more discrete than continuous in nature.

In the light of this evidence it is believed widely that extreme gust events pertinent to aircraft limit load cases are better described by isolated gust procedures and that response to discrete gusts will continue to play a major role in load requirements for aircraft. Such a need becomes even more imperative as new aircraft designs evolve, since structural optimization and active control system design based upon inappropriate or restricted assumptions about the nature of the atmosphere could lead to inaccurate conclusions about the degree of strength necessary to provide a level of safety equivalent to that achieved by current designs. For this reason it must be expected that any development in airworthiness regulations will continue to maintain discrete gust requirements in addition to continuous turbulence requirements.

2. DISCRETE GUST STATISTICS AND COMPARISON WITH REQUIREMENTS (V. Card, CAA)

The basic philosophy behind most structural load requirements is the definition of a loading condition that approximates to the most severe that an aircraft is likely to encounter in service (a limit load condition) and then ensure that the structure has sufficient strength to withstand 1.5 times the resulting loads.

For discrete gust requirements this has hitherto been done through a standard design envelope approach in which limit gust velocities are defined as a function of altitude. The aircraft is required to be able to withstand the loads resulting from encounter with these gusts at all altitudes and with all practicable combinations of weight, fuel, payload, etc. No account is taken of the joint probability of meeting the design limit gust and being in the critical operating state. A graphical representation of the gust velocity distribution used in the current requirements for transport aircraft is given in Figure 1. However, this distribution does not compare well with the known characteristics of the atmosphere as represented by gust statistics based upon operational data. Using such gust load factor data as that presented in

Reference 2 a more realistic derived gust probability model can be established. The curves shown in Figure 2 are based upon the data recorded by six types of aircraft fitted with cloud warning radar, but these correlate well with data taken from other sources (e.g. Reference 3). The derived gust velocity values shown have been established from measured values through the use of an extreme value probability distribution to allow extrapolation to the extremely improbable event. A comparison between the operational gust probability model and the V_c gust velocity from the requirements is shown in Figure 3. It is particularly noticeable that the trend of gust velocity with altitude in the requirement shows significant departure from a constant probability line at altitudes below 20,000 feet.

Working on the basis that the requirement gust velocities are used to define the maximum load occurring in a typical aircraft lifetime (say 50,000 hours) it would appear that the requirement gust velocities are possibly too severe between 14,000 feet and 40,000 feet and not severe enough below 14,000 feet. Alternatively, if the achieved airworthiness level is satisfactory for a turboprop powered aircraft predominately operating at or below, say, 15,000 feet, too severe a target might be being set for a pure jet aircraft which would mainly operate at higher altitudes. This is in opposition to one fundamental objective of an airworthiness code which is to establish a common, minimum level of safety for all types of aircraft to which that code applies. Any development of discrete gust requirements must take into account the probability of meeting the critical gust condition.

Other factors which should be taken into account are as follows:

(1) The need for a full aircraft dynamic model

(2) The need for simplicity of interpretation

(3) The need for a uniform standard of application from one manufacturer to another and from one authority to another.

(4) The need for a consistent approach between gust loads with high lift and high drag devices deployed and clean aircraft conditions.

(5) Design loads must be consistent with the strength of past satisfactory designs.

3. THE POWER SPECTRAL DENSITY (PSD) CONCEPT (T. Barnes, FAA)

The power spectral density (PSD) concept, which was well known in electrical engineering, was recognized as the analytical tool to account for the continuous nature of atmospheric turbulence. Around 1952, efforts were initiated to apply the Power Spectral Density methods of Generalized Harmonic Analysis to gust analyses, both in describing models of atmospheric turbulence, and on the response of the airplane. The classic diagram shown in Figure 4 demonstrates the basic relations. The top sketch characterizes the atmosphere (the power spectrum of the turbulence), the second sketch characterizes the airplane, being a transfer function between input and output, and the third sketch characterizes the output response under consideration. This allowed study over the entire frequency range for which response values were needed covering multiple degrees of freedom. In effect, the power spectral approach allowed for a much more rational treatment of gust loads, since many of the assumptions made in the discrete gust treatments were alleviated. The area under the output response spectra in Figure 4 equals the mean square value of response, while the moment of inertia of this area around the vertical axis gives the number of zero crossings per second.

Development of PSD concept for use in transport aircraft design was initiated by the FAA. Two contracts were let to U.S. industry.

The results of study contracts let to Lockheed and Boeing for the purpose of helping FAA define procedures and criteria are summarized in Reference 5.

In ADS-53, Reference 5, three alternate forms of gust loads criteria based on power-spectral concepts were developed. These included a mission analysis criterion, a design envelope criterion, and a criterion combining the advantages of each. The latter was recommended for design use. Design levels were determined based on the strength of three existing satisfactory airplanes, the Lockheed Model 749 (Constellation) and Model 188 (Electra) and the Boeing Model 720B. The determination of a design load level involved dynamic gust analysis of the three airplanes, taking into account the significant rigid body and elastic modes, for both vertical and lateral gust inputs, as well as detailed stress analysis using the resulting loads.

Two techniques were developed for integrating the statistical determination of loads with the detailed stress analysis. One is the matching condition technique, in which design conditions are generated to closely envelope the statistically defined loads, with phase relations of the various load or stress components properly accounted for. The other is the joint probability technique, in which the joint probability density of axial and shear stresses is determined at all potentially critical locations in the structure and related to the respective strength envelopes. The sensitivity of results to variations in input data was investigated.

ADS-54 (Reference 6) presents a dynamic gust analysis of the Boeing Model 720B airplane and outlines two procedures for assessing gust design strength for future civil transports. The procedures outlined are based on two approaches. The first is the design envelope approach, the second is the flight profile approach. In the design envelope approach, certain flight conditions are established by successive analyses to determine the most critical flight condition for a given portion or component of the airplane for either vertical of lateral gust loads. The one-factor level flight load added to the rms load times a particular constant will gust equal the limit design strength of the component. The constant, $\sigma_w \zeta_d$, represents an effective gust intensity which would just stress the structure to its limit design strength.

The object of the flight profile approach is to determine the expected number of flight hours that the airplane could be operated before the limit design strength of any of its major components would be exceeded. The flight profile approach requires a description of airplane operation in terms of flight profiles that best typify the airplane usage. A separate power spectral analysis is conducted for each of the profile conditions. In addition, a description of the atmosphere applicable to the condition altitude is determined. From this information, the expected number of hours required to exceed the limit strength is computed.

The 720B airplane was studied for both concepts, first, by using the bending moment on the wing, fuselage, and vertical tail as indices of their strengths. This procedure was used to locate critical flight conditions, critical portions of the structure, and to obtain preliminary values of $\sigma_w \zeta_d$ by the design envelope approach, and expected hours to fly to exceed limit design strength by the flight profile approach.

The second step was to study the more critical structural areas using a joint probability stress analysis approach developed by Boeing. The critical values of $\sigma_w \zeta_d$ and hours to fly to exceed limit design strength of each structural element in the critical area were determined.

Initial FAA design criteria for PSD that the FAA incorporated into the regulations as Appendix G to FAR 25 in September 1990 were the result of extensive negotiations between FAA and U.S. Industry. The primary difference between the criteria prescribed in FAA-ADS-53 and current FAA criteria are in the specified design gust velocities and their variation with altitude. These FAA criteria provided the basis for all current continuous turbulence criteria, regardless of the certifying agency.

Current FAA design criteria for PSD reflect a change that was incorporated to give credit for a designers previous history of successful designs, or dynamic similarity to another successful design. Basically, this change allowed a reduction in the gust intensity factor used in the design envelope procedure from 85 to 75 feet per second. This change was incorporated at the request of U.S. Industry which supplied additional supporting data.

The initial FAA design criterion included design envelope capability of 85 feet per second. The actual capability of various transports for which data were presented is given on Figure 5 and Figure 6.

The FAA decision was made to retain 85 feet per second as the general rule and permit a decrease in design gust intensity to as low as 75 feet per second for aircraft whose transfer function and mission profile characteristics are comparable to a previous design with extensive good service experience. The previous design must have been shown to be adequate for the lower gust intensity chosen for the new design. This permits a new configuration which could otherwise comply with the new standard at a design envelope gust level

less than 85 feet per second by choosing the mission analysis option, to show compliance at lower gust intensity levels with the design envelope option alone.

Whether or not the technical information concerning a similar configuration is available to a designer, the option to comply with the mission analysis method is available to establish adequate strength in combination with design envelope gust intensity values as low as 60 feet per second.

Use of the PSD results has given rise to problems which have been solved by various different approaches. The difficulty using the current PSD criteria to produce design loads is how to fit them into the routine by which design loads are obtained and stress analysis is conducted. Normal stress analysis practice utilizes design conditions each of which is defined over the whole of some major structural component at a given instant. Power-spectral methods, however, do not result in this sort of design condition. They lead, instead, to individual design-level values of load of equal probability at various points in the structure, or of various components of load such as wing shear, being moment, and torsion, with the phasing undetermined. For example, it is not determined whether maximum up shear combines with maximum nose-up or maximum nose-down torsion or with some intermediate value. This difficulty can be circumvented to some extent by determining design-level values of internal loads or stresses, such as front and rear beam shear flows. Although mathematical relationships between the various output load parameters can be developed, and other methods can be used to develop a most likely balanced loads solution, this involves a separate additional step in the analysis procedure.

In Reference 7 presented at the AGARD Conference in Cezme, Turkey, October 1987, Mr. Moon of Lockheed summarized some of the methods that are currently used by U.S. Airframe manufacturers.

FAA is sponsoring an evaluation of new methods that consider the response of airplanes to continuous turbulence and produce complete sets of correlated loads on an airplane. Included in this is an evaluation of the Statistical Discrete Gust (SDG) Analysis Method described in Reference 8.

A new procedure which uses matched filter theory to develop design load sets is presented in Reference 9.

Introduction of non-linear aircraft systems has resulted in the need to re-evaluate the adequacy of the PSD method, which is based on the presumption that it is applied to linear systems. Current jet transports generally have a yaw damper in addition to a limited authority autopilot. The Lockheed L-1011-500 and the Airbus A320 have systems which interact with vertical gust response, and have significant non-linear characteristics. Even though FAA prepared special conditions for the certification of these airplanes, they discussed the technical concerns without defining an acceptable means of compliance. As more airplanes are certified with increasing level of system interaction with structure, the need for changes in the regulations increases.

4. REFERENCES

1) K. G. Pratt and W. G. Walker — A Revised Gust Load Formula and a Re-Evaluation of V-G Data Taken on Civil Transport Airplanes from 1933 to 1950 NACA Report 1206

2) I. W. Kaynes — A Summary of the Analysis of Gust Loads Recorded by Counting Accelerometers on Seventeen Types of Aircraft. AGARD-R-605

3) J. B. de Jonge and D. J. Spiekhout — Assessment of Service Load Experience Using Aids Recorded Data. NLR MP 77011 U

4) Anon — Average Gust Frequencies for Subsonic Transport Aircraft. Engineering Sciences Data Sheet 69023

5) F. M. Hoblit, N. Paul, J. D. Shelton and F. E. Ashford — Development of a Power-Spectral Gust Design Procedure for Civil Aircraft. FAA-ADS-53

6) J. R. Fuller, L. D. Richmond, C. D. Larkins and S. W. Russell — Contributions to the Development of a Power-Spectral Gust Design Procedure for Civil Aircraft. FAA-ADS-53

7) R. Moon — A Summary of Methods for Establishing Airframe Design Loads from Continuous Gust Design Criteria. AGARD-R-734 Addendum

8) J. G. Jones — On the Formulation of Gust Load Requirements in terms of the Statistical Discrete Gust Method. RAE Tech Memo FS 208

9) T. A. Zieler and A. S. Pototzky — On the Relationship Between Matched Filter Theory as Applied to Gust Loads and Phased Design Loads Analysis. NASA Contractor Report 181802

Figure 1
Discrete Gust Velocities
Ref. FAR/JAR 25.341(a)

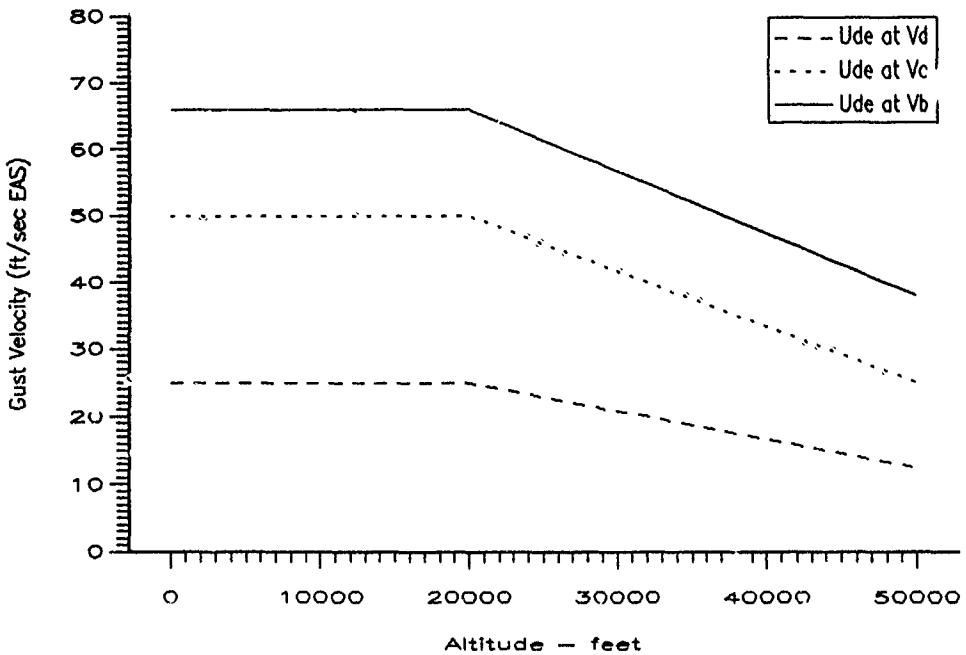

Figure 2
Discrete Gust Probabilities
per nautical mile

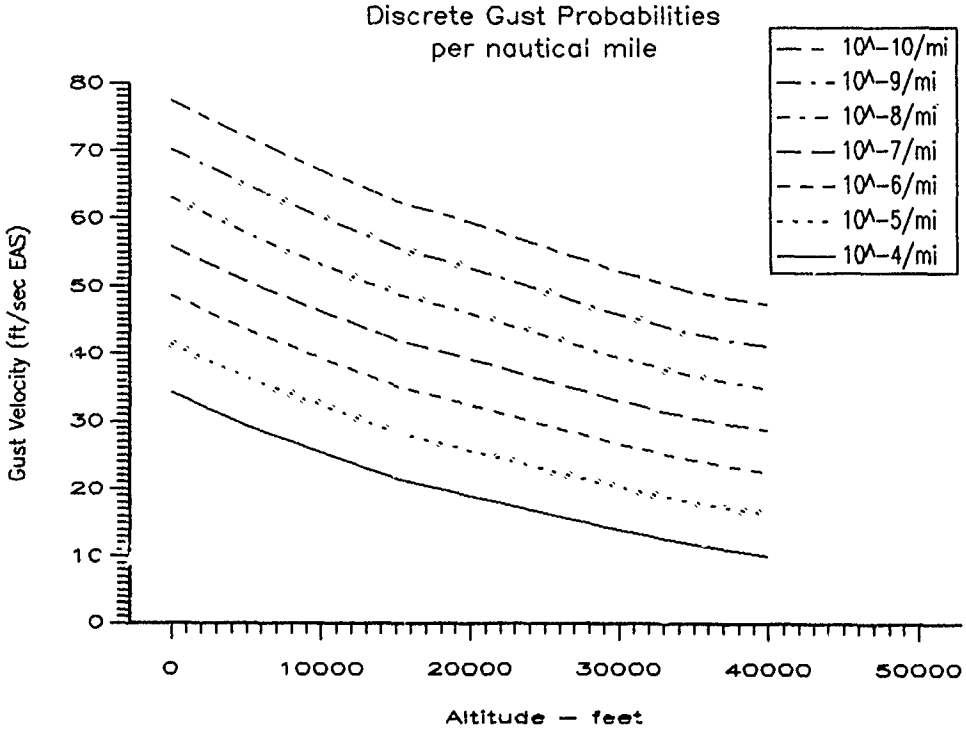

Figure 3

Discrete Gust Probabilities Compared With Requirements

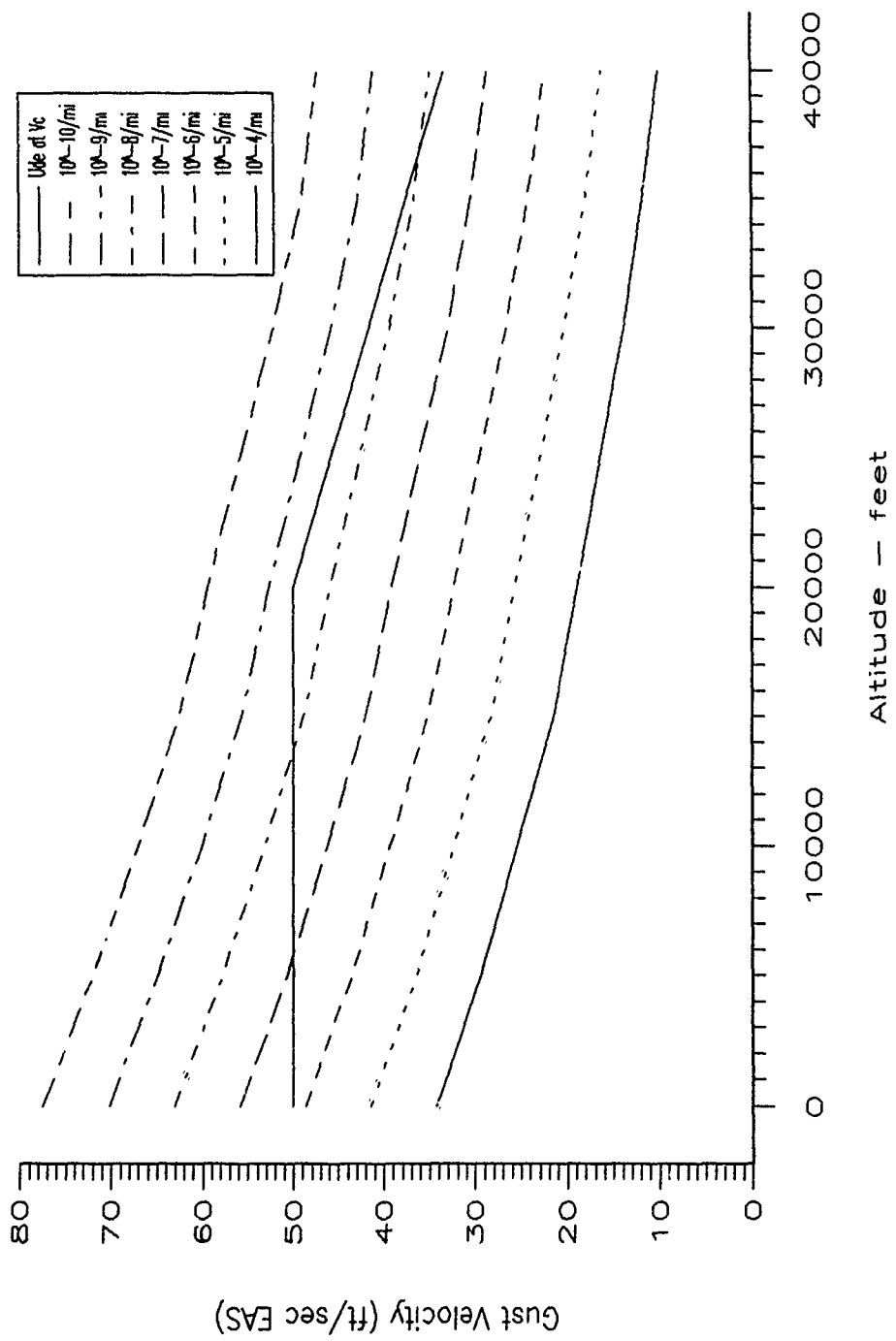

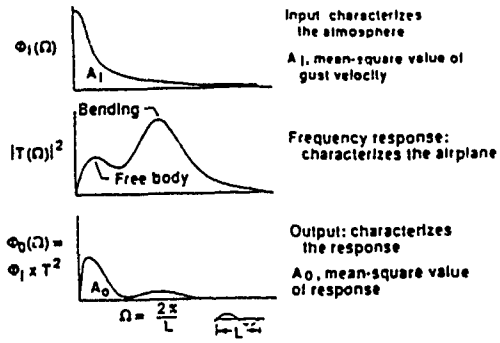

Gust response determination through use of generalized harmonic analysis

FIGURE 4

SUMMARY OF DESIGN
STRENGTH CAPABILITY FOR CONTINUOUS TURBULENCE
(DESIGN ENVELOPE)

NOTE: Uσ values are based on zero margin of safety..

AIRPLANE	ALTITUDE 1000 FT	Uσ, FPS
720B	23.5	62
727-100	20.0	74
727-200	20.0	64
737-200	23.5	70
747-100	20.0	62
Constellation Model 749	7.0	65
Electra Model 188	12.0	60
L-1011	26.2	76
DC-9-30	20.0	97
DC-10-10	24.8	71.4

Figure 5

Figure 6

GUST STRENGTH LEVELS FOR CURRENT AIRPLANES
BASED ON ZERO MARGIN OF SAFETY

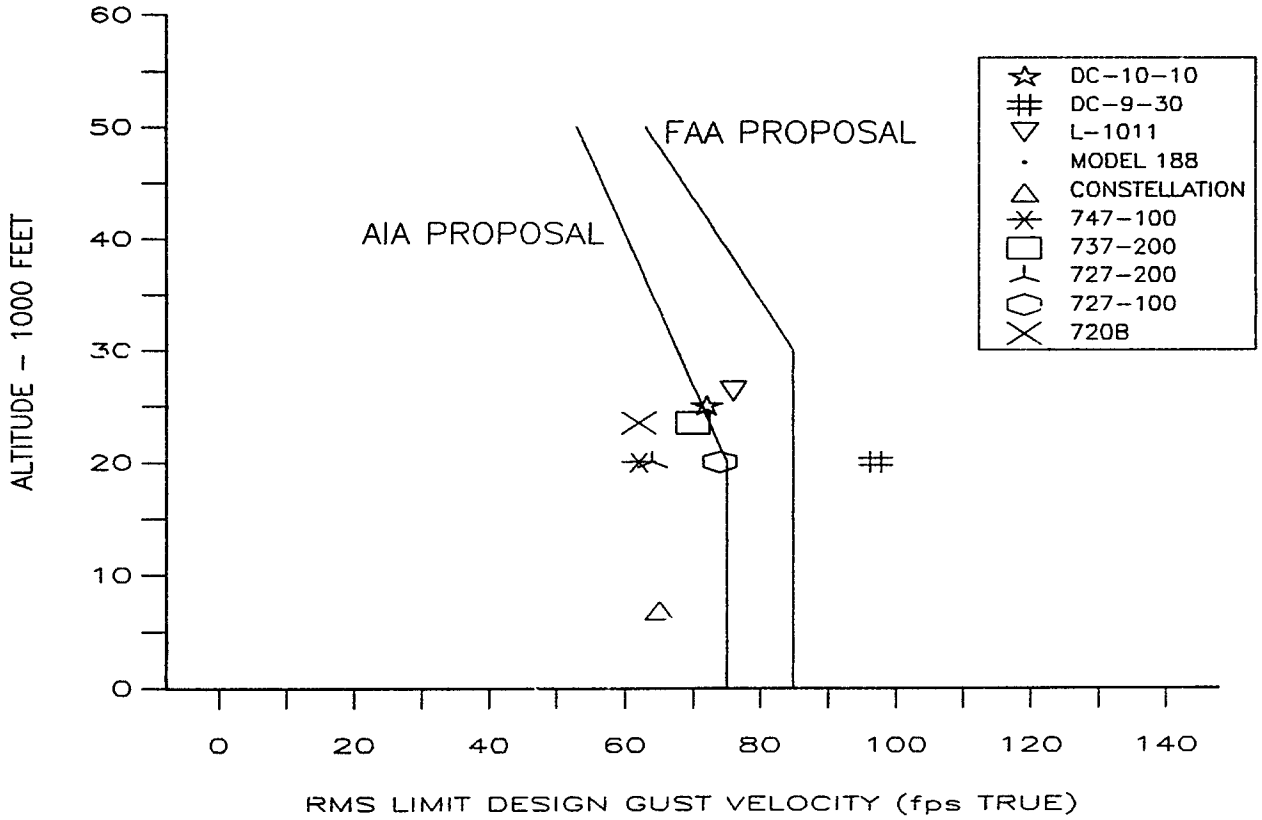

REPORT DOCUMENTATION PAGE

1. Recipient's Reference	2. Originator's Reference	3. Further Reference	4. Security Classification of Document
	AGARD-AG-317	ISBN 92-835-0617-0	UNCLASSIFIED

5. Orginator Advisory Group for Aerospace Research and Development
North Atlantic Treaty Organization
7 rue Ancelle, 92200 Neuilly sur Seine, France

6. Title MANUAL ON THE FLIGHT OF FLEXIBLE AIRCRAFT IN TURBULENCE

7. Presented at

8. Author(s)/Editor(s) Edited by John C. Houbolt

9. Date May 1991

10. Author's/Editor's Address

11. Pages 170

12. Distribution Statement This document is distributed in accordance with AGARD policies and regulations, which are outlined on the back covers of all AGARD publications.

13. Keywords/Descriptors

Aerodynamic loads
Aircraft
Design
Turbulence
Reviews

14. Abstract

In the course of the past few years the Structures and Materials Panel of AGARD has considered a number of aspects of the turbulence problem as it affects aircraft. The present publication constitutes a review document in which is distilled the experience of specialists from amongst the aircraft manufacturing nations of NATO. It is aimed at those in design offices concerned with the problems of turbulences and resultant loads.

This AGARDograph was sponsored by the Structures and Materials Panel of AGARD.

AGARDograph No.317 Advisory Group for Aerospace Research and Development, NATO MANUAL ON THE FLIGHT OF FLEXIBLE AIRCRAFT IN TURBULENCE Edited by John C. Houbolt Published May 1991 170 pages In the course of the past few years the Structures and Materials Panel of AGARD has considered a number of aspects of the turbulence problem as it affects aircraft The present publication constitutes a review document in which is distilled the experience of specialists from amongst the aircraft manufacturing nations of NATO. It is aimed at those in design offices concerned with the problems of turbulences and resultant loads P.T.O	AGARD-AG-317 Aerodynamic loads Aircraft Design Turbulence Reviews	AGARDograph No 317 Advisory Group for Aerospace Research and Development, NATO MANUAL ON THE FLIGHT OF FLEXIBLE AIRCRAFT IN TURBULENCE Edited by John C. Houbolt Published May 1991 170 pages In the course of the past few years the Structures and Materials Panel of AGARD has considered a number of aspects of the turbulence problem as it affects aircraft The present publication constitutes a review document in which is distilled the experience of specialists from amongst the aircraft manufacturing nations of NATO. It is aimed at those in design offices concerned with the problems of turbulences and resultant loads P.T.O	AGARD-AG-317 Aerodynamic loads Aircraft Design Turbulence Reviews
AGARDograph No.317 Advisory Group for Aerospace Research and Development, NATO MANUAL ON THE FLIGHT OF FLEXIBLE AIRCRAFT IN TURBULENCE Edited by John C. Houbolt Published May 1991 170 pages In the course of the past few years the Structures and Materials Panel of AGARD has considered a number of aspects of the turbulence problem as it affects aircraft The present publication constitutes a review document in which is distilled the experience of specialists from amongst the aircraft manufacturing nations of NATO It is aimed at those in design offices concerned with the problems of turbulences and resultant loads. P.T.O.	AGARD-AG-317 Aerodynamic loads Aircraft Design Turbulence Reviews	AGARDograph No.317 Advisory Group for Aerospace Research and Development NATO MANUAL ON THE FLIGHT OF FLEXIBLE AIRCRAFT IN TURBULENCE Edited by John C. Houbolt Published May 1991 170 pages In the course of the past few years the Structures and Materials Panel of AGARD has considered a number of aspects of the turbulence problem as it affects aircraft The present publication constitutes a review document in which is distilled the experience of specialists from amongst the aircraft manufacturing nations of NATO. It is aimed at those in design offices concerned with the problems of turbulences and resultant loads. P.T.O.	AGARD-AG-317 Aerodynamic loads Aircraft Design Turbulence Reviews

This AGARDograph was sponsored by the Structures and Materials Panel of AGARD. ISBN 92-835 0617-0	This AGARDograph was sponsored by the Structures and Materials Panel of AGARD. ISBN 92-835-0617-0
This AGARDograph was sponsored by the Structures and Materials Panel of AGARD. ISBN 92-835-0617-0	This AGARDograph was sponsored by the Structures and Materials Panel of AGARD. ISBN 92-835-0617-0

AGARD
NATO OTAN
7 RUE ANCELLE · 92200 NEUILLY-SUR-SEINE
FRANCE
Téléphone (1)47.38.57.00 · Télex 610 176
Télécopie (1)47.38.57.99

DIFFUSION DES PUBLICATIONS AGARD NON CLASSIFIEES

L'AGARD ne détient pas de stocks de ses publications, dans un but de distribution générale à l'adresse ci-dessus. La diffusion initiale des publications de l'AGARD est effectuée auprès des pays membres de cette organisation par l'intermédiaire des Centres Nationaux de Distribution suivants. A l'exception des Etats-Unis, ces centres disposent parfois d'exemplaires additionnels; dans les cas contraire, on peut se procurer ces exemplaires sous forme de microfiches ou de microcopies auprès des Agences de Vente dont la liste suite

CENTRES DE DIFFUSION NATIONAUX

ALLEMAGNE
Fachinformationszentrum,
Karlsruhe
D-7514 Eggenstein-Leopoldshafen 2

BELGIQUE
Coordonnateur AGARD-VSL
Etat-Major de la Force Aérienne
Quartier Reine Elisabeth
Rue d'Evere, 1140 Bruxelles

CANADA
Directeur du Service des Renseignements Scientifiques
Ministère de la Défense Nationale
Ottawa, Ontario K1A 0K2

DANEMARK
Danish Defence Research Board
Ved Idraetsparken 4
2100 Copenhagen Ø

ESPAGNE
INTA (AGARD Publications)
Pintor Rosales 34
28008 Madrid

ETATS-UNIS
National Aeronautics and Space Administration
Langley Research Center
M/S 180
Hampton, Virginia 23665

FRANCE
O.N.E.R.A. (Direction)
29, Avenue de la Division Leclerc
92320, Châtillon sous Bagneux

GRECE
Hellenic Air Force
Air War College
Scientific and Technical Library
Dekelia Air Force Base
Dekelia, Athens TGA 1010

ISLANDE
Director of Aviation
c/o Flugrad
Reykjavik

ITALIE
Aeronautica Militaire
Ufficio del Delegato Nazionale all'AGARD
3 Piazzale Adenauer
00144 Roma EUR

LUXEMBOURG
Voir Belgique

NORVEGE
Norwegian Defence Research Establishment
Attn: Biblioteket
P.O. Box 25
N-2007 Kjeller

PAYS-BAS
Netherlands Delegation to AGARD
National Aerospace Laboratory NLR
Kluyverweg 1
2629 HS Delft

PORTUGAL
Portuguese National Coordinator to AGARD
Gabinete de Estudos e Programas
CLAFA
Base de Alfragide
Alfragide
2700 Amadora

ROYAUME UNI
Defence Research Information Centre
Kentigern House
65 Brown Street
Glasgow G2 8EX

TURQUIE
Milli Savunma Başkanlığı (MSB)
ARGE Daire Başkanlığı (ARGE)
Ankara

LE CENTRE NATIONAL DE DISTRIBUTION DES ETATS-UNIS (NASA) NE DETIENT PAS DE STOCKS DES PUBLICATIONS AGARD ET LES DEMANDES D'EXEMPLAIRES DOIVENT ETRE ADRESSEES DIRECTEMENT AU SERVICE NATIONAL TECHNIQUE DE L'INFORMATION (NTIS) DONT L'ADRESSE SUIT

AGENCES DE VENTE

National Technical Information Service
(NTIS)
5285 Port Royal Road
Springfield, Virginia 22161
Etats-Unis

ESA/Information Retrieval Service
European Space Agency
10, rue Mario Nikis
75015 Paris
France

The British Library
Document Supply Division
Boston Spa, Wetherby
West Yorkshire LS23 7BQ
Royaume Uni

Les demandes de microfiches ou de photocopies de documents AGARD (y compris les demandes faites auprès du NTIS) doivent comporter la dénomination AGARD, ainsi que le numéro de série de l'AGARD (par exemple AGARD-AG-315) Des informations analogues, telles que le titre et la date de publication sont souhaitables Veuiller noter qu'il y a lieu de spécifier AGARD-R-nnn et AGARD-AR-nnn lors de la commande de rapports AGARD et des rapports consultatifs AGARD respectivement. Des références bibliographiques complètes ainsi que des résumés des publications AGARD figurent dans les journaux suivants:

Scientifique and Technical Aerospace Reports (STAR)
publié par la NASA Scientific and Technical
Information Division
NASA Headquarters (NTT)
Washington D.C. 20546
Etats-Unis

Government Reports Announcements and Index (GRA&I)
publié par le National Technical Information Service
Springfield
Virginia 22161
Etats-Unis

(accessible également en mode interactif dans la base de données bibliographiques en ligne du NTIS, et sur CD-ROM)

Imprimé par Specialised Printing Services Limited
40 Chigwell Lane, Loughton, Essex IG10 3TZ

AGARD
NATO · OTAN
7 RUE ANCELLE · 92200 NEUILLY-SUR-SEINE
FRANCE
Telephone (1)47.38.57.00 · Telex 610 176
Telefax (1)47.38.57.99

DISTRIBUTION OF UNCLASSIFIED AGARD PUBLICATIONS

AGARD does NOT hold stocks of AGARD publications at the above address for general distribution. Initial distribution of AGARD publications is made to AGARD Member Nations through the following National Distribution Centres.Further copies are sometimes available from these Centres (except in the United State.), but if not may be purchased in Microfiche or Photocopy form from the Sales Agencies listed below.

NATIONAL DISTRIBUTION CENTRES

BELGIUM
Coordonnateur AGARD — VSL
Etat-Major de la Force Aérienne
Quartier Reine Elisabeth
Rue d'Evere, 1140 Bruxelles

CANADA
Director Scientific Information Services
Dept of National Defence
Ottawa, Ontario K1A 0K2

DENMARK
Danish Defe
Ved Idraets
2100 Cope

FRANCE
O.N.E.R.A
29 Avenue
92320 Châ

GERMANY
Fachinform
Karlsruhe
D-7514 Eg

GREECE
Hellenic A
Air War C
Scientific a
Dekelia Ai
Dekelia, A

ICELAND
Director of
c/o Flugra
Reykjavik

ITALY
Aeronautica Militare
Ufficio del Delegato Nazionale all'AGARD
3 Piazzale Adenauer
00144 Roma/EUR

LUXEMBOURG
See Belgium

NETHERLANDS
Netherlands Delegation to AGARD
National Aerospace Laboratory, NLR
Kluyverweg 1
2629 HS Delft

NORWAY
Norwegian Defence Research Establishment
Attn: Biblioteket
P.O. Box 25

NASA
National Aeronautics and Space Administration
Washington, DC 20546

Postage an Fees Paid
National Aeronautics and Space Administration
NASA-451

Official Business
Penalty for Private Use $300

SPECIAL FOURTH CLASS MAIL BOOK

RD

L4 001 AGARDAL 31791 03306 7306
DEPT OF DEFENSE
DEFENSE TECHNICAL INFORMATION CENTER
OTIC FDAC
CAMERON STATION BLDG 5
ALEXANDRIA VA 22304614

UNITED STATES
National Aeronautics and Space Administration (NASA)
Langley Research Center
M/S 180
Hampton, Virginia 23665

THE UNITED STATES NATIONAL DISTRIBUTION CENTRE (NASA) DOES NOT HOLD STOCKS OF AGARD PUBLICATIONS, AND APPLICATIONS FOR COPIES SHOULD BE MADE DIRECT TO THE NATIONAL TECHNICAL INFORMATION SERVICE (NTIS) AT THE ADDRESS BELOW.

SALES AGENCIES

National Technical
Information Service (NTIS)
5285 Port Royal Road
Springfield, Virginia 22161
United States

ESA/Information Retrieval Service
European Space Agency
10, rue Mario Nikis
75015 Paris
France

The British Library
Document Supply Centre
Boston Spa, Wetherby
West Yorkshire LS23 7BQ
United Kingdom

Requests for microfiches or photocopies of AGARD documents (including requests to NTIS) should include the word 'AGARD' and the AGARD serial number (for example AGARD-AG-315). Collateral information such as title and publication date is desirable. Note that AGARD Reports and Advisory Reports should be specified as AGARD-R-nnn and AGARD-AR-nnn, respectively. Full bibliographical references and abstracts of AGARD publications are given in the following journals:

Scientific and Technical Aerospace Reports (STAR)
published by NASA Scientific and Technical
Information Division
NASA Headquarters (NTT)
Washington D.C. 20546
United States

Government Reports Announcements and Index (GRA&I)
published by the National Technical Information Service
Springfield
Virginia 22161
United States
(also available online in the NTIS Bibliographic Database or on CD-ROM)

Printed by Specialised Printing Services Limited
40 Chigwell Lane, Loughton, Essex IG10 3TZ

ISBN 92-835-0617-0

AG 317

MANUAL ON THE FLIGHT OF FLEXIBLE AIRCRAFT IN TURBULENCE